



University of Kentucky
UKnowledge

Theses and Dissertations--Pharmacy

College of Pharmacy

2015

DESIGN, SYNTHESIS, AND PHARMACOLOGICAL EVALUATION OF THREE SERIES OF LOBELANE ANALOGS AS INHIBITORS OF THE VESICULAR MONOAMINE TRANSPORTER (VMAT2)

John P. Culver
University of Kentucky, johnculver@hotmail.com

[Right click to open a feedback form in a new tab to let us know how this document benefits you.](#)

Recommended Citation

Culver, John P., "DESIGN, SYNTHESIS, AND PHARMACOLOGICAL EVALUATION OF THREE SERIES OF LOBELANE ANALOGS AS INHIBITORS OF THE VESICULAR MONOAMINE TRANSPORTER (VMAT2)" (2015). *Theses and Dissertations--Pharmacy*. 46.
https://uknowledge.uky.edu/pharmacy_etds/46

This Doctoral Dissertation is brought to you for free and open access by the College of Pharmacy at UKnowledge. It has been accepted for inclusion in Theses and Dissertations--Pharmacy by an authorized administrator of UKnowledge. For more information, please contact UKnowledge@lsv.uky.edu.

STUDENT AGREEMENT:

I represent that my thesis or dissertation and abstract are my original work. Proper attribution has been given to all outside sources. I understand that I am solely responsible for obtaining any needed copyright permissions. I have obtained needed written permission statement(s) from the owner(s) of each third-party copyrighted matter to be included in my work, allowing electronic distribution (if such use is not permitted by the fair use doctrine) which will be submitted to UKnowledge as Additional File.

I hereby grant to The University of Kentucky and its agents the irrevocable, non-exclusive, and royalty-free license to archive and make accessible my work in whole or in part in all forms of media, now or hereafter known. I agree that the document mentioned above may be made available immediately for worldwide access unless an embargo applies.

I retain all other ownership rights to the copyright of my work. I also retain the right to use in future works (such as articles or books) all or part of my work. I understand that I am free to register the copyright to my work.

REVIEW, APPROVAL AND ACCEPTANCE

The document mentioned above has been reviewed and accepted by the student's advisor, on behalf of the advisory committee, and by the Director of Graduate Studies (DGS), on behalf of the program; we verify that this is the final, approved version of the student's thesis including all changes required by the advisory committee. The undersigned agree to abide by the statements above.

John P. Culver, Student

Dr. Peter A. Crooks, Major Professor

Dr. Jim Pauly, Director of Graduate Studies

DESIGN, SYNTHESIS, AND PHARMACOLOGICAL EVALUATION OF THREE
SERIES OF LOBELANE ANALOGS AS INHIBITORS OF THE VESICULAR
MONOAMINE TRANSPORTER (VMAT2)

DISSERTATION

A dissertation submitted in partial fulfillment of the requirements for the degree of
Doctor of Philosophy in the College of Pharmacy at the University of Kentucky

By

John P. Culver

Lexington, Kentucky

Director: Dr. Peter A. Crooks, Professor and Chairman, Department of Pharmaceutical
Sciences

Little Rock, Arkansas

2015

Copyright © John P. Culver 2015

ABSTRACT OF DISSERTATION

DESIGN, SYNTHESIS, AND PHARMACOLOGICAL EVALUATION OF THREE SERIES OF LOBELANE ANALOGS AS INHIBITORS OF THE VESICULAR MONOAMINE TRANSPORTER (VMAT2)

Methamphetamine (METH) abuse is a serious problem in the United States and worldwide. The reward experienced by METH users is due to the increase in extracellular dopamine (DA) concentrations caused by an interaction between METH and the DA transporter (DAT) as well as the Vesicular Monoamine Transporter-2 (VMAT2). The reward felt by users of METH leads to further use of the drug and subsequent abuse. The current project examined the ability of three novel series of lobelane analogs to interact with a binding site on the Vesicular Monoamine Transporter-2 (VMAT2) in an attempt to inhibit the effects of METH. Lobelane is a defunctionalized analog of Lobeline, a natural product found in *Lobelia inflata* which has been shown to bind to VMAT2 and inhibit its function. Rational drug design methodology and organic synthesis was used to generate a library of three series of lobelane analogs. In total, 107 compounds were synthesized and examined. Compounds were assayed for affinity in a high-throughput [^3H] dihydrotetrabenazine (DTBZ) radioligand binding screen as well as for function in a [^3H] DA uptake assay. Several compounds were identified which possess affinity as well as selectivity for the DTBZ binding site on VMAT2 [JPC-077 ($K_i=0.19\ \mu\text{M}$), JPC-094 ($K_i=0.15\ \mu\text{M}$), JPC-096 ($K_i=0.19\ \mu\text{M}$), and JPC-106 ($K_i=0.19\ \mu\text{M}$)]. The same four compounds exhibited inhibition of [^3H]DA uptake [JPC-077 ($K_i=9.3\ \text{nM}$), JPC-094 ($K_i=13\ \text{nM}$), JPC-096 ($K_i=20\ \text{nM}$), and JPC-106 ($K_i=83\ \text{nM}$)]. With the assay data generated from the library of compounds, several structure activity relationship (SAR) based ligand based pharmacophore models were developed to guide future ligand design.

Keywords: lobeline, lobelane, vesicular monoamine transporter-2, VMAT2, methamphetamine, affinity, binding site

John P. Culver

Student's Signature

July 8, 2014

Date

STUDENT AGREEMENT:

I represent that my thesis or dissertation and abstract are my original work. Proper attribution has been given to all outside sources. I understand that I am solely responsible for obtaining any needed copyright permissions. I have obtained and attached hereto needed written permission statements(s) from the owner(s) of each third-party copyrighted matter to be included in my work, allowing electronic distribution (if such use is not permitted by the fair use doctrine). I hereby grant to The University of Kentucky and its agents the non-exclusive license to archive and make accessible my work in whole or in part in all forms of media, now or hereafter known. I agree that the document mentioned above may be made available immediately for worldwide access unless a preapproved embargo applies. I retain all other ownership rights to the copyright of my work. I also retain the right to use in future works (such as articles or books) all or part of my work. I understand that I am free to register the copyright to my work.

REVIEW, APPROVAL AND ACCEPTANCE

The document mentioned above has been reviewed and accepted by the student's advisor, on behalf of the advisory committee, and by the Director of Graduate Studies (DGS), on behalf of the program; we verify that this is the final, approved version of the student's dissertation including all changes required by the advisory committee. The undersigned agree to abide by the statements above.

John P. Culver, Student

Dr. Peter A. Crooks, Major Professor

Dr. Jim Pauly, Director of Graduate Studies

DEDICATION

This work is dedicated to my wife, parents, family, and friends. Thank you for all of the support and understanding you have shown throughout this process.

ACKNOWLEDGEMENTS

The dissertation that follows came about through a blend of collaboration, teamwork, and determination. The guidance, support, and resources of Dr. Peter Crooks and Dr. Linda Dwoskin made this dissertation possible. The advice of Dr. Guangrong Zheng was instrumental in helping solve synthesis challenges, and I am thankful to him for helping making the time in the lab productive, challenging, and enjoyable. Dr. Justin Nickell was indispensable in the assaying and testing of the final compounds, and my thanks also go out to him for his patience and cooperation in explaining the results and how they were obtained. Thanks go also to Dr. Vinod Kasam for sharing his knowledge in molecular modeling and helping me to generate the pharmacophore models that form the basis for Chapter 6.

I am in addition thankful to the members of my graduate committee for their guidance and patience. These members include Drs. Peter Crooks, Linda Dwoskin, John Littleton, Jim Pauly, and Lowell Bush. A special thank you to all of the members of Dr. Crooks' and Dr. Dwoskin's research groups, both past and present, is owed. Of these, my comrades in this process must be noted and I am thankful for their friendship. They include: Josh Eldridge, Mike Smith, Ujjwal Chakraborty, Harpreet Dhooper, Nikhil Madadi, David Horton, and Mikolaj Milewski.

Final thanks are to be given to my wife, Tabitha, whose patience throughout this process has been remarkable, my family, especially my sister, Susan, whose help in taking care of my daughter, Kate, was priceless during the writing process.

TABLE OF CONTENTS

Acknowledgements	iii
List of Tables	vi
List of Schemes	viii
List of Figures	xii
Chapter 1: Goals of the study and literature review	1
1.1 Hypotheses	1
1.2 Overall Aims	1
1.3 Methodology to be utilized in this study	2
1.4 Overview of Drug Discovery	3
1.5 Methamphetamine abuse prevalence and limitations of viable therapies and treatments	11
1.6 Methamphetamine Mechanism of Action, and the Role of VMAT2	19
1.7 Methamphetamine Mechanism of Action	24
1.8 Lobeline Background and Mechanism of Action as a Treatment for METH abuse	26
1.9 Review of Structural Modifications of Lobeline and lobelane to afford VMAT2 Inhibitors	34
1.10 Portions of the lobelane scaffold that are critical in binding to VMAT2	89
1.11 Modification and optimization of the lobelane scaffold	90
Chapter 2: Synthesis of 2,6-disubstituted piperidine analogs structurally related to lobelane	92
2.1 Prior studies with this scaffold	92
2.2 Design and synthesis of the 2,6-disubstituted piperidine scaffold	92

2.3 Summary of the 2,6-disubstituted piperidine analog series	116
Chapter 3: Design and Synthesis of 1,4-Disubstituted Piperidine Analogs of lobelane	117
3.1 Prior studies with the 1,4-disubstituted scaffold	117
3.2 Design and Synthesis of 1,4-substituted piperidine scaffold analogs	117
3.3 Summary of the 1,4-disubstituted piperidine analog series	199
Chapter 4: Design and Synthesis of 1,4-substituted piperazine scaffold analogs of lobelane	200
4.1 Experiments in the 1,4-disubstituted piperazine scaffold	200
4.2 Summary of the 1,4-disubstituted piperazine analog series	231
Chapter 5: Pharmacology Assays and Data	232
5.1 [³ H] Dihydrotrabenazine Binding Assay and [³ H] Dopamine Uptake Assay Background	232
5.2 [³ H] Dihydrotrabenazine Binding Assay and [³ H] Dopamine Uptake Assay Results	237
5.3 [³ H] Dihydrotrabenazine Binding Assay and [³ H] Dopamine Uptake Assay Results Discussion	253
Chapter 6: Ligand based pharmacophore modeling of the VMAT2 binding site	268
6.1 Background of computational modeling	268
6.2 Model Methods of automatic pharmacophore modeling of VMAT2 inhibitors	269
6.3 Results of automatic pharmacophore modeling of VMAT2 inhibitors	271
6.4 Model Methods of manual pharmacophore modeling of VMAT2 inhibitors	275
6.5 Results of manual pharmacophore modeling of VMAT2 inhibitors	278
Chapter 7: Review and Discussion	280
References	285
Vita	301

LIST OF TABLES

Table 1.1	Binding affinity of LOB, lobelanine, ketoalkene, and lobelanidine at $\alpha 4\beta 2^*$ and $\alpha 7^*$ nAChRs, and at VMAT2	37
Table 1.2	Binding affinity of <i>des</i> -keto LOB analogs at $\alpha 4\beta 2^*$ and $\alpha 7^*$ nAChRs, and at VMAT2	40
Table 1.3	Binding affinity of “des-oxygen” LOB analogs at $\alpha 4\beta 2^*$ & $\alpha 7^*$ nAChRs, and at VMAT2	44
Table 1.4	Binding affinity of acyclic fragmented lobelane analogs at $\alpha 4\beta 2^*$ & $\alpha 7^*$ nAChRs, and at VMAT2	50
Table 1.5	Structures of substituted phenyl analogs of lobelane and assay data from [³ H]NIC Binding $\alpha 4\beta 2^*$ nAChR, [³ H]MLA Binding $\alpha 7^*$ nAChR, [³ H]DTBZ Binding VMAT2, and VMAT2 [³ H]DA Uptake	55
Table 1.6	Structures and Binding affinity of heteroaromatic substituted and symmetrical lobelane analogs for VMAT2	60
Table 1.7	Compound structures and $\alpha 4\beta 2^*$ & $\alpha 7^*$ nAChRs, and VMAT2 binding affinity of isomerized lobelane analogs with phenethyl linkers in the N1, C2; N1, C3; N1, C4; C2, C4 and C3, C5 positions	67
Table 1.8	Compound structures and VMAT2 binding affinity of modified lobelane analogs with differing intramolecular distances between the piperidine ring and the phenyl rings in the molecule	80
Table 1.9	Compound structures and VMAT2 binding affinity of modified lobelane analogs	82
Table 1.10	Structures and VMAT2 binding affinities of modified lobelane analogs	88

Table 5.1	[³ H] Dihydrotetrabenazine Binding Assay Data and [³ H] Dopamine Uptake Assay Data for JPC compounds in the 2,6-substituted piperidine analog scaffold of lobelane	240
Table 5.2	[³ H] Dihydrotetrabenazine Binding Assay Data and [³ H] Dopamine Uptake Assay Data for JPC compounds in the 1,4-substituted piperidine Analog scaffold of lobelane	249
Table 5.3	[³ H] Dihydrotetrabenazine Binding Assay Data and [³ H] Dopamine Uptake Assay Data for JPC compounds in the 1,4-substituted piperazine and diazepane analog scaffolds of lobelane and similar compounds	252
Table 6.1	Statistics of best pharmacophore model query obtained by using the MOE pharmacophore elucidator (automatic pharmacophore modeling)	272

LIST OF SCHEMES

Scheme 1.1. Synthetic routes to lobelanine, lobelanidine, and the ketoalkene [2-((2 <i>R</i> , 6 <i>S</i>)-1-methyl-6-styrylpiperidine-2-yl)-1-phenylethanone	36
Scheme 1.2. The synthetic route to <i>des</i> -keto analogs of lobeline (Adapted from Crooks, et al., 2011)	38
Scheme 1.3. Synthetic routes to LOB analogs in which all oxygen functionalities have been removed (defunctionalized LOB analogs) (adapted from Crooks et al., 2011)	41
Scheme 1.4. Synthetic methods used in generating fragmented lobelane analogs (Zheng et al., 2005; Crooks et al., 2011)	47
Scheme 1.5. Synthetic methods for generation of symmetrically substituted phenyl ring analogs of lobelane (Zheng et al., 2005)	51
Scheme 1.6 Synthetic methods for generation of symmetrically substituted heteroaromatic ring analogs of lobelane (Varkat et al., 2010)	57
Scheme 1.7 Synthetic methods for the generation of asymmetrical lobelane analogs (Crooks, et al., 2011)	58
Scheme 1.8 Synthetic methods for generation of isomerized lobelane analogs (Zheng et al., 2005; Crooks et al., 2011)	62
Scheme 1.9 Synthetic methods for generation of isomerized lobelane analogs with phenethyl linkers in the 2,4 and 3,5 position of the piperidine ring (Zheng et al., 2005; Crooks et al., 2011)	63

Scheme 1.10	Synthesis of a symmetrical lobelane analog with zero methylene groups between the piperidine ring and the phenyl rings (Zheng et al., 2008; Crooks et al., 2011)	68
Scheme 1.11	Synthesis of the symmetrical lobelane analog with one methylene group between the piperidine ring and the phenyl rings (Zheng et al., 2008; Crooks et al., 2011)	69
Scheme 1.12	Synthesis of the symmetrical lobelane analog with three methylene groups between the piperidine ring and the phenyl rings (Zheng et al., 2008; Crooks et al., 2011)	70
Scheme 1.13	Synthesis of an asymmetrical lobelane analog with zero carbons and one carbon in the linkers between the piperidine ring and the phenyl rings (Zheng et al., 2008; Crooks et al., 2011)	71
Scheme 1.14	Synthesis of asymmetrical lobelane analog with zero methylene units and either two or three methylene units in the linkers between the piperidine ring and the phenyl rings (Zheng et al., 2008; Crooks et al., 2011)	73
Scheme 1.15	Synthesis of the asymmetrical lobelane analog with one methylene units and two methylene units in the linkers between the piperidine ring and the phenyl rings (Zheng et al., 2008; Crooks et al., 2011)	75
Scheme 1.16	Synthesis of an asymmetrical lobelane analog with one methylene unit and two methylene units in the linkers between the piperidine ring and the phenyl rings (Zheng et al., 2008; Crooks et al., 2011)	76

Scheme 1.17	Synthesis of an asymmetrical lobelane analog with two methylene units and three methylene units in the linkers between the piperidine ring and the phenyl rings (Zheng et al., 2008; Crooks et al., 2011)	77
Scheme 1.18	Synthetic outline for generation of piperazine analogs of lobelane	84
Scheme 1.19	Synthesis of tropane analogs of lobelane (Zheng et al., 2005)	85
Scheme 1.20	Synthesis of tropane analogs of lobelane with extended linkers (Zheng et al., 2005)	85
Scheme 2.1	Synthesis of the 2,6-substituted piperidine analog scaffold of lobelane	93
Scheme 3.1	Synthetic route to the 1,4-disubstituted piperidine analogs of lobelane	118
Scheme 3.2	Synthetic route to the phenethyl substituted 4-benzyl-1-phenethylpiperidine analogs of lobelane	166
Scheme 3.3	Synthetic route to the substituted 1-benzyl-4-phenethylpiperidine analogs of lobelane	172
Scheme 3.4	Synthesis of the 4-phenethyl-1-(1-phenylpropan-2-yl)piperidine and 4-benzyl-1-(1-phenylpropan-2-yl)piperidine series of lobelane analogs	180
Scheme 3.5	Synthesis of the 4-phenethyl-1-(2-(piperidin-1-yl)ethyl)piperidine and 4-(2-(4-phenethylpiperidin-1-yl)ethyl)morpholine series of lobelane analogs	186
Scheme 4.1	Synthesis of the symmetrical 1,4-substituted piperazine analog scaffold	201
Scheme 4.2	Synthesis of the asymmetrical 1,4-piperazine scaffold	208
Scheme 4.3	Synthesis of the symmetrical 1,4-diazepane series of analogs	215
Scheme 4.4	Synthesis of 1,2- <i>bis</i> (4-benzylpiperidin-1-yl)ethane and 1,2- <i>bis</i> (4-phenethylpiperidin-1-yl)ethane	223

Scheme 4.5 Synthesis of the 1-phenethyl-4-(1-phenylpropan-2-yl)piperazine set of
Compounds

227

LIST OF FIGURES

Figure 1.1	Flow chart overview of the drug discovery process. Rational design and synthesis and high throughput synthesis generate the libraries of compounds that are then assayed for activity at the biomolecular target of interest. Each cycle of the flow chart represents a single generation of compounds. SAR analysis can accelerate the cycle time, with each generation yielding a new lead compound that is a more suitable drug candidate.	10
Figure 1.2	Chemical Structures of Cocaine and Methamphetamine	15
Figure 1.3	Structure of the neurotransmitter dopamine (DA)	16
Figure 1.4	Illustration of METH's effects on the dopaminergic neuron (Adapted from G. Zheng, with permission)	25
Figure 1.5	The chemical structures of lobeline (LOB) and structurally related alkaloids present in <i>Lobelia inflata</i>	27
Figure 1.6	Likely process of Lobeline epimerization (adapted from Crooks et al., 2011)	28
Figure 1.7	Lobeline's Mechanism of Action at the Dopaminergic Neuron (Adapted from G. Zheng, With Permission)	33
Figure 1.8	Lobeline's inhibition of Methamphetamine (Adapted from G. Zheng, With Permission)	34
Figure 1.9.	Structures of acyclic fragmented lobelane analogs	48
Figure 1.10	Graphical representation of the lobelane scaffold depicting the parts of the molecule that are essential for binding to VMAT2	89
Figure 2.1	Structure of (2 <i>S</i> ,6 <i>R</i>)-2,6- <i>bis</i> (3,5-difluorophenethyl)piperidine (JPC-001)	98

Figure 2.2	Structure of (2 <i>S</i> ,6 <i>R</i>)-2,6- <i>bis</i> (3,5-difluorophenethyl)-1-methylpiperidine (JPC-011)	99
Figure 2.3	Structure of (2 <i>S</i> ,6 <i>R</i>)-2,6- <i>bis</i> (3-chlorophenethyl)piperidine (JPC-002)	100
Figure 2.4	Structure of 3,3'-(2,2'-((2 <i>S</i> ,6 <i>R</i>)-piperidine-2,6-diyl) <i>bis</i> (ethane-2,1-diyl)) dianiline (JPC-008)	101
Figure 2.5	Structure of (2 <i>S</i> ,6 <i>R</i>)-2,6- <i>bis</i> (2-cyclohexylethyl)piperidine (JPC-003)	102
Figure 2.6	Structure of (2 <i>S</i> ,6 <i>R</i>)-2,6- <i>bis</i> (2-cyclohexylethyl)-1-methylpiperidine (JPC-007)	103
Figure 2.7	Structure of (2 <i>S</i> ,6 <i>R</i>)-2,6- <i>bis</i> (2,4-difluorophenethyl)piperidine(JPC-130a)	104
Figure 2.8	Structure of (2 <i>S</i> ,6 <i>R</i>)-2,6- <i>bis</i> (2,4-difluorophenethyl)-1-methylpiperidine (JPC-130b)	105
Figure 2.9	Structure of (2 <i>S</i> ,6 <i>R</i>)-2,6- <i>bis</i> (3,5-dimethoxyphenethyl)piperidine (JPC-004)	106
Figure 2.10	Structure of (2 <i>S</i> ,6 <i>R</i>)-2,6- <i>bis</i> (3,5-dimethoxyphenethyl)-1-methylpiperidine (JPC-010)	107
Figure 2.11	Structure of (2 <i>S</i> ,6 <i>R</i>)-2,6- <i>bis</i> (3,4-dimethoxyphenethyl)piperidine (JPC-033)	108
Figure 2.12	Structure of (2 <i>S</i> ,6 <i>R</i>)-2,6- <i>bis</i> (3,4-dimethoxyphenethyl)-1-methylpiperidine (JPC-034)	109
Figure 2.13	Structure of (2 <i>S</i> ,6 <i>R</i>)-2,6- <i>bis</i> (2,3-dimethoxyphenethyl)piperidine (JPC-035)	110
Figure 2.14	Structure of (2 <i>S</i> ,6 <i>R</i>)-2,6- <i>bis</i> (2,3-dimethoxyphenethyl)-1-Methylpiperidine (JPC-036)	111
Figure 2.15	Structure of (2 <i>S</i> ,6 <i>R</i>)-2,6- <i>bis</i> (2,5-dimethoxyphenethyl)piperidine (JPC-041)	112

Figure 2.16	Structure of (2 <i>S</i> ,6 <i>R</i>)-2,6- <i>bis</i> (2,5-dimethoxyphenethyl)-1-Methylpiperidine (JPC-042)	113
Figure 2.17	Structure of (2 <i>S</i> ,6 <i>R</i>)-2,6- <i>bis</i> (4-fluoro-3-methoxyphenethyl)piperidine (JPC-161b)	114
Figure 2.18	Structure of (2 <i>S</i> ,6 <i>R</i>)-2,6- <i>bis</i> (4-fluoro-3-methoxyphenethyl)-1-methylpiperidine (JPC-161c)	115
Figure 3.1	Structure of 1-(2-methoxyphenethyl)-4-phenethylpiperidine (JPC-57)	123
Figure 3.2	Structure of 1-(3,4-dimethoxyphenethyl)-4-phenethylpiperidine (JPC-058)	124
Figure 3.3	Structure of 1-(3-methoxyphenethyl)-4-phenethylpiperidine (JPC-059)	125
Figure 3.4	Structure of 1-(4-methoxyphenethyl)-4-phenethylpiperidine (JPC-060)	126
Figure 3.5	Structure of 1-(2-chlorophenethyl)-4-phenethylpiperidine (JPC-072)	127
Figure 3.6	Structure of 1-(4-fluorophenethyl)-4-phenethylpiperidine (JPC-073)	128
Figure 3.7	Structure of 4-(2-methoxyphenethyl)-1-phenethylpiperidine (JPC-078)	129
Figure 3.8	Structure of 1,4- <i>bis</i> (2-methoxyphenethyl)piperidine (JPC-077)	130
Figure 3.9	Structure of 4-(2-methoxyphenethyl)-1-(3-methoxyphenethyl)piperidine (JPC-094)	131
Figure 3.10	Structure of 4-(2-methoxyphenethyl)-1-(4-methoxyphenethyl)piperidine (JPC-095)	132
Figure 3.11	Structure of 4-(2-methoxyphenethyl)-1-(2-chlorophenethyl)piperidine (JPC-096)	133
Figure 3.12	Structure of 4-(2-methoxyphenethyl)-1-(4-fluorophenethyl)piperidine (JPC-097)	134
Figure 3.13	Structure of 4-(3-methoxyphenethyl)-1-phenethylpiperidine (JPC-079)	135

Figure 3.14	Structure of 1-(2-methoxyphenethyl)-4-(3-methoxyphenethyl)piperidine (JPC-080)	136
Figure 3.15	Structure of 1,4- <i>bis</i> (3-methoxyphenethyl)piperidine (JPC-081)	137
Figure 3.16	Structure of 1-(4-methoxyphenethyl)-4-(3-methoxyphenethyl)piperidine (JPC-082)	138
Figure 3.17	Structure of 1-(2-chlorophenethyl)-4-(3-methoxyphenethyl)piperidine (JPC-083)	139
Figure 3.18	Structure of 1-(4-fluorophenethyl)-4-(3-methoxyphenethyl)piperidine (JPC-084)	140
Figure 3.19	Structure of 4-(4-methoxyphenethyl)-1-phenethylpiperidine (JPC-085)	141
Figure 3.20	Structure of 1-(2-methoxyphenethyl)-4-(4-methoxyphenethyl)piperidine (JPC-086)	142
Figure 3.21	Structure of 1-(3-methoxyphenethyl)-4-(4-methoxyphenethyl)piperidine (JPC-087)	143
Figure 3.22	Structure of 1,4- <i>bis</i> (4-methoxyphenethyl)piperidine (JPC-088)	144
Figure 3.23	Structure of 1-(2-chlorophenethyl)-4-(4-methoxyphenethyl)piperidine (JPC-089)	145
Figure 3.24	Structure of 1-(4-fluorophenethyl)-4-(4-methoxyphenethyl)piperidine (JPC-090)	146
Figure 3.25	Structure of 4-(2,4-difluorophenethyl)-1-phenethylpiperidine (JPC-098)	147
Figure 3.26	Structure of 4-(2,4-difluorophenethyl)-1-(2-methoxyphenethyl)piperidine (JPC-099)	148

Figure 3.27	Structure of 4-(2,4-difluorophenethyl)-1-(3-methoxyphenethyl) piperidine (JPC-100)	149
Figure 3.28	Structure of 4-(2,4-difluorophenethyl)-1-(4-methoxyphenethyl) Piperidine (JPC-101)	150
Figure 3.29	Structure of 1-(2-chlorophenethyl)-4-(2,4-difluorophenethyl)piperidine (JPC-102)	151
Figure 3.30	Structure of 4-(2,4-difluorophenethyl)-1-(4-fluorophenethyl)piperidine (JPC-103)	152
Figure 3.31	Structure of 4-(2-fluoro-4-methoxyphenethyl)-1-phenethylpiperidine (JPC-104)	153
Figure 3.32	Structure of 4-(2-fluoro-4-methoxyphenethyl)-1-(2-methoxyphenethyl) piperidine (JPC-105)	154
Figure 3.33	Structure of 4-(2-fluoro-4-methoxyphenethyl)-1-(3-methoxyphenethyl) piperidine (JPC-106)	155
Figure 3.34	Structure of 4-(2-fluoro-4-methoxyphenethyl)-1-(4-methoxyphenethyl) piperidine (JPC-107)	156
Figure 3.35	Structure of 1-(2-chlorophenethyl)-4-(2-fluoro-4-methoxyphenethyl) piperidine (JPC-108)	157
Figure 3.36	Structure of 4-(2-fluoro-4-methoxyphenethyl)-1-(4-fluorophenethyl) piperidine (JPC-109)	158
Figure 3.37	Structure of 4-(3,5-difluorophenethyl)-1-phenethylpiperidine (JPC-110)	159
Figure 3.38	Structure of 4-(3,5-difluorophenethyl)-1-(2-methoxyphenethyl) piperidine (JPC-111)	160

Figure 3.39	Structure of 4-(3,5-difluorophenethyl)-1-(3-methoxyphenethyl) Piperidine (JPC-112)	161
Figure 3.40	Structure of 4-(3,5-difluorophenethyl)-1-(4-methoxyphenethyl) piperidine (JPC-113)	162
Figure 3.41	Structure of 1-(2-chlorophenethyl)-4-(3,5-difluorophenethyl)piperidine (JPC-114)	163
Figure 3.42	Structure of 4-(3,5-difluorophenethyl)-1-(4-fluorophenethyl)piperidine (JPC-115)	164
Figure 3.43	Structure of 1-phenethyl-4-(2,4,5-trimethoxyphenethyl)piperidine (JPC-068)	165
Figure 3.44	Structure of 4-benzyl-1-(2-methoxyphenethyl)piperidine (JPC-061)	168
Figure 3.45	Structure of 4-benzyl-1-(3-methoxyphenethyl)piperidine (JPC-062)	169
Figure 3.46	Structure of 4-benzyl-1-(3,4-dimethoxyphenethyl)piperidine (JPC-063)	170
Figure 3.47	Structure of 4-benzyl-1-(4-methoxyphenethyl)piperidine (JPC-064)	171
Figure 3.48	Structure of 1-benzyl-4-phenethylpiperidine (JPC-152)	174
Figure 3.49	Structure of 1-(2-methoxybenzyl)-4-phenethylpiperidine (JPC-153)	175
Figure 3.50	Structure of 1-(3-methoxybenzyl)-4-phenethylpiperidine (JPC-154)	176
Figure 3.51	Structure of 1-(4-methoxybenzyl)-4-phenethylpiperidine (JPC-155)	177
Figure 3.52	Structure of 1-(2-chlorobenzyl)-4-phenethylpiperidine (JPC-156)	178
Figure 3.53	Structure of 1-(4-fluorobenzyl)-4-phenethylpiperidine (JPC-157)	179
Figure 3.54	Structure of racemic 4-benzyl-1-(1-phenylpropan-2-yl)piperidine (JPC-174)	182

Figure 3.55	Structure of racemic 4-phenethyl-1-(1-phenylpropan-2-yl)piperidine (JPC-175)	183
Figure 3.56	Structure of racemic 4-benzyl-1-(1-(4-bromophenyl)propan-2-yl) piperidine (JPC-171)	184
Figure 3.57	Structure of racemic 1-(1-(4-bromophenyl)propan-2-yl)-4- phenethylpiperidine (JPC-172)	185
Figure 3.58	Structure of 4-phenethyl-1-(2-(piperidin-1-yl)ethyl)piperidine (JPC-116)	188
Figure 3.59	Structure of 4-(2-(4-phenethylpiperidin-1-yl)ethyl)morpholine (JPC-117)	189
Figure 3.60	Structure of 4-(2-methoxyphenethyl)-1-(2-(piperidin-1-yl)ethyl) Piperidine (JPC-118)	190
Figure 3.61	Structure of 4-(2-(4-(2-methoxyphenethyl)piperidin-1-yl)ethyl) Morpholine (JPC-119)	191
Figure 3.62	Structure of 4-(3-methoxyphenethyl)-1-(2-(piperidin-1-yl)ethyl) piperidine (JPC-120)	192
Figure 3.63	Structure of 4-(2-(4-(3-methoxyphenethyl)piperidin-1-yl)ethyl) morpholine (JPC-121)	193
Figure 3.64	Structure of 4-(4-methoxyphenethyl)-1-(2-(piperidin-1-yl)ethyl) Piperidine (JPC-122)	194
Figure 3.65	Structure of 4-(2-(4-(4-methoxyphenethyl)piperidin-1-yl)ethyl) Morpholine (JPC-123)	195
Figure 3.66	Structure of 4-(2,4-difluorophenethyl)-1-(2-(piperidin-1-yl)ethyl) piperidine (JPC-124)	196

Figure 3.67	Structure of 4-(2-(4-(2,4-methoxyphenethyl)piperidin-1-yl)ethyl) morpholine (JPC-125)	197
Figure 3.68	Structure of 4-(2-fluoro-4-methoxyphenethyl)-1-(2-(piperidin-1-yl)ethyl)piperidine (JPC-126)	198
Figure 4.1	Structure of 1,4-diphenethylpiperazine (JPC-134)	202
Figure 4.2	Structure of 1,4- <i>bis</i> (2-methoxyphenethyl)piperazine (JPC-135)	203
Figure 4.3	Structure of 1,4- <i>bis</i> (3-methoxyphenethyl)piperazine (JPC-137)	204
Figure 4.4	Structure of 1,4- <i>bis</i> (4-methoxyphenethyl)piperazine (JPC-138)	205
Figure 4.5	Structure of 1,4- <i>bis</i> (2-chlorophenethyl)piperazine (JPC-139)	206
Figure 4.6	Structure of 1,4- <i>bis</i> (4-fluorophenethyl)piperazine (JPC-140)	207
Figure 4.7	Structure of 1-(2-methoxyphenethyl)-4-phenethylpiperazine (JPC-141)	210
Figure 4.8	Structure of 1-(3-methoxyphenethyl)-4-phenethylpiperazine (JPC-142)	211
Figure 4.9	Structure of 1-(4-methoxyphenethyl)-4-phenethylpiperazine (JPC-143)	212
Figure 4.10	Structure of 1-(2-chlorophenethyl)-4-phenethylpiperazine (JPC-144)	213
Figure 4.11	Structure of 1-(4-fluorophenethyl)-4-phenethylpiperazine (JPC-145)	214
Figure 4.12	Structure of 1,4-diphenethyl-1,4-diazepane (JPC-146)	217
Figure 4.13	Structure of 1,4- <i>bis</i> (2-methoxyphenethyl)-1,4-diazepane (JPC-147)	218
Figure 4.14	Structure of 1,4- <i>bis</i> (3-methoxyphenethyl)-1,4-diazepane (JPC-148)	219
Figure 4.15	Structure of 1,4- <i>bis</i> (4-methoxyphenethyl)-1,4-diazepane (JPC-149)	220
Figure 4.16	Structure of 1,4- <i>bis</i> (2-chlorophenethyl)-1,4-diazepane (JPC-150)	221
Figure 4.17	Structure of 1,4- <i>bis</i> (4-fluorophenethyl)-1,4-diazepane (JPC-151)	222
Figure 4.18	Structure of 1,2- <i>bis</i> (4-benzylpiperidin-1-yl)ethane (JPC-132)	225
Figure 4.19	Structure of 1,2- <i>bis</i> (4-phenethylpiperidin-1-yl)ethane (JPC-133)	226

Figure 4.20	Structure of racemic 1-phenethyl-4-(1-phenylpropan-2-yl)piperazine (JPC-176)	229
Figure 4.21	Structure of racemic 1-(1-(4-bromophenyl)propan-2-yl)-4- phenethylpiperazine (JPC-173)	230
Figure 6.1	The most reliable pharmacophore model generated by automatic pharmacophore model generation in the MOE pharmacophore elucidator. The spheres in green represent the hydrophobic features and the blue sphere represents the central cation feature.	273
Figure 6.2	The most reliable pharmacophore model generated by automatic pharmacophore model generation in the MOE pharmacophore elucidator with all active compounds aligned in their best fit to the pharmacophore model.	274
Figure 6.3	Pharmacophoric features derived manually using compound JPC-077. The four pharmacophore features are displayed in red (anionic/acceptor), green (hydrophobic), and purple (cationic/donor) colored spheres.	276
Figure 6.4	Pharmacophoric features derived manually using lobelane. The four pharmacophore features are displayed in green (hydrophobic) and purple (cationic/donor) colored spheres.	277
Figure 6.5	Pharmacophoric features derived manually using the compound lobeline. The four pharmacophore features are displayed in yellow (hydrophobic), green (hydrophobic) and purple (cationic/donor) colored spheres.	278

Chapter 1

Goals of the study and literature review

1.1 Hypotheses

This study involved three central hypotheses. One hypothesis of this work was that structural analogs of lobelane that maintain the 2,6-diphenethylpiperidine scaffold but introduce preferred moieties into the phenyl rings present in lobelane can be designed and synthesized that increase binding affinity for the vesicular monoamine transporter-2 (VMAT2), and that these analogs will increase the functional inhibition of VMAT2 and modify the effects of Methamphetamine (METH) on VMAT2. A second hypothesis of this work is that structural analogs of lobelane in which the 2,6-phenethyl moieties lobelane are changed to 1,4-phenethyl moieties will lead to a further increase in affinity for VMAT2, and also increase potency to functionally inhibit VMAT2 to better modify the effect of METH on VMAT2. A third hypothesis of this work was that introduction of heteroatoms into the piperidine ring of the lobelane scaffold will result in compounds with increased water solubility, while maintaining improved affinity for VMAT2 when compared to lobelane.

1.2 Overall Aims

Psychostimulant abuse has become a severe worldwide problem that has shown no sign of lessening the hold that it has on much of mainstream society. There exists an ongoing need for new therapies and medications that can provide efficacy in the treatment of psychostimulant abuse. METH especially is identified as an addictive and increasingly popular psychostimulant drug, and there are no effective Food and Drug Administration (FDA) approved pharmacological treatments available for the addicts

who wish to quit. This project has been designed to address those people who currently abuse psychostimulants such as METH and need an effective therapy that will help them to break away from their addiction. Within the following dissertation, the design and synthesis of a library of analogs similar to lobelane is described, with alterations designed into the molecules in an attempt to make them more potent at the target protein: VMAT2, and to ultimately provide one or multiple candidates that could ultimately become a treatment for psychostimulant abuse for the part of the population that currently abuses psychostimulants but wishes to quit.

1.3 Methodology to be utilized in this study

- To utilize the established drug discovery process to afford likely candidates for treatment of METH abuse
- To design molecules that can be synthesized that have characteristics that would increase the likelihood of their affinity and functional inhibition of VMAT2
- To use organic chemistry methods to synthesize and purify the previously designed molecules in sufficient quantities as to afford their testing via high throughput affinity assays as well as functional assays
- Once pharmacological assay data has been obtained, to use modern methods of ligand based pharmacophore modeling of the VMAT2 binding/uptake sites that may allow further generations of molecules to be developed that show even further enhanced potency and selectivity at VMAT2

1.4 Overview of Drug Discovery

Drug discovery consists of the combined processes in which new drugs are invented, evaluated for their pharmacological activity and thereby selected for lead molecule identification and subsequent optimization. A flow chart describing the drug design process is shown in figure 1.1. Rational drug design is the inventive process by which new medications are found based on a discovered target of biological origin. Drugs are commonly small organic molecules that either activate or inhibit the normal function of a protein or biomolecule target, and that interaction leads to a therapeutic benefit or advantage in the patient to which the designed drug is given (Drews, J., 2000). Prior scientific investigation reveals the key biological workings and mechanisms of both the normal physiological function of the protein or biomolecule target and also the altered state of function that is caused by a disease or other outside influence, such as drug abuse. The identified mechanisms by which the proteins in question work provide drug discovery scientists areas to manipulate, probe, and take overall advantage of in hopes of developing novel pharmacotherapeutics that can provide a controlled curative medical intervention. As these discovered physiological mechanisms are elucidated, their processes and inner workings are seen as prime potential novel drug targets to the drug discovery scientist. When considered in the most basic way, drug design involves the design and synthesis of small molecules that are complementary to and correspond with the shape and local net charge of the biomolecular target with which they are designed to target and which therefore bind to the biomolecular target being queried. As far as the overall scale of the biomolecular targets, they can truly be as small as molecular in scale, for example peptides, receptors on a protein (for example a binding site on VMAT2), or

they can be comprised of entire cellular and systemic scale processes (Drews, J., 2000). Once the target has been recognized, it is the overriding goal of the drug design/discovery scientists to produce a drug that can be used for further experimental purposes that can lead to therapeutic medical intervention. It is also extremely important that the drug designed for the specific target should be designed in such a way that the lead drug molecule should not affect any other important biomolecules that are deemed off target, as the drug molecule may stray from the designed course of action and produce undesirable side effects in the patient.

There are at least four primary steps involved in the drug discovery process. These are listed here in order of occurrence, but are equally important, and include 1.) overall drug design, 2.) synthesis of the designed drug molecule, 3.) pharmacological assay evaluation of the targeted and desired physiological/biological effect, and 4.) structure-activity relationship (SAR) analysis of the data collected in order to generate the subsequent generation of drug compounds that perform even better than the prior generation. The results of SAR analysis are then mined for a better understanding of the overall biological workings and mechanisms in place. It is key that the next generation of drug candidates be improved in as many ways as possible, if not all aspects, when compared to the first phase of drug synthesis.

There are also numerous important facets that must be taken into consideration when entering the drug design phase. The overall structure of the biomolecular target, the target's location within the body, the distinct environmental surroundings in the area of the target, the overall number of the biomolecular targets in the area of the body to be effected by the drug, the stability of the drug molecule itself, and the potential for binding

to other “off-target” sites that may result in side-effects. These are just a few of the factors that must be considered when designing small molecule candidates that are to be used to produce the desired effect on the targeted biomolecule and therefore on the target’s subsequent function. These complications are a part of what makes drug design a stimulating yet challenging process. Many of these challenges can be overcome or avoided outright by utilization of the knowledge gathered about the nature of the prospective drug target.

In the past, most drugs have been discovered by one of two ways. Either natural products were isolated from plant sources that were known to have medicinal properties (Sneader, 1985) or through unexpected and or unplanned discoveries in the laboratory that reveal that a compound may have the desired effect (Drews, 2000). Drug design and discovery scientists cannot depend on luck to provide the desired drug candidates, therefore the most fruitful traditional method for providing promising drug candidates has been through isolation and purification of compounds from both newly discovered species and traditional medicinal sources such as plants. Currently there is a marked emphasis on more modern strategies for the discovery of new drug entities. The more modern methods consist of rational drug design and high-throughput synthesis and subsequent high-throughput pharmacological assays of small organic molecules (Drews, 2000).

Rational drug design is, at its core, based on a thorough understanding of the biomolecular target and the overall mechanism of the disease or abuse process and uses this knowledge to build molecules that will be likely target specific, with known mechanisms of action and prior knowledge of the likely molecular interactions. In an

ideal world, rational drug design would allow for immediate improved drug activity profiles, with higher potency and selectivity, while still introducing minimal toxicity into the system. This is due to some prior knowledge of the target and the drug molecule libraries that are constructed and customized to interact with the previously known structural target. With all previously acquired knowledge of the location, nature of the target, and the target's function, relatively complicated organic synthetic chemistry methodology can be used to generate families of compounds within the library that are specifically constructed to interact and bind to the known molecular topographic features of the target. Therefore, ideally, rational drug design can, in just one step, improve the overall hit rate of the constructed compound library, while improving the lead compound's potency, selectivity, and toxicity profiles.

With the utilization of high throughput synthesis coupled to high throughput screening methods, the synthesis of a vast number of compounds that can be made in a relatively simple manner, with a low number of synthetic steps, with overall yield balancing between cost of synthesis and the amount necessary for initial and subsequent testing is the focus of synthetic drug discovery chemist. High throughput synthesis coupled to high throughput screening attempts to discover active compounds by applying the muscle of large scale library building medicinal chemistry such as parallel organic chemistry (used in this work), or microwave based chemistry, to generate a large number of compounds that will be screened to afford a small number of candidates. High throughput synthesis must be coupled to high throughput screening methods due to the volume of time that it characteristically takes to manage and test large libraries of compounds (Drews, 2000). One major limitation of high throughput synthesis derives

from the focus on the large number of compounds generated without initial concern for the initial hit rate, drugability factors, or toxicity profile of the compounds generated. The utter volume of compounds generated by the high throughput synthesis can offset the issues of low initial hit rates and drugability factors. The number of initial hits and preliminary drug candidates can allow for the drugability and toxicity profiles to come into play after the preliminary screening. The ultimate and overriding goal of high throughput synthesis and screening is to massively reduce the initial cost of distinguishing high quality lead compounds for the desired pharmacological target of interest. Another desirable aspect of high throughput synthesis coupled to high throughput screening derives from the creativity possible when generating the compound libraries. Often novel compounds that may have otherwise not been investigated are generated when the medicinal chemist is compiling a compound library that lead to unforeseen advancements and allow expedited optimization of novel lead drug candidates.

Pharmacological evaluation processes are required to be developed into a much more streamlined procedure when they are part of a large drug discovery process. Much of the time, in the early testing process, the evaluation of compounds is limited to a single screening effort where compounds are evaluated for one biological effect. Compounds that show promise in the initial screen are then selected and considered as hits. These hit compounds are then subjected to further biological testing (Drews, 2000). This is done to reduce the number of compounds that require further biological consideration in an effort to minimize the testing response time and therefore reducing cost, both in valuable scientist hours and in monetary expense. It is in this manner that compounds deemed

ineffectual can be discarded in favor of compounds that obtain a set level of drug potential. This prevents the time-consuming and expensive in-depth pharmacological tests from being carried out on compounds that hold little promise of becoming lead drugs for the target of interest.

An important aspect of high throughput screening is that the data generated, both of the positive and negative variety of results, from a large library of compounds is invaluable in later compound modification and refinement. This characterization and evaluation of the data generated is known as structure activity relationship (SAR) analysis, and can reveal significant features about both the biomolecular target as well as the interactions that the lead drug compounds has with the target. SAR analysis is a key tool of the drug design/discovery scientist and is best defined as the science of quantifying and evaluating interactions at the molecular level between the drug molecule and the target it is interacting with. Modern SAR efforts require the use of computational resources and programs that use mathematical models of the drug molecule and target. This part of the drug discovery pathway has become more and more complex as it evolves. Entire research groups are dedicated to the “virtual synthesis” and “virtual screening” of molecules and drug targets. These virtual efforts go hand in hand with traditional drug discovery procedures, and are mainly used to support the continuing synthetic efforts to make more and more efficient drug candidates. By taking advantage of the information gleaned from prior synthetic efforts and biological experimentation, computational SAR can uncover the required molecular features of the lead compounds from past generations of synthesis and provide direction and novel ideas for structural chemical modification.

The computational methods for computational SAR differ depending on the circumstances and information at hand. The different methods are described as: 1.) development of ligand-receptor models also known as docking models, and these are used specifically for situations where the receptor or biomolecular target structure has been previously identified through methods such as x-ray crystallography, or 2.) development of a pharmacophore based model, also known as a ligand based model, which consists of SAR modeling based on certain molecular features of the ligand molecules from the constructed compound library, and these are used in situations where less information is known about the drug target or when the critical molecular structural features of the target are not well defined, as in this case with VMAT2. Once the nature of the molecular interactions between the ligand and the target site has been elucidated, SAR based computational models can be further used as a tool to predict new compounds and structural motifs that should be improved in their drug candidate qualities. It is in this manner that SAR leads to advancement in the next generation of compounds synthesized, and in theory should lead to improvements in all aspects of the next lead molecule, including potency and selectivity, and thereby enhance the toxicity and side effect profile as well. It is through these combined efforts that improved pharmacotherapies can be discovered to intervene in the disease/abuse process.

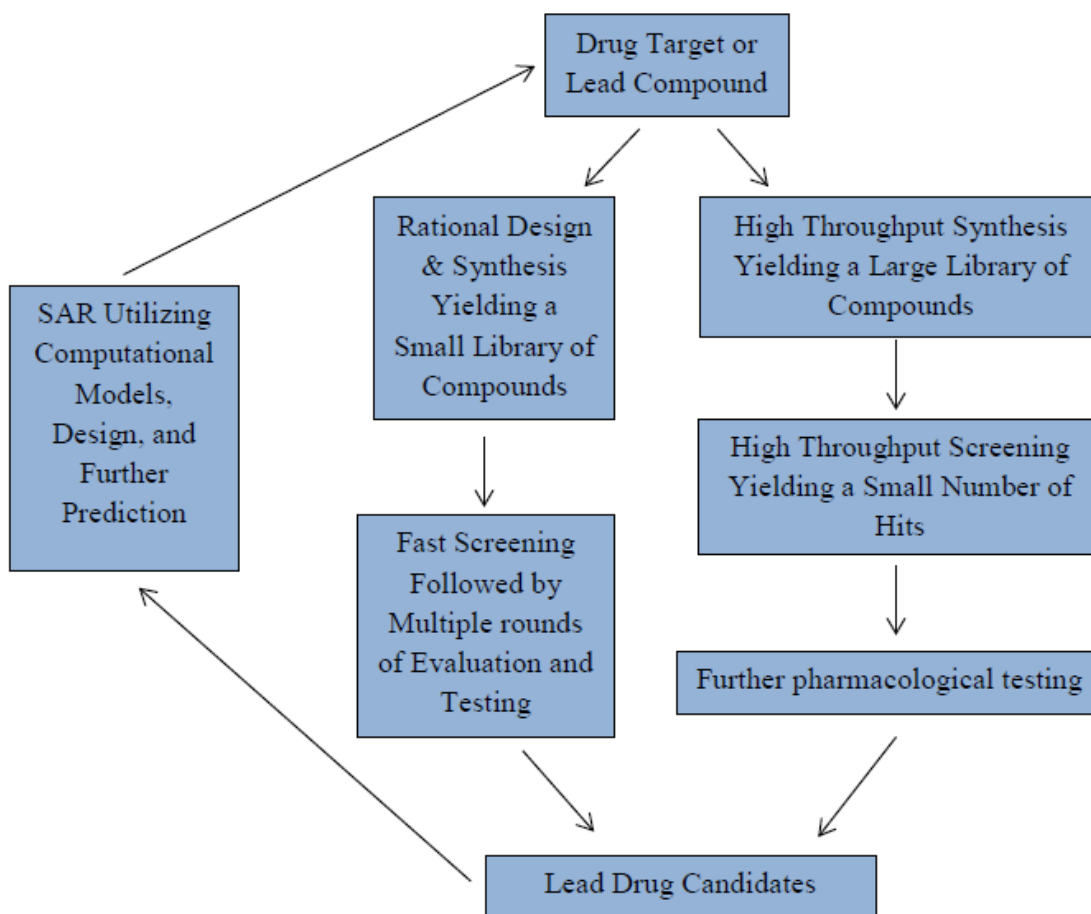


Figure 1.1 Flow chart overview of the drug discovery process. Rational design and synthesis and high throughput synthesis generate the libraries of compounds that are then assayed for activity at the biomolecular target of interest. Each cycle of the flow chart represents a single generation of compounds. SAR analysis can accelerate the cycle time, with each generation yielding a new lead compound that is a more suitable drug candidate.

1.5 Methamphetamine abuse prevalence and limitations of viable therapies and treatments

Psychostimulant abuse has become a severe worldwide problem that has shown no sign of lessening the hold it has on much of mainstream society. METH is an addictive and increasingly popular psychostimulant drug that affects the central nervous system. METH is also known to users of the drug as chalk, ice and crystal. Currently and most significantly there are no effective and accepted pharmacological treatments available for addicts who wish to quit. METH exists in its pure form as a white crystalline powder that is odorless, bitter tasting and readily soluble in water or alcohol, and can be self-administered by several delivery routes. Users of METH have various methods of delivery that include: nasal inhalation, smoking and inhalation into the lungs, or via injection. The oral route of administration has not gained prevalence due to the delayed onset of reward, and the relatively low bioavailability when compared to the injection route. While the preferred method of abusing the drug varies by region, smoking METH is the most common way of introducing the drug into the body. Whatever the route of administration, the users quickly develop a strong desire to continue using it due to the false sense of happiness and well-being associated with METH's use. Users report a rush or feeling of strength and invulnerability as well as a surge of confidence, hyperactivity, and a drastic increase in energy level. As with many stimulants, METH is often abused in a "binge and crash" manner. The "rush" felt by users of the drug is maintained for a very short amount of time, sometimes only minutes, and the users attempt to maintain the high by taking more and more of the drug. It has been documented in many cases that abusers take part in a form of bingeing known on the

street as a “run”, in which the user forgoes food and sleep for several days while continuing to self-administer the drug (National Institute on Drug Abuse, 2013). In 2012, approximately 1.2 million people (about 0.4% of the United States population) reported using METH when asked. While this number is slightly down from previous estimates, METH continues to exhibit regional variability, and abuse is strongest on the West coast and in parts of the Midwest.

METH was developed in the laboratory from the parent drug, amphetamine, and is considered the first purely synthetic drug of abuse. It was developed early in the twentieth century and was used for a time as a nasal decongestant and to relieve bronchial health issues in the form of an inhalable powder. METH was first synthesized from ephedrine in 1893 by Japanese chemist Nagai Nagayoshi and in 1919 the hydrochloride salt was synthesized by the pharmacologist Akira Ogata via a simple reduction of ephedrine utilizing red phosphorus (commonly found in certain types of matches) and iodine (Vermont, 2013). During World War II, METH was used extensively by the Axis forces for its stimulant effects (Defalque, 2011). METH was synthesized in Germany in 1937 and subsequently was commercially released in 1938. It quickly became a popular stimulant for workers in the “German War Machine” and also gained popularity as a recreational drug for young people until the middle of 1941 when it became a controlled substance inside Germany as well. METH continued to be abused by the German armed forces during World War II when it was commonly distributed by commanding officers (occasionally over the objections of the units' physicians) to prevent or treat the fatigue of overworked troops and thus allow them to continue fighting (Defalque, 2011).

METH does differ greatly from amphetamine in that, when used at the same dosage level, it is a much more potent stimulant as it crosses the blood-brain barrier at a greater rate. Due to the presence of the α -methyl group, it has a longer-lasting effect and therefore has greater harmful effects on the central nervous system. METH has been classified as a Schedule II stimulant by the United States Drug Enforcement Administration, and while it can be legally prescribed in a non-refillable prescription, it is rarely prescribed due mainly to the large abuse liability. In the medical field, it can still be prescribed for the treatment of attention deficit hyperactivity disorder, and narcolepsy, and can be utilized as a short-term component of weight loss treatments, albeit at doses much lower than those that are readily abused (National Institute on Drug Abuse, 2013).

It is widely accepted that the vast majority of the METH abused in the United States is illegally manufactured here in the United States or is made in Mexico and trafficked into the United States. One of the major hurdles in combatting the illegal manufacture of METH is due to the ease with which it can be prepared. Multiple synthetic methods exist, and are easily found via search engines on the internet. METH is easily made in small, readily mobile, covert “laboratories” (examples include automobile trunks, rental storage units, hotel rooms and more recently, recreational vehicles). Requiring inexpensive ingredients such as pseudoephedrine and relatively easily to obtain ammonia (a common fertilizer used on farms across the United States), combatting METH at its source is problematic, if not impossible.

Many users of METH liken its effects to that of cocaine, and the two drugs have similar behavioral and physiological effects. There are however, several important differences found in the mechanisms by which they produce the reward or “rush” felt by

their users. One important aspect in which METH and cocaine differ is the duration of time they remain in the body. The half-life (time it takes for the body to remove half of the dose absorbed) of cocaine is roughly one hour; however, the half-life of METH is much longer, approximately 12 hours (NIDA, 2013, Barr et al., 2006). Cocaine is relatively quickly removed from the body and much of the dose is completely metabolized within in the body in a short time; whereas METH has a much longer duration of action, and is more slowly metabolized so that a larger percent of the dose absorbed into the body remains unchanged. METH is metabolized into two primary metabolites, amphetamine and 4-hydroxymethamphetamine (Keueger et al., 2005, Yamada et al., 1984, Cashman et al., 1999) with amphetamine belonging to the same class of stimulant compounds as METH and likely contributes to the pharmacological activity felt by the users, while 4-hydroxymethamphetamine (also known as Pholedrine as used in a clinical setting) does stimulate the sympathetic nervous system, it is not thought to produce the same pharmacological affect as the parent drug, METH (Dasgupta et al., 2012). It is administered in the clinical setting as a topical eye drop form for the purpose of dilating the pupil and can be used to diagnose Horner's syndrome (Bates et al., 1995). Thus, METH remains in the brain longer, and affords prolonged stimulant and rewarding effects. Both cocaine and METH produce their reward through increased levels of dopamine (DA) within the synapse of dopaminergic nerve terminals, but is has been shown in studies in animal model that following administration of METH, the levels of DA are much higher than when animals are administered cocaine (Barr et al., 2006, NIDA, 2013, Wilson et al., 1996). The structural differences between METH and cocaine are shown in Figure 1.2.

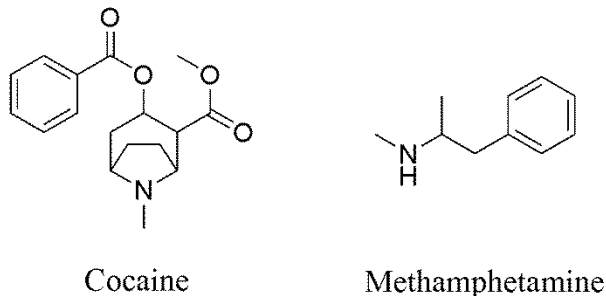
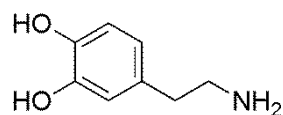


Figure 1.2 Chemical Structures of Cocaine and Methamphetamine

METH has many effects on the human body, and these effects differ greatly depending on the length of time a METH user has been abusing the drug. Short term effects from the use of METH, even at what are considered small doses, include increased activity, increased attention, increased respiration and rapid and or irregular heartbeat, hyperthermia, decreased fatigue, decreased appetite, as well as the main effect that METH users desire: quick onset of the rush and euphoria that leads to abuse. Hyperthermia (increased core body temperature) and convulsions can occur after using METH and are mainly associated with METH overdose, and if not treated by trained medical professionals immediately can result in death (NIDA, 2013). It is widely accepted that the main pleasurable effects the users feel when using METH stem from the release of large concentrations of DA in the brain. DA is a neurotransmitter that involved in motor function (as seen in Parkinson's disease), motivation, and the experience of pleasure. It is also believed that the high levels of DA released by METH causes some of METH's harmful effects on dopaminergic neurons in the brain (Barr, et al., 2006, NIDA, 2013). The structure of DA is shown in Figure 1.3.



Dopamine

Figure 1.3 Structure of the neurotransmitter dopamine (DA)

The long term effects of METH abuse has many more significant detrimental consequences, not the least of which is a strong addiction to the drug. Addiction is defined as the continued repetition of a behavior even though the behavior has strong adverse consequences. Addiction, in the case of METH, is considered a chronic, relapsing disease, that is characterized by an overwhelming compulsion to seek out more of the drug and is also associated with molecular and functional changes within the addict's brain (NIDA, 2013, Wimalasena, 2011). Another long term effect of METH, as is found with many drugs, is that tolerance develops quickly to METH's desired pleasurable effects when METH is taken repeatedly. Chronic users of the drug find themselves needing to take higher and higher doses of the drug, in more frequent administrations, or change the method of administration to achieve the same desired rush and euphoria effect. It is also common for chronic users of METH to be unable to find anything in life that provides them pleasure except for the drug, which in turn reinforces the need for the METH. When users are unable to find or afford the drug, or have looked for treatment in a clinical atmosphere, users experience extreme withdrawal symptoms that include severe depression, fatigue, anxiety, dysphoric mood, increased appetite, increased movement or decreased movement, lack of motivation, sleeplessness or sleepiness, vivid or lucid dreams, violent behavior, memory loss and of course, an intense, overwhelming craving for the drug (Shoptaw, 2009). Chronic abusers of METH

can also display numerous symptoms of psychosis that include paranoia, hallucinations and delusions, an example of which is known by a common name “Meth Bugs” in which the abuser has an intense sensation of insects crawling beneath their skin. Skin sores are apparent in the users of METH experiencing this specific type of delusion, and are the result of the addict scratching and picking at their skin in an attempt to relieve themselves from the insects they imagine to be crawling underneath. These signs of psychosis can last for years after a user has been drug free, and even small amounts of stress can bring about recurrence of METH psychosis events (Barr et al., 2006, Iyo et al., 1997).

These types of symptoms allude to the substantial changes in the brain of abusers of METH. In adults who used METH, magnetic resonance imaging (MRI) has shown enlarged striatal volumes (Chang et al., 2005, Chang et al., 2007). In comparison, children that have been exposed to prenatal METH show smaller striatal structures (Chang, et al., 2007). Positron emission tomography (PET) studies have revealed that several other functional aspects within the striatum have been altered. These include: reduced dopamine transporter (DAT) density and reduced dopamine D(2) receptors in the striatum of METH users (Volkow et al., 2001, McCann, et al., 1998, Sekine et al., 2001, Iyo et al., 2004). PET studies also found lower levels of serotonergic transporter density and vesicular monoamine transporter (VMAT2) density in the striatum, as well as altered brain glucose metabolism (Chang et al., 2007), which were linked with the overall severity of psychiatric symptoms in the limbic and orbitofrontal regions of the brain (Chang et al., 2007).

Some of the changes in the brain of chronic METH abusers do appear to be at least partially reversible. These neuronal recoveries take over a year of abstinence from

METH, and were linked with improvements in both motor skills and verbal memory examinations. Substantial damage to some brain regions of addicts does not show marked signs of recovery even after the one year abstinence time frame, which indicates that some of the METH-induced damage is very long lasting, if not permanent. Further damage to the brain can occur due to an increased risk in METH abusers to experience a stroke, which can cause death or in many cases irreversible and severe damage to the brain (McIntosh, 2006). It has also been shown that as a consequence of METH's effect on the levels of DA in the brain, there is a greater occurrence of Parkinson's disease in a population of abusers of METH (Callaghan, 2011).

The detrimental effects that derive from METH abuse are numerous and severe. The fact that there are currently no effective and accepted pharmacological treatments available for the addicts that wish to quit makes it much more difficult to break the cycle of addiction. Medications have been shown effective for treating other substance abuse disorders, for example three drugs exist to treat alcoholism: disulfiram, naltrexone, and acamprostate. No medications exist that counteract the effect of METH at the biomolecular level or prolong abstinence from or reduce the abuse of METH by an individual that has become addicted to the drug (NIDA, 2013). Currently the most effective treatments for METH addiction are behavioral therapies that include cognitive-behavioral therapy and contingency-management interventions (NIDA, 2013). Results from these behavioral therapies have proven somewhat effective, but treatment depends much on the individual addict's dedication to become drug free. It is clear that a therapeutic treatment for METH abuse is needed, and must be a priority for the future treatment of METH addicts.

1.6 Methamphetamine Mechanism of Action, and the Role of VMAT2

The abuse liability of METH is thought mainly to be a product of an interaction and subsequent alteration of the brain's dopaminergic system. Inside the presynaptic dopaminergic neuron METH interacts with the dopamine transporter (DAT), the vesicular monoamine transporter-2 (VMAT2), and with monoamine oxidase (MAO) (Dwoskin and Crooks, 2002). Signal transduction within monoaminergic neurons is dependent on monoamine neurotransmission in the synaptic region of the neuron. (Henry et al., 1998; Schuldiner et al., 1996; Rudnick, 1998). Monoamine neurotransmission can be apportioned between several principle steps: (1) the initial biosynthesis of monoaminergic neurotransmitters from their biochemical precursors within the cytoplasm, followed by their active sequestration and accumulation into synaptic storage vesicles utilizing an uptake mechanism driven by a proton gradient, (2) the constant biosynthetic conversions within the synaptic vesicles, (3) the release of the monoaminergic neurotransmitter via exocytosis or diffusion, chiefly the former in response to a physiological stimulus, into the synaptic cleft, (4) interaction of the neurotransmitter with the target receptor on the postsynaptic membrane (the distinct act of signal transduction), and (5) the dissociation of the neurotransmitter molecule from the target receptor and the subsequent reuptake into the cytosol of the presynaptic terminal by plasma membrane monoamine transporters, of which the dopamine transporter (DAT) is an example. DAT is a membrane spanning protein that functions to pump DA out of the synapse back into cytosol, from which VMAT2 sequester DA into vesicles for later storage and release. DA reuptake via DAT provides the primary mechanism through which DA is removed from synapses, which effectively terminates the neurotransmitter

signal across the neuron's synaptic cleft, and provides a method for DA to be recycled within the neuron rather than repeatedly biosynthesized when needed. DAT is also referred to as a symporter, or a transporter that is involved in the movement of two or more species of molecules or ions across a membrane. Ions that are transported are generally moving down the concentration gradient, and that in turn allows the molecule being co-transported to be moved against the concentration gradient. In this case, DAT moves DA across the cell membrane by linking the movement of DA to the energetically-favorable movement of sodium ions moving from high to low concentration into the cell. To be specific, the function of DAT requires the sequential binding and co-transport of two positively charged sodium ions and one negatively charged chloride ion in order to transport one molecule of DA. The movement of the sodium and chloride ions is considered facilitated diffusion, while DA is being actively transported into the presynaptic terminal from the synaptic cleft. The overall driving force for DAT-mediated DA reuptake is the ion concentration gradient generated by the plasma membrane sodium/potassium adenosine triphosphatase (Torres, 2003).

Those monoaminergic neurotransmitters not taken back up into the presynaptic terminal are subject to monoamine metabolizing enzymes in the extracellular space, and consequent inactivation, making it necessary for the biosynthesis of the neurotransmitter to be repeated. Metabolizing enzymes are not allocated only within the extracellular space, and the neurotransmitter can be metabolized within the cytosol itself by specific enzymes, of which monoamine oxidase (MAO) is an example. Accordingly, the efficient reuptake of the neurotransmitter from the synaptic cleft via plasma membrane monoamine transporters, and their subsequent sequestration and reaccumulation into

synaptic vesicles via vesicular monoamine transporters (VMATs), is vital to the process of monoamine neurotransmission within monoaminergic synaptic neurons.

Vesicular monoamine transporters are in control of and responsible for the process and mechanism of uptake of cytosolic monoamines into synaptic vesicles found within monoaminergic neurons (Wimalasena, 2011). The VMAT exists as two distinct isoforms: VMAT1 and VMAT2 (Erickson and Eiden, 1993; Erickson et al., 1992; Peter et al., 1994; Zheng et al., 2006). Remarkably, the distribution of the two isoforms of VMAT appears to vary from species to species. In the human, VMAT1 is primarily expressed in neuroendocrine cells which include chromaffin cells of the adrenal medulla, as well as enterochromaffin cells of the intestine (Peter et al., 1995; Weihe et al., 1994; Stern-Bach et al., 1992; Howell et al., 1994). While recent studies have shown that the VMAT1 isoform is also expressed in the brain (Lohoff et al., 2006), the VMAT2 isoform is expressed in sympathetic postganglionic neurons in addition to adult human and monoaminergic neurons of the central nervous system (Erickson et al., 1996; Peter et al., 1995; Weihe et al., 1994; Stern-Bach et al., 1992; Howell et al., 1994) and is considered the main transporter protein involved in the sequestration of cytoplasmic neurotransmitters into vesicles for storage, as well as their subsequent release. The accumulation and storage of the monoamines dopamine (DA), serotonin, norepinephrine, and histamine are essential to the regulatory processes governing the concentrations of these endogenous neurotransmitters available in the cytosol of monoaminergic neurons (Erikson et al., 1996). The active transport of cytosolic monoamines into vesicles for storage, against a high concentration gradient (synaptic vesicles can contain concentrations of monoamines up to 0.5 M), is propelled by the pH gradient across the

plasma membrane in vesicles as well as the electrochemical gradient originating from the H^+ -ATPase in the chromaffin granule membrane (Wimalasena, 2011; Eiden et al., 2004; Schuldiner, 1994; Gasnier, 2000; Henry et al., 1994).

VMAT1 and VMAT2 are glycoproteins with a molecular weight of 40 kDa (Liu et al. 1992; Erickson and Eiden, 1993; Erickson et al., 1992). The origin of VMAT1 and VMAT2 has been determined to be from two distinct genes; however they show high sequence homology (Parsons, 2000; Bravo and Parsons, 2002). The crystallographic structures have not yet been resolved for VMAT1 or VMAT2, the sequences have been analyzed and related proteins suggest that their structure is consistent with transmembrane proteins consisting of 12 transmembrane spanning domains similar in structure to plasma membrane monoamine transporters such as the dopamine transporter (DAT). It is believed that both the *C*-terminus as well as the *N*-terminus of the VMAT series of transporters are located within the cytoplasmic side of the vesicle, and this is supported by studies that show a lack of a cleavable sequence in VMAT2 (Erickson et al., 1992).

Without a crystal structure determination of the crystallized protein, probes into the tertiary structure of the protein are inconclusive at this time. Several studies have investigated structure-function relationships of VMAT at the molecular level. Such studies utilize mutations of specific amino acids and determine what effect such a mutation has on the binding affinity of the protein for a specific substrate or molecule. In what have been called the original studies in this field, (Shirvan et al., 1994) has shown that when His419 (found to be His414 in human VMAT2, and located in the cytoplasmic side of the membrane between TMDs X and XI) is mutated to either Arg or to Cys, the

accumulation of serotonin (5-HT) and DA drop to zero, and a mutation at the same site strongly inhibits the pH-dependent binding of Reserpine (RES) (Wimalasena, 2011). These observations have led to the logical conclusion that His419 (His414 in human VMAT2) plays a primary role in monoamine transport, likely through aiding the initial proton-dependent conformational change of the transporter (Shirvan et al., 1994). It has also been proposed that RES likely binds to this new conformation, and in the mutated form of the transporter, the interaction has been impeded.

Another single-point mutation at the Asp431 (Asp426 in human VMAT2 found in TMD XI) with either Glu or Ser again inhibits 5-HT transport without changing the rate of RES binding to the preferred RES binding site (Steiner-Mordoch et al., 1996). Similar to conclusions have been drawn from His419 mutations, and it has been postulated that Asp431 (Asp426 in human VMAT2) is necessary for the completion of the substrate transport cycle, and the concomitant proposed second conformational change of the protein releasing the amine into the cytosol, in the same proposed model of VMAT function. In contrast, a mutation replacing Asp404 (Asp399 in human VMAT2) in TMD X with Cys or Ser does inhibit 5HT transport and also affects RES binding in rat VMAT1, but when Asp404 (Asp399 in human VMAT2) is replaced with Glu, neither 5HT transport nor the binding of RES and tetrabenazine (TBZ) is altered in a significant manner. The rationale behind this discovery is thought to be the presence of the carboxyl moiety shared in Asp and Glu, but lacking in Ser and Cys. The presence of the carboxyl group appears to play a vital function at site 404 (399 in human VMAT2) if VMAT is to operate normally (Steiner-Mordoch et al., 1996).

Other research has focused on the primary structure of the protein: the VMAT sequence homology itself. Without lengthy mutation studies, it is possible to analyze portions of the amino acid sequence, and, when overlaid, to find the portions of the sequence that have been conserved between VMATs. This simple analysis has shown that four Asp residues in TMD I, VI, X, and XI as well as a Lys residue found in TMD II are conserved among all members of the VMAT protein family. Since they have been dutifully conserved by evolution, it is likely that they have a critical role in both the structure and function of this family of VMAT proteins.

1.7 Methamphetamine Mechanism of Action

Delving deeper into METH's mechanism of action at the dopaminergic neuron, specifically at DAT, VMAT2 and MAO, Figure 1.4 illustrates the numerous effects that METH has at the biomolecular level.

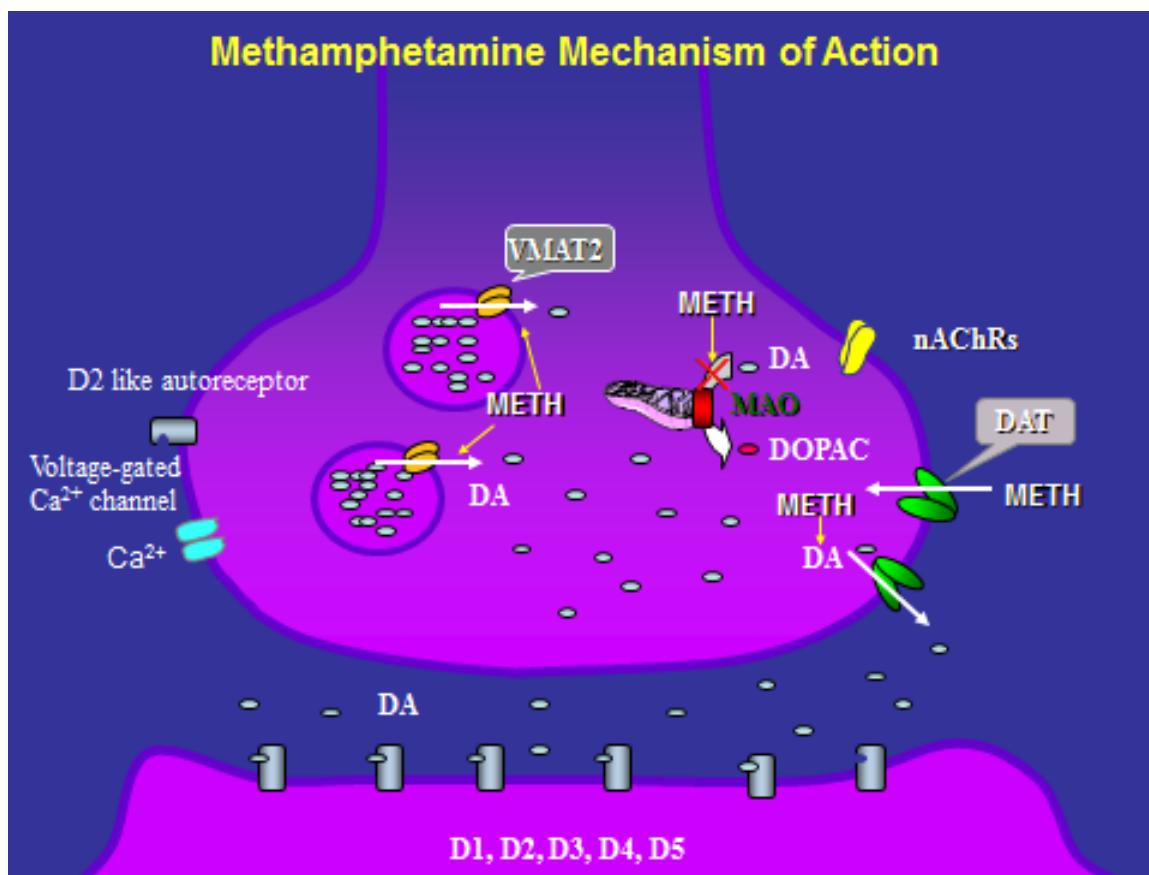


Figure 1.4 Illustration of METH's effects on the dopaminergic neuron

(Adapted from G. Zheng, with permission)

METH effectively reverses the normal function of both DAT and VMAT2, greatly increasing the free DA present in the cytosol and in the extracellular space/synaptic cleft. METH also blocks the normal function of MAO, preventing the metabolism of the DA into 3,4-dihydroxyphenylacetic acid (DOPAC), such that DA may be released from the vesicles into the cytosol and then the extracellular space (Dwoskin & Crooks, 2002).

VMAT2 is a relevant biomolecular target in the search for a viable treatment for METH abuse (Sulzer et al., 2005). METH inhibits DA uptake at VMAT2 and promotes

DA release from vesicles to increase cytosolic DA. Therefore, pharmacological compounds that modulate VMAT2 function or effectively redistribute DA from presynaptic vesicles, in effect limiting vesicular and cytosolic DA available for METH-induced reverse transport, should be suitable candidates for the treatment of METH addiction. Studies utilizing VMAT2 knockout mice demonstrate reduced drug-seeking behavior compared to wild-type rats in locomotor response studies that included an array of drugs, including amphetamine and cocaine (Takahashi et al., 1997; Wang et al., 1997).

1.8 Lobeline Background and Mechanism of Action as a Treatment for METH abuse

(-)-Lobeline (LOB) is the major alkaloidal constituent of *Lobelia inflata*, which is more commonly known as Indian tobacco. The common name “Indian tobacco” most likely originated when Europeans new to the North American continent found that Native Americans smoked the dried leaves of the plants (Millspaugh, 1974). In 1938, Proctor prepared a liquid alkaloid extract from the plant and named it lobeline (Millspaugh, 1974). Since that time, the alkaloidal extract of *Lobelia inflata* has been used medically as an expectorant, emetic, antiasthmatic, antispasmodic, respiratory stimulant, general muscular relaxant, diaphoretic, diuretic, stimulant, and it has even been used to treat narcotic overdose (Crooks et al., 2011). In the *Lobelia inflata* plant, LOB is by far the most abundant alkaloid, as well as the most pharmacologically active constituent of more than twenty related piperidine alkaloids (Felpin et al., 2004). The other alkaloids include, but are not limited to, lobelanine, *nor*-lobelanine, lobelanidine, and *nor*-lobelanidine. The structures of these alkaloids are shown in Figure 1.5.

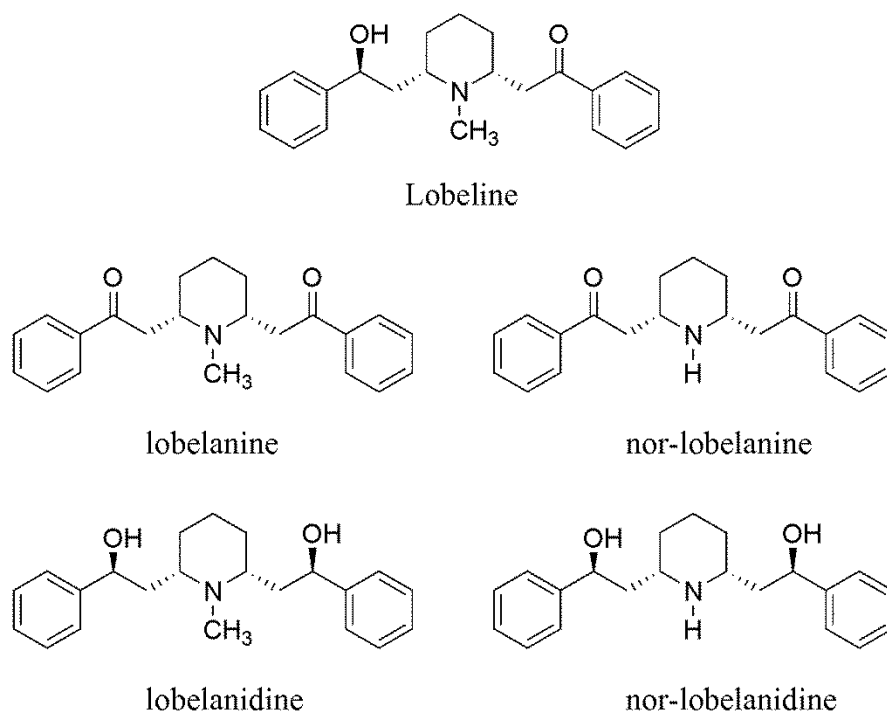


Figure 1.5 The chemical structures of lobeline (LOB) and structurally related alkaloids present in *Lobelia inflata*.

The LOB molecule was purified and isolated from the plant extract and characterized by Wieland (Wieland, 1921; Wieland, et al., 1925; Wieland, et al., 1929). Wieland followed the purification and isolation of LOB with the subsequent total synthesis of the molecule to confirm the structure proposed in 1921 (Wieland, et al., 1929). Following Wieland's total synthesis, multiple synthetic methods for the preparation of LOB have been reported either via racemic methodology (Scheuing, et al., 1929; Schoepf, et al., 1935) or via the asymmetric synthesis approach (Schoepf, et al., 1965; Compere, et al., 1999; Felpin, et al., 2002; Klinger, et al., 2006; Birman et al., 2007).

The free base form of LOB, as well as the sulfate and hydrochloride salt forms of LOB, are stable to degradation in the solid, crystalline form. Conversely, when in solution, LOB quickly undergoes a pH-dependent epimerization at carbon-2 (C2) of the piperidine ring that yields a mixture of *cis*-LOB and *trans*-LOB (Compere, et al., 1999; Felpin, et al., 2002; Zheng, et al., 2004). This epimerization is thought to ensue via the transitory retro-aza Michael addition product. This process is shown in Figure 1.6.

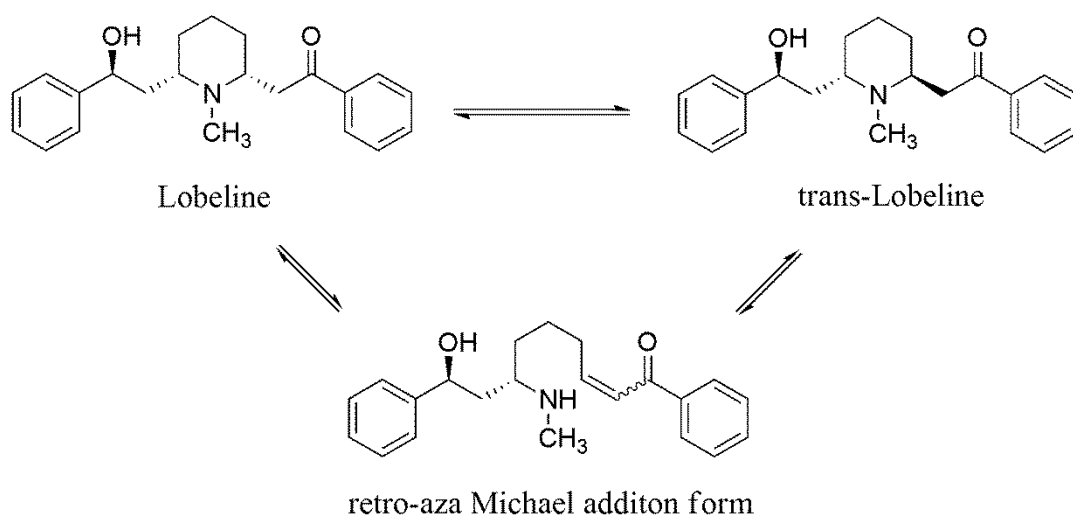


Figure 1.6 Likely process of Lobeline epimerization (adapted from Crooks, et al, 2011)

Compounds possessing a β -aminoketone moiety do have a tendency to exhibit stability issues, such as the epimerization process shown in Figure 1.6, as well as an elimination process, thought to be due to the molecule's predisposition to undergo retro-aza Michael addition processes. Many of the cases where retro-aza Michael addition pathways have been shown to occur happen under acidic conditions (Vazquez, et al., 2001; Davis, et al., 2005), but the epimerization process does not occur in aqueous solutions at a pH of 3.0 (Crooks, et al., 2011). This is quite useful information, and was

used in a “quench” technique (after a set time at a higher pH, an aqueous solution of LOB is decreased to a pH below 3.0, effectively terminating the epimerization process at that point) (Crooks, et al., 2011). The quench technique was used to determine the kinetics of epimerization and high performance liquid chromatography (HPLC) techniques were used to determine the ratio of the two resulting epimers.

When in aqueous solution at room temperature, LOB epimerization proceeds to afford an approximate 65:35 ratio of *cis:trans*, and the equilibrium stops at that point. Interestingly, when in solution in chloroform, the ratio of *cis:trans* is 46:54 in favor of the *trans*-isomer. More surprisingly, the *cis:trans* ratio within human plasma after sublingual administration of LOB sulfate reaches 1:19 in favor of the *trans*-isomer. This is reversed in rat plasma, after the same sublingual administration of LOB sulfate, i.e. the ratio is 16:1 in favor of the *cis* isomer (Crooks et al., 2011).

Several reviews on the pharmacology of LOB exist in the literature (Zheng et al., 2006; Dwoskin et al., 2002; Felpin et al., 2004; McCurdy et al., 2000). LOB is known to display high affinity for nicotinic acetylcholine receptors (nAChRs) (Court et al., 1994; Damaj et al., 1997; Flammia et al., 1999; Miller et al., 2004), and has been shown to have many effects similar to nicotine, such as tachycardia (increased heart rate) and hypertension (increased blood pressure) (Korczyński et al., 1969), analgesia (Damaj et al., 1997), nausea (Bevan et al., 1966), improvement in learning and memory tests (Decker et al., 1993), anxiolytic activity (Brioni et al., 1993), and hyperalgesic actions (Hamann et al., 1994). In consequence, LOB has been characterized as a nicotinic receptor agonist, despite the lack of structural similarities between LOB and nicotine (NIC) and further SAR studies do not support LOB and NIC possessing the same pharmacophore profile

(Barlow et al., 1989). It is not thought that LOB and NIC act via the same mechanism, and this is supported by studies that show LOB and NIC have different effects in both behavioral as well as neurochemical studies (Dwoskin & Crooks, 2002). In contrast to NIC, LOB very marginally supports self-administration in mice (Rasmussen et al., 1998), and does not show support for self-administration of any type in rats (Harrod et al., 2003). As further evidence that LOB and NIC do not act via the same mechanism, chronic administration of LOB does not increase locomotor activity in rats (Fudala et al., 1986; Stolerman et al., 1995). In contrast, LOB diminishes hyperactivity induced by repeated nicotine administration in rats (Miller et al., 2003). More specifically, LOB has been shown to inhibit NIC-evoked [³H]DA overflow from striatal slices from rat brain with an IC₅₀ of approximately 1 μM, which suggests that LOB and NIC not only do not act via the same mechanism, but demonstrate that LOB acts as an antagonist at nAChRs that mediate NIC-evoked DA release (Miller et al., 2000). LOB has also been shown to bind to α4β2 nAChRs with high affinity ($K_i = 4$ nM), while inhibiting NIC-evoked ⁸⁶Rb⁺ (radiolabeled Rubidium) efflux from rat synaptosomes (IC₅₀ = 0.7 μM), which further supports contention that LOB is an antagonist at α4β2 nAChRs (Miller et al., 2000). In addition, LOB has been shown to be an antagonist (IC₅₀ = 8.5 μM) at human α7 nAChR subtypes expressed in *Xenopus* oocytes (Briggs et al., 1998). The combined results from the above studies suggest that LOB is not correctly categorized as a nicotinic receptor agonist, but that it also acts as a potent, albeit nonselective, nAChR antagonist.

Along with the interaction of LOB with nAChRs, LOB also interacts with DAT and VMAT2. LOB inhibits [³H]dihydrotrabenazine (DTBZ) binding to VMAT2 (IC₅₀ = 0.9 μM) and also inhibits [³H]DA uptake into vesicle preparations from rat striatum

($IC_{50} = 0.88 \mu\text{M}$) (Teng et al., 1997; Teng et al., 1998). Although LOB does inhibit [^3H]DA uptake into synaptosomal preparations from rat striatum ($IC_{50} = 80 \mu\text{M}$) via DAT, it is noteworthy that the inhibition of DAT is of nearly 100-fold weaker in comparison to LOB's inhibition of VMAT2 (Teng et al., 1997). When VMAT2 and DAT are both present on a co-expressed cell line, LOB was shown to induce [^3H]DA release through its interaction with VMAT2, rather than through an interaction with DAT (Wilhelm et al., 2004). This finding was also supported with later data showing that LOB caused a decrease in METH-evoked [^3H]DA release (Wilhelm et al., 2008).

Research has shown that LOB inhibits the behavioral consequences of amphetamine as well as the neurochemical effects of the drug in both rats and mice. LOB decreases amphetamine-induced and METH-induced hyperactivity in rats and mice, and has been shown to inhibit amphetamine-evoked DA release from superfused (the process by which the maintenance of the normal metabolic or physiological activity of the tissue by submitting it to a continuous flow of a sustaining medium over the outside) slices from rat brain striatum (Miller et al., 2001). Most importantly, it was found that LOB decreased METH self-administration in rats without acting as a substitute reinforcer (Harrod et al., 2001; Harrod et al., 2003), and this is in accord with LOB not supporting self-administration in rats (Harrod et al., 2000) suggesting a lack of abuse liability for LOB.

Further behavioral studies in rats have demonstrated that LOB has significant potential as a therapeutic agent for treatment of psychostimulant abuse. When administered as a pretreatment, LOB reduces the intensity of METH-induced stereotypy (a repetitive or ritualistic movement, posture, or utterance) in adolescent mice (Tatsuta, et

al., 2006). While, LOB has also been shown to attenuate cocaine self-administration in rats (Neugebauer, et al., 2007), the effects that LOB has on cocaine-induced hyperactivity in rats are multifaceted and intricate. When administered acutely, LOB did not decrease the effect that cocaine had on hyperactivity in rats. Conversely, when LOB was given via repeated administration, it attenuated cocaine-induced hyperactivity in rats. LOB was also found to prevent rats from becoming sensitized to cocaine (Crooks et al, 2011). Phase 1b clinical evaluation of LOB is completed, and found that LOB is safe in human METH addicted subjects (Clinical Trial ID #NCT00439504), and awaits investigation in Phase II trials as a pharmacological treatment for METH abuse (Crooks et al., 2011).

The current understanding of the mechanism by which LOB reduces the rewarding effects desired by abusers of psychostimulants such as amphetamine and METH involves LOB's alteration of DA concentrations within dopaminergic synapses through an interaction with both VMAT2 and DAT (Dwoskin & Crooks, 2002; Crooks et al., 2011). It is more plausible that the interaction between LOB and VMAT2 is more essential to LOB's inhibition of the behavioral effects of psychostimulant abuse, due to LOB having an approximate 100-fold greater affinity for VMAT2 than for DAT (Teng, et al, 1997; Dwoskin & Crooks, 2002; Crooks et al., 2011). A distinct and important difference between LOB and METH is with respect to their actions on MAO. LOB does not interfere with MAO, allowing the increased levels of DA within the cytosol to be oxidized into dihydroxyphenylacetic acid (DOPAC), which does not interact with DA receptors on the postsynaptic terminal (Alachar, et al., 2012). With these data considered, the mechanism of action for LOB in the inhibition of METH induced behavioral effects is due to the interaction of LOB with the DTBZ allosteric binding site

on VMAT2, effectively inhibiting DA uptake into synaptic vesicles while promoting DA release from the same storage vesicles within the presynaptic terminals of the dopaminergic neuron (Dwoskin & Crooks, 2002; Crooks et al., 2011). Through this mechanism, LOB diminishes the total DA pool available for reverse transport through DAT to be released into the synaptic cleft. In that manner, less DA is available for METH to be released from the presynaptic terminal, even if the addict fails to remain drug free during treatment. Figures 1.7 and 1.8 illustrate the mechanism by which LOB attenuates METH's effect at the dopaminergic neuron.

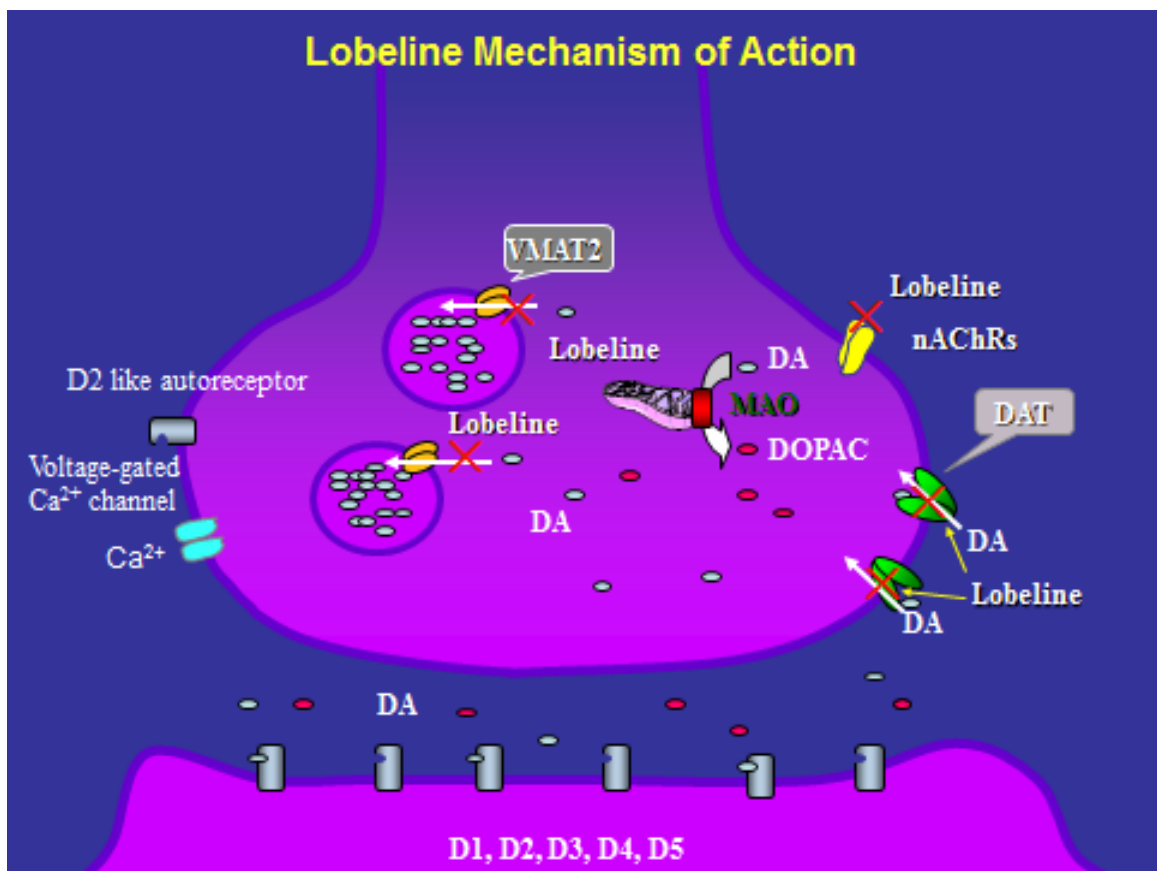


Figure 1.7 Lobeline's Mechanism of Action at the Dopaminergic Neuron

(Adapted from G. Zheng, With Permission)

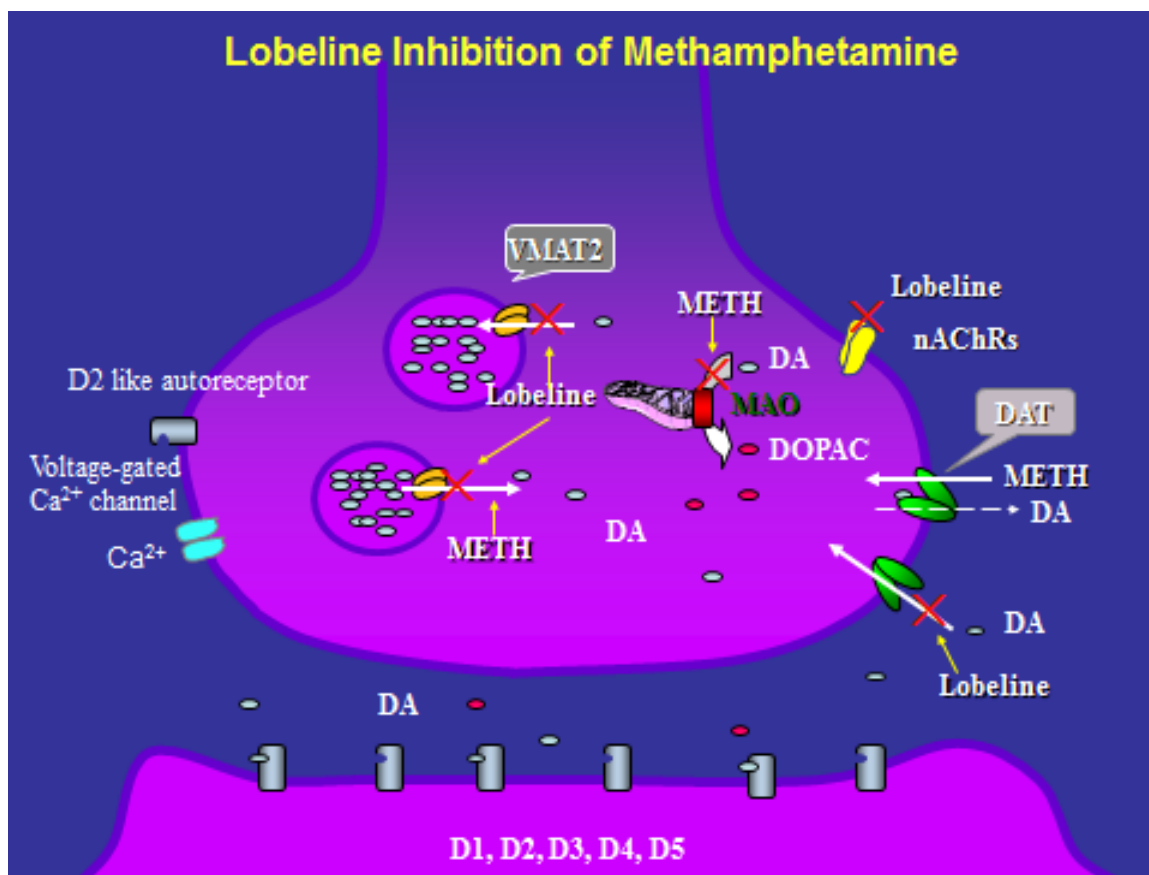


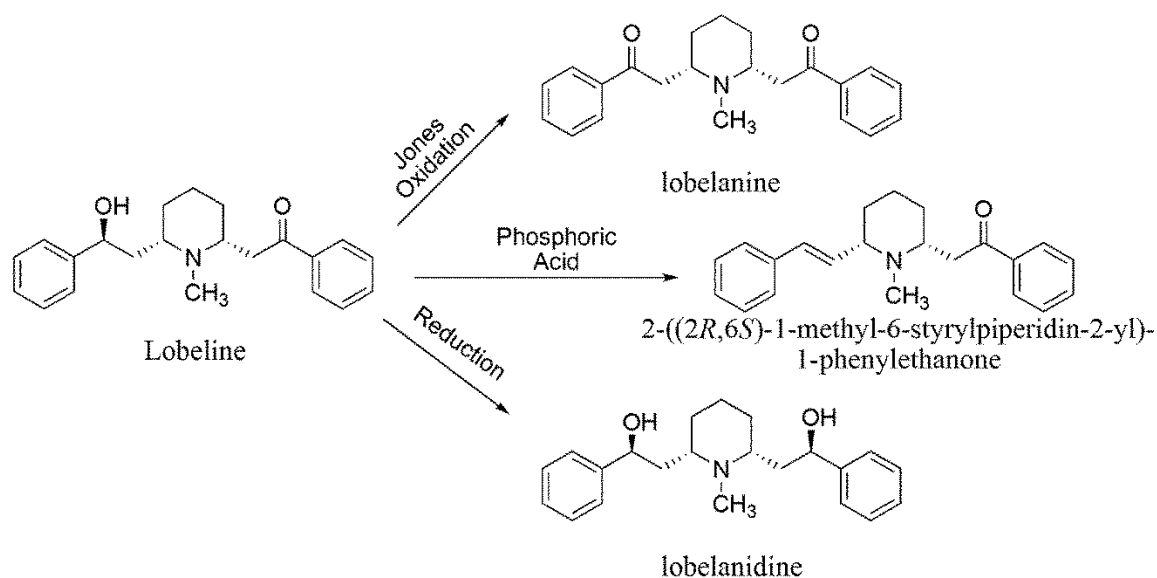
Figure 1.8 Lobeline's inhibition of Methamphetamine

(Adapted from G. Zheng, With Permission)

1.9 Review of Structural Modifications of Lobeline and Lobelane to afford VMAT2 Inhibitors

The discovery of LOB as a VMAT2 ligand presents a novel scaffold and lead molecule with which to explore inhibition of VMAT2, and this section is designed to provide background information regarding previous studies that have been conducted in this area prior to this author's entrance into the area of study. Albeit, LOB is a molecule that has been shown to interact with and bind to a number of biomolecular targets, including nAChRs (Teng et al., 1997; Dwoskin & Crooks, 2002; Miller et al., 2000;

Hillmer et al., 2013; Kaniakova et al., 2011; Hojamat et al., 2010; Horton, et al., 2011), opiate receptors (Hart, et al., 2010; Miller et al., 2007; Miller et al., 2011), VMAT2 (Meyer et al., 2013; Dimatelis, et al., 2012; Horton et al., 2011; Dwoskin & Crooks, 2002; Crooks et al., 2011; Horton et al., 2011; Nickell et al., 2010; Nickell et al., 2011; Hojamat et al., 2010; Varkat et al., 2009; Wilhelm et al., 2004; Wilhelm et al., 2008; Zheng et al., 2005; Zheng et al., 2006; Miller et al., 2004; Teng et al, 1998), and DAT (Smith, et al., 2012; Horton et al, 2011; Nickell et al., 2010; Wilhelm et al, 2008; Li et al., 2007;). Significant quantities of time and effort have been allocated to structurally modifying the LOB molecule to improve potency and selectivity at VMAT2 while limiting the effects at other neurotransmitter transporters and nAChRs (Crooks, et al.; 2011). A review of the studies conducted follows, with a linear timeline of strategies attempted. Some of the first structural modifications attempted on the LOB scaffold where oxidation and dehydration reactions under acidic conditions (these reactions are shown in Scheme 1.1). When LOB is subjected to oxidizing conditions, the alcohol functionality converts to a ketone (Jones oxidation with chromium (VI) oxide) affording lobelanine. Acid-catalyzed (phosphoric acid) degradation of LOB yields the ketoalkene (2-((2*R*, 6*S*)-1-methyl-6-styrylpiperidine-2-yl)-1-phenylethanone), and when LOB is subjected to mild reduction conditions (sodium borohydride) the keto functionality is reduced to afford the stereospecific product, lobelanidine.



Scheme 1.1. Synthetic routes to lobelanine, lobelanidine, and the ketoalkene [2-((2R, 6S)-1-methyl-6-styrylpiperidine-2-yl)-1-phenylethanone

When compared to LOB (data shown in Table 1.1), lobelanine, ketoalkene, and lobelanidine all showed decreased binding to $\alpha 4\beta 2^*$ nAChRs by greater than 100-fold to almost 10000-fold differences. At the $\alpha 7^*$ nAChRs, affinity was only slightly modified, however, a 4-fold increase in affinity for VMAT2 was observed with the ketoalkene analog. The radiolabeled ligands are: [^3H]nicotine ([^3H]NIC), for the nicotine binding site on $\alpha 4\beta 2^*$ nAChRs, [^3H]methyllycaconitine ([^3H]MLA), for the MLA binding site on $\alpha 7^*$ nAChRs, and [^3H]methoxytetrabenazine ([^3H]MTBZ), for the tetrabenazine (TBZ) binding site on VMAT2. From these data, it can be determined that the presence of a second keto moiety in the LOB scaffold causes a decrease in affinity for $\alpha 4\beta 2^*$ and $\alpha 7^*$ nAChRs, but only slightly improved potency at VMAT2. Removal of the alcohol moiety in LOB results in a ketoalkene analog that exhibits moderately decreased affinity for $\alpha 4\beta 2^*$ and $\alpha 7^*$ nAChRs, but exhibits 4-fold increase in affinity for the TBZ binding

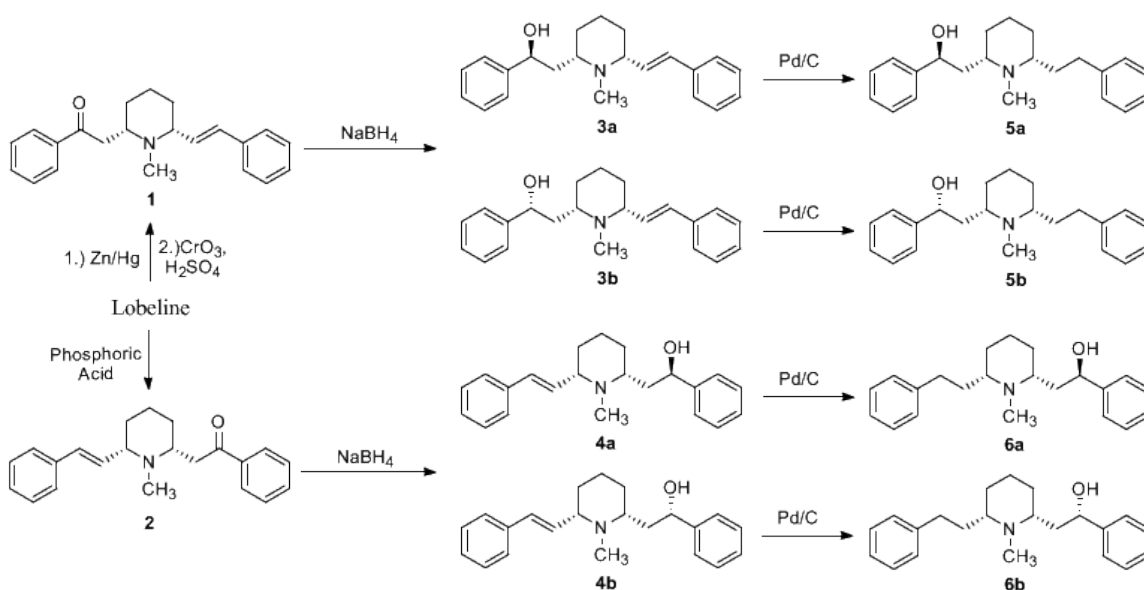
site on VMAT2. Reduction of the keto moiety in LOB yields lobelanidine, which has two alcohol moieties; when compared to LOB, lobelanidine shows less affinity for $\alpha 4\beta 2^*$ nAChRs, slightly greater affinity than LOB at $\alpha 7^*$ nAChRs, and 5-fold less affinity for VMAT2 (Crooks, et al., 2011).

Compound	Values are K_i , μM		
	$[^3\text{H}]\text{NIC}$ Binding $\alpha 4\beta 2^*$ nAChR	$[^3\text{H}]\text{MLA}$ Binding $\alpha 7^*$ nAChR	$[^3\text{H}]\text{MTBZ}$ Binding VMAT2
LOB	0.004	11.6	5.46
lobelanine	37.1	22.7	2.41
ketoalkene (2)	3.10	3.29	25.9
lobelanidine	0.44	34.2	1.35

Table 1.1. Binding affinity of LOB, lobelanine, ketoalkene, and lobelanidine at $\alpha 4\beta 2^*$ and $\alpha 7^*$ nAChRs, and at VMAT2.

With this data in hand, both carboxylate and sulfonate esters of LOB were synthesized. When assayed (data not shown; Hojamat et al., 2010), it was apparent that the above modifications of the alcohol moiety of LOB affected the way in which the compound bound to both $\alpha 4\beta 2^*$ and $\alpha 7^*$ nAChRs, but did not effectively increase affinity at VMAT2.

In order to systematically determine the SAR for the LOB scaffold, the next logical step was to reduce/remove the keto functionality completely from the molecule. To this end, the reactions outlined in Scheme 1.2 were conducted, and the products isolated and characterized (Zheng et al., 2006).



Scheme 1.2. The synthetic route to *des*-keto analogs of lobeline (Adapted from Crooks, et al., 2011)

The aim of the synthetic work described in Scheme 1.2 was to produce a series of LOB analogs with the keto group removed. To afford compound 1, a Clemmenson reduction of LOB was used to remove the carboxyl moiety entirely, and this was followed by oxidation of the alcohol to a ketone, which was then reduced to afford both stereoisomers (R & S) of the corresponding alcohol (3a & 3b), as the synthesis of both stereoisomers was desired. The oxidation step followed by reduction with sodium borohydride was done to make it possible to obtain compounds 3a and 3b as a separable mixture that each be isolated and purified by silica column chromatography. A portion of the total synthesized amount of compounds 3a and 3b were then subjected to hydrogenation conditions (hydrogen gas under pressure with palladium-on-charcoal) to reduce the alkene moiety and afford compounds 5a and 5b, which were also separable via silica column chromatography (Zheng, et al., 2006; Crooks et al., 2011). The process that

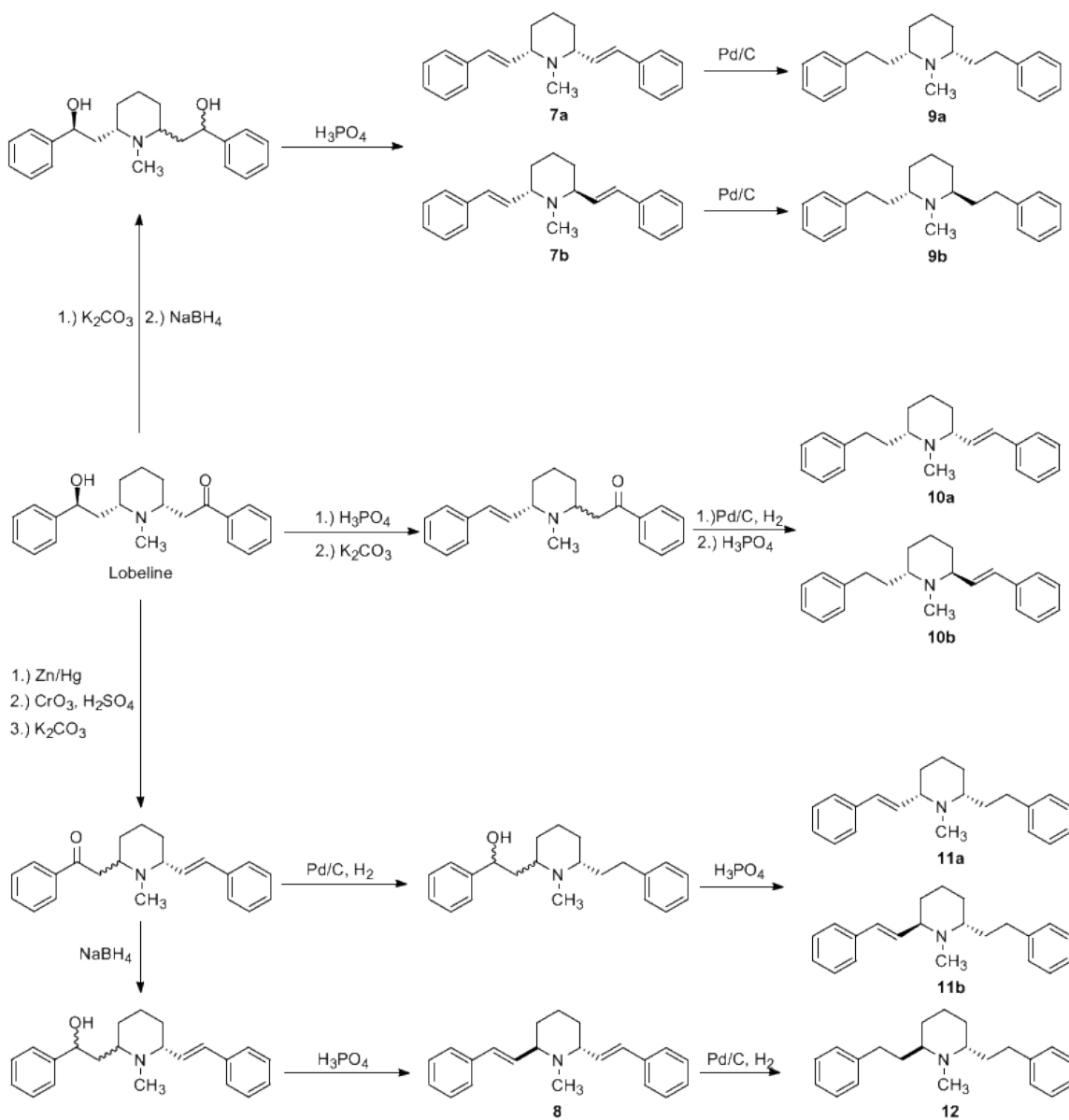
affords the keto alkene (2) is illustrated in Scheme 1.1. Products 4a and 4b, and 6a and 6b can then be synthesized via the same route as used in the preparation of 3a and 3b and 5a and 5b (i.e reduction of the ketone to an alcohol, separation and purification, then hydrogenation followed by silica column separation and purification). The pure compounds were assayed for biological activity as described in Table 1.1, with one exception; rather than using [³H]methoxytetrabenazine ([³H]MTBZ, as the radioligand [³H]dihydroxytetrabenazine ([³H]DTBZ) was used as the radioligand for the tetrabenazine (TBZ) binding site on VMAT2, and the two radioligands have been used interchangeably as ligands for the TBZ site on VMAT2. DTBZ is less susceptible to metabolism in the periphery when compared to TBZ and MTBZ, so in in vivo studies, it is preferred (Welch et al., 2012). The biological data for the eight *des*-keto compounds are shown in Table 1.2 (Zheng et al., 2006). LOB is included as well for comparison.

Compound	Values are $K_i \pm \text{SEM}$, μM		
	$[^3\text{H}]\text{NIC}$ Binding $\alpha 4\beta 2^*$ nAChR	$[^3\text{H}]\text{MLA}$ Binding $\alpha 7^*$ nAChR	$[^3\text{H}]\text{DTBZ}$ Binding VMAT2
LOB	0.004 ± 0.000	6.26 ± 1.30	2.76 ± 0.64
3a	9.75 ± 0.91	>100	6.44 ± 0.54
3b	>100	>100	0.59 ± 0.15
4a	4.19 ± 0.80	1.70 ± 0.32	5.16 ± 0.30
4b	>100	>100	6.06 ± 0.45
5a	1.77 ± 0.61	39.3 ± 12.9	3.09 ± 0.41
5b	>100	>100	6.60 ± 2.96
6a	2.36 ± 0.18	1.21 ± 0.09	1.98 ± 0.31
6b	33.6 ± 8.54	>100	3.01 ± 0.44

Table 1.2. Binding affinity of *des*-keto LOB analogs at $\alpha 4\beta 2^*$ and $\alpha 7^*$ nAChRs, and at VMAT2

The data shown in Table 1.2 clearly show that when the keto functionality is removed from the LOB scaffold, the affinity for $\alpha 4\beta 2^*$ and $\alpha 7^*$ nAChRs dropped considerably (in the order of 25000-fold). Interestingly, when the keto group was removed from the LOB molecule, the resultant analogs had affinities for VMAT2 comparable to that of LOB. To summarize: the keto functionality in LOB appears to be important for maintaining high affinity for nAChRs, but the same cannot be stated with respect to VMAT2. In continuation of the systematic approach for studying the SAR of

the LOB scaffold, the next step was to generate analogs in which all oxygen functionalities in the LOB molecule are removed.



Scheme 1.3. Synthetic routes to LOB analogs in which all oxygen functionalities have been removed (defunctionalized LOB analogs)) (adapted from Crooks et al., 2011).

The synthesis of defunctionalized LOB analogs is described in Scheme 1.3. It is through this synthetic modification of the LOB molecule that a compound of significant

interest was discovered, i.e. lobelane (Zheng, et al., 2005). All synthetic compounds generated in Scheme 1.3 began with LOB as the starting material. The synthesis of compounds 7a and 7b began with epimerization of the LOB starting material by subjecting LOB to a basic solution via addition of potassium carbonate in methanol. This was followed by reduction with sodium borohydride to yield a mixture of lobelanidine isomers (structure of this compound illustrated previously in Scheme 1.1). The mixture of dihydroxyl isomers was treated with phosphoric acid to promote removal of both hydroxyl moieties via dehydration to form C-C double bonds. The resulting mixture of 7a (*meso*-transdiene) and 7b ((-)-*trans*-transdiene) were separable via silica column chromatography to afford pure samples of 7a and 7b. Compounds 7a and 7b were each subjected to hydrogenation conditions (hydrogen gas, palladium-on-carbon) to reduce the double bonds in the phenethylene linkers, yielding 9a (*cis*-lobelane) and 9b ((2S,6S)-1-methyl-2,6-diphenethylpiperidine).

The synthesis of compounds 10a and 10b also began with LOB as the starting material. The same ketoalkene analog synthesized in Scheme 1.1 was again generated, and then subjected to epimerization via potassium carbonate in methanol, yielding a mixture of *cis*-ketoalkene and *trans*-ketoalkene isomers. This mixture was subjected to catalytic hydrogenation conditions, to yield a mixture of four isomers, which was then subjected to acid catalyzed dehydration with phosphoric acid, to yield a separable mixture of the two products, 10a ((2S,6R)-1-methyl-2-phenethyl-6-styrylpiperidine) and 10b ((2S,6S)-1-methyl-2-phenethyl-6-styrylpiperidine).

Starting with LOB, compounds 11a and 11b were prepared via a five step process, with Clemmenson reduction followed by Jones oxidation, compound 1 was generated via

the same methodology as in Scheme 1.2, and then subjected to epimerization with potassium carbonate in methanol. This mixture of epimers then underwent catalytic hydrogenation to yield a mixture of four isomers, which was then subjected to acid catalyzed dehydration to yield a mixture of 11a ((2R,6S)-1-methyl-2-phenethyl-6-styrylpiperidine and 11b ((2R,6R)-1-methyl-2-phenethyl-6-styrylpiperidine) which were separable via silica column chromatography to yield the pure samples of each compound.

The synthesis of compounds 8 and 12 in Scheme 1.3 also began with LOB, and followed the same synthetic route, beginning with epimerization of the LOB starting material by subjecting LOB to a basic solution via addition of potassium carbonate in methanol. This was followed by reduction with sodium borohydride to yield a mixture of lobelanidine isomers (structure of this compound illustrated previously in Scheme 1.1), at which point the mixture of epimers was then subjected to reduction via sodium borohydride, then to acid catalyzed dehydration of the alcohol with phosphoric acid to yield a mixture of compounds 7a and 8. The isomeric mixture of compounds 7a and 8 was then purified via silica column chromatography to yield two pure compounds: the previously synthesized 7a and 8 ((2R,6R)-1-methyl-2,6-distyrylpiperidine). When analog 8 was subjected to catalytic hydrogenation, compound 12 ((2R,6R)-1-methyl-2,6-diphenethylpiperidine) was obtained.

The results for the ten *des*-oxygen compounds are shown in Table 1.3 (Zheng et al., 2005). LOB is included as well for easy comparison. Compound 7a (*meso*-transdiene; MTD), is an unsaturated, fully deoxygenated analog of LOB, and was found to have little to no affinity at either $\alpha 4\beta 2^*$ (11.6 μ M) or $\alpha 7^*$ (>100 μ M) nAChRs, but had comparable affinity for VMAT2 as LOB (i.e. less than 4-fold difference).

Compound	Values are $K_i \pm \text{SEM}$, μM		
	[³ H]NIC Binding $\alpha 4\beta 2^*$ nAChR	[³ H]MLA Binding $\alpha 7^*$ nAChR	[³ H]DTBZ Binding VMAT2
LOB	0.004 \pm 0.000	6.26 \pm 1.30	2.76 \pm 0.64
7a	11.6 \pm 2.01	>100	9.88 \pm 2.22
7b	>100	>100	19.4 \pm 1.25
8	>100	>100	7.09 \pm 2.42
9a (lobelane)	14.9 \pm 1.67	26.0 \pm 6.57	0.97 \pm 0.19
9b	>100	25.3 \pm 4.27	5.32 \pm 0.45
10a	>100	>100	2.50 \pm 0.23
10b	>100	55.1 \pm 13.3	5.27 \pm 1.32
11a	>100	>100	2.67 \pm 0.56
11b	>100	25.2 \pm 3.00	>100
12	>100	40.0 \pm 14.1	6.46 \pm 1.70

Table 1.3. Binding affinity of “*des-oxygen*” LOB analogs at $\alpha 4\beta 2^*$ & $\alpha 7^*$ nAChRs, and at VMAT2

Compounds 7b [(-)-*trans-trans*diene] and 8, are the two *trans*-enantiomers of MTD, and both showed no affinity for either $\alpha 4\beta 2^*$ (>100 μM) or $\alpha 7^*$ (>100 μM) nAChRs, so they were more selective than LOB for VMAT2, but were less potent than LOB at VMAT2 with affinities of 19.4 and 7.09 μM respectively. When MTD and the two enantiomers of the *trans-trans*diene were subjected to hydrogenation, two compounds were generated, viz.: 9a (*cis*-lobelane) and 9b (*trans*-lobelane). The *cis*-

isomer of lobelane (9a) (hereafter referred to as simply lobelane) showed selectivity for VMAT2, with approximately 4000-fold less affinity for $\alpha 4\beta 2^*$ (14.9 μM) or $\alpha 7^*$ (26.0 μM) nAChRs, and had the greatest affinity of any of the compounds in Table 3 for VMAT2 (0.97 μM). The *trans*-isomer of lobelane, 9b, showed similar selectivity for VMAT2, but was not quite as potent (5.32 μM).

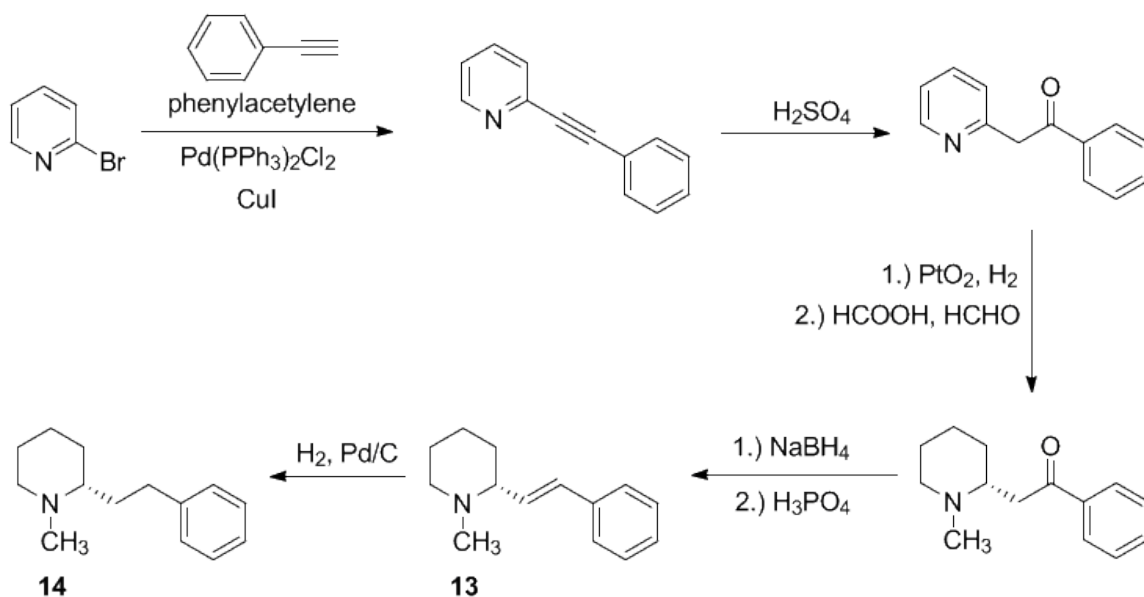
Nearly all the other defunctionalized analogs of LOB followed suit, with one exception: compounds 10a, 10b, 11a and 11b possess little to no affinity at $\alpha 4\beta 2^*$ or $\alpha 7^*$ nAChRs, and 10a, 10b, and 11a have similar affinities for VMAT2 as does LOB, however, 11b, the (2R,6R)-1-methyl-2-phenethyl-6-styrylpiperidine compound lacked affinity for VMAT2 (>100 μM). The TBZ binding site on VMAT2 was unable to distinguish between the (2S,6R) stereochemistry of compound 10a, the (2S,6S) stereochemistry of compound 10b, and the (2R,6S) stereochemistry of compound 11a, but was not as efficient at recognizing the (2R,6R) stereochemistry of compound 11b, and it is noteworthy that VMAT2 could differentiate between these subtle changes in stereochemistry (Zheng et al., 2005; Crooks et al., 2011).

Most importantly, for studies focused on targeting VMAT2, a new lead compound was identified, lobelane (9a), that was specific for VMAT2 over $\alpha 4\beta 2^*$ or $\alpha 7^*$ nAChRs, and had greater affinity for the TBZ binding site of VMAT2 than LOB. At this point, emphasis shifted from structural modification of LOB to structural modification of the defunctionalized analog, lobelane. The second iteration of the SAR flowchart cycle had begun with lobelane, the second generation lead compound.

The systematic approach to the alteration of the lobelane scaffold progressed in a similar manner to the approach taken with LOB modification; however, a study of greater

depth was undertaken for each remaining functionality of the lobelane scaffold. First, synthesis was undertaken that effectively fragmented the lobelane scaffold to better determine which portion(s) of the molecule were most important in binding to the TBZ site on VMAT2. Second, the phenyl rings in the lobelane scaffold were modified, either by addition of aromatic substituents, or by replacing the phenyl moieties with other aromatic ring systems. Third, the lobelane scaffold was isomerized with respect to the location and stereochemistry of the 2,6-substituents on the central piperidine ring. Fourth, the length of the ethylene linkers between the central piperidine ring and the phenyl groups were varied. Fifth, the *N*-methyl substituent of the lobelane molecule was modified, either by increasing the length of the methyl group, or by introducing a variety of other substituents with greater organic functionality and polarity. Sixth, the central piperidine ring in lobelane was altered by replacement with other heterocycles, e.g. a piperazino ring or a five membered pyrrolidine ring, as well as with conformationally restricted ring systems, such as the tropane ring. Each of these structural modifications provided important information and the vast amount of work completed has been reviewed (Crooks et al., 2011).

Structural fragmentation of the lobelane scaffold was undertaken to determine if the complete lobelane scaffold was necessary to maintain potent binding to the TBZ site on VMAT2. The synthetic methodology used in generating fragmented lobelane analogs is shown in Scheme 1.4.



Scheme 1.4. Synthetic methods used in generating fragmented lobelane analogs (Zheng et al., 2005; Crooks et al., 2011).

The methodology used to generate analogs 13 and 14 in Scheme 4 involved seven steps. Beginning with 2-bromopyridine, Sonogashira coupling chemistry was used to couple phenylacetylene to 2-bromopyridine to generate 2-(phenylethynyl)pyridine, which was further modified under acidic conditions (sulfuric acid/reflux) to the ketone to yield 1-phenyl-2-(pyridin-2-yl)ethanone. The keto compound was hydrogenated with Adam's catalyst (platinum (IV) oxide) to reduce the pyridine ring to a piperidine ring, and set the stereochemistry of the phenethyl linker, yielding the *nor*-(*R*)-1-phenyl-2-(piperidin-2-yl)ethanone. *N*-methylation via formaldehyde addition afforded the *N*-methyl analog, (*R*)-2-(1-methylpiperidin-2-yl)-1-phenylethanone. The keto functionality was then reduced with sodium borohydride and dehydrated under acidic conditions with phosphoric acid to produce compound 13, (*R,E*)-1-methyl-2-styrylpiperidine. A portion

of this product was again subjected, in the final step, to hydrogenation conditions (hydrogen gas, palladium-on-carbon) to yield the lobelane fragment analog compound 14, (*R*)-1-methyl-2-phenethylpiperidine (Zheng, et al., 2005).

Four acyclic compounds in which the piperidine ring was removed in favor of acyclic analogs were also prepared as lobelane fragment analogs. Two compounds, 15 ((*S*)-*N*-methyl-1,9-diphenylnonan-3-amine) and 16 ((*R*)-*N*-methyl-1,9-diphenylnonan-3-amine) were fortuitously formed as side products and separated via silica column chromatography from the hydrogenation of the previously discussed compounds 7b ((-)-*trans*-transdiene) and compound 8 respectively, formed via ring opening during the hydrogenation process. Two compounds, 17 ((*E*)-*N*-cinnamyl-*N*-methyl-3-phenylprop-2-en-1-amine) (Blickle et al., 1939) and 18 (*N*-methyl-3-phenyl-*N*-(3-phenylpropyl)propan-1-amine) (Stuhmer et al., 1954) were synthesized via established methods. These four acyclic analogs of lobelane are shown in Figure 1.9.

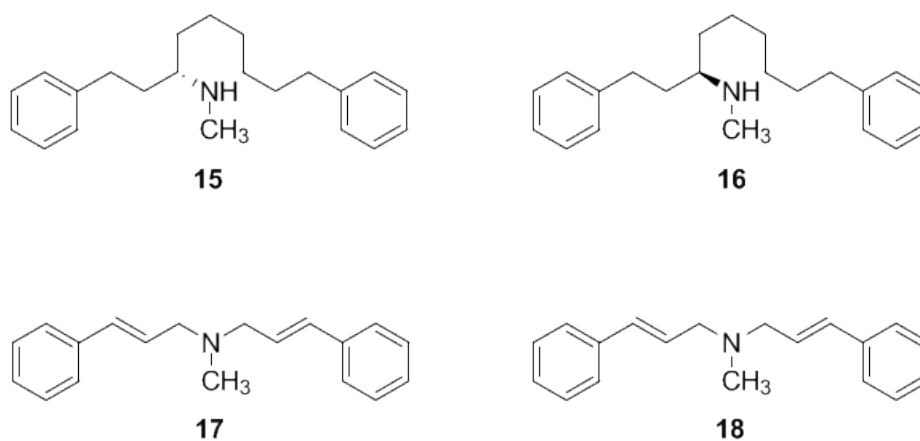


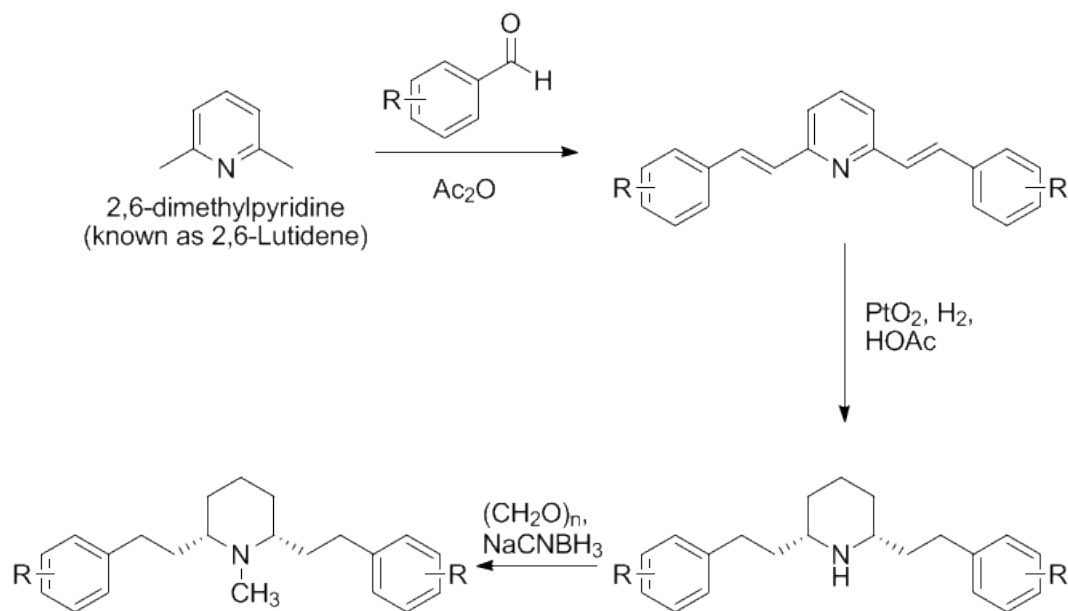
Figure 1.9. Structures of acyclic fragmented lobelane analogs

The biological results for the six fragmented lobelane analogs are shown in Table 1.4 (Zheng et al., 2005). Compound 13, the fragmented MTD analog, (*R,E*)-1-methyl-2-styrylpiperidine, had no affinity for any of the receptors tested ($IC_{50} > 100 \mu M$). Compound 14, the lobelane fragment analog, (*R*)-1-methyl-2-phenethylpiperidine, showed only slight affinity for the $\alpha 4\beta 2^*$ nAChR, but had no affinity for the $\alpha 7^*$ nAChR, and surprisingly had no affinity at VMAT2 ($IC_{50} > 100 \mu M$). These data indicate that both side chain linkers are required for the lobelane scaffold to bind to VMAT2. The acyclic fragments of lobelane, compounds 15, 16, 17, and 18 had no affinity for either $\alpha 4\beta 2^*$ or $\alpha 7^*$ nAChRs, but had similar binding affinity as LOB at VMAT2, but slightly decreased affinity for VMAT2 when compared to lobelane. The combined data from Table 1.4 indicate that the amine moiety and the two phenethyl moieties are required for binding to the TBZ site on VMAT2, and in the case of the acyclic analogs, the data suggests that an intact piperidine ring may be needed to maintain affinity for the TBZ site on VMAT2.

Compound	Values are $K_i \pm \text{SEM}$, μM		
	[³ H]NIC Binding $\alpha 4\beta 2^*$ nAChR	[³ H]MLA Binding $\alpha 7^*$ nAChR	[³ H]DTBZ Binding VMAT2
LOB	0.004 ± 0.000	6.26 ± 1.30	2.76 ± 0.64
lobelane	14.9 ± 1.67	26.0 ± 6.57	0.97 ± 0.19
13	>100	>100	>100
14	4.52 ± 0.58	>100	>100
15	>100	>100	5.21 ± 1.23
16	>100	>100	3.96 ± 0.80
17	>100	>100	2.37 ± 0.55
18	>100	>100	3.07 ± 1.72

Table 1.4 Binding affinity of acyclic fragmented lobelane analogs
at $\alpha 4\beta 2^*$ & $\alpha 7^*$ nAChRs, and at VMAT2

The next phase of modification of the lobelane scaffold involved alteration of the phenyl rings, either by addition of aromatic substituents, or by replacing the phenyl rings with other aromatic ring systems into those positions of the scaffold. Scheme 1.5 outlines the chemistry necessary for the synthesis of symmetrically substituted phenyl ring modification of the lobelane scaffold.



Scheme 1.5. Synthetic methods for generation of symmetrically substituted phenyl ring analogs of lobelane (Zheng et al., 2005).

Synthesis of symmetrical substituted phenyl ring analogs of lobelane utilizes 2,6-methylpyridine as a starting material, which undergoes a condensation type reaction with substituted aryl aldehydes when refluxed in acetic anhydride to yield the corresponding 2,6-distyrylpyridine with a variety of substituted phenyl rings. The phenyl substituted 2,6-distyrylpyridine compounds are then subjected to hydrogenation conditions with Adam's catalyst (platinum(IV)oxide) to reduce the central pyridine ring to a piperidine ring (affording 2,6-*cis*-stereochemistry) and the two alkene moieties to alkanes. At this stage of the synthesis, phenyl substituted (2*S*,6*R*)-2,6-diphenethylpiperidine is generated. If all positions on the phenyl rings are hydrogen rather than other functionalities, the compound generated is *nor*-lobelane, (des-methyl lobelane). To introduce the *N*-methyl group present in Lobeline and lobelane, the phenyl substituted (2*S*,6*R*)-2,6-diphenethylpiperidine intermediates were exposed to reductive amination conditions with

paraformaldehyde and sodium cyanoborohydride in methanol to yield the corresponding phenyl substituted (2S,6R)-1-methyl-2,6-diphenethylpiperidine scaffold. Symmetrical phenyl substituted analogs of both lobelane and *nor*-lobelane were generated via this methodology, and their structures and binding affinities for $\alpha 4\beta 2^*$ & $\alpha 7^*$ nAChRs, and for VMAT2 are included in Table 1.5.

Compound Identifier	Compound Structure	Values are $K_i \pm \text{SEM}$, μM			
		[³ H]NIC Binding $\alpha 4\beta 2^*$ nAChR	[³ H]MLA Binding $\alpha 7^*$ nAChR	[³ H]DTBZ Binding VMAT2	VMAT2 [³ H]DA Uptake
LOB		0.004 \pm 0.000	6.26 \pm 1.30	2.76 \pm 0.64	0.47 \pm 0.045
lobelane		14.9 \pm 1.67	26.0 \pm 6.57	0.97 \pm 0.19	0.045 \pm 0.002
<i>Nor</i> -lobelane		>100	>100	2.31 \pm 0.21	0.043 \pm 0.008
19a		>100	>100	1.60 \pm 0.10	0.042 \pm 0.011
19b		>100	>100	1.07 \pm 0.07	0.057 \pm 0.010

Table 1.5 (continued)

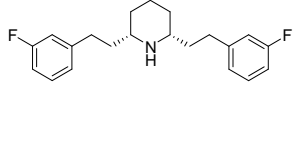
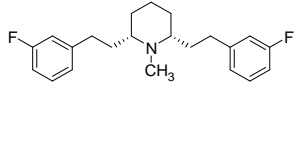
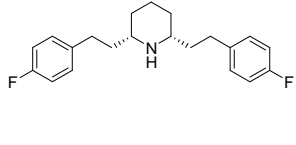
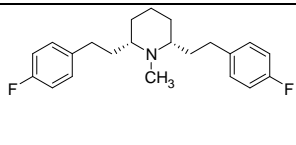
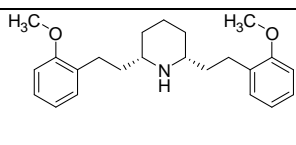
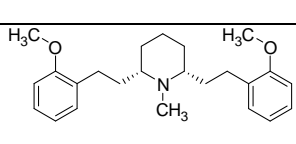
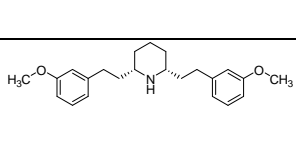
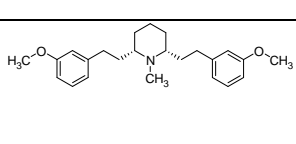
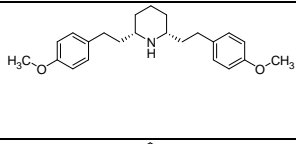
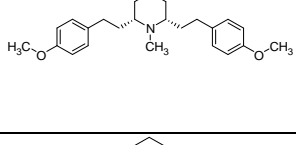
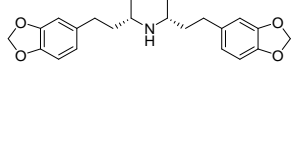
20a		>100	49.2 ± 21.3	1.60 ± 0.08	0.036 ± 0.006
20b		>100	16.6 ± 3.47	0.57 ± 0.07	0.093 ± 0.018
21a		>100	>100	1.25 ± 0.08	0.021 ± 0.004
21b		>100	>100	0.98 ± 0.31	0.030 ± 0.008
22a		>100	>100	1.87 ± 0.19	0.026 ± 0.004
22b		>100	29.7 ± 7.73	0.58 ± 0.04	0.026 ± 0.004
23a		>100	>100	1.67 ± 0.07	0.040 ± 0.006
23b		>100	25.1 ± 2.23	0.43 ± 0.03	0.030 ± 0.005
24a		>100	>100	3.32 ± 0.82	0.013 ± 0.003
24b		>100	>100	1.73 ± 0.20	0.015 ± 0.002
25a		>100	>100	2.34 ± 0.16	0.191 ± 0.146

Table 1.5 (continued)

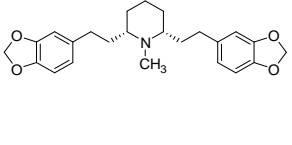
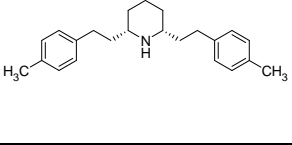
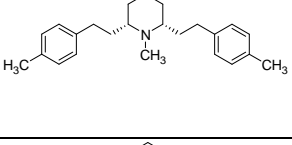
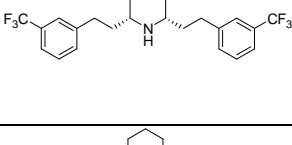
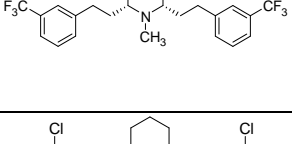
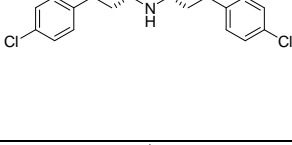
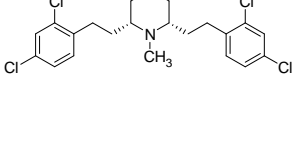
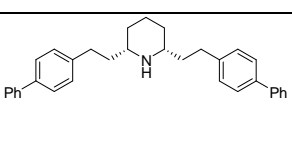
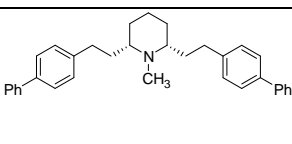
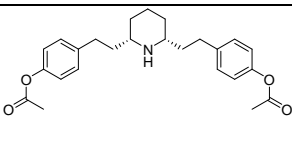
25b		>100	18.2 ± 6.87	0.52 ± 0.25	0.043 ± 0.011
26a		>100	>100	3.23 ± 0.10	0.59 ± 0.010
26b		>100	>100	4.36 ± 0.18	0.154 ± 0.008
27a		>100	>100	9.90 ± 2.01	0.836 ± 0.361
27b		>100	>100	1.51 ± 0.07	0.19 ± 0.015
28a		>100	>100	1.32 ± 0.18	0.182 ± 0.005
28b		>100	>100	1.04 ± 0.06	0.016 ± 0.005
29a		>100	>100	>100	0.127 ± 0.034
29b		>100	>100	10.7 ± 6.60	0.034 ± 0.008
30		>100	>100	5.96 ± 1.76	0.247 ± 0.042

Table 1.5 (continued)

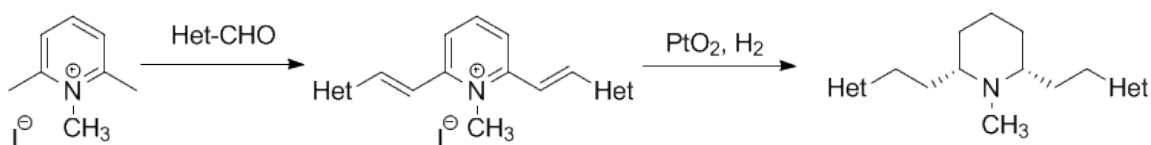
31		>100	>100	5.26 ± 0.47	0.047 ± 0.017
32a		>100	>100	4.68 ± 0.70	*
32b		>100	>100	0.63 ± 0.16	*
33a		>100	>100	>100	*
33b		>100	>100	2.03 ± 0.45	*

Table 1.5 Structures of substituted phenyl analogs of lobelane and assay data from [³H]NIC Binding $\alpha 4\beta 2^*$ nAChR, [³H]MLA Binding $\alpha 7^*$ nAChR, [³H]DTBZ Binding VMAT2, and VMAT2 [³H]DA Uptake

Twenty eight lobelane analogs with a variety of substitutions in the phenyl rings were synthesized in this series. All of the compounds within this series had either lower or comparable affinities at $\alpha 4\beta 2^*$ & $\alpha 7^*$ nAChRs when compared to lobelane, with the exception of compounds 29a ((2*S*,6*R*)-2,6-*bis*(2-(biphenyl-4-yl)ethyl)piperidine) and 33a ((2*S*,6*R*)-2,6-*bis*(2-(naphthalen-2-yl)ethyl)piperidine), which were both *nor*-analogs with bulky biphenyl (compound 29a) and 2-naphthyl (compound 33a) analogs, all compounds had comparable affinity to lobelane at VMAT2. Analogs 20b ((2*S*,6*R*)-2,6-*bis*(3-fluorophenethyl)-1-methylpiperidine), 22b ((2*S*,6*R*)-2,6-*bis*(2-methoxyphenethyl)-1-

methylpiperidine), and 23b ((2*S*,6*R*)-2,6-*bis*(3-methoxyphenethyl)-1-methylpiperidine) had the highest affinity for VMAT2 with K_i values of 0.57, 0.58, and 0.43 μM , respectively. Also the *N*-methyl analogs consistently exhibited higher affinity at VMAT2 when compared to their corresponding *nor*-counterparts. All in all, modification of the phenyl rings in the lobelane scaffold via addition of a variety of aromatic substituents that were either electron withdrawing, electron donating, or replacement of the phenyl rings with more bulky aromatic moieties was successful in further reducing the affinity of these analogs at $\alpha 4\beta 2^*$ & $\alpha 7^*$ nAChRs, while maintaining and perhaps slightly improving affinity for the TBZ binding site on VMAT2. The compounds that had the greatest affinity for the TBZ binding site on VMAT2 and their corresponding aromatic substituents were 19b (2-fluoro substituted phenyl), 20b (3-fluoro substituted phenyl), 21b (4-fluoro substituted phenyl), 22b (2-methoxy substituted phenyl), 23b (3-methoxy substituted phenyl), 24b (4-methoxy substituted phenyl), 25b (3,4-methylenedioxy substituted phenyl), and 28b (2,4-dichloro substituted phenyl), each of which possessed affinity for the TBZ site on VMAT2 of approximately 1 μM and each possessed a *N*-methyl moiety. This subgroup of eight compounds also had correspondingly potent values in the VMAT2 [^3H]DA Uptake assay with values ranging from 15-93 nM. It cannot be overstated that the importance of the VMAT2 [^3H]DA Uptake assay is much greater than that of the TBZ site binding assay. The TBZ binding assay does determine the affinity of the ligand in question for the TBZ binding site on VMAT2, but the VMAT2 [^3H]DA Uptake assay accurately determines the effect of the ligand on the functioning vesicles' ability to sequester DA into the vesicle for storage and later use/release. More information on these two assays will be addressed in Chapter 5.

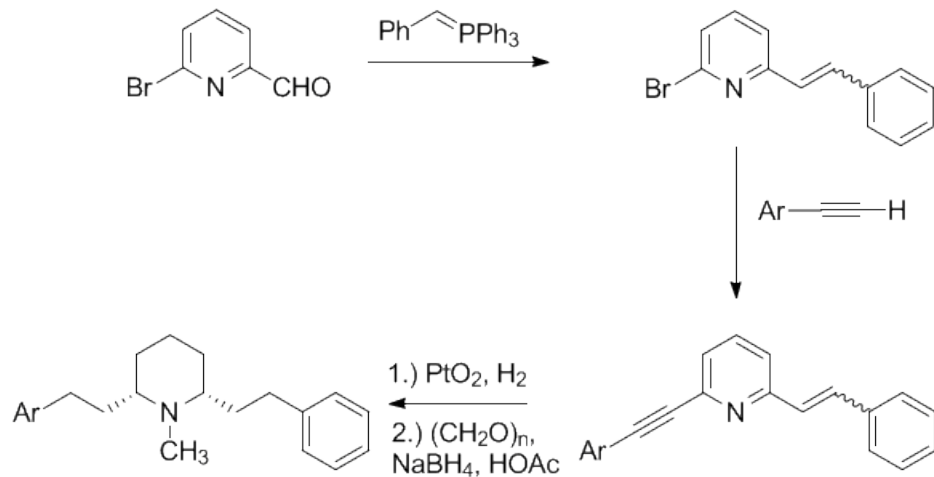
Two further synthetic schemes were designed to modify the phenyl moieties present in the lobelane scaffold. Scheme 1.6 outlines the synthesis of lobelane analogs possessing heteroaromatic rings in place of the phenyl rings, and Scheme 1.7 outlines the synthesis of asymmetric lobelane analogs that possess two different aromatic moieties in place of the two phenyl rings of the lobelane scaffold.



Scheme 1.6 Synthetic methods for generation of symmetrically substituted heteroaromatic ring analogs of lobelane (Varkat et al., 2010).

The synthetic procedure illustrated in Scheme 1.6 began with *N*-methylated 2,6-dimethylpyridinium iodide as the starting material. The starting material underwent a condensation reaction with the required heteroaromatic aldehyde to form the conjugated backbone of the scaffold. When subjected to hydrogenation conditions (Adam's catalyst and hydrogen gas), five final products with heteroaromatic moieties in place of the phenyl rings found in the lobelane scaffold were generated. Their structures and binding affinities at VMAT2 are included in Table 1.6.

Asymmetric lobelane analogs which integrate two non-identical aromatic functionalities into the lobelane scaffold were also being prepared. The synthesis of these asymmetric lobelane analogs is outlined in Scheme 1.7.



Scheme 1.7 Synthetic methods for the generation of asymmetrical lobelane analogs (Crooks, et al., 2011)

Two asymmetric analogs were prepared via the chemistry outlined in Scheme 1.7. Beginning with 2-bromo-6-pyridinecarboxaldehyde as the starting material, a Wittig reaction with a benzyl ylid afforded a *cis-trans* mixture of 2-bromo-6-styrylpyridine. This *cis-trans* mixture was taken without isolation and subjected to Sonogashira coupling chemistry with either 1-ethynynaphthalene or 3-ethynylanisole to afford the conjugated intermediates, 2-(naphthalen-1-ylethynyl)-6-styrylpyridine and 2-((3-methoxyphenyl)ethynyl)-6-styrylpyridine respectively.

The two conjugated intermediates (2-(naphthalen-1-ylethynyl)-6-styrylpyridine and 2-((3-methoxyphenyl)ethynyl)-6-styrylpyridine) were first subjected to hydrogenation conditions with Adam's catalyst and hydrogen gas, and then *N*-methylated via reductive amination. The two final products, compound 39, (2*S*,6*R*)-1-methyl-2-(2-(naphthalen-1-yl)ethyl)-6-phenethylpiperidine, and compound 40 (2*S*,6*R*)-2-(3-

methoxyphenethyl)-1-methyl-6-phenethylpiperidine and their binding affinities for VMAT2 are included in Table 1.6.

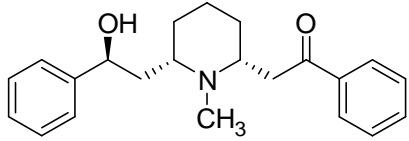
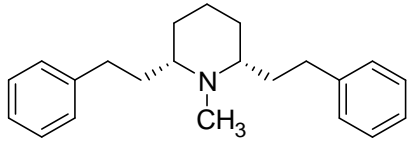
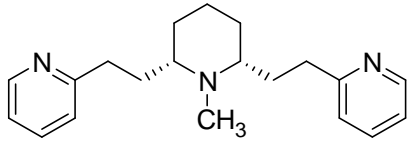
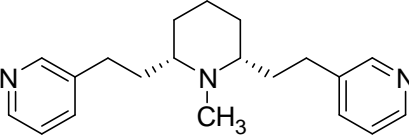
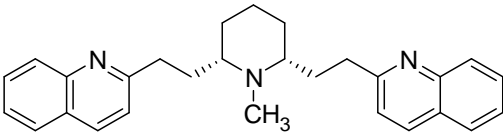
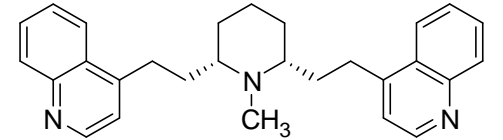
Compound Identifier	Compound Structure	Values are $K_i \pm$ SEM, μM
		$[^3\text{H}]\text{DTBZ}$ Binding VMAT2
LOB		2.76 ± 0.64
lobelane		0.97 ± 0.19
34		5.87 ± 1.72
35		33.3 ± 16.3
36		0.96 ± 0.37
37		2.64 ± 1.41

Table 1.6 (continued)

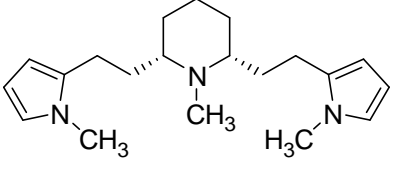
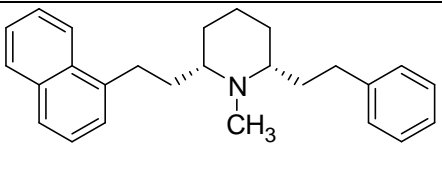
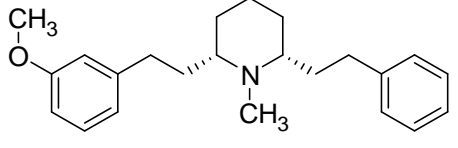
38		9.21 ± 1.65
39		1.02 ± 0.30
40		0.83 ± 0.23

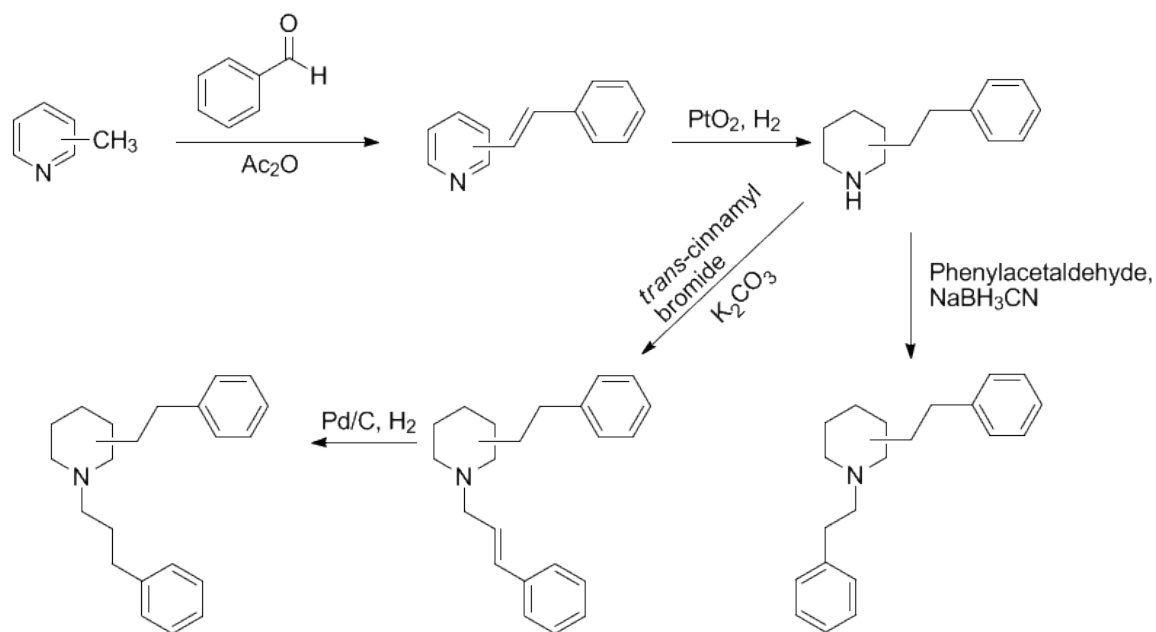
Table 1.6 Structures and Binding affinity of heteroaromatic substituted and asymmetrical lobelane analogs for VMAT2

Of the five analogs that were designed and synthesized to contain two heteroaromatic ring substituents instead of rather than the two phenyl rings found in lobelane, three (i.e. compounds 34, 35, and 38) will be positively charged due to protonation at physiological pH, i.e. nitrogen moieties with pK_a 's greater than 7.2-7.4 at three distinct sites on the molecule. The majority of the compounds containing nitrogen atoms susceptible to protonation at physiological pH exhibited lower affinities for the TBZ binding site on VMAT2 (compounds 34, 35, 37 and 38). The lone exception was compound 36, where the phenyl rings that are found in lobelane have been replaced by two 2-quinolinyl moieties; this analog showed similar affinity to lobelane at VMAT2 (Varkat, et al., 2010). This is important information, since it shows that the TBZ binding site on VMAT2 prefers neutral aryl substituents in order to bind effectively.

The two asymmetric analogs of lobelane (compounds 39 and 40) exhibited similar affinities as lobelane at the TBZ binding site on VMAT2. Compound 39, containing one naphthyl ring and one phenyl ring did have slightly less affinity than the symmetrical naphthyl analog (1.02 μM vs 0.63 μM , respectively). Compound 40, containing one anisole ring and one phenyl ring also had slightly less affinity for VMAT2 than the symmetrical 3-anisoyl analog (0.83 μM vs 0.43 μM).

The next two phases of modification of the lobelane scaffold involved altering both the location of attachment of the phenethyl linkers on the central piperidine ring as well as varying the length of the methylene linkers that connect the aryl rings to the central piperidine ring, in order to determine the importance of the intramolecular distance between the piperidine ring amine moiety and the phenyl rings (Crooks et al., 2011). Schemes 1.8, and 1.9 outline the chemistry used in these modifications of the lobelane scaffold.

Scheme 1.8 illustrates the synthesis of isomerized lobelane analogs in which the phenethyl linkers have been moved from the 2,6 positions of the piperidine ring to the 1,2-, 1,3-, and 1,4-positions. Several analogs were also generated that contained a three-carbon linker between the piperidine ring and the phenyl rings. The synthesis utilizes an appropriate 2-methylpyridine, 3-methylpyridine, or 4-methylpyridine, depending on the desired attachment point of the linker on the piperidine ring. The starting material is condensed with benzaldehyde in refluxing acetic anhydride to yield the conjugated 2, 3, or 4 substituted (*E*)-styrylpyridine. These conjugated products are then subjected to hydrogenation conditions with Adam's catalyst (platinum(IV) oxide) and hydrogen gas to yield the appropriate 2, 3, or 4 substituted phenethylpiperidine.

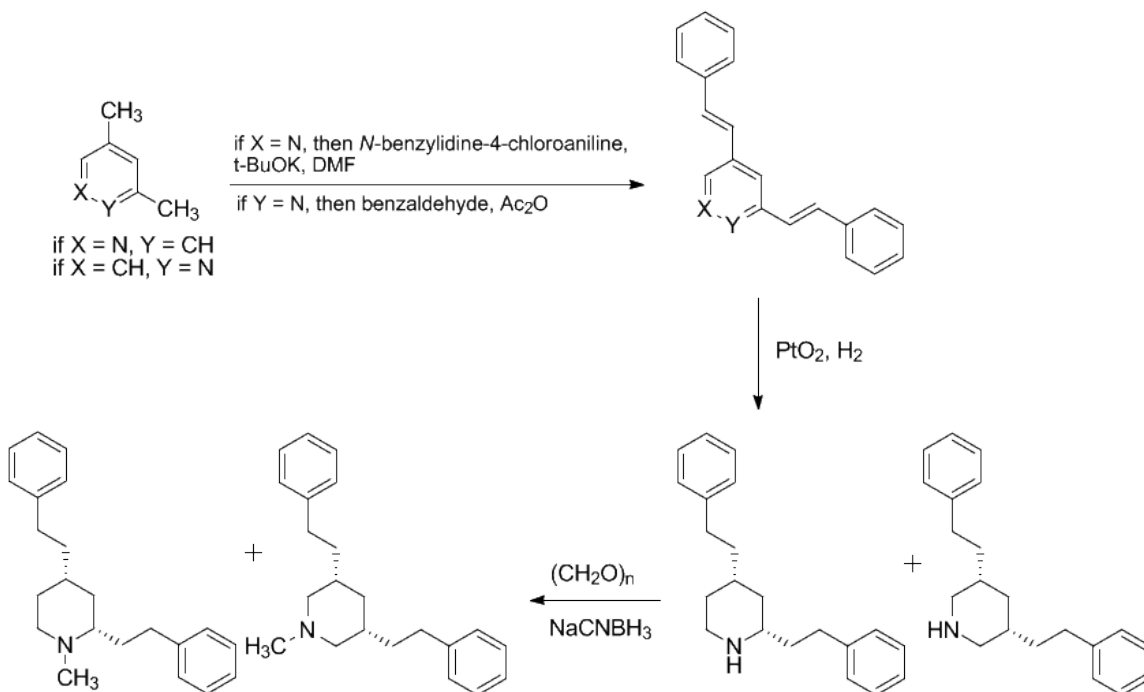


Scheme 1.8 Synthetic methods for generation of isomerized lobelane analogs (Zheng et al., 2005; Crooks et al., 2011)

The substituted phenethylpiperidines were reacted via one of two methods to yield either N1 linked phenethyl analogs or N1 linked phenpropyl analogs. In the case of the N1 substituted phenethyl compounds, the substituted phenethylpiperidines were reacted with phenylacetaldehyde and sodium cyanoborohydride to yield the desired series of products. In the case of the N1 substituted phenpropyl compounds, the substituted phenethylpiperidines were reacted with *trans*-cinnamyl bromide with potassium carbonate serving as a base, to yield the desired series of products. The exact structures of the analogs generated in Scheme 1.8 and the resultant binding affinities at $\alpha 4\beta 2^*$ & $\alpha 7^*$ nAChRs, and at VMAT2 are shown in Table 1.7.

Scheme 1.9 outlines the chemistry used in generating a series of four compounds where the phenethyl linkers have been moved to the 2,4 and 3,5 positions of the central

piperidine ring of the lobelane scaffold. In order to more clearly indicate where the amine moiety is in the ring, it has been given a marker labeled as such in the scheme.



Scheme 1.9 Synthetic methods for generation of isomerized lobelane analogs with phenethyl linkers in the 2,4 and 3,5 position of the piperidine ring (Zheng et al., 2005; Crooks et al., 2011)

The synthesis of the four analogs generated in Scheme 1.9 necessitated two different reaction conditions for the appropriate starting materials. When the starting material was 2,4-lutidine, also known as 2,4-dimethylpyridine, the hydrogen atoms on the methyl groups were sufficiently acidic to allow condensation reaction to be utilized. 2,4-Lutidine was subjected to condensation reaction conditions with benzaldehyde in refluxing acetic anhydride to yield the desired conjugated intermediate, 2,4-distyrylpyridine. However, the presence of the methyl groups in the 3 and 5 positions of

the pyridine ring in 3,5-lutidine (also known as 3,5-dimethylpyridine) made the hydrogen atoms on the methyl groups less acidic, and a different chemistry was required to generate the conjugated intermediate, 3,5-distyrylpyridine. Starting with 3,5-lutidine, the condensation reaction proceeded only with an activated form of benzaldehyde, i.e. *N*-benzylidene-4-chloroaniline, using potassium *t*-butoxide as a base in dimethylformamide. The two appropriately substituted conjugated intermediates, 2,4-distyrylpyridine and 3,5-distyrylpyridine, were then subjected to hydrogenation conditions with Adam's catalyst and hydrogen gas to yield *nor*-(2*S*,4*S*)-2,4-diphenethylpiperidine and *nor*-(3*R*,5*S*)-3,5-diphenethylpiperidine, respectively. In order to introduce the *N*-methyl moiety, the *nor*-compounds were exposed to reductive amination conditions with paraformaldehyde and sodium cyanoborohydride in methanol to generate analogs (2*S*,4*S*)-1-methyl-2,4-diphenethylpiperidine and (3*R*,5*S*)-1-methyl-3,5-diphenethylpiperidine. The binding affinities of the four analogs generated in Scheme 1.9 at $\alpha 4\beta 2^*$ & $\alpha 7^*$ nAChRs, and at VMAT2 are shown in Table 1.7.

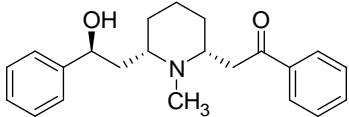
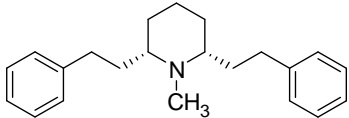
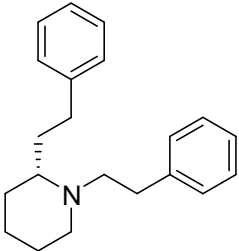
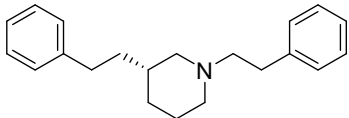
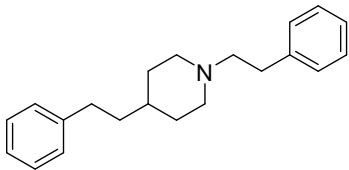
Compound Identifier	Compound Structure	Values are $K_i \pm \text{SEM}$, μM		
		$[^3\text{H}]\text{NIC}$ Binding $\alpha 4\beta 2^*$ nAChR	$[^3\text{H}]\text{MLA}$ Binding $\alpha 7^*$ nAChR	$[^3\text{H}]\text{DTBZ}$ Binding VMAT2
LOB		0.004 ± 0.000	6.26 ± 1.30	2.76 ± 0.64
lobelane		14.9 ± 1.67	26.0 ± 6.57	0.97 ± 0.19
41		>100	66.9 ± 27.4	3.32 ± 0.74
42		>100	>100	3.95 ± 0.61
43		7.62 ± 1.47	>100	1.87 ± 0.25

Table 1.7 (continued)

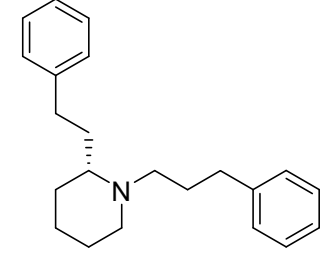
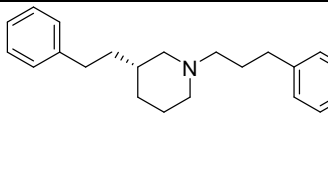
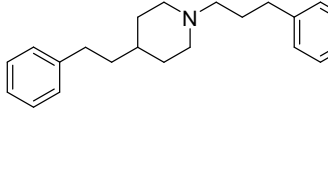
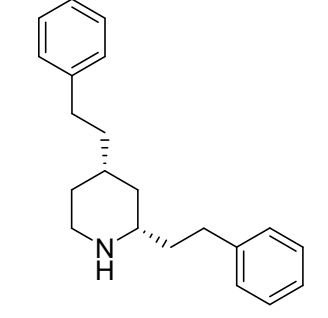
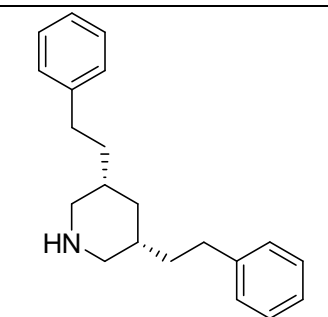
44		>100	9.02 ± 1.54	3.35 ± 0.80
45		>100	>100	4.04 ± 1.76
46		>100	>100	2.47 ± 0.70
47		>100	>100	1.36 ± 0.11
48		>100	>100	6.11 ± 0.92

Table 1.7 (continued)

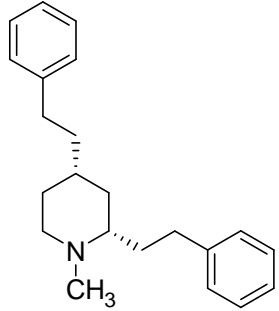
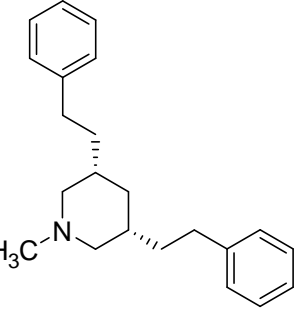
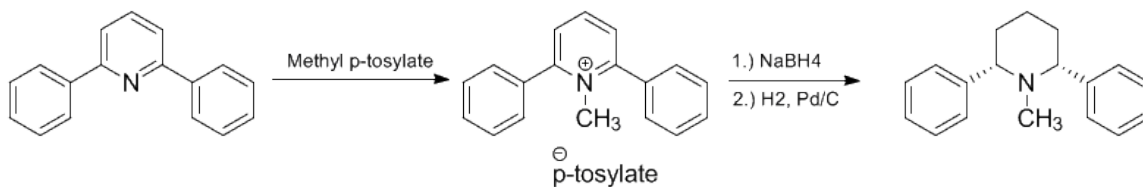
49		>100	>100	2.62 ± 0.51
50		>100	>100	11.7 ± 0.65

Table 1.7 Compound structures and $\alpha 4\beta 2^*$ & $\alpha 7^*$ nAChRs, and VMAT2 binding affinity of isomerized lobelane analogs with phenethyl linkers in the N1, C2; N1, C3; N1, C4; C2, C4 and C3, C5 positions.

The above isomerized analogs of lobelane had the low affinities at $\alpha 4\beta 2^*$ & $\alpha 7^*$ nAChRs, and interestingly maintained similar affinities to lobelane at the TBZ binding site on VMAT2 (within one order of magnitude). Compounds 43, 46, and 49 were especially interesting, since they exhibited binding affinity better than most other analogs in the table; the linkers in these analogs were in the C2, C4 and N1, C4 positions. The extra carbon in the N1 linker of compound 46 only moderately decreased the analog's affinity for VMAT2. These data indicate that isomerization of the lobelane scaffold to afford compounds with linkers in varying positions of attachment around central

piperidine ring does not greatly hinder binding to VMAT2, and allows for interesting opportunities involving scaffold optimization and chemical space.

The fourth stage of the systematic approach to the alteration of the lobelane scaffold comprised of designing analogs with variable methylene linker lengths between the central piperidine ring of the scaffold and the phenyl rings, therefore increasing and decreasing intramolecular distances between the amine moiety and the phenyl rings. The number of carbon atoms between the piperidine ring and the phenyl rings was varied from zero to three in the C2 and C6 positions, affording 17 compounds in this series (Zheng et al., 2008; Crooks et al., 2011). Schemes 1.10, 1.11, and 1.12 outline the chemistry designed to produce the three symmetrical scaffolds.

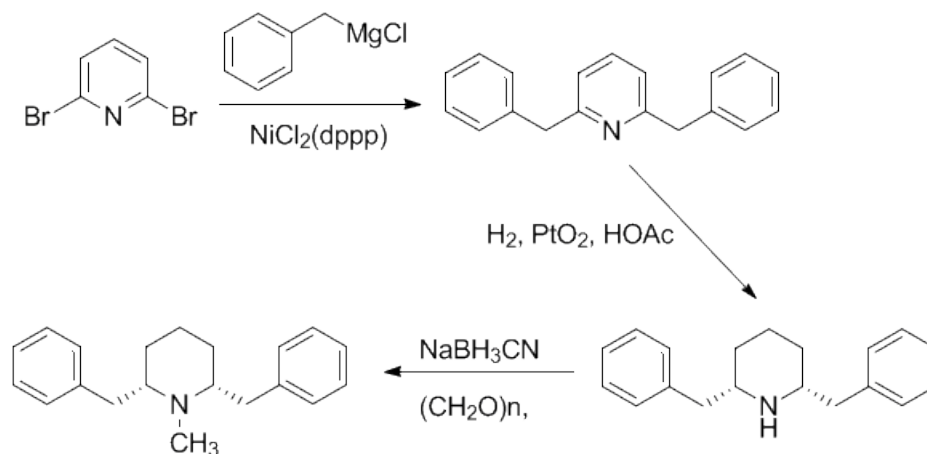


Scheme 1.10 Synthesis of a symmetrical lobelane analog with zero methylene groups between the piperidine ring and the phenyl rings (Zheng et al., 2008; Crooks et al., 2011)

Synthesis of the symmetrical lobelane analog with no carbon atoms between the piperidine ring and the two phenyl rings (i.e. a molecule which is devoid of methylene units between the central piperidine ring and two phenyl rings) was synthesized by initial *N*-methylation of the starting material, 2,6-bisphenylpyridine, via reaction with methyl *p*-tosylate, generating the quaternary ammonium salt as an intermediate. Subsequent two step reduction of the quaternary ammonium salt with NaBH₄, followed by catalytic

hydrogenation with palladium- on-carbon and hydrogen gas afforded the desired compound, (2*S*,6*R*)-1-methyl-2,6-diphenylpiperidine.

The synthesis of the symmetrical lobelane analog with one methylene group between the piperidine ring and the two phenyl rings is shown in Scheme 1.11.



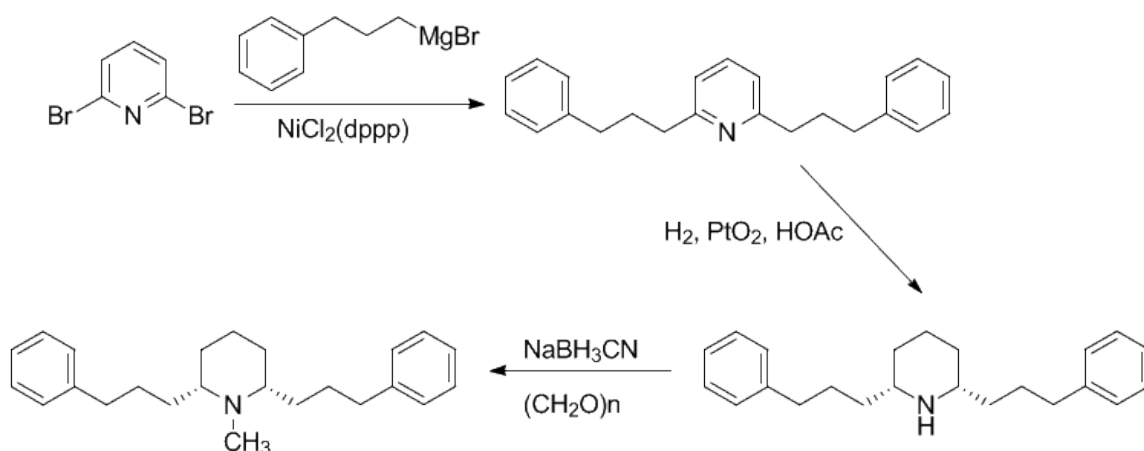
Scheme 1.11 Synthesis of the symmetrical lobelane analog with one methylene group between the piperidine ring and the phenyl rings (Zheng et al., 2008; Crooks et al., 2011)

The synthesis of the symmetrical analog with one methylene group between the piperidine ring and the two phenyl rings utilized 2,6-dibromopyridine as the starting material.

Application of Kumada coupling chemistry, which consists of a cross coupling reaction, which is widely used in organic synthesis for generating carbon–carbon bonds by the reaction of a Grignard reagent, in this case (3-phenylpropyl)magnesium bromide and an organic halide, i.e. 2,6-dibromopyridine . The Kumada coupling procedure uses transition metal catalysts, in this case dichloro[1,3-bis(diphenylphosphino)propane]nickel, to couple the 2,6-dibromopyridine starting material with (3-phenylpropyl)magnesium bromide to afford the desired 2,6-dibenzylpyridine intermediate. Reduction of this intermediate via

hydrogenation conditions utilizing Adam's catalyst and hydrogen gas yielded *nor*-(2*S*,6*R*)-2,6-dibenzylpiperidine. In order to introduce the *N*-methyl moiety the *nor*-compound was exposed to reductive amination conditions with paraformaldehyde and sodium cyanoborohydride in methanol to generate lobelane analog (2*S*,6*R*)-2,6-dibenzyl-1-methylpiperidine.

A similar synthetic strategy for the symmetrical lobelane analog with three methylene groups between the piperidine ring and the two phenyl rings is shown in Scheme 1.12.

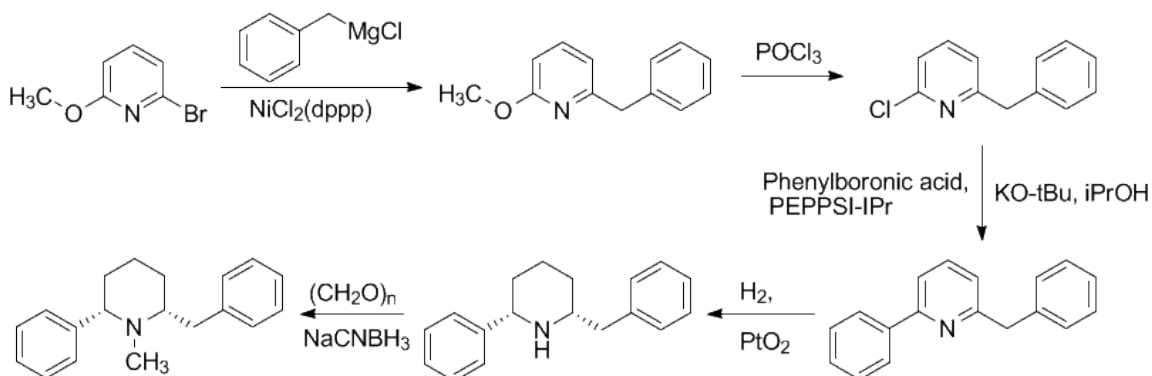


Scheme 1.12 Synthesis of the symmetrical lobelane analog with three methylene groups between the piperidine ring and the phenyl rings (Zheng et al., 2008; Crooks et al., 2011)

The synthesis of the symmetrical analog with three methylene groups linking the piperidine ring and the two phenyl rings also utilized 2,6-dibromopyridine as the starting material. Again, via the application of Kumada coupling chemistry to couple the 2,6-dibromopyridine starting material with (3-phenylpropyl)magnesium bromide afford the desired 2,6-bis(3-phenylpropyl)pyridine intermediate. Reduction of the intermediate via

hydrogenation conditions with Adam's catalyst and hydrogen gas yielded the *nor*-(2*R*,6*S*)-2,6-bis(3-phenylpropyl)piperidine compound. In order to introduce the *N*-methyl moiety found in the lobelane scaffold, the *nor*-compounds were exposed to reductive amination conditions with paraformaldehyde and sodium cyanoborohydride in methanol to generate lobelane analog (2*R*,6*S*)-1-methyl-2,6-bis(3-phenylpropyl)piperidine.

The asymmetric compounds in this series required more involved chemistry and multiple synthetic steps. The synthesis of the analog containing zero carbons between the piperidine ring and the phenyl ring on one side of the molecule and one carbon between the piperidine ring and the phenyl ring on the opposite side of the molecule is outlined in Scheme 1.13.

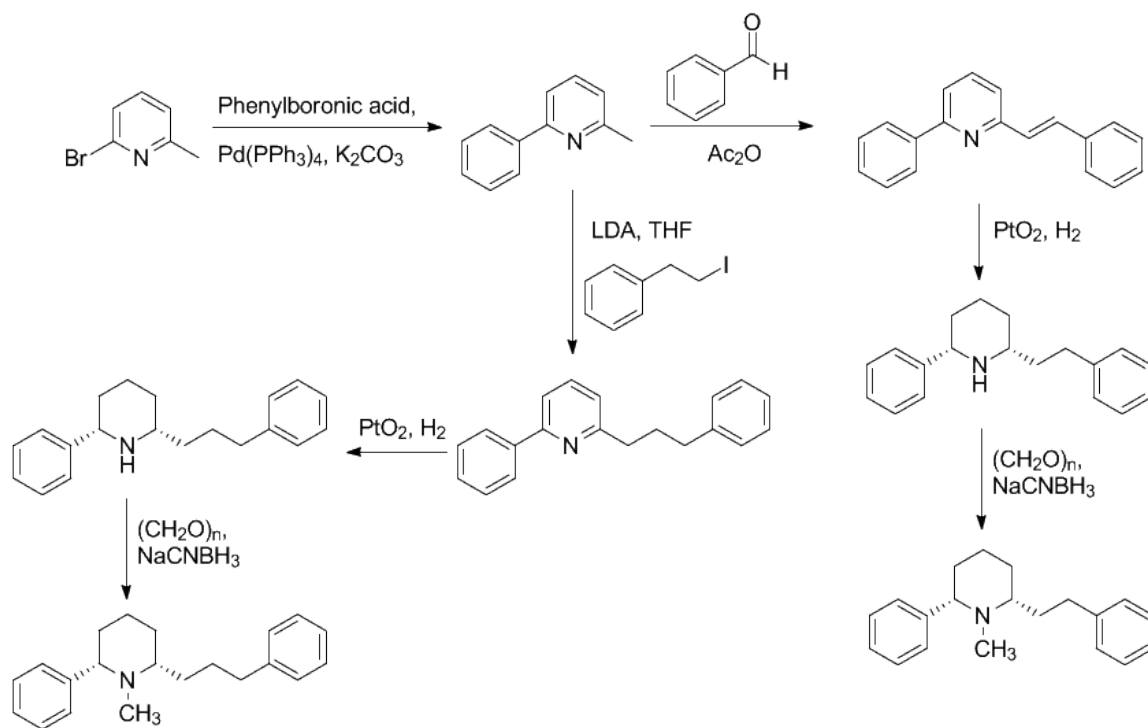


Scheme 1.13 Synthesis of an asymmetrical lobelane analog with zero carbons and one carbon in the linkers between the piperidine ring and the phenyl rings (Zheng et al., 2008; Crooks et al., 2011).

The starting material for the synthesis outlined in Scheme 1.13 was 2-bromo-6-methoxypyridine. Application of Kumada coupling chemistry with benzylmagnesium chloride afforded the 2-benzyl-6-methoxypyridine intermediate, which was then

subjected to reaction with phosphoryl chloride to transform the methoxy group to a chlorine functionality, which yielded the 2-benzyl-6-chloropyridine intermediate. This in turn, was subjected to Suzuki coupling with phenylboronic acid catalyzed with [1,3-bis(2,6-diisopropylphenyl)imidazol-2-ylidene](3-chloropyridyl)-palladium(II) dichloride (PEPPSI-IPr) and KOtBu as base in isopropanol, to yield the 2-benzyl-6-phenylpyridine intermediate. Reduction of this intermediate via hydrogenation with Adam's catalyst and hydrogen gas yielded the *nor*- (2*R*,6*S*)-2-benzyl-6-phenylpiperidine. In order to introduce the *N*-methyl moiety, the *nor*-compound was exposed to reductive amination conditions with paraformaldehyde and sodium cyanoborohydride in methanol to generate the lobelane analog (2*R*,6*S*)-2-benzyl-1-methyl-6-phenylpiperidine.

The synthesis of the analogs containing zero methylene units between the piperidine ring and the phenyl ring on one side of the molecule and either two methylene units or three methylene units between the piperidine ring and the phenyl ring on the opposite side of the molecule is outlined in Scheme 1.14.

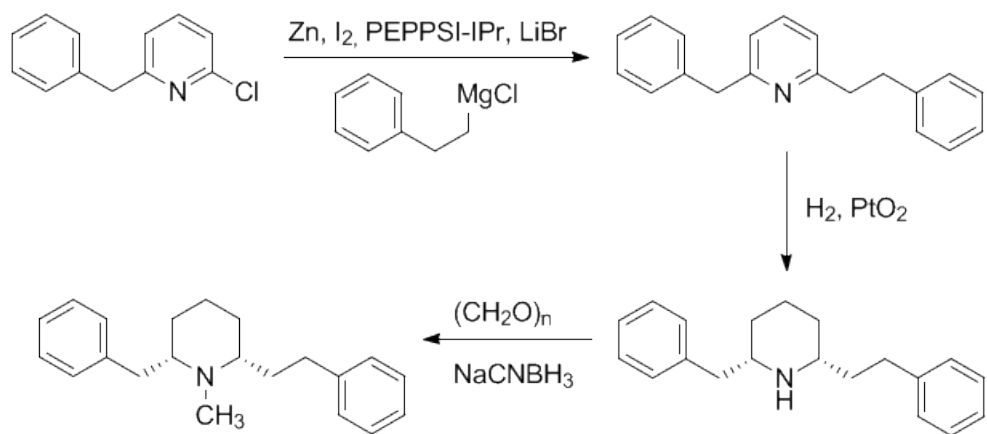


Scheme 1.14 Synthesis of asymmetrical lobelane analog with zero methylene units and either two or three methylene units in the linkers between the piperidine ring and the phenyl rings (Zheng et al., 2008; Crooks et al., 2011).

The synthesis of both asymmetrical compounds began with 2-bromo-6-methylpyridine as the starting material, which was reacted with phenylboronic acid under Suzuki coupling conditions to yield the common intermediate, 2-methyl-6-phenylpyridine. From this point the syntheses diverged. To make the asymmetrical compound with zero and two methylene units in the linkers, the common intermediate was subjected to a condensation reaction with benzaldehyde in refluxing acetic anhydride. This afforded the conjugated product (*E*)-2-phenyl-6-styrylpyridine, which was then reduced under hydrogenation conditions to *nor*-(2*R*,6*S*)-2-phenethyl-6-phenylpiperidine. The *N*-methyl group was introduced utilizing reductive amination

conditions with paraformaldehyde and sodium cyanoborohydride in methanol to generate the desired product, (2*R*,6*S*)-1-methyl-2-phenethyl-6-phenylpiperidine. To prepare the asymmetrical compound with zero and three carbons in the linker units, the common intermediate 2-methyl-6-phenylpyridine was subjected to deprotonation of the 2-methyl group followed by an S_N2 reaction with 2-iodoethylbenzene to afford 2-phenyl-6-(3-phenylpropyl)pyridine, which was then reduced under hydrogenation conditions to *nor*-(2*S*,6*S*)-2-phenyl-6-(3-phenylpropyl)piperidine followed by *N*-methylation to afford the desired product, (2*S*,6*S*)-1-methyl-2-phenyl-6-(3-phenylpropyl)piperidine.

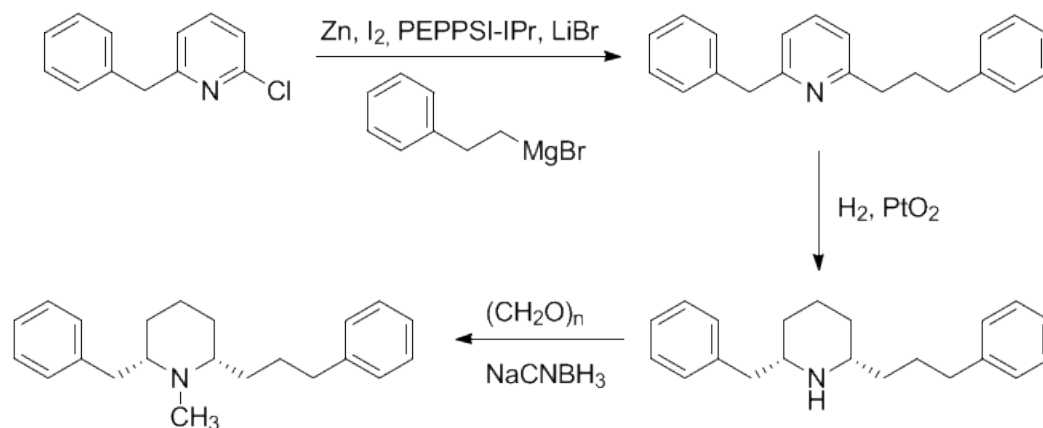
The synthesis of the analog containing one methylene unit between the piperidine ring and the phenyl ring on one side of the molecule and two methylene units between the piperidine ring and the phenyl ring on the opposite side of the molecule is outlined in Scheme 1.15. Starting with 2-benzyl-6-chloropyridine, Negishi coupling of the starting material with 2-phenyl-1-ethylzinc iodide (generated in situ) using PEPPSI-IPr as a catalyst afforded 2-benzyl-6-phenethylpyridine, which was then subjected to catalytic hydrogenation to yield *nor*-(2*S*,6*R*)-2-benzyl-6-phenethylpiperidine and *N*-methylated with paraformaldehyde and sodium cyanoborohydride in methanol to generate the desired product, (2*S*,6*R*)-2-benzyl-1-methyl-6-phenethylpiperidine.



Scheme 1.15 Synthesis of the asymmetrical lobelane analog with one methylene units and two methylene units in the linkers between the piperidine ring and the phenyl rings

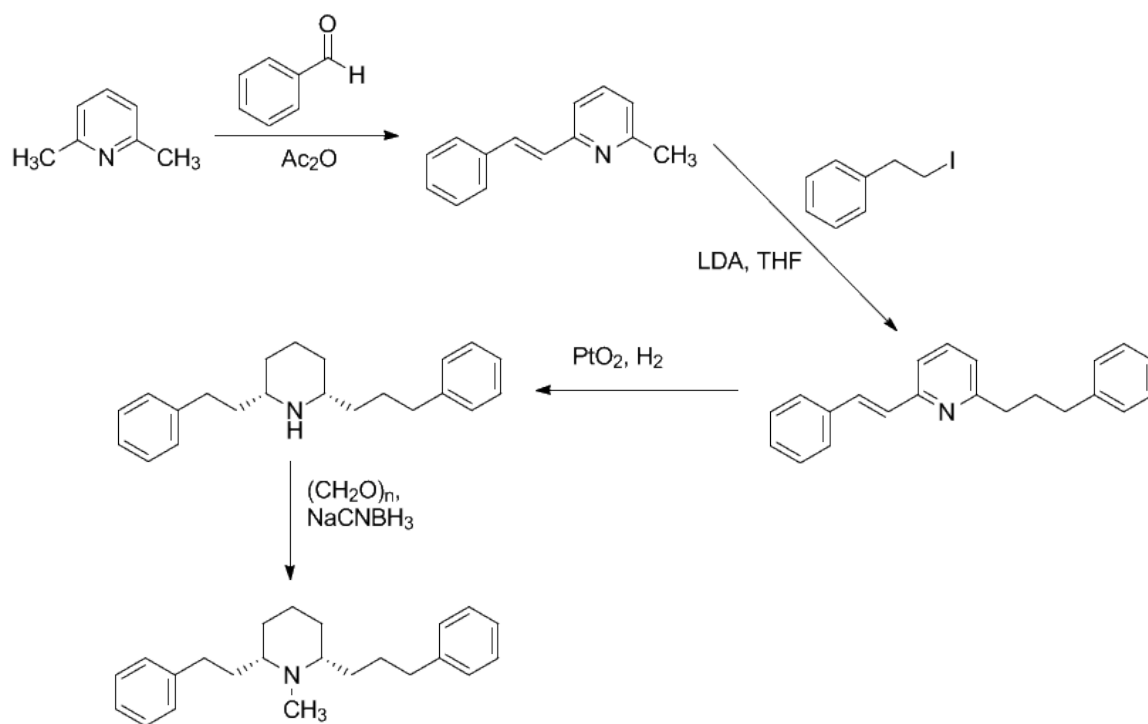
(Zheng et al., 2008; Crooks et al., 2011).

The synthesis of the analog containing one methylene unit between the piperidine ring and the phenyl ring on one side of the molecule and three methylene units between the piperidine ring and the phenyl ring on the opposite side of the molecule is outlined in Scheme 1.16. Starting with 2-benzyl-6-chloropyridine, Negishi coupling of the starting material with 3-phenyl-1-propylzinc iodide (generated in situ) using PEPPSI-IPr as a catalyst afforded 2-benzyl-6-(3-phenylpropyl)pyridine, which was then subjected to catalytic hydrogenation to yield *nor*- (2*S*,6*S*)-2-benzyl-6-(3-phenylpropyl)piperidine. *N*-methyl under reductive amination conditions with paraformaldehyde and sodium cyanoborohydride in methanol afforded the desired product, (2*S*,6*S*)-2-benzyl-1-methyl-6-(3-phenylpropyl)piperidine.



Scheme 1.16 Synthesis of an asymmetrical lobelane analog with one methylene unit and two methylene units in the linkers between the piperidine ring and the phenyl rings (Zheng et al., 2008; Crooks et al., 2011).

The synthesis of the analog containing two methylene units between the piperidine ring and the phenyl ring on one side of the molecule and three methylene units between the piperidine ring and the phenyl ring on the opposite side of the molecule is outlined in Scheme 1.17. The starting material, 2,6-lutidine, was subjected to mono-condensation with benzaldehyde (both mono and disubstituted products were produced, and the mono product was separated via column chromatography), to afford the conjugated product, (*E*)-2-methyl-6-styrylpyridine. The conjugated product was then subjected to deprotonation of the 2-methyl group followed by S_N2 reaction with (2-iodoethyl)benzene to yield (*E*)-2-(3-phenylpropyl)-6-styrylpyridine, which was subjected to catalytic hydrogenation to yield *nor*-(2*S*,6*S*)-2-phenethyl-6-(3-phenylpropyl)piperidine and *N*-methylated to afford the desired product, (2*S*,6*S*)-1-methyl-2-phenethyl-6-(3-phenylpropyl)piperidine.



Scheme 1.17 Synthesis of an asymmetrical lobelane analog with two methylene units and three methylene units in the linkers between the piperidine ring and the phenyl rings (Zheng et al., 2008; Crooks et al., 2011).

The 17 lobelane analogs generated in this fourth stage of the systematic approach to the alteration of the lobelane scaffold comprised of designing analogs with modified lengths between the central piperidine ring of the scaffold, therefore varying the intramolecular distance between the amine moiety and the phenyl rings; their binding affinities at the TBZ binding site on VMAT2 are shown in Table 1.8.

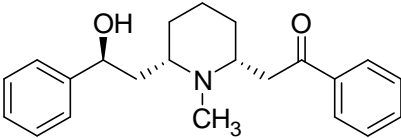
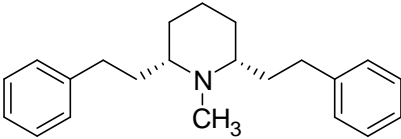
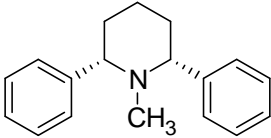
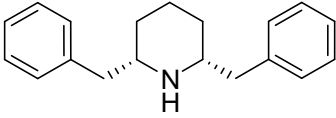
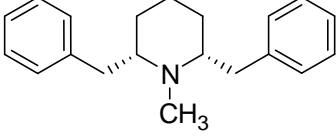
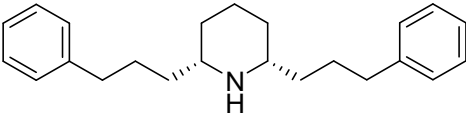
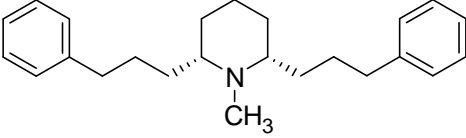
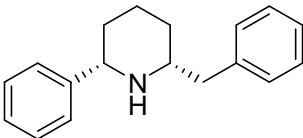
Compound Identifier	Compound Structure	Values are $K_i \pm \text{SEM}$, μM
		[^3H]DTBZ Binding VMAT2
LOB		2.76 ± 0.64
lobelane		0.97 ± 0.19
51		>100
52a		7.68 ± 1.44
52b		10.5 ± 3.36
53a		4.50 ± 1.02
53b		1.00 ± 0.23
54a		24.1 ± 6.10

Table 1.8 (continued)

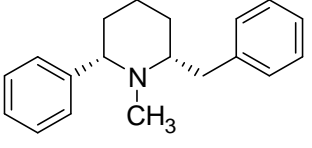
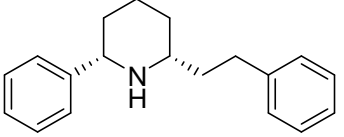
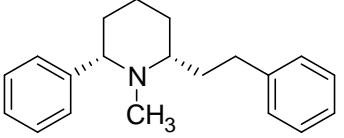
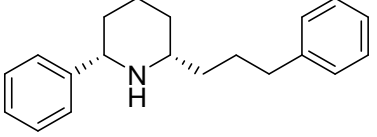
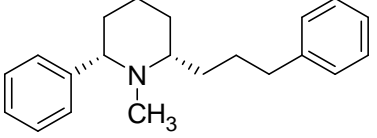
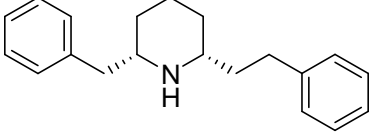
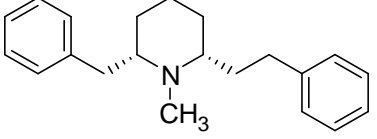
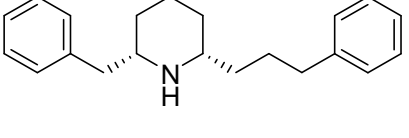
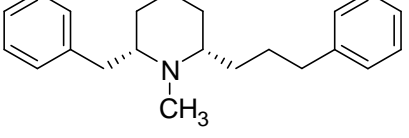
54b		13.6 ± 8.14
55a		28.4 ± 7.30
55b		16.1 ± 4.07
56a		28.6 ± 2.44
56b		62.5 ± 16.6
57a		12.2 ± 0.19
57b		2.77 ± 1.77
58a		1.13 ± 0.28
58b		1.62 ± 0.39

Table 1.8 (continued)

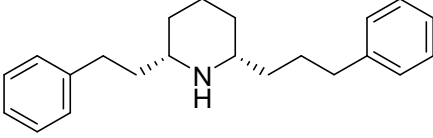
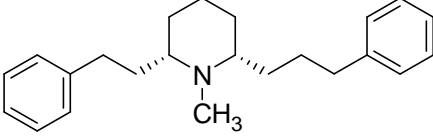
59a		4.60 ± 0.56
59b		0.88 ± 0.30

Table 1.8 Compound structures and VMAT2 binding affinity of modified lobelane analogs with differing intramolecular distances between the piperidine ring and the phenyl rings in the molecule (Zheng et al., 2008; Crooks et al., 2011).

From the data in Table 1.8, it has been shown that altering the intramolecular distance between the piperidine ring and the phenyl rings on the lobelane scaffold has dramatic effects on the ability of the analogs to bind to the TBZ binding site on VMAT2. The removal of the ethylene linker on both sides of the piperidine ring of lobelane to afford compound 51 resulted in a complete loss of affinity for the TBZ binding site on VMAT2. When the linkers are one methylene unit in length some of the affinity for VMAT2 returns, but then only moderately, as compound 52b still exhibited a 10-fold decrease in affinity compared to lobelane. In order to bind to the TBZ site on VMAT2, it appears that it is necessary to extend the length of the methylene linkers between the piperidine ring and the phenyl rings to at least two carbons (the distance found in lobelane) or longer. Compound 53b, which is a symmetrical analog of lobelane (three carbons in each linker), exhibits the same affinity for VMAT2 as does lobelane ($K_i = 1.00 \mu\text{M}$). The asymmetric analog 59b also had an affinity similar to lobelane ($K_i = 0.88 \mu\text{M}$),

and the linkers between the piperidine ring and the phenyl rings were two and three methylene units in length.

In the fifth stage of the systematic approach to alteration of the lobelane scaffold, the *N*-methyl group of lobelane was modified, either by increasing the length of the alkyl-moiety, or by replacing the methyl group with a variety of other *N*-substituents with greater organic functionality and polarity. The seven compounds generated in this series of structural modifications and their affinities for the TBZ binding site on VMAT2 are shown in Table 1.9.

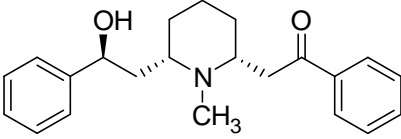
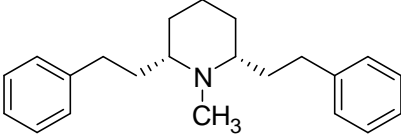
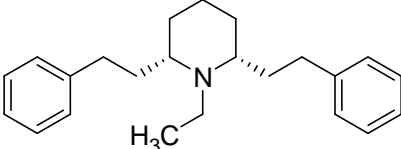
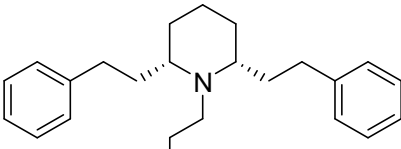
Compound Identifier	Compound Structure	Values are $K_i \pm \text{SEM}$, μM
		[³ H]DTBZ Binding VMAT2
LOB		2.76 ± 0.64
lobelane		0.97 ± 0.19
60		3.41 ± 0.67
61		1.87 ± 0.25

Table 1.9 (continued)

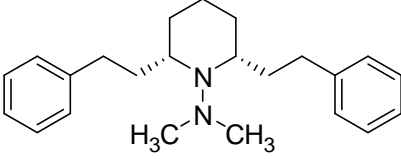
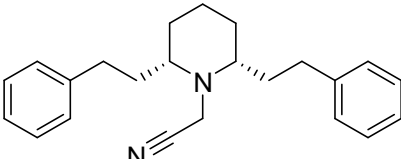
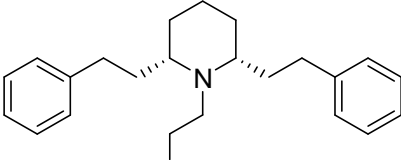
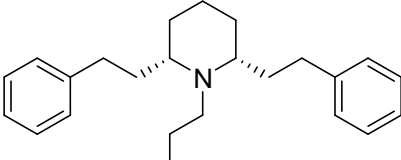
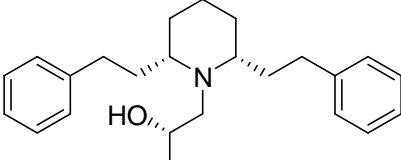
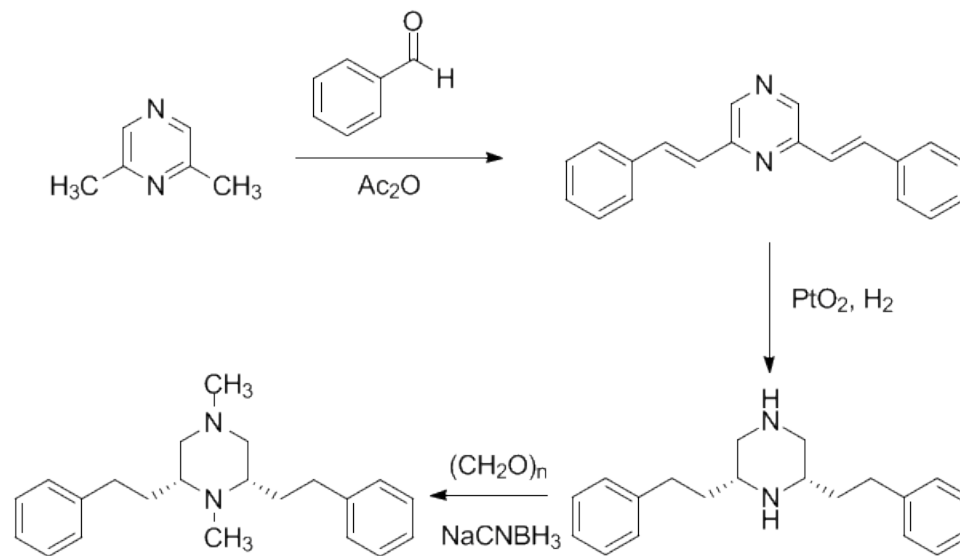
62		>100
63		22.6 ± 0.23
64		5.59 ± 0.94
65		9.59 ± 1.47
66		0.56 ± 0.08

Table 1.9 Compound structures and VMAT2 binding affinity of modified lobelane analogs (Crooks et al., 2011)

In compounds 60 and 61 the length of the *N*-methyl substituent has been increased from methyl to ethyl and propyl. The *N*-ethyl and *N*-propyl analogs exhibited slightly lower affinity at VMAT2 compared to lobelane. By replacing the *N*-methyl group with a dimethylhydrazine moiety, as in compound 62, led to a complete loss of

affinity for the TBZ site on VMAT2. When the *N*-methyl group was replaced with a cyanomethyl moiety (compound 63), aminoethyl (compound 64), or a dimethylaminoethyl moiety (compound 65), the affinity for VMAT2 was also reduced by about one order of magnitude (5-20 fold) when compared to lobelane (Crooks et al., 2011). One very interesting compound was discovered in this series (compound 66), in which the *N*-methyl group was replaced with a 1,2(*R*)-dihydroxypropyl moiety. Compound 66, (*R*)-3-((2*S*,6*R*)-2,6-diphenethylpiperidin-1-yl)propane-1,2-diol, exhibited slightly better affinity than lobelane for the TBZ binding site on VMAT2, and was much more water soluble than lobelane, which is a highly desirable characteristic in compounds selected for further study in animals and humans.

In the sixth phase of the systematic approach to structural changes in the lobelane scaffold, the central piperidine ring was subjected to structural modification. The piperidine ring was altered by incorporating an additional heteroatom, to afford a piperazine ring system. The piperidine ring was also replaced with a smaller five-membered pyrrolidine ring, as well as with a larger conformationally restricted tropane ring system. The synthesis of the piperazine ring analogs is outlined in Scheme 1.18.

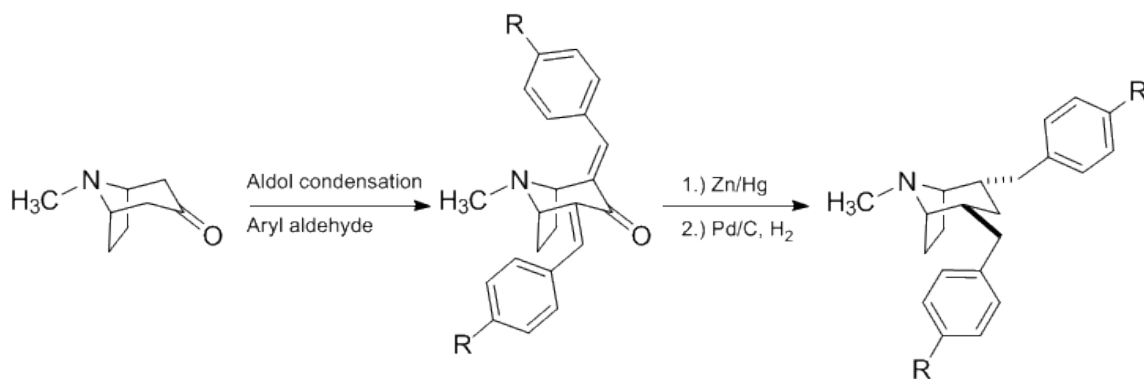


Scheme 1.18 Synthetic outline for generation of piperazine analogs of lobelane

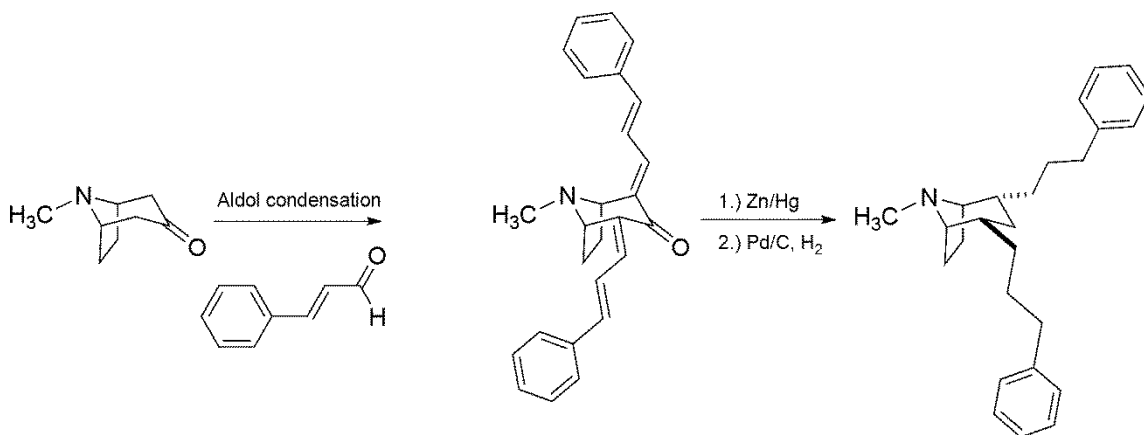
Two compounds were constructed in the piperazine series of analogs, viz., (2*R*,6*S*)-2,6-diphenethylpiperazine and (2*R*,6*S*)-1,4-dimethyl-2,6-diphenethylpiperazine. The chemistry involved in making these two compounds differs only in the starting material when compared to the synthesis of the piperidine analogs in Scheme 1.5, since 2,6-dimethylpyrazine is used in place of 2,6-dimethylpyridine. The two piperazine compounds generated in this series and their affinities for the TBZ binding site on VMAT2 are shown in Table 1.9.

The piperidine ring was also replaced with a five-membered pyrrolidine ring, and the structures and affinities of such compounds at the TBZ binding site on VMAT2 are also shown in Table 1.9.

Finally, the piperidine ring was replaced with a more conformationally restricted tropane ring. The outline of the chemistry used to synthesize the seven compounds in this series is shown in Schemes 1.19 and 1.20.



Scheme 1.19 Synthesis of tropane analogs of lobelane (Zheng et al., 2005)



Scheme 1.20 Synthesis of tropane analogs of lobelane with extended linkers
(Zheng et al., 2005)

Briefly, the synthesis of the seven analogs in the tropane series began with tropinone as the starting material, which was subjected to an Aldol condensation reaction with either aryl aldehydes or *trans*-cinnamaldehyde. Clemmenson reduction of the conjugated Aldol products followed by catalytic hydrogenation with palladium-on-carbon and hydrogen gas afforded the substituted (2*R*,4*S*)-2,4-dibenzyl-8-methyl-8-

azabicyclo[3.2.1]octane and (2*R*,4*S*)-8-methyl-2,4-*bis*(3-phenylpropyl)-8-azabicyclo[3.2.1]octane analogs of lobelane.

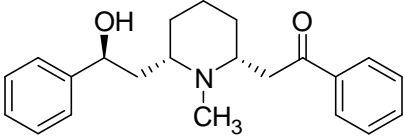
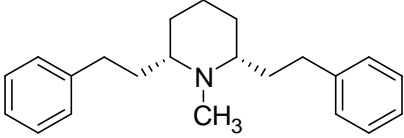
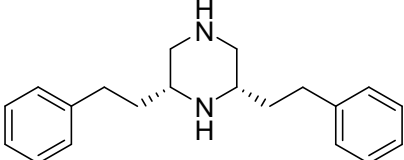
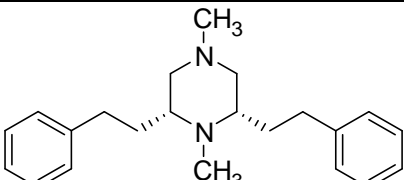
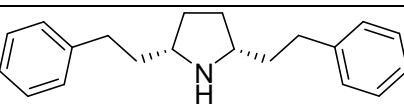
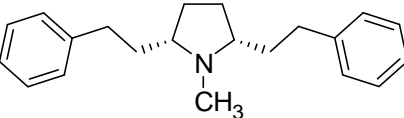
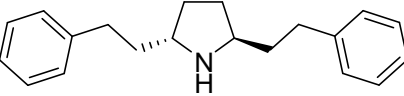
Compound Identifier	Compound Structure	Values are $K_i \pm \text{SEM}$, μM
		[³ H]DTBZ Binding VMAT2
LOB		2.76 ± 0.64
lobelane		0.97 ± 0.19
67		37.6 ± 20.3
68		6.09 ± 0.19
69		1.50 ± 0.22
70		14.5 ± 2.13
71		3.02 ± 0.17

Table 1.10 (continued)

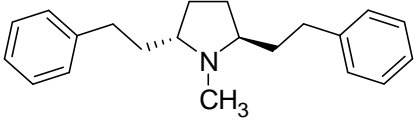
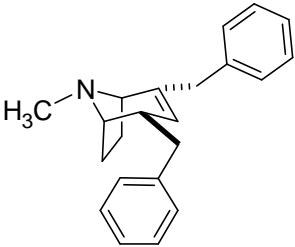
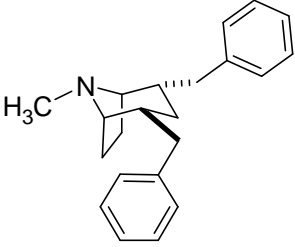
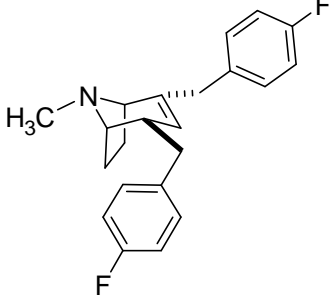
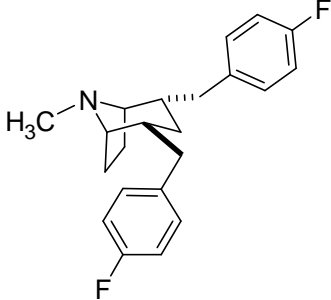
72		8.80 ± 2.30
73		1.30 ± 0.21
74		>100
75		1.38 ± 0.20
76		>100

Table 1.10 (continued)

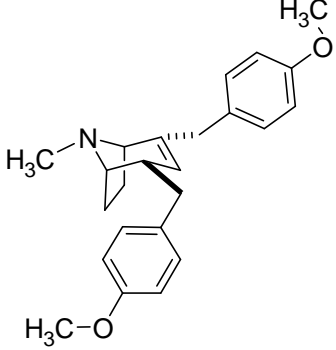
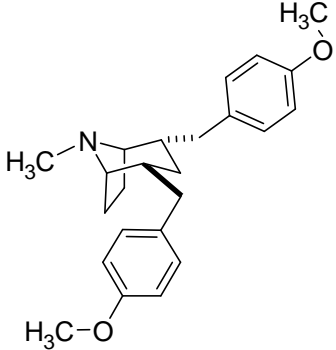
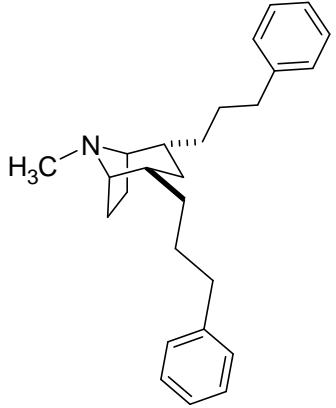
77		4.80 ± 1.70
78		3.88 ± 0.90
79		3.95 ± 0.54

Table 1.10 Structures and VMAT2 binding affinities of modified lobelane analogs

(Zheng et al., 2005; Crooks et al., 2011)

In the piperazine series of compounds, only compound 68 ((2*R*,6*S*)-1,4-dimethyl-2,6-diphenethylpiperazine) had similar affinity to lobelane at VMAT2. In the pyrrolidine series of analogs, affinities for VMAT2 were lower in all compounds, but interestingly

the *nor*-compounds had higher affinities than their *N*-methyl counterparts, which contrasts greatly compared to the previous piperidine series of lobelane analogs. In the tropane series of analogs,, compounds 73 and 75 had affinities similar to lobelane, while their saturated counterparts had no affinity for VMAT2 ($IC_{50} > 100 \mu M$). The double bond present in the tropane ring of compounds 73 and 75 appear to be important in providing the correct configuration of the tropane ring, as well as the orientations of the two phenethyl side chains.

1.10 Portions of the lobelane scaffold that are critical in binding to VMAT2

From the library of compounds designed, synthesized, and evaluated for their affinity for VMAT2, it is possible to infer which portions of the lobelane scaffold is essential for the molecule to bind to VMAT2. A graphical representation of each section of the molecule that must be conserved in order to maintain affinity for VMAT2 is shown in Figure 1.9.

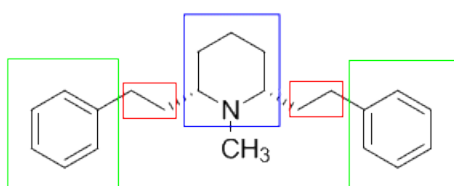


Figure 1.10 Graphical representation of the lobelane scaffold depicting the parts of the molecule that are essential for binding to VMAT2

Three distinct sections of the lobelane scaffold have been shown to be important with respect to binding to VMAT2. First, a cationic nitrogen moiety must be present

(depicted in Figure 1.9 in blue), and preferably the nitrogen atom is located inside a cyclic system such as the piperidine ring. Second, two hydrophobic moieties must be present (depicted in Figure 1.9 in green), preferably both phenyl rings. Substitution of the phenyl rings with fluoro or methoxy moieties can improve affinity for the VMAT2 binding site. Third, the cationic site and the two hydrophobic sites must be linked together via methylene linkers (depicted in Figure 1.9 in red) of at least two methylene units in length. The methylene linkers can be attached at the 2,6 or 1,4 positions on the central nitrogen containing ring without a decrease in binding affinity for the VMAT2 binding site.

1.11 Modification and optimization of the lobelane scaffold

With the data from all six stages of lobelane scaffold modifications in hand, three structural groups within the library of compounds appear to be prime candidates for optimization and further exploration. These three areas are 1.) further studies on the design and synthesis of structural analogs of lobelane that maintain the 2,6-substituted piperidine scaffold but introduced preferred moieties, i.e. chloro, fluoro, or methoxy moieties, into the phenyl rings present in lobelane, 2.) further studies into structural analogs of lobelane that move the phenethyl linkers present in the 2,6-substituted position on the piperidine ring in lobelane to the 1,4-substituted position could be designed and synthesized that also include the preferred moieties, i.e. chloro, fluoro, or methoxy moieties to enhance their affinity and function at VMAT2, and 3.) further studies into lobelane analogs that introduce an additional nitrogen atom into the piperidine ring of the

lobelane scaffold that would increase water- solubility while maintaining similar affinity for VMAT2. These three areas are explored in Chapters 2, 3, and 4, and have become the main focus of this work.

Chapter 2.

Synthesis of 2,6-disubstituted piperidine analogs structurally related to lobelane

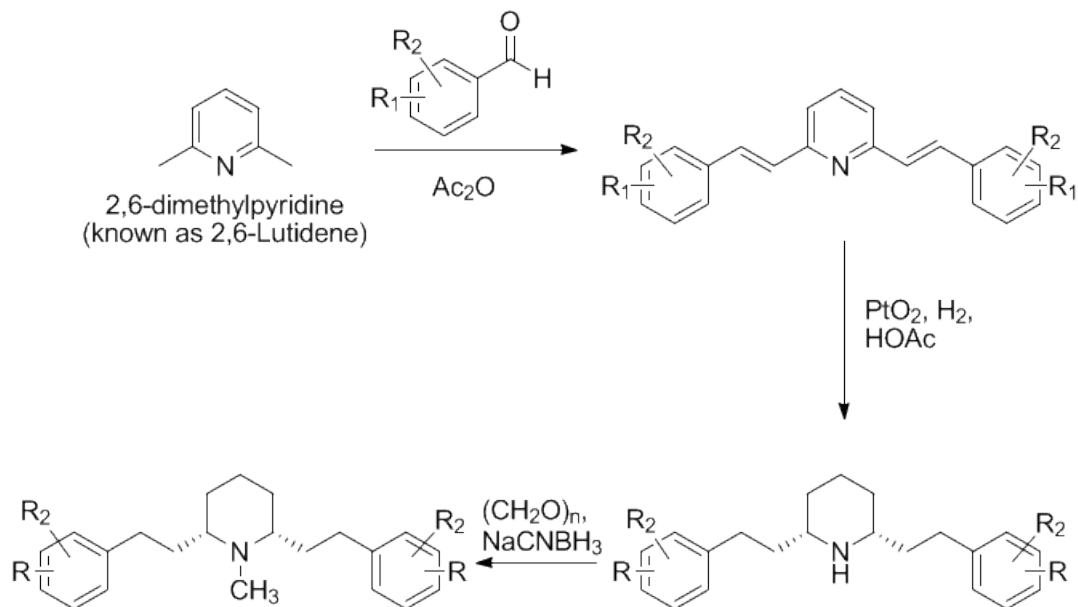
2.1 Prior studies with this scaffold

As discussed in Chapter 1 of this dissertation, (section 1.8), a series of 28 symmetrical 2,6-substituted lobelane analogs have previously been synthesized and their affinities at $\alpha 4\beta 2^*$ & $\alpha 7^*$ nAChRs and at the TBZ binding site on VMAT2 have been evaluated. All of the compounds within this series had either lower or comparable affinities at $\alpha 4\beta 2^*$ & $\alpha 7^*$ nAChRs when compared to lobelane, with the exception of compounds 29a ((2*S*,6*R*)-2,6-*bis*(2-(biphenyl-4-yl)ethyl)piperidine) and 33a ((2*S*,6*R*)-2,6-*bis*(2-(naphthalen-2-yl)ethyl)piperidine), which were both *nor*-analogs with bulky biphenyl (compound 29a) and 2-naphthyl (compound 33a) aromatic rings incorporated into the molecule in place of the phenyl moieties. These compounds had comparable affinity to lobelane at VMAT2. Analogs 20b ((2*S*,6*R*)-2,6-*bis*(3-fluorophenethyl)-1-methylpiperidine), 22b ((2*S*,6*R*)-2,6-*bis*(2-methoxyphenethyl)-1-methylpiperidine), and 23b ((2*S*,6*R*)-2,6-*bis*(3-methoxyphenethyl)-1-methylpiperidine) had the highest affinity for VMAT2 with K_i values of 0.57, 0.58, and 0.43 μ M respectively. Also the *N*-methyl analogs consistently exhibited higher affinity at VMAT2 when compared to the corresponding *nor*-counterparts.

2.2 Design and synthesis of the 2,6-disubstituted piperidine scaffold

Further optimization and study was needed to ascertain if addition of different substituents into the phenyl ring would enhance binding affinity at VMAT2. Addition of two substituents into the phenyl ring was also explored in order to determine if multiple substituents could also improve affinity. The synthesis of eighteen compounds in this

series was accomplished. The general synthetic scheme that was utilized is shown in Scheme 2.1, and the structures and analytical data follow in Figures 2.1 through 2.18.



Scheme 2.1 Synthesis of the 2,6-substituted piperidine analog scaffold of lobelane

The general synthetic scheme begins with 2,6-dimethylpyridine as the starting material, which is subjected to condensation reaction conditions with the appropriate mono-substituted or di-substituted aryl aldehyde. This affords the appropriate crude 2,6-distyrylpyridine compound (purified by crystallization or via silica column chromatography), which was then exposed to acidic hydrogenation conditions with Adam's catalyst (platinum(IV)oxide) and hydrogen gas in acetic acid. After 18-72 hours, depending on the aromatic substitution pattern of the distyrylpyridine, the reaction yields the appropriate *nor*-(2*S*,6*R*)-2,6-diphenethylpiperidine (purified via silica column chromatography), as the meso-isomer (cis stereochemistry at the C2 and C6 positions on the piperidine ring). *N*-methylation was accomplished by exposing the *nor*-compounds to reductive amination conditions with paraformaldehyde and sodium cyanoborohydride in

methanol to generate lobelane analogs containing the *N*-methyl moiety (purified by silica column chromatography). The structures of the compounds synthesized in this series and the structural analytical data for each compound are shown in Figures 2.1 through 2.20. NMR spectra were recorded in either CDCl₃ or DMSO-d₆ (as designated) on one of three Varian instruments (300 MHz, 400 MHz, or 500 MHz) as indicated are reported in ppm relative to either TMS as internal standard or as relative to the solvent peak present in ¹³C spectra. GC-mass spectra were recorded on an Agilent 6890 GC incorporating an Agilent 7683 autosampler and an Agilent 5973 MSD. All compounds were converted to their hydrochloric acid salts prior to submission for pharmacological evaluation. A detailed example of the procedure used in the synthesis of the 2,6-substituted piperidine series of lobelane analogs follows (example procedure is for the synthesis of JPC-001 and JPC-011).

Condensation reaction procedure: To a clean, dry 250 ml round bottom flask equipped with a magnetic stirbar and a water jacketed condenser was added 3.772 grams (0.0352 moles) of 2,6-lutidine, 10.0 grams (0.071 moles) of 3,5-difluorobenzaldehyde, and 10 ml of acetic anhydride. The reaction mass was heated to reflux and maintained at reflux for 72 hours. The reaction was then cooled to room temperature and the excess solvent was removed under vacuum. The gummy residue was purified via silica column chromatography (300 grams of 400 mesh silica) utilizing a 10:1 mixture of hexane:ethyl acetate. The excess solvent was removed from the product fraction via vacuum, and a solid white product was isolated. The product (2,6-bis(3,5-difluorostyryl)pyridine) was isolated in 52% yield (6.5 grams (0.0183 moles)).

Hydrogenation reaction procedure: 2.0 grams (5.63 mmol) of the product of the condensation reaction (2,6-bis(3,5-difluorostyryl)pyridine) was placed in a clean, dry 250 ml Parr hydrogenation flask and brought into solution with 50 ml of concentrated acetic acid. To this was added 0.5 mole % (6.3 mg (0.0282 mmol)) of Adam's catalyst (platinum (IV) oxide). This heterogeneous catalyst reaction mass was placed on a Parr hydrogenator and purged three times with hydrogen gas with shaking. The reaction was then pressurized to 50 psi (3.45 atm) with hydrogen gas under room temperature. The Parr hydrogenator's shaking function was used and the reaction allowed to proceed for 18 hours. The pressure was then released and the reaction was filtered through a pad of celite to remove the platinum catalyst. The remaining filtrate was subjected to reduced pressure under vacuum to remove excess acetic acid. The reaction mass was then basified with a saturated solution of sodium bicarbonate in water, and extracted three times with dichloromethane. The organic layer was dried with sodium sulfate, filtered, and the dichloromethane removed under reduced pressure. The remaining gummy residue was purified via column chromatography (60 grams of silica (400 mesh)) utilizing a solvent mixture of 50:1:0.2 chloroform: methanol: ammonium hydroxide. The product fractions were combined, and the solvent removed via vacuum to yield 1.52 grams (4.16 mmol (73.9% isolated yield) of (2*S*,6*R*)-2,6-*bis*(3,5-difluorophenethyl)piperidine (JPC-001) as a gummy material. The purified product was converted to the hydrochloride salt by dissolving the gum residue in a minimum amount of dichloromethane and adding 1.0 M hydrochloric acid in dry diethyl ether dropwise until a precipitate formed. This reaction mass was stirred for four hours at room

temperature and the excess solvent removed via reduced pressure. The residue was triturated in dry diethyl ether until a white powder of the hydrochloride salt of the product formed. The powder was filtered off and dried under vacuum overnight to yield 1.35 grams (3.36 mmol) of (2S,6R)-2,6-bis(3,5-difluorophenethyl)piperidinium chloride in 80.75% isolated yield.

Reductive amination procedure: 1.0 grams (2.49 mmol) of (2S,6R)-2,6-bis(3,5-difluorophenethyl)piperidinium chloride product was added to a clean, dry 50 ml round bottom flask and brought into solution with 10 ml of methanol. 210 mg (2.49 mmol) of dry sodium bicarbonate was added to the solution and stirred for thirty minutes to convert the hydrochloride salt to the freebase form. To the reaction mass was added five equivalents of sodium cyanoborohydride (783 mg (12.45 mmol)) and ten equivalents (748 mg (24.9 mmol)) of paraformaldehyde, and this reaction was stirred under room temperature for 18 hours. The excess solvent was then removed via reduced pressure and the reaction mass was subjected to extraction with saturated sodium chloride in water and dichloromethane three times. The organic layer was then collected, combined, and dried with sodium sulfate and filtered. The excess dichloromethane was removed under reduced pressure to yield a gummy residue which was purified via silica column chromatography (30 grams of silica (400 mesh)) via a solvent mixture of 50:1:0.2 chloroform:methanol: ammonium hydroxide. The product fractions were combined, and the solvent removed via reduced pressure to yield the pure product (2S,6R)-2,6-bis(3,5-difluorophenethyl)-1-methylpiperidine (JPC-011) as a gummy material. The yield of the product was (746 mg (1.97 mmol) or 79% yield. The freebase product was a gummy, oily residue and was therefore brought up in a minimum volume of dichloromethane to

which 1.0 M hydrochloric acid in dry diethyl ether was added until a precipitate began to form. This mixture was stirred under room temperature for four hours at which time the solvent was removed via reduced pressure. The residue was triturated with dry diethyl ether until a white powder of the hydrochloride salt formed. The powder was filtered off and dried under vacuum to yield 594 mg (1.43 mmol) of (2S,6R)-2,6-bis(3,5-difluorophenethyl)-1-methylpiperidinium chloride resulting in a 72.5% isolated yield for the hydrochloride salt formation.

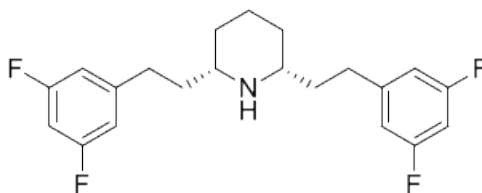


Figure 2.1 Structure of (2*S*,6*R*)-2,6-*bis*(3,5-difluorophenethyl)piperidine (JPC-001)

Chemical Formula: C₂₁H₂₃F₄N Molecular Weight: 365.41

This molecule was designed to evaluate the effect of 3,5-difluoro substituents on VMAT2 binding. Since the fluoro-moieties are very electronegative they cause inductive withdrawal, or withdrawal of electrons from the phenyl rings, but since the fluoro-moieties have non-bonding electrons they can donate electron density through pi bonding or resonance donation. The synthesis utilized 2,6-dimethylpyridine as the starting material, which was subjected to Aldol condensation with 3,5-difluorobenzaldehyde to yield 2,6-*bis*(3,5-difluorostyryl)pyridine. Catalytic hydrogenation of the styryl intermediate afforded (2*S*,6*R*)-2,6-*bis*(3,5-difluorophenethyl)piperidine (JPC-001).

¹H NMR (500 MHz, CDCl₃): δ 1.28-1.81 (m, 10H), 2.11 (s, 1H), 2.33-2.41 (m, 2H), 2.70 (t, 4H), 6.53-6.62 (m, 2H), 6.68-6.73 (m, 4H) ppm.

¹³C NMR (125 MHz, CDCl₃): δ 25.3, 31.9, 32.3, 35.6, 63.1, 101.8, 113.6, 147.1, 164.2 ppm.

MS (EI) m/z 365 (M⁺).

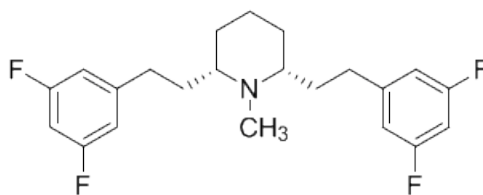


Figure 2.2 Structure of *(2S,6R)*-2,6-*bis*(3,5-difluorophenethyl)-1-methylpiperidine (JPC-011) Chemical Formula: C₂₂H₂₅F₄N Molecular Weight: 379.43

This molecule was designed to evaluate the effect of 3,5-difluoro substitution of lobelane on VMAT2 binding similar to JPC-001, but to also preserve the *N*-methyl substituent on the amine. *(2S,6R)*-2,6-*bis*(3,5-difluorophenethyl)piperidine (JPC-001) was *N*-methylated by exposed to reductive amination conditions with paraformaldehyde and sodium cyanoborohydride in methanol to provide *N*-methylated *(2S,6R)*-2,6-*bis*(3,5-difluorophenethyl)-1-methylpiperidine (JPC-011).

¹H NMR (500 MHz, CDCl₃): δ 1.31-1.84 (m, 10H), 2.14 (s, 3H), 2.36-2.40 (m, 2H), 2.66 (t, 4H), 6.59-6.64 (m, 2H), 6.71-6.74 (m, 4H) ppm.

¹³C NMR (125 MHz, CDCl₃): δ 25.5, 31.8, 32.3, 35.9, 40.5, 62.4, 101.5, 111.6, 147.4, 164.5 ppm.

MS (EI) m/z 379 (M⁺).

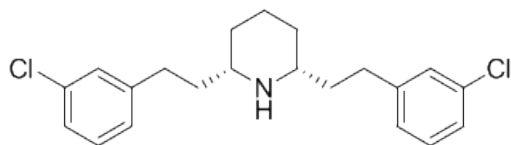


Figure 2.3 Structure of (2*S*,6*R*)-2,6-*bis*(3-chlorophenethyl)piperidine (JPC-002)

Chemical Formula: C₂₁H₂₅Cl₂N Molecular Weight: 362.34

This molecule was designed to evaluate the effect of the 3-chloro substitution of lobelane on VMAT2 binding. The chlorine atom is an electron-withdrawing aromatic substituent and can cause similar inductive and resonance based electron effects on the phenyl rings as the fluoro substituent, however the chlorine atom is larger in radius, and slightly more polarizable than the fluoro moiety. The synthesis began with 2,6-dimethylpyridine as the starting material, which was subjected to Aldol condensation with 3-chlorobenzaldehyde to yield 2,6-*bis*(3-chlorostyryl)pyridine. Subsequent catalytic hydrogenation afforded (2*S*,6*R*)-2,6-*bis*(3-chlorophenethyl)piperidine (JPC-002). However, during hydrogenation, reductive dechlorination occurred, leading to a difficult separation and very little JPC-002 was isolated, even when scaled up to larger reaction amounts. For this reason alone, the *N*-methyl analog was not prepared.

¹H NMR (300 MHz, CDCl₃): δ 1.37-1.78 (m, 10H), 2.11 (s, 1H), 2.33-2.41 (m, 2H), 2.60 (t, 4H), 7.13-7.21 (m, 2H), 7.34-7.46 (m, 4H), 7.51, (s, 2H) ppm.

¹³C NMR (75 MHz, CDCl₃): δ 22.3, 30.5, 32.8, 35.8, 58.1, 121.6, 121.9, 128.5, 129.1, 136.3, 142.2 ppm.

MS (EI) *m/z* 361 (M⁺).

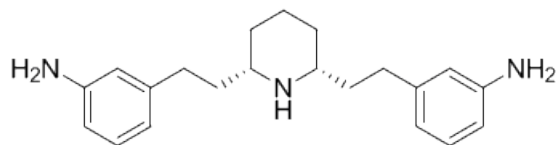


Figure 2.4 Structure of 3,3'-(2,2'-((2*S*,6*R*)-piperidine-2,6-diyl)*bis*(ethane-2,1-diyl))dianiline (JPC-008) Chemical Formula: C₂₁H₂₉N₃ Molecular Weight: 323.48

This molecule was designed to evaluate the effect of introducing a 3-amino substituent into the lobelane scaffold on VMAT2 binding. The amino moiety is an electron donating group that donates some of its electron density into the conjugated π system of the phenyl ring. The 2,6-dimethylpyridine starting material was subjected to Aldol condensation reaction conditions with 3-nitrobenzaldehyde to yield 2,6-bis(3-nitrostyryl)pyridine. Subsequent catalytic hydrogenation afforded the desired compound, 3,3'-(2,2'-((2*S*,6*R*)-piperidine-2,6-diyl)*bis*(ethane-2,1-diyl))dianiline (JPC-008).

¹H NMR (300 MHz, CDCl₃): δ 1.35-1.83 (m, 10H), 2.08 (s, 1H), 2.56 (t, 4H), 2.71 (m, 2H), 5.24 (s, 4H), 6.43-6.48 (m, 2H), 6.59-6.67 (m, 4H), 7.10, (m, 2H)ppm.

¹³C NMR (75 MHz, CDCl₃): δ 21.5, 29.7, 32.3, 35.9, 54.8, 111.6, 114.7, 117.3, 127.1, 138.2, 147.5 ppm.

MS (EI) m/z 323 (M⁺).

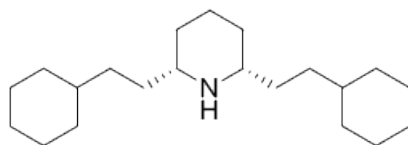


Figure 2.5 Structure of (2*S*,6*R*)-2,6-*bis*(2-cyclohexylethyl)piperidine (JPC-003)

Chemical Formula: C₂₁H₃₉N Molecular Weight: 305.54

This molecule was designed to evaluate the effect of complete saturation of the phenyl rings in *nor*-lobelane to cyclohexyl moieties on VMAT2 binding (Note, this compound and the *N*-methyl derivative has been prepared previously) (Zheng et al., 2005). 2,6-Dimethylpyridine was the starting material, which was subjected to Aldol condensation reaction conditions with benzaldehyde to yield the intermediate 2,6-*bis*(styryl)pyridine. Catalytic hydrogenation with Adam's catalyst (PtO₂) and hydrogen gas afforded of the desired compound, (2*S*,6*R*)-2,6-*bis*(2-cyclohexylethyl)piperidine (JPC-003).

¹H NMR (300 MHz, CDCl₃): δ 1.37-2.38 (m, 36H), 2.05 (s, 1H), 2.67 (m, 2H) ppm.

¹³C NMR (75 MHz, CDCl₃): δ 20.7, 24.7, 25.3, 28.6, 29.8, 32.7, 33.0, 33.1, 49.8 ppm.

MS (EI) *m/z* 305 (M⁺).

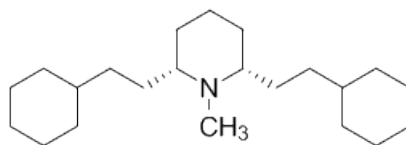


Figure 2.6 Structure of (2*S*,6*R*)-2,6-*bis*(2-cyclohexylethyl)-1-methylpiperidine (JPC-007)

Chemical Formula: C₂₂H₄₁N Molecular Weight: 319.57

This molecule was designed to evaluate the effect of complete saturation of the phenyl rings in Lobeline to cyclohexyl moieties, while preserving the *N*-methyl substituent, on VMAT2 binding. (2*S*,6*R*)-2,6-*bis*(2-cyclohexylethyl)piperidine (JPC-003) was exposed to reductive amination conditions with paraformaldehyde and sodium cyanoborohydride in methanol to afford *N*-methylated (2*S*,6*R*)-2,6-*bis*(2-cyclohexylethyl)-1-methylpiperidine (JPC-007).

¹H NMR (300 MHz, CDCl₃): δ 1.45-2.34 (m, 36H), 2.08 (m, 2H), 2.17 (s, 3H) ppm.

¹³C NMR (75 MHz, CDCl₃): δ 21.1, 24.9, 25.6, 28.7, 29.6, 32.9, 33.4, 33.9, 38.8, 54.6 ppm.

MS (EI) m/z 319 (M⁺).

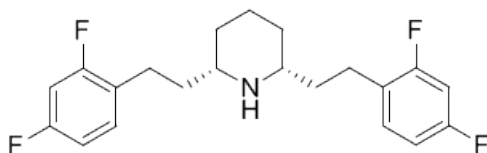


Figure 2.7 Structure of (2*S*,6*R*)-2,6-*bis*(2,4-difluorophenethyl)piperidine (JPC-130a)

Chemical Formula: C₂₁H₂₃F₄N Molecular Weight: 365.41

This molecule was designed to evaluate the effect of introducing 2,4-difluoro aromatic substituents into the *nor*-lobelane structure on VMAT2 binding. Again, since the fluoro-substituents are electronegative they cause inductive withdrawal of electrons from the aromatic ring, but since the fluoro-moieties have non-bonding electrons they can also donate electron density through pi bonding or resonance donation. Synthesis began with 2,6-dimethylpyridine as the starting material, which was subjected to Aldol condensation reaction conditions with 2,4-difluorobenzaldehyde to yield 2,6-*bis*(2,4-difluorostyryl)pyridine. Catalytic hydrogenation with Adam's catalyst (PtO₂) and hydrogen gas afforded the desired product, (2*S*,6*R*)-2,6-*bis*(2,4-difluorophenethyl)piperidine (JPC-130a).

¹H NMR (500 MHz, CDCl₃): δ 1.28-1.73 (m, 10H), 2.17 (s, 1H), 2.30-2.41 (m, 2H), 2.73 (t, 4H), 6.60-6.67 (m, 2H), 6.87-6.95 (m, 2H), 7.17-7.23 (m, 2H) ppm.

¹³C NMR (125 MHz, CDCl₃): δ 24.3, 25.6, 31.7, 32.3, 60.3, 101.8, 109.4, 120.9, 128.9, 161.1, 164.2 ppm.

MS (EI) m/z 365 (M⁺).

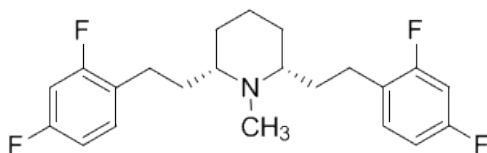


Figure 2.8 Structure of (2*S*,6*R*)-2,6-*bis*(2,4-difluorophenethyl)-1-methylpiperidine (JPC-130b) Chemical Formula: C₂₂H₂₅F₄N Molecular Weight: 379.43

This molecule was designed to evaluate the effect of introducing 2,4-difluoro aromatic substituents into lobelane on VMAT2 binding, while retaining the *N*-methyl substituent on the piperidine ring. (2*S*,6*R*)-2,6-*bis*(2,4-difluorophenethyl)piperidine (JPC-130a) was exposed to reductive amination conditions with paraformaldehyde and sodium cyanoborohydride in methanol to provide the desired compound, *N*-methylated (2*S*,6*R*)-2,6-*bis*(2,4-difluorophenethyl)-1-methylpiperidine (JPC-130b).

¹H NMR (500 MHz, CDCl₃): δ 1.35-1.76 (m, 10H), 2.15 (s, 3H), 2.35 (m, 2H), 2.65 (t, 4H), 6.73-6.78 (m, 4H), 7.13-7.15 (m, 2H) ppm.

¹³C NMR (125 MHz, CDCl₃): δ 25.1, 25.2, 26.8, 29.9, 34.9, 62.6, 103.7, 111.0, 122.7, 131.3, 160.6, 162.5 ppm.

MS (EI) m/z 379 (M⁺).

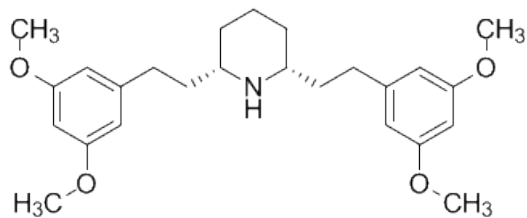


Figure 2.9 Structure of (2*S*,6*R*)-2,6-*bis*(3,5-dimethoxyphenethyl)piperidine (JPC-004)

Chemical Formula: C₂₅H₃₅NO₄ Molecular Weight: 413.55

This molecule was designed to evaluate the effect of introducing 3,5-dimethoxy aromatic substituents into the *nor*-lobelane molecule on VMAT2 binding. Since the methoxy substituents are electronegative they cause inductive withdrawal, or withdrawal of electrons from the carbon atom of benzene, but since they also have non-bonding electrons they can donate electron density through pi bonding or resonance donation. The methoxy group is substantially larger than fluoro group in the previous compounds, and will provide some steric effects at the binding site of VMAT2, if space on the site is limited around the phenyl ring binding regions. The starting material, 2,6-dimethylpyridine was reacted with 3,5-dimethoxybenzaldehyde under Aldol condensation reaction conditions to yield 2,6-*bis*(3,5-dimethoxystyryl)pyridine. Catalytic hydrogenation with Adam's catalyst (PtO₂) and hydrogen gas afforded (2*S*,6*R*)-2,6-*bis*(3,5-dimethoxyphenethyl)piperidine (JPC-004).

¹H NMR (300 MHz, CDCl₃): δ 1.33-1.82 (m, 10H), 2.20 (s, 1H), 2.41 (m, 2H), 2.65 (t, 4H), 3.78 (s, 12H), 6.52-6.64 (m, 6H) ppm.

¹³C NMR (75 MHz, CDCl₃): δ 21.6, 29.6, 32.6, 39.9, 55.6, 58.3, 97.2, 106.3, 143.9, 160.1 ppm.

MS (EI) m/z 413 (M⁺).

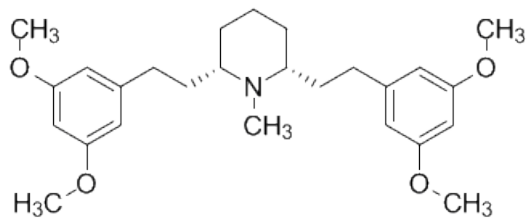


Figure 2.10 Structure of *(2S,6R)*-2,6-*bis*(3,5-dimethoxyphenethyl)-1-methylpiperidine (JPC-010) Chemical Formula: $C_{26}H_{37}NO_4$ Molecular Weight: 427.58

This molecule was designed to evaluate the effect of introducing 3,5-dimethoxy aromatic substituents into the lobelane scaffold on VMAT2 binding, while retaining the *N*-methyl substituent on the piperidine ring. *(2S,6R)*-2,6-*bis*(3,5-dimethoxyphenethyl)piperidine (JPC-004) was exposed to reductive amination conditions with paraformaldehyde and sodium cyanoborohydride in methanol to afford *(2S,6R)*-2,6-*bis*(3,5-dimethoxyphenethyl)-1-methylpiperidine (JPC-010).

^1H NMR (300 MHz, CDCl_3): δ 1.26-1.87 (m, 10H), 2.22 (s, 3H), 2.35 (m, 2H), 2.63 (t, 4H), 3.78 (s, 12H), 6.31-6.36 (m, 6H) ppm.

^{13}C NMR (75 MHz, CDCl_3): δ 21.6, 29.6, 30.9, 32.6, 33.1, 39.9, 55.2, 97.9, 106.2, 144.8, 160.6 ppm.

MS (EI) m/z 427 (M^+).

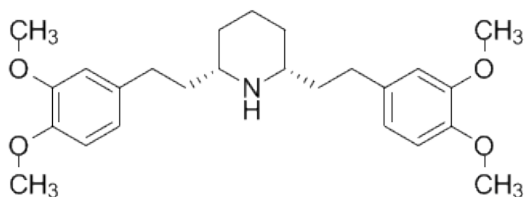


Figure 2.11 Structure of (2*S*,6*R*)-2,6-bis(3,4-dimethoxyphenethyl)piperidine (JPC-033)

Chemical Formula: C₂₅H₃₅NO₄ Molecular Weight: 413.55

This molecule was designed to evaluate the effect of introducing 3,4-dimethoxy aromatic substituents into the *nor*-lobelane scaffold on VMAT2 binding. Synthesis began with 2,6-dimethylpyridine as the starting material, which was subjected to Aldol condensation with 3,4-dimethoxybenzaldehyde to yield 2,6-*bis*(3,4-dimethoxystyryl)pyridine. Catalytic hydrogenation afforded (2*S*,6*R*)-2,6-*bis*(3,4-dimethoxyphenethyl)piperidine (JPC-033).

¹H NMR (300 MHz, CDCl₃): δ 1.30-1.75 (m, 10H), 2.17 (s, 1H), 2.49 (m, 2H), 2.57 (t, 4H), 3.79 (s, 12H), 6.72-6.87 (m, 6H) ppm.

¹³C NMR (75 MHz, CDCl₃): δ 23.6, 29.3, 31.2, 35.9, 55.3, 62.4, 107.9, 111.5, 119.9, 134.5, 146.2, 148.1 ppm

MS (EI) m/z 413 (M⁺).

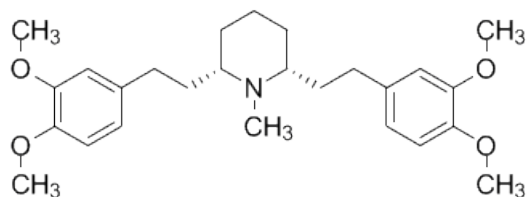


Figure 2.12 Structure of (2*S*,6*R*)-2,6-*bis*(3,4-dimethoxyphenethyl)-1-methylpiperidine

(JPC-034) Chemical Formula: C₂₆H₃₇NO₄ Molecular Weight: 427.58

This molecule was designed to evaluate the effect of introducing 3,4-dimethoxy aromatic substituents into the lobelane scaffold on VMAT2 binding, while retaining the *N*-methyl moiety on the piperidine ring. The synthesis utilized (2*S*,6*R*)-2,6-*bis*(3,4-dimethoxyphenethyl)piperidine (JPC-033) which was exposed to reductive amination conditions with paraformaldehyde and sodium cyanoborohydride in methanol to afford (2*S*,6*R*)-2,6-*bis*(3,4-dimethoxyphenethyl)-1-methylpiperidine (JPC-034).

¹H NMR (300 MHz, CDCl₃): δ 1.30-1.95 (m, 10H), 2.20 (s, 3H), 2.45 (m, 2H), 2.61 (t, 4H), 3.86 (s, 12H), 6.76 (m, 6H) ppm.

¹³C NMR (75 MHz, CDCl₃): δ 24.8, 26.3, 30.2, 31.9, 36.3, 55.7, 62.4, 110.9, 111.5, 119.9, 135.0, 146.7, 148.4 ppm.

MS (EI) *m/z* 427 (M⁺).

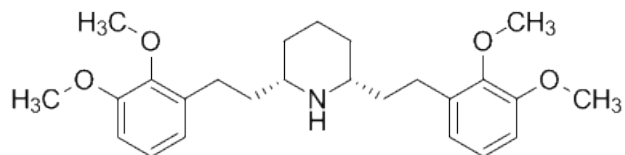


Figure 2.13 Structure of (2*S*,6*R*)-2,6-*bis*(2,3-dimethoxyphenethyl)piperidine (JPC-035)

Chemical Formula: C₂₅H₃₅NO₄ Molecular Weight: 413.55

This molecule was designed to evaluate the effect of introducing 2,3-dimethoxy aromatic substituents into the nor-lobelane scaffold on VMAT2 binding. The starting material, 2,6-dimethylpyridine, was subjected to Aldol condensation with 2,3-dimethoxybenzaldehyde to yield 2,6-*bis*(2,3-dimethoxystyryl)pyridine. Catalytic hydrogenation with Adam's catalyst (PtO₂) and hydrogen gas afforded (2*S*,6*R*)-2,6-*bis*(2,3-dimethoxyphenethyl)piperidine (JPC-035).

¹H NMR (300 MHz, CDCl₃): δ 1.30-1.85 (m, 10H), 2.13 (s, 1H), 2.41 (m, 2H), 2.62 (t, 4H), 3.81 (s, 12H), 6.77-6.94 (m, 6H) ppm.

¹³C NMR (75 MHz, CDCl₃): δ 23.4, 25.7, 27.8, 33.1, 55.9, 60.7, 62.2, 111.2, 121.1, 123.0, 130.1, 146.1, 152.0 ppm.

MS (EI) *m/z* 413 (M⁺).

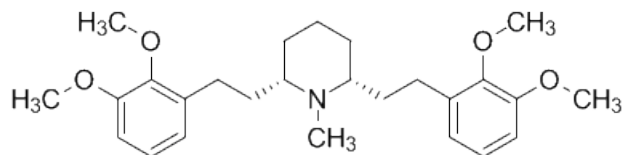


Figure 2.14 Structure of (2*S*,6*R*)-2,6-*bis*(2,3-dimethoxyphenethyl)-1-methylpiperidine

(JPC-036) Chemical Formula: C₂₆H₃₇NO₄ Molecular Weight: 427.58

This molecule was designed to evaluate the effect of introducing 2,3-dimethoxy aromatic substituents into the lobelane scaffold on VMAT2 binding, while retaining the *N*-methyl moiety on the piperidine ring. (2*S*,6*R*)-2,6-*bis*(2,3-dimethoxyphenethyl)piperidine (JPC-035) was exposed to reductive amination conditions with paraformaldehyde and sodium cyanoborohydride in methanol to afford (2*S*,6*R*)-2,6-*bis*(2,3-dimethoxyphenethyl)-1-methylpiperidine (JPC-036).

¹H NMR (300 MHz, CDCl₃): δ 1.30-1.95 (m, 10H), 2.27 (s, 3H), 2.45 (m, 2H), 2.68 (t, 4H), 3.83 (s, 12H), 6.77-6.98 (m, 6H) ppm.

¹³C NMR (75 MHz, CDCl₃): δ 24.6, 26.4, 27.0, 31.0, 35.2, 55.5, 60.5, 63.2, 109.8, 121.7, 123.6, 136.1, 146.7, 152.4 ppm

MS (EI) *m/z* 427 (M⁺).

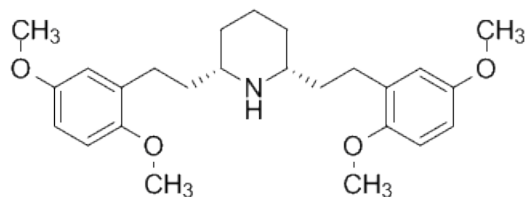


Figure 2.15 Structure of (2*S*,6*R*)-2,6-*bis*(2,5-dimethoxyphenethyl)piperidine (JPC-041)

Chemical Formula: C₂₅H₃₅NO₄ Molecular Weight: 413.55

This molecule was designed to evaluate the effect of introducing 2,5-dimethoxy aromatic substituents into *nor*-lobelane on VMAT2 binding. 2,6-Dimethylpyridine was subjected to Aldol condensation with 2,5-dimethoxybenzaldehyde to yield 2,6-*bis*(2,5-dimethoxystyryl)pyridine. Catalytic hydrogenation with Adam's catalyst (PtO₂) and hydrogen gas afforded (2*S*,6*R*)-2,6-*bis*(2,5-dimethoxyphenethyl)piperidine (JPC-041).
¹H NMR (300 MHz, CDCl₃): δ 1.39-1.85 (m, 10H), 2.21 (s, 1H), 2.35 (m, 2H), 2.65 (t, 4H), 3.74 (s, 12H), 6.63-6.76 (m, 6H) ppm.

¹³C NMR (75 MHz, CDCl₃): δ 22.3, 26.2, 31.9, 34.9, 55.1, 55.7, 62.9, 110.4, 110.6, 110.8, 116.0, 132.3, 151.4, 153.1 ppm.

MS (EI) m/z 413 (M⁺).

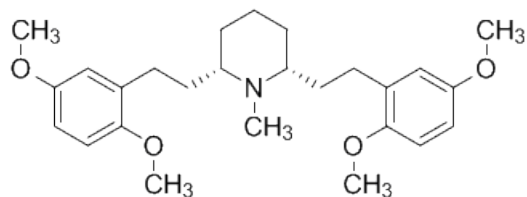


Figure 2.16 Structure of (2*S*,6*R*)-2,6-*bis*(2,5-dimethoxyphenethyl)-1-methylpiperidine

(JPC-042) Chemical Formula: C₂₆H₃₇NO₄ Molecular Weight: 427.58

This molecule was designed to evaluate the effect of introducing 2,5-dimethoxy aromatic substituents into the lobelane scaffold on VMAT2 binding, while retaining the *N*-methyl moiety on the piperidine ring. (2*S*,6*R*)-2,6-*bis*(2,5-dimethoxyphenethyl)piperidine (JPC-041) which was exposed to reductive amination conditions with paraformaldehyde and sodium cyanoborohydride in methanol to afford (2*S*,6*R*)-2,6-*bis*(2,5-dimethoxyphenethyl)-1-methylpiperidine (JPC-041).

¹H NMR (300 MHz, CDCl₃): δ 1.25-1.90 (m, 10H), 2.20 (s, 3H), 2.35 (m, 2H), 2.63 (t, 4H), 3.72 (s, 12H), 6.63-6.76 (m, 6H) ppm.

¹³C NMR (75 MHz, CDCl₃): δ 25.0, 27.0, 27.2, 31.2, 34.7, 55.4, 55.7, 62.9, 110.4, 110.8, 116.0, 132.3, 151.4, 153.1 ppm.

MS (EI) m/z 427 (M⁺).

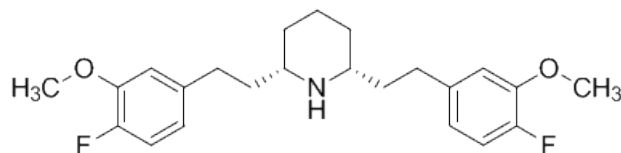


Figure 2.17 Structure of (2*S*,6*R*)-2,6-*bis*(4-fluoro-3-methoxyphenethyl)piperidine

(JPC-161b) Chemical Formula: C₂₃H₂₉F₂NO₂ Molecular Weight: 389.48

This molecule was designed to evaluate the effect of introducing 4 fluoro,3-methoxy aromatic substituents on VMAT2 binding. 2,6-Dimethylpyridine was subjected to Aldol condensation with 4-fluoro-3-methoxybenzaldehyde to yield 2,6-*bis*(4-fluoro-3-methoxystyryl)pyridine. Subsequent catalytic hydrogenation with Adam's catalyst (PtO₂) and hydrogen gas afforded (2*S*,6*R*)-2,6-*bis*(4-fluoro-3-methoxyphenethyl)piperidine (JPC-161b).

¹H NMR (300 MHz, CDCl₃): δ 1.30-1.75 (m, 10H), 2.09 (s, 1H), 2.53 (m, 2H), 2.62 (t, 4H), 3.81 (s, 6H), 6.72-7.10 (m, 6H) ppm.

¹³C NMR (75 MHz, CDCl₃): δ 22.6, 29.9, 32.3, 36.5, 55.3, 61.4, 109.7, 114.1, 123.9, 136.1, 148.4, 148.6 ppm.

MS (EI) m/z 389 (M⁺).

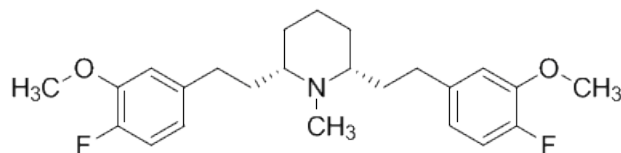


Figure 2.18 Structure of (2*S*,6*R*)-2,6-*bis*(4-fluoro-3-methoxyphenethyl)-1-methylpiperidine (JPC-161c)

Chemical Formula: C₂₄H₃₁F₂NO₂ Molecular Weight: 403.51

This molecule was designed to evaluate the effect of introducing 4 fluoro,3-methoxy aromatic substituents into the lobelane scaffold on VMAT2 binding while retaining the *N*-methyl moiety on the piperidine ring. (2*S*,6*R*)-2,6-*bis*(4-fluoro-3-methoxy-phenethyl)piperidine (JPC-161b) was exposed to reductive amination with paraformaldehyde and sodium cyanoborohydride in methanol to afford (2*S*,6*R*)-2,6-*bis*(4-fluoro-3-methoxyphenethyl)-1-methylpiperidine (JPC-161c).

¹H NMR (300 MHz, CDCl₃): δ 1.35-1.75 (m, 10H), 2.17 (s, 3H), 2.43 (m, 2H), 2.58 (t, 4H), 3.87 (s, 6H), 6.70-7.10 (m, 6H) ppm.

¹³C NMR (75 MHz, CDCl₃): δ 21.9, 30.2, 31.9, 34.5, 38.2, 55.8, 61.9, 111.3, 114.0, 123.7, 138.1, 148.2, 148.5 ppm.

MS (EI) m/z 403 (M⁺).

2.3 Summary of the 2,6-disubstituted piperidine analog series

In summary, eighteen compounds were designed and synthesized in the 2,6-disubstituted piperidine scaffold of lobelane, fourteen of which contained two substituents in each of the phenyl rings. These substituents consisted of difluoro-, dimethoxy-, and 4-fluoro-3-methoxyphenyl substituents. Seven of the compounds were analogs of the *nor*-lobelane scaffold, and seven analogs were analogs of the lobelane scaffold. Their affinities for the TBZ site of VMAT2, as well as their functional ability to prevent DA uptake into the vesicles of the dopaminergic neuron are discussed in Chapter 5.

Chapter 3.

Design and Synthesis of 1,4-Disubstituted Piperidine Analogs of lobelane

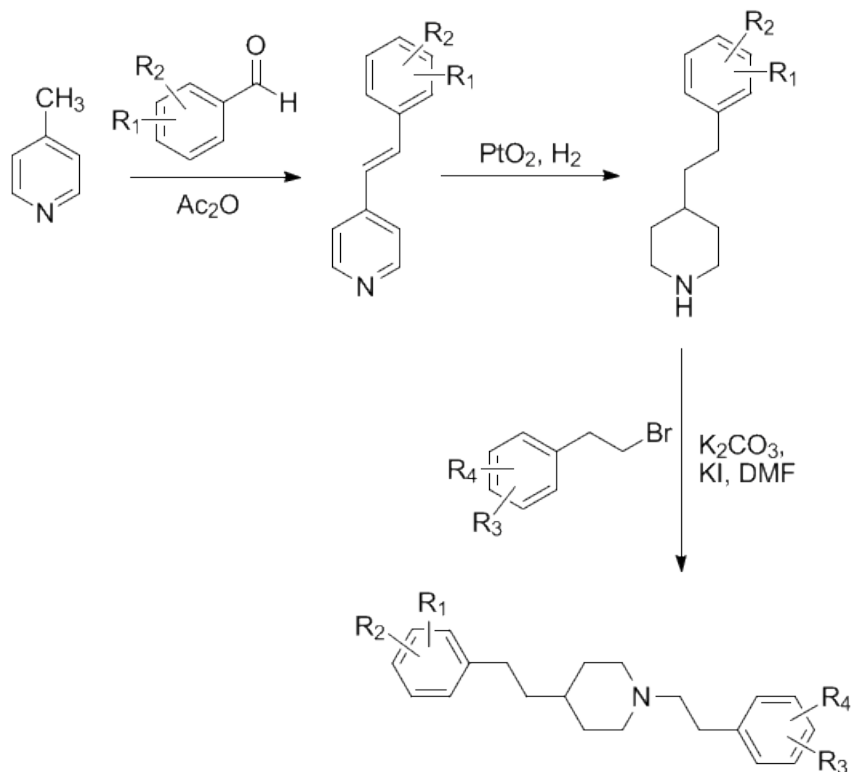
3.1 Prior studies with the 1,4-disubstituted scaffold

As discussed in Chapter 1, (section 1.8), a series of isomerized lobelane analogs have been designed and synthesized. These analogs have different positions of attachment of the phenethyl moieties around the central piperidine ring. Of these structural modifications, the analogs with phenethyl moieties in the N1 and C4 positions of the piperidine ring showed more promise for optimization and further study, since their binding affinities at VMAT2 were quite similar to lobelane, and they exhibited little to no affinity for $\alpha 4\beta 2^*$ & $\alpha 7^*$ nAChRs. The symmetry present in the 1,4-substituted scaffold allows for the relatively fast synthesis of a library of compounds with a variety of substituents in the phenyl rings, and also provides opportunities to explore the introduction of non-aromatic functionalities in place of one of the phenyl rings in lobelane, resulting in analogs with higher polarity improved water solubility characteristics, which is a desirable property in the development of drugs with improved bioavailability over lobelane.

3.2 Design and Synthesis of 1,4-substituted piperidine scaffold analogs

Further optimization and study was needed to ascertain if addition of different substituents into the phenyl rings of the 1,4-substituted lobelane scaffold would enhance binding affinity at VMAT2. Addition of multiple aromatic substituents into the phenyl rings was also explored in order to determine if multiple substituents could also improve affinity. The synthesis of 43 compounds in this series were designed and synthesized.

The general synthetic scheme is shown in Scheme 3.1, and the structures and analytical data follow in Figures 3.1 through 3.43.



Scheme 3.1 Synthetic route to the 1,4-disubstituted piperidine analogs of lobelane

The general synthetic route to the 1,4-disubstituted piperidine analogs of lobelane began with 4-picoline (also known as 4-methylpyridine) as the starting material. Similar chemistry to that used in the 2,6-disubstituted piperidine scaffold was utilized. The starting material was subjected to Aldol condensation with the appropriately substituted benzaldehyde in refluxing acetic anhydride to afford the corresponding (*E*)-4-styrylpyridine intermediate. After purification via silica gel column chromatography, this intermediate was subjected to catalytic hydrogenation with Adam's catalyst and hydrogen gas in acetic acid to afford the appropriately substituted 4-phenethylpiperidine

intermediate, which was then subjected to a S_N2 reaction with potassium carbonate and the appropriately substituted bromoethylbenzene to yield the final 1,4-disubstituted piperidine analogs of lobelane. A detailed example of the procedure used in the synthesis of the 1,4-disubstituted piperidine analogs of lobelane is given below (example is for JPC-077 (1,4-bis(2-methoxyphenethyl)piperidine)). The exact structures of the compounds synthesized and the analytical data for each compound are shown in Figures 3.1 through 3.43. NMR spectra were recorded in either $CDCl_3$ or $DMSO-d_6$ (as designated) on one of three Varian instruments (300 MHz, 400 MHz, or 500 MHz) as indicated are reported in ppm relative to either TMS as internal standard or as relative to the solvent peak present in ^{13}C spectra. GC-mass spectra were recorded on an Agilent 6890 GC incorporating an Agilent 7683 autosampler and an Agilent 5973 MSD. All compounds were converted into their hydrochloride or fumarate salt forms prior to use in pharmacological assay experiments.

Condensation reaction procedure: To a clean, dry 250 ml round bottom flask equipped with a magnetic stirbar and a water jacketed condenser was added 2.30 grams (0.0247 moles) of 3-picoline, 5.044 grams (0.0371 moles) of 2-methoxybenzaldehyde, and 25 ml of acetic anhydride. The reaction mass was heated to reflux and maintained at reflux for 72 hours. The reaction was then cooled to room temperature and the excess solvent was removed under vacuum. The gummy residue was purified via silica column chromatography (200 grams of 400 mesh silica) utilizing a 5:1 mixture of hexane:ethyl acetate. The excess solvent was removed from the product fraction via vacuum, and a

solid off-white product isolated. The product (E)-4-(2-methoxystyryl)pyridine was isolated in 54% yield (2.81 grams (0.0133 moles)).

Hydrogenation reaction procedure: 2.0 grams (9.47 mmol) of the product of the condensation reaction ((E)-4-(2-methoxystyryl)pyridine) was placed in a clean, dry 250 ml Parr hydrogenation flask and brought into solution with 50 ml of concentrated acetic acid. To this was added 0.5 mole % (10.75 mg (0.0473 mmol)) of Adam's catalyst (platinum (IV) oxide). This heterogeneous catalyst reaction mass was placed on a Parr hydrogenator and purged three times with hydrogen gas and shaking. The reaction was then pressurized to 50 psi (3.45 atm) with hydrogen gas under room temperature. The Parr hydrogenator's shaking function was used and the reaction was allowed to proceed for 72 hours. The pressure was then released and the reaction was filtered through a pad of celite to remove the platinum catalyst. The remaining filtrate was subjected to reduced pressure under vacuum to remove excess acetic acid. The reaction mass was then basified with a saturated solution of sodium bicarbonate in water, and extracted three times with dichloromethane. The organic layer was dried with sodium sulfate, filtered, and the dichloromethane removed under reduced pressure. The remaining gummy residue was purified via column chromatography (60 grams of silica (400 mesh)) utilizing a solvent mixture of 10:1:0.2 dichloromethane: methanol: ammonium hydroxide. The product fractions were combined, and the solvent removed via vacuum to yield 1.39 grams (6.35 mmol (67.0% isolated yield) of 4-(2-methoxyphenethyl)piperidine as a gummy material. The purified product was converted to the hydrochloride salt by dissolving the gum residue in a minimum amount of

dichloromethane and adding 1.0 M hydrochloric acid in dry diethyl ether dropwise until a precipitate formed. This reaction mass was stirred for four hours at room temperature and the excess solvent was removed via reduced pressure. The residue was triturated in dry diethyl ether until a white powder of the hydrochloride salt of the product formed. The powder was filtered off and dried under vacuum overnight to yield 1.27 grams (4.97 mmol) of 4-(2-methoxyphenethyl)piperidinium chloride in 78.2% isolated yield.

N-alkylation reaction procedure (S_N2 reaction): To a clean, dry 100 ml round bottomed flask that has been purged with argon gas and equipped with a magnetic stirbar and a water jacketed condenser was added 350 mg (1.37 mmol) of 4-(2-methoxyphenethyl)piperidinium chloride (from the hydrogenation reaction above), 325 mg (1.51 mmol) of 2-methoxyphenethylbromide, and 10 ml of dimethylformamide (DMF) as solvent. To this reaction mass was added 500 mg (3.43 mmol) of potassium carbonate and 11.6 mg (0.07 mmol) of potassium iodide. Under an argon atmosphere the reaction mass was heated in an oil bath (with stirring) to 60° C and maintained at that temperature for 18 hours. The reaction flask was then subjected to reduced pressure while maintaining the heat in the oil bath in order to remove excess DMF from the reaction mixture. The residue from this procedure was subjected to extraction with dichloromethane and saturated sodium chloride (brine solution) in water three times. The organic layers are combined, dried with sodium sulfate, filtered, and the combined filtrate was subjected to reduced pressure to remove the dichloromethane solvent. The residue from this procedure was purified via silica column chromatography (20 g of silica (400 mesh)) utilizing a 20:1 mixture of dichloromethane: methanol. The fractions containing the product were combined and the solvents removed under reduced pressure. The

residue of the pure compound JPC-077 (1,4-bis(2-methoxyphenethyl)piperidine) (356 mg, 1.01 mmol, 73.7% yield) was a thick oil at this stage, so the purified product was converted to the hydrochloride salt by dissolving the gum residue in a minimum amount of dichloromethane and adding 1.0 M hydrochloric acid in dry diethyl ether dropwise until a precipitate formed. This reaction mass was stirred for four hours at room temperature and the excess solvent was removed via reduced pressure. The residue was triturated in dry diethyl ether until a white powder of the hydrochloride salt of the product formed. The powder was filtered off and dried under vacuum overnight to yield 276 mg (0.702 mmol) of (1,4-bis(2-methoxyphenethyl)piperidinium chloride in 70.2% yield.

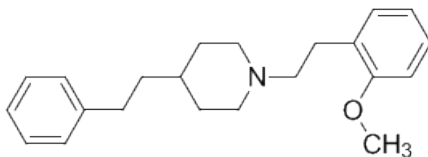


Figure 3.1 Structure of 1-(2-methoxyphenethyl)-4-phenethylpiperidine (JPC-57)

Chemical Formula: $C_{22}H_{29}NO$ Molecular Weight: 323.47

This molecule was designed to evaluate the effect of introducing a 2-methoxy substituent into the phenyl ring of the phenethyl moiety attached to N1 in the 1,4-disubstituted piperidine scaffold on VMAT2 binding. 4-Methylpyridine was subjected to Aldol condensation with benzaldehyde in refluxing acetic anhydride to yield (*E*)-4-styrylpyridine (which was purified via silica column chromatography before use). Catalytic hydrogenation with Adam's catalyst (PtO_2) and hydrogen gas afforded 4-phenethylpiperidine (purified via silica column chromatography before use), which was then reacted via an S_N2 reaction with potassium carbonate and 1-(2-bromoethyl)-2-methoxybenzene to yield the final product, 1-(2-methoxyphenethyl)-4-phenethylpiperidine (JPC-57) (purified via column chromatography).

1H NMR (300 MHz, $CDCl_3$): δ 1.38-1.80 (m, 7H), 2.52-3.01 (m, 10H), 3.78 (s, 3H), 6.83-7.31(m, 9H) ppm.

^{13}C NMR (75 MHz, $CDCl_3$): δ 27.8, 32.7, 34.1, 35.4, 37.0, 54.2, 55.1, 61.1, 110.2, 120.9, 127.1, 127.9, 128.8, 128.9, 129.6, 131.4, 140.7, 157.2 ppm.

MS (EI) m/z 323 (M^+).

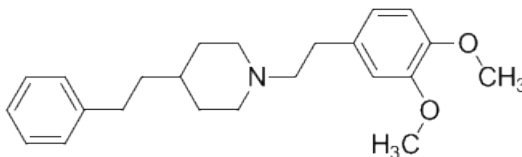


Figure 3.2 Structure of 1-(3,4-dimethoxyphenethyl)-4-phenethylpiperidine (JPC-058)

Chemical Formula: $C_{23}H_{31}NO_2$ Molecular Weight: 353.50

This molecule was designed to evaluate the effect of introducing 3,4-dimethoxy substituents into the phenyl ring of the phenethyl moiety attached to N1 in the 1,4-disubstituted piperidine scaffold on VMAT2 binding. Synthesis began with the common intermediate 4-phenethylpiperidine prepared previously, which was reacted via an S_N2 reaction with potassium carbonate and 1-(2-bromoethyl)-3,4-dimethoxybenzene to yield the final product 1-(3,4-dimethoxyphenethyl)-4-phenethylpiperidine (JPC-058) after purification via silica gel column chromatography.

1H NMR (300 MHz, $CDCl_3$): δ 1.19-2.07 (m, 10H), 2.51-3.07 (m, 7H), 3.81 (s, 6H), 6.70-6.76(m, 5H), 7.11-7.21 (m, 3H) ppm.

^{13}C NMR (75 MHz, $CDCl_3$): δ 29.7, 32.6, 34.1, 35.8, 37.6, 54.0, 55.1, 61.7, 110.4, 111.6, 114.7, 114.8, 120.7, 121.3, 129.1, 129.3, 140.4, 144.1, 157.3 ppm.

MS (EI) m/z 353 (M^+).

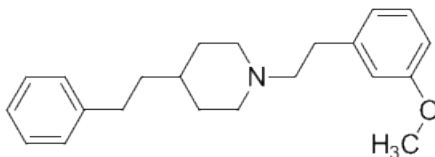


Figure 3.3 Structure of 1-(3-methoxyphenethyl)-4-phenethylpiperidine (JPC-059)

Chemical Formula: $C_{22}H_{29}NO$ Molecular Weight: 323.47

This molecule was designed to evaluate the effect of the introducing the 3-methoxy substituent into the phenyl ring of the phenethyl linker attached to N1 in the 1,4-disubstituted piperidine scaffold on VMAT2 binding. Synthesis began with the common intermediate 4-phenethylpiperidine, which was reacted with potassium carbonate and 1-(2-bromoethyl)-3-methoxybenzene to yield the final product 1-(3-methoxyphenethyl)-4-phenethylpiperidine (JPC-059) after was purification via silica gel column chromatography.

1H NMR (300 MHz, $CDCl_3$): δ 1.24-1.98 (m, 10H), 2.51-2.98 (m, 7H). 3.80 (s, 3H), 6.73-7.23 (m, 9H) ppm.

^{13}C NMR (100 MHz, $CDCl_3$): δ 28.7, 29.3, 32.0, 32.6, 37.2, 38.9, 51.6, 55.0, 56.5, 112.2, 114.3, 120.8, 125.7, 128.2, 128.3, 129.6, 138.9, 141.9, 159.4 ppm.

MS (EI) m/z 323 (M^+).

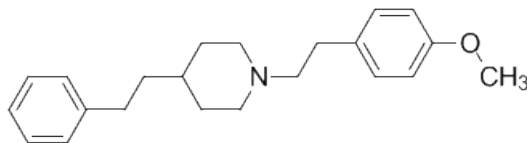


Figure 3.4 Structure of 1-(4-methoxyphenethyl)-4-phenethylpiperidine (JPC-060)

Chemical Formula: $C_{22}H_{29}NO$ Molecular Weight: 323.47

This molecule was designed to evaluate the effect of introducing the 4-methoxy substituent into the phenyl ring of the phenethyl moiety attached to N1 in the 1,4-substituted piperidine scaffold on VMAT2 binding. Synthesis began with the common intermediate 4-phenethylpiperidine, which was reacted via a S_N2 reaction with potassium carbonate and 1-(2-bromoethyl)-4-methoxybenzene to yield the final product 1-(4-methoxyphenethyl)-4-phenethylpiperidine (JPC-060) after purification via silica gel column chromatography.

1H NMR (300 MHz, $CDCl_3$): δ 1.18-1.94 (m, 10H), 2.38-2.95 (m, 7H), 3.82 (s, 3H), 6.78-7.21 (m, 9H) ppm.

^{13}C NMR (100 MHz, $DMSO-d_6$): δ 28.4, 28.7, 32.0, 32.6, 37.2, 38.9, 51.6, 55.0, 56.9, 114.0, 125.7, 128.2, 128.3, 129.1, 129.6, 141.9, 158.0 ppm.

MS (EI) m/z 323 (M^+).

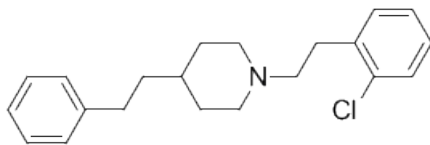


Figure 3.5 Structure of 1-(2-chlorophenethyl)-4-phenethylpiperidine (JPC-072)

Chemical Formula: $C_{21}H_{26}ClN$ Molecular Weight: 327.89

This molecule was designed to evaluate the effect of introducing the 2-chloro substituent into the phenyl ring of the phenethyl linker attached to N1 in the 1,4-substituted piperidine scaffold on VMAT2 binding. 4-Phenethylpiperidine was reacted with potassium carbonate and 1-(2-bromoethyl)-2-chlorobenzene to afford the final product 1-(2-chlorophenethyl)-4-phenethylpiperidine (JPC-072) after purification via silica gel column chromatography.

1H NMR (300 MHz, $CDCl_3$): δ 1.39-1.77 (m, 7H), 2.10-3.09 (m, 10H), 7.08-7.28 (m, 9H) ppm.

^{13}C NMR (75 MHz, $CDCl_3$): δ 31.0, 31.9, 33.3, 35.2, 38.4, 53.9, 58.6, 125.8, 127.1, 127.9, 128.5, 129.6, 131.1, 134.0, 142.6 ppm.

MS (EI) m/z 327 (M^+).

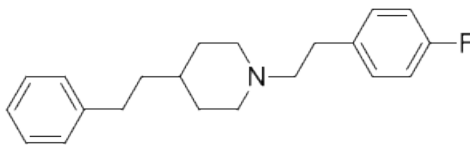


Figure 3.6 Structure of 1-(4-fluorophenethyl)-4-phenethylpiperidine (JPC-073)

Chemical Formula: $C_{21}H_{26}FN$ Molecular Weight: 311.44

This molecule was designed to evaluate the effect of the introducing a 4-chloro substituent into the phenyl ring of the phenethyl linker attached to N1 in the 1,4-disubstituted piperidine scaffold on VMAT2 binding. 4-Phenethylpiperidine was reacted with potassium carbonate and 1-(2-bromoethyl)-4-fluorobenzene to yield the final product, 1-(4-fluorophenethyl)-4-phenethylpiperidine (JPC-073) after purification via silica column chromatography.

1H NMR (300 MHz, $CDCl_3$): δ 1.32-2.01 (m, 10H), 2.51-3.01 (m, 7H), 6.93-6.99 (m, 2H), 7.12-7.31 (m, 7H) ppm.

^{13}C NMR (75 MHz, $CDCl_3$): δ 32.6, 33.3, 33.4, 35.6, 38.7, 54.2, 61.3, 115.1, 115.4, 125.8, 128.4, 130.1, 130.2, 136.2, 142.9 ppm.

MS (EI) m/z 311 (M^+).

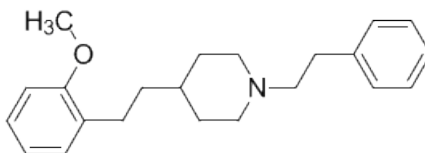


Figure 3.7 Structure of 4-(2-methoxyphenethyl)-1-phenethylpiperidine (JPC-078)

Chemical Formula: $C_{22}H_{29}NO$ Molecular Weight: 323.47

This molecule was designed to evaluate the effect of introducing a 2-methoxy substituent into the phenyl ring of the phenethyl moiety attached to C4 in the piperidine ring of the 1,4-disubstituted piperidine scaffold on VMAT2 binding. 4-Methylpyridine was subjected to Aldol condensation with 2-methoxybenzaldehyde in refluxing acetic anhydride to yield (*E*)-4-(2-methoxystyryl)pyridine (purified via silica column chromatography). Catalytic hydrogenation with Adam's catalyst (PtO_2) and hydrogen gas afforded 4-(2-methoxyphenethyl)piperidine (purified via silica column chromatography), which was reacted with potassium carbonate and (2-bromoethyl)benzene to yield the final product, 4-(2-methoxyphenethyl)-1-phenethylpiperidine (JPC-078) after purification via silica gel column chromatography.

1H NMR (300 MHz, $CDCl_3$): δ 1.32-1.98 (m, 7H), 2.54-2.98 (m, 10H), 3.81 (s, 3H), 6.83-7.31(m, 9H) ppm.

^{13}C NMR (75 MHz, $CDCl_3$): δ 27.6, 32.7, 34.2, 35.9, 37.0, 54.3, 55.5, 61.4, 110.4, 120.5, 126.1, 126.9, 128.5, 128.8, 129.7, 131.4, 140.8, 157.5 ppm.

MS (EI) m/z 323 (M^+).

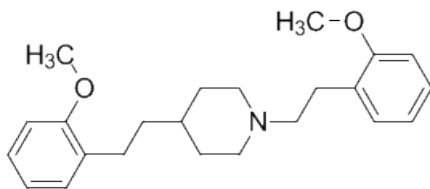


Figure 3.8 Structure of 1,4-*bis*(2-methoxyphenethyl)piperidine (JPC-077)

Chemical Formula: $C_{23}H_{31}NO_2$ Molecular Weight: 353.50

This molecule was designed to evaluate the effect of introducing the combination of a 2-methoxy substituent into the phenyl ring of the phenethyl linker attached to N1, and a 2-methoxy substituent into the phenyl ring of the phenethyl linker attached to C4 of the piperidine ring in the 1,4-disubstituted piperidine scaffold on VMAT2 binding. 4-(2-Methoxyphenethyl)piperidine was reacted with potassium carbonate and 1-(2-bromoethyl)-2-methoxybenzene to yield the final product, 1,4-bis(2-methoxyphenethyl)piperidine (JPC-077) after was purification via silica gel column chromatography.

^1H NMR (300 MHz, CDCl_3): δ 1.32-2.02 (m, 7H), 2.52-3.06 (m, 10H). 3.83 (s, 6H), 6.84-7.27 (m, 8H) ppm.

^{13}C NMR (75 MHz, CDCl_3): δ 27.6, 28.3, 32.7, 35.9, 37.0, 54.2, 55.5, 59.5, 110.4, 110.5, 120.5, 120.6, 126.9, 127.4, 129.7, 130.4, 131.4, 157.5, 157.6 ppm.

MS (EI) m/z 353 (M^+).

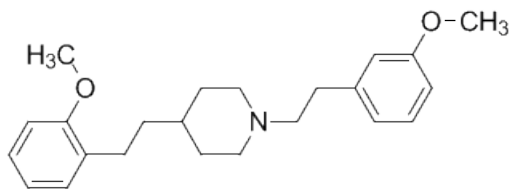


Figure 3.9 Structure of 4-(2-methoxyphenethyl)-1-(3-methoxyphenethyl)piperidine (JPC-094)

Chemical Formula: $C_{23}H_{31}NO_2$ Molecular Weight: 353.50

This molecule was designed to evaluate the effect of introducing the combination of a 3-methoxy substituent into the phenyl ring of the phenethyl linker attached to N1, and a 2-methoxy substituent into the phenyl ring of the phenethyl linker attached to C4 of the piperidine ring in the 1,4-disubstituted piperidine scaffold on VMAT2 binding. Synthesis began with 4-(2-methoxyphenethyl)piperidine which was reacted with potassium carbonate and 1-(2-bromoethyl)-3-methoxybenzene to yield the final product, 4-(2-methoxyphenethyl)-1-(3-methoxyphenethyl)- piperidine (JPC-094) which was purified via column chromatography.

^1H NMR (300 MHz, CDCl_3): δ 1.27-1.98 (m, 7H), 2.48-3.04 (m, 10H). 3.82 (s, 6H), 6.89-7.22 (m, 8H) ppm.

^{13}C NMR (100 MHz, DMSO-d_6): δ 28.5, 28.7, 29.3, 32.9, 35.8, 51.6, 55.0, 55.21, 55.22, 56.5, 109.5, 110.6, 112.2, 114.3, 120.3, 120.8, 124.4, 127.1, 129.6, 138.9, 157.0, 159.4 ppm.

MS (EI) m/z 353 (M^+).

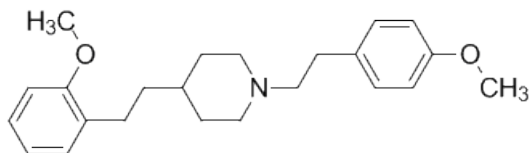


Figure 3.10 Structure of 4-(2-methoxyphenethyl)-1-(4-methoxyphenethyl)piperidine (JPC-095)

Chemical Formula: $C_{23}H_{31}NO_2$ Molecular Weight: 353.50

This molecule was designed to evaluate the effect of introducing the combination of a 4-methoxy substituent into the phenyl ring of the phenethyl linker attached to N1, and a 2-methoxy substituent into the phenyl ring of the phenethyl linker attached to C4 of the piperidine ring in the 1,4-disubstituted piperidine scaffold on VMAT2 binding. Synthesis began with the common intermediate 4-(2-methoxyphenethyl)piperidine that had been prepared previously, which was reacted with potassium carbonate and 1-(2-bromoethyl)-4-methoxybenzene to yield the final product 4-(2-methoxyphenethyl)-1-(4-methoxyphenethyl) piperidine (JPC-095) after purification via silica gel column chromatography.

^1H NMR (300 MHz, CDCl_3): δ 1.28-2.04 (m, 7H), 2.44-2.91 (m, 10H). 3.80 (s, 6H), 6.81-7.30 (m, 8H) ppm.

^{13}C NMR (100 MHz, DMSO-d_6): δ 26.5, 28.4, 28.7, 32.9, 35.8, 43.3, 51.6, 55.0, 55.2, 56.9, 109.4, 110.6, 120.3, 127.1, 129.1, 129.5, 129.7, 157.0, 158.0 ppm.

MS (EI) m/z 353 (M^+).

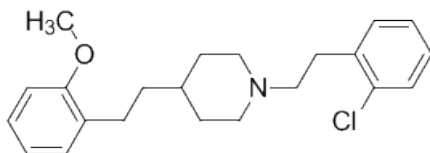


Figure 3.11 Structure of 4-(2-methoxyphenethyl)-1-(2-chlorophenethyl)piperidine (JPC-096)

Chemical Formula: $C_{22}H_{28}ClNO$ Molecular Weight: 357.92

This molecule was designed to evaluate the effect of introducing the combination of a 2-chloro substituent into the phenyl ring of the phenethyl linker attached to N1 and a 2-methoxy substituent into the phenyl ring of the phenethyl linker attached to C4 of the piperidine ring in the 1,4-disubstituted piperidine scaffold on VMAT2 binding. The combination of methoxy and chloro substituents had not previously been investigated in any lobelane scaffold thus far. 4-(2-Methoxyphenethyl)piperidine was reacted with potassium carbonate and 1-(2-bromoethyl)-2-chlorobenzene to yield the final product 4-(2-methoxyphenethyl)-1-(2-chlorophenethyl)piperidine (JPC-096) after purification via silica gel column chromatography.

1H NMR (300 MHz, $CDCl_3$): δ 1.30-1.97 (m, 10H), 2.48-2.94 (m, 7H), 3.81 (s, 3H), 6.80-7.28 (m, 8H) ppm.

^{13}C NMR (100 MHz, $DMSO-d_6$): δ 26.5, 27.8, 28.7, 32.8, 35.8, 43.3, 51.6, 54.9, 55.2, 110.6, 120.2, 127.1, 127.6, 128.9, 129.4, 129.5, 129.7, 131.1, 133.0, 134.8, 157.0 ppm.

MS (EI) m/z 357 (M^+).

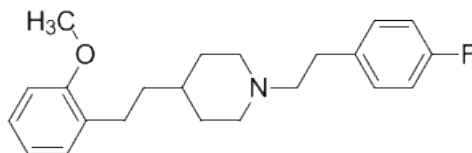


Figure 3.12 Structure of 4-(2-methoxyphenethyl)-1-(4-fluorophenethyl)piperidine

(JPC-097) Chemical Formula: $C_{22}H_{28}FNO$ Molecular Weight: 341.46

This molecule was designed to evaluate the effect of introducing the combination of a 4-fluoro substituent into the phenyl ring of the phenethyl linker attached to N1 and a 2-methoxy substituent into the phenyl ring of the phenethyl linker attached to C4 of the piperidine ring in the 1,4-disubstituted piperidine scaffold on VMAT2 binding. 4-(2-Methoxyphenethyl)piperidine was reacted with potassium carbonate and 1-(2-bromoethyl)-4-fluorobenzene to yield the final product, 4-(2-methoxyphenethyl)-1-(4-fluorophenethyl)piperidine (JPC-097) after purification via silica gel column chromatography.

^1H NMR (300 MHz, CDCl_3): δ 1.30-1.97 (m, 10H), 2.50-3.00 (m, 7H), 3.81 (s, 3H), 6.82-7.25(m, 8H) ppm.

^{13}C NMR (75 MHz, CDCl_3): δ 27.6, 32.7, 33.3, 35.9, 37.0, 54.3, 55.5, 61.4, 110.3, 115.1, 115.3, 120.5, 127.0, 129.6, 130.1, 130.2, 131.3, 136.3, 136.4, 157.4, 163.0 ppm.

MS (EI) m/z 341 (M^+).

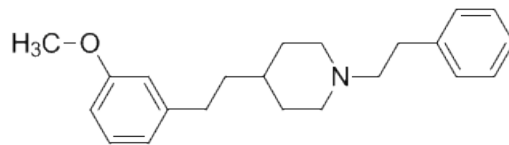


Figure 3.13 Structure of 4-(3-methoxyphenethyl)-1-phenethylpiperidine (JPC-079) Chemical Formula: $C_{22}H_{29}NO$ Molecular Weight: 323.47

This molecule was designed to evaluate the effect of introducing a 3-methoxy substituent into the phenyl ring of the phenethyl linker attached to C4 in the piperidine ring of the 1,4-disubstituted piperidine scaffold on VMAT2 binding. 4-Methylpyridine was subjected to Aldol condensation with 3-methoxybenzaldehyde in refluxing acetic anhydride to yield (*E*)-4-(3-methoxystyryl)pyridine (purified via silica column chromatography). Catalytic hydrogenation with Adam's catalyst (PtO_2) and hydrogen gas afforded 4-(3-methoxyphenethyl)piperidine (purified via silica column chromatography), which was reacted with potassium carbonate and (2-bromoethyl)benzene to yield the final product, 4-(3-methoxyphenethyl)-1-phenethylpiperidine (JPC-079) after purification via silica gel column chromatography.

1H NMR (300 MHz, $CDCl_3$): δ 1.25-2.03 (m, 7H), 2.55-3.03 (m, 10H), 3.80 (s, 3H), 6.71-7.31 (m, 9H) ppm.

^{13}C NMR (75 MHz, $CDCl_3$) δ 25.6, 30.7, 34.1, 36.3, 37.0, 49.3, 55.6, 59.9, 110.9, 113.8, 120.5, 126.1, 128.5, 128.8, 129.7, 139.4, 140.8, 159.5 ppm.

MS (EI) m/z 323 (M^+).

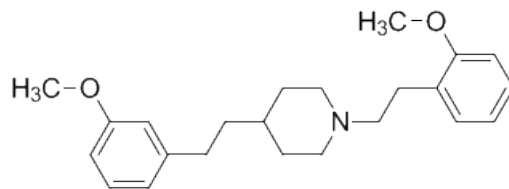


Figure 3.14 Structure of 1-(2-methoxyphenethyl)-4-(3-methoxyphenethyl)piperidine (JPC-080)

Chemical Formula: $C_{23}H_{31}NO_2$ Molecular Weight: 353.50

This molecule was designed to evaluate the effect of introducing the combination of a 2-methoxy substituent into the phenyl ring of the phenethyl linker attached to N1 and a 3-methoxy substituent into the phenyl ring of the phenethyl linker attached to C4 of the piperidine ring in the 1,4-disubstituted piperidine scaffold on VMAT2 binding. 4-(3-methoxyphenethyl)piperidine was reacted with potassium carbonate and 1-(2-bromoethyl)-2-methoxybenzene to yield the final product 1-(2-methoxyphenethyl)-4-(3-methoxyphenethyl)-piperidine (JPC-080) after purification via silica gel column chromatography.

1H NMR (300 MHz, $CDCl_3$): δ 1.21-2.04 (m, 10H), 2.42-3.07 (m, 7H), 3.77 (s, 6H), 6.65-6.89(m, 4H), 7.11-7.21 (m, 4H) ppm.

^{13}C NMR (75 MHz, $CDCl_3$): δ 28.3, 32.7, 33.5, 35.7, 38.6, 53.7, 54.1, 55.4, 55.5, 59.5, 110.4, 111.0, 114.3, 120.5, 120.9, 127.3, 129.1, 129.4, 130.3, 144.6, 157.6, 159.7 ppm.

MS (EI) m/z 353 (M^+).

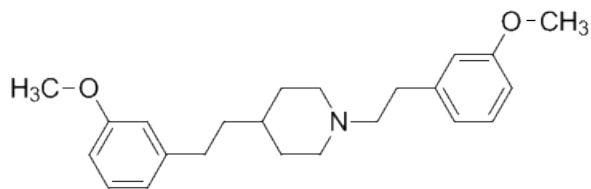


Figure 3.15 Structure of 1,4-*bis*(3-methoxyphenethyl)piperidine (JPC-081)

Chemical Formula: $C_{23}H_{31}NO_2$ Molecular Weight: 353.50

This molecule was designed to evaluate the effect of introducing the combination of a 3-methoxy substituent into the phenyl ring of the phenethyl linker attached to N1, and a 3-methoxy substituent into the phenyl ring of the phenethyl linker attached to C4 of the piperidine ring in the 1,4-disubstituted piperidine scaffold on VMAT2 binding. 4-(3-Methoxyphenethyl) was reacted with potassium carbonate and 1-(2-bromoethyl)-3-methoxybenzene to yield the final product 1,4-bis(3-methoxyphenethyl)- piperidine (JPC-081) after purification via silica gel column chromatography.

^1H NMR (300 MHz, CDCl_3): δ 1.19-2.07 (m, 10H), 2.51-3.07 (m, 7H). 3.79 (s, 6H), 6.73-6.76(m, 5H), 7.15-7.21 (m, 3H) ppm.

^{13}C NMR (75 MHz, CDCl_3): δ 32.7, 33.5, 34.2, 35.6, 38.6, 54.2, 55.4, 61.2, 111.0, 111.4, 114.3, 114.7, 120.9, 121.3, 129.4, 129.5, 142.4, 144.6, 159.7 ppm.

MS (EI) m/z 353 (M^+).

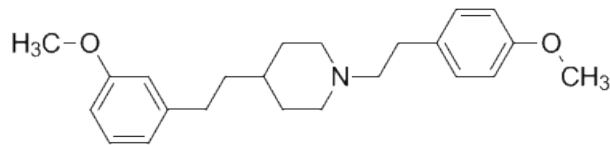


Figure 3.16 Structure of 1-(4-methoxyphenethyl)-4-(3-methoxyphenethyl)piperidine (JPC-082)

Chemical Formula: $C_{23}H_{31}NO_2$ Molecular Weight: 353.50

This molecule was designed to evaluate the effect of introducing the combination of a 4-methoxy substituent into the phenyl ring of the phenethyl linker attached to N1, and a 3-methoxy substituent into the phenyl ring of the phenethyl linker attached to C4 of the piperidine ring in the 1,4-disubstituted piperidine scaffold on VMAT2 binding. 4-(3-Methoxyphenethyl)piperidine was reacted with potassium carbonate and 1-(2-bromoethyl)-4-methoxybenzene to yield the final product, 1-(4-methoxyphenethyl)-4-(3-methoxyphenethyl)piperidine (JPC-082) after purification via silica gel column chromatography.

^1H NMR (300 MHz, CDCl_3): δ 1.21-1.96 (m, 7H), 2.41-2.97 (m, 10H). 3.82 (s, 6H), 6.81-7.23 (m, 8H) ppm.

^{13}C NMR (100 MHz, DMSO-d_6): δ 28.2, 28.7, 32.0, 32.6, 37.1, 43.3, 51.6, 54.9, 55.0, 56.9, 109.5, 111.1, 113.9, 114.0, 120.5, 129.0, 129.3, 129.6, 143.6, 158.1, 159.3 ppm.

MS (EI) m/z 353 (M^+).

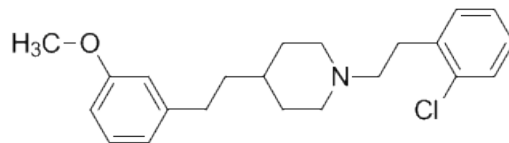


Figure 3.17 Structure of 1-(2-chlorophenethyl)-4-(3-methoxyphenethyl)piperidine (JPC-083)

Chemical Formula: $C_{22}H_{28}ClNO$ Molecular Weight: 357.92

This molecule was designed to evaluate the effect of introducing the combination of a 2-chloro substituent into the phenyl ring of the phenethyl linker attached to N1, and a 3-methoxy substituent into the phenyl ring of the phenethyl linker attached to C4 of the piperidine ring in the 1,4-disubstituted piperidine scaffold on VMAT2 binding. 4-(3-Methoxyphenethyl)piperidine was reacted with potassium carbonate and 1-(2-bromoethyl)-2-chlorobenzene to yield the final product 1-(2-chlorophenethyl)-4-(3-methoxyphenethyl)piperidine (JPC-083) was after purification via silica gel column chromatography.

1H NMR (300 MHz, $CDCl_3$): δ 1.22-1.94 (m, 10H), 2.43-2.99 (m, 7H), 3.80 (s, 3H), 6.88-7.32 (m, 8H) ppm.

^{13}C NMR (100 MHz, $DMSO-d_6$): δ 27.4, 28.3, 28.9, 32.1, 37.2, 43.4, 51.8, 55.0, 111.2, 114.1, 120.6, 127.7, 129.4, 131.2, 133.2, 134.1, 134.9, 143.7, 159.3, 166.4 ppm.

MS (EI) m/z 357 (M^+).

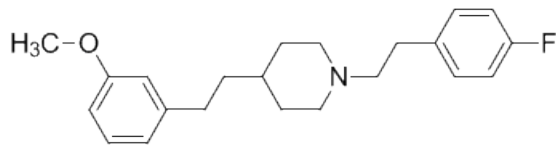


Figure 3.18 Structure of 1-(4-fluorophenethyl)-4-(3-methoxyphenethyl)piperidine (JPC-084) Chemical Formula: $C_{22}H_{28}FNO$ Molecular Weight: 341.46

This molecule was designed to evaluate the effect of introducing the combination of a 4-fluoro substituent into the phenyl ring of the phenethyl linker attached to N1, and a 3-methoxy substituent into the phenyl ring of the phenethyl linker attached to C4 of the piperidine ring in the 1,4-disubstituted scaffold on VMAT2 binding. 4-(3-Methoxyphenethyl)piperidine was reacted with potassium carbonate and 1-(2-bromoethyl)-4-fluorobenzene to yield the final product 1-(4-fluorophenethyl)-4-(2-chlorophenethyl)piperidine (JPC-084) after purification via silica gel column chromatography.

^1H NMR (300 MHz, CDCl_3): δ 1.24-1.96 (m, 10H), 2.46-3.02 (m, 7H), 3.80 (s, 3H), 6.83-7.21(m, 8H) ppm.

^{13}C NMR (100 MHz, DMSO-d_6): δ 28.4, 28.7, 32.0, 32.6, 37.1, 43.3, 51.6, 54.9, 56.6, 111.1, 113.9, 115.2, 115.4, 120.5, 129.3, 130.5, 130.6, 133.5, 143.6, 159.3, 162.3 ppm.

MS (EI) m/z 341 (M^+).

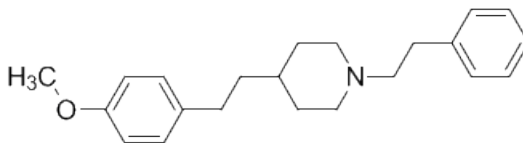


Figure 3.19 Structure of 4-(4-methoxyphenethyl)-1-phenethylpiperidine (JPC-085) Chemical Formula: C₂₂H₂₉NO Molecular Weight: 323.47

This molecule was designed to evaluate the effect of introducing a 4-methoxy substituent into the phenyl ring of the phenethyl linker attached to C4 in the piperidine ring of the 1,4-disubstituted piperidine scaffold on VMAT2 binding. 4-Methylpyridine was subjected to Aldol condensation with 4-methoxybenzaldehyde in refluxing acetic anhydride to yield (*E*)-4-(4-methoxystyryl)pyridine (purified via silica gel column chromatography). Catalytic hydrogenation with Adam's catalyst (PtO₂) and hydrogen gas afforded 4-(4-methoxyphenethyl)piperidine (purified via silica gel column chromatography), which was reacted with potassium carbonate and (2-bromoethyl)benzene to yield the final product 4-(4-methoxyphenethyl)-1-phenethylpiperidine (JPC-085) after purification via silica gel column chromatography.

¹H NMR (300 MHz, CDCl₃): δ 1.21-1.97 (m, 10H), 2.36-2.91 (m, 7H), 3.83 (s, 3H), 6.81-7.24 (m, 9H) ppm.

¹³C NMR (100 MHz, DMSO-d₆): δ 28.7, 29.3, 31.0, 32.5, 37.4, 43.3, 51.6, 54.9, 56.6, 109.5, 113.7, 126.7, 128.60, 128.61, 129.1, 133.72, 137.4, 157.3 ppm.

MS (EI) m/z 323 (M⁺).

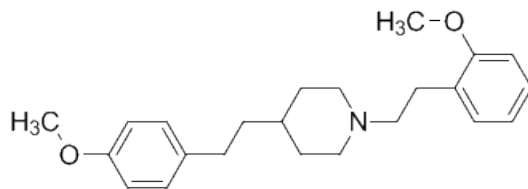


Figure 3.20 Structure of 1-(2-methoxyphenethyl)-4-(4-methoxyphenethyl)piperidine (JPC-086)

Chemical Formula: $C_{23}H_{31}NO_2$ Molecular Weight: 353.50

This molecule was designed to evaluate the effect of introducing the combination of a 2-methoxy substituent into the phenyl ring of the phenethyl linker attached to N1, and a 4-methoxy substituent into the phenyl ring of the phenethyl linker attached to C4 of the piperidine ring in the 1,4-disubstituted piperidine scaffold on VMAT2 binding. 4-(4-Methoxyphenethyl)piperidine was reacted with potassium carbonate and 1-(2-bromoethyl)-2-methoxybenzene to yield the final product 1-(2-methoxyphenethyl)-4-(4-methoxyphenethyl)piperidine (JPC-086) after purification via silica gel column chromatography.

^1H NMR (300 MHz, CDCl_3): δ 1.27-2.06 (m, 7H), 2.48-3.05 (m, 10H). 3.84 (s, 6H), 6.87-7.30 (m, 8H) ppm.

^{13}C NMR (100 MHz, DMSO-d_6): δ 24.3, 28.7, 31.0, 32.5, 37.4, 43.3, 51.5, 54.9, 55.3, 55.4, 110.9, 113.7, 120.5, 124.4, 125.0, 128.3, 129.1, 130.0, 133.7, 157.0, 157.3 ppm.

MS (EI) m/z 353 (M^+).

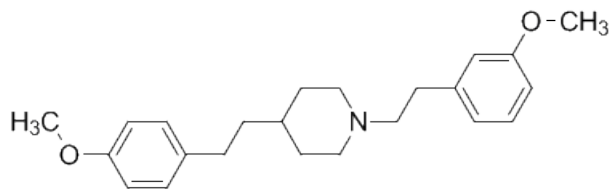


Figure 3.21 Structure of 1-(3-methoxyphenethyl)-4-(4-methoxyphenethyl)piperidine (JPC-087)

Chemical Formula: $C_{23}H_{31}NO_2$ Molecular Weight: 353.50

This molecule was designed to evaluate the effect of introducing the combination of a 3-methoxy substituent into the phenyl ring of the phenethyl linker attached to N1, and a 4-methoxy substituent into the phenyl ring of the phenethyl linker attached to C4 of the piperidine ring in the 1,4-disubstituted scaffold on VMAT2 binding. 4-(4-Methoxyphenethyl)piperidine was reacted with potassium carbonate and 1-(2-bromoethyl)-3-methoxybenzene to yield the final product 1-(3-methoxyphenethyl)-4-(4-methoxyphenethyl)piperidine (JPC-087), after purification via silica gel column chromatography.

^1H NMR (300 MHz, CDCl_3): δ 1.23-1.98 (m, 7H), 2.38-2.94 (m, 10H). 3.81 (s, 6H), 6.87-7.28 (m, 8H) ppm.

^{13}C NMR (100 MHz, DMSO-d_6): δ 28.7, 29.3, 31.0, 32.5, 37.4, 43.3, 51.6, 54.9, 55.0, 56.5, 112.2, 113.7, 114.3, 120.8, 129.1, 129.6, 133.7, 138.9, 157.3, 159.4 ppm.

MS (EI) m/z 353 (M^+).

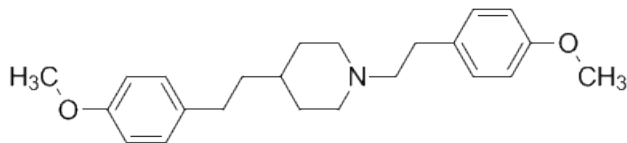


Figure 3.22 Structure of 1,4-*bis*(4-methoxyphenethyl)piperidine (JPC-088)

Chemical Formula: $C_{23}H_{31}NO_2$ Molecular Weight: 353.50

This molecule was designed to evaluate the effect of introducing the combination of a 4-methoxy substituent into the phenyl ring of the phenethyl linker attached to N1, and a 4-methoxy substituent into the phenyl ring of the phenethyl linker attached to C4 of the piperidine ring in the 1,4-disubstituted piperidine scaffold on VMAT2 binding. 4-(4-Methoxyphenethyl)piperidine was reacted with potassium carbonate and 1-(2-bromoethyl)-4-methoxybenzene to yield the final product 1-(4-methoxyphenethyl)-4-(4-methoxyphenethyl)piperidine (JPC-088) after purification via silica gel column chromatography.

^1H NMR (300 MHz, CDCl_3): δ 1.21-2.05 (m, 7H), 2.38-2.91 (m, 10H), 3.82 (s, 6H), 6.76-7.23 (m, 8H) ppm.

^{13}C NMR (100 MHz, DMSO-d_6): δ 28.4, 28.7, 31.1, 32.6, 37.5, 51.6, 54.95, 55.04, 56.9, 109.5, 113.7, 114.0, 124.4, 129.08, 129.12, 129.7, 133.8, 157.4, 158.1 ppm.

MS (EI) m/z 353 (M^+).

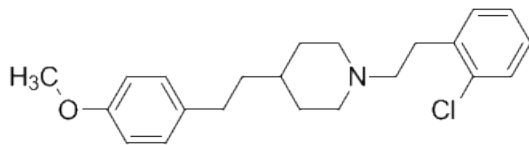


Figure 3.23 Structure of 1-(2-chlorophenethyl)-4-(4-methoxyphenethyl)piperidine (JPC-089)

Chemical Formula: $C_{22}H_{28}ClNO$ Molecular Weight: 357.92

This molecule was designed to evaluate the effect of introducing the combination of a 2-chloro substituent into the phenyl ring of the phenethyl linker attached to N1, and a 4-methoxy substituent into the phenyl ring of the phenethyl linker attached to C4 of the piperidine ring in the 1,4-disubstituted piperidine scaffold on VMAT2 binding. 4-(4-Methoxyphenethyl)piperidine was reacted with potassium carbonate and 1-(2-bromoethyl)-2-chlorobenzene to yield the final product, 1-(2-chlorophenethyl)-4-(4-methoxyphenethyl)piperidine (JPC-089) after purification via silica gel column chromatography.

1H NMR (300 MHz, $CDCl_3$): δ 1.26-1.95 (m, 10H), 2.41-3.02 (m, 7H), 3.81 (s, 3H), 6.84-7.33 (m, 8H) ppm.

^{13}C NMR (100 MHz, $DMSO-d_6$): δ 27.2, 28.7, 31.1, 32.5, 37.4, 43.3, 51.6, 55.0, 109.5, 113.7, 124.4, 127.6, 128.9, 129.3, 131.1, 133.1, 133.8, 134.8, 157.4, 165.9 ppm.

MS (EI) m/z 357 (M^+).

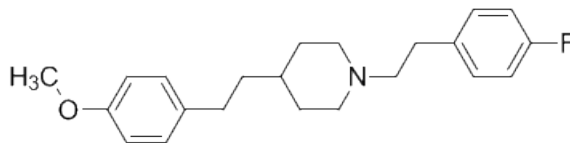


Figure 3.24 Structure of 1-(4-fluorophenethyl)-4-(4-methoxyphenethyl)piperidine (JPC-090) Chemical Formula: $C_{22}H_{28}FNO$ Molecular Weight: 341.46

This molecule was designed to evaluate the effect of introducing the combination of a 4-fluoro substituent into the phenyl ring of the phenethyl linker attached to N1, and a 4-methoxy substituent into the phenyl ring of the phenethyl linker attached to C4 of the piperidine ring in the 1,4-disubstituted piperidine scaffold on VMAT2 binding. 4-(4-Methoxyphenethyl)piperidine was reacted with potassium carbonate and 1-(2-bromoethyl)-4-fluorobenzene to yield the final product 1-(4-fluorophenethyl)-4-(4-methoxyphenethyl)piperidine (JPC-090) after purification via silica gel column chromatography.

1H NMR (300 MHz, $CDCl_3$): δ 1.21-1.94 (m, 10H), 2.49-3.07 (m, 7H), 3.83 (s, 3H), 6.87-7.28(m, 8H) ppm.

^{13}C NMR (100 MHz, $DMSO-d_6$): δ 28.4, 28.7, 31.0, 32.5, 37.4, 51.6, 54.9, 56.5, 113.7, 115.2, 115.4, 124.4, 129.1, 130.5, 130.6, 133.50, 133.53, 133.7, 159.9, 162.3 ppm.

MS (EI) m/z 341 (M^+).

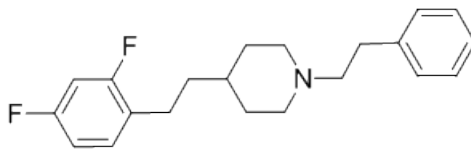


Figure 3.25 Structure of 4-(2,4-difluorophenethyl)-1-phenethylpiperidine (JPC-098) Chemical Formula: $C_{21}H_{25}F_2N$ Molecular Weight: 329.43

This molecule was designed to evaluate the effect of introducing 2,4-difluoro substituents into the phenyl ring of the phenethyl linker attached to C4 in the piperidine ring of the 1,4-disubstituted scaffold on VMAT2 binding. 4-Methylpyridine was subjected to Aldol condensation with 2,4-difluorobenzaldehyde in refluxing acetic anhydride to yield (*E*)-4-(2,4-difluorostyryl)pyridine (purified via silica gel column chromatography). Catalytic hydrogenation with Adam's catalyst (PtO_2) and hydrogen gas afforded 4-(2,4-difluorophenethyl)piperidine (purified via silica gel column chromatography), which was reacted with potassium carbonate and (2-bromoethyl)benzene to yield the final product 4-(2,4-difluorophenethyl)-1-phenethylpiperidine (JPC-098) after purification via silica gel column chromatography.

1H NMR (300 MHz, $CDCl_3$): δ 1.31-1.95 (m, 9H), 2.44-3.02 (m, 8H), 6.65-6.91(m, 6H), 7.13-7.30 (m, 2H) ppm.

^{13}C NMR (100 MHz, $DMSO-d_6$): δ 24.7, 28.6, 29.3, 32.7, 35.9, 43.29, 43.30, 51.6, 56.6, 103.6, 109.5, 111.4, 124.4, 126.7, 128.6, 131.7, 137.3, 142.2 ppm.

MS (EI) m/z 329 (M^+).

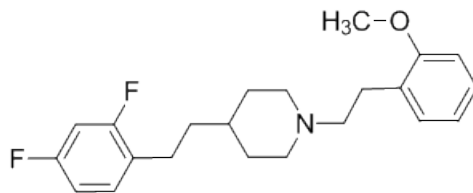


Figure 3.26 Structure of 4-(2,4-difluorophenethyl)-1-(2-methoxyphenethyl)piperidine (JPC-099)

Chemical Formula: $C_{22}H_{27}F_2NO$ Molecular Weight: 359.45

This molecule was designed to evaluate the effect of introducing the combination of a 2-methoxy substituent into the phenyl ring of the phenethyl linker attached to N1, and 2,4-difluoro substituents into the phenyl ring of the phenethyl linker attached to C4 of the piperidine ring in the 1,4-disubstituted piperidine scaffold on VMAT2 binding. 4-(2,4-Difluorophenethyl)piperidine was reacted with potassium carbonate and 1-(2-bromoethyl)-2-methoxybenzene to yield the final product, 4-(2,4-difluorophenethyl)-1-(2-methoxyphenethyl)piperidine (JPC-099) after purification via silica gel column chromatography.

1H NMR (300 MHz, $CDCl_3$): δ 1.28-2.02 (m, 9H), 2.51-3.00 (m, 8H), 3.81 (s, 3H), 6.65-6.81(m, 5H), 7.11-7.26 (m, 2H) ppm.

^{13}C NMR (100 MHz, $DMSO-d_6$): δ 24.3, 24.7, 28.6, 32.6, 35.8, 43.3, 51.5, 55.3, 55.4, 103.5, 109.5, 110.9, 111.2, 120.5, 124.4, 125.0, 128.3, 130.0, 157.1 ppm.

MS (EI) m/z 359 (M^+).

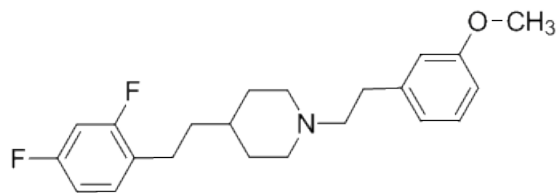


Figure 3.27 Structure of 4-(2,4-difluorophenethyl)-1-(3-methoxyphenethyl)piperidine (JPC-100)

Chemical Formula: $C_{22}H_{27}F_2NO$ Molecular Weight: 359.45

This molecule was designed to evaluate the effect of introducing the combination of a 3-methoxy substituent into the phenyl ring of the phenethyl linker attached to N1, and 2,4-difluoro substituents in the phenyl ring of the phenethyl linker attached to C4 of the piperidine ring in the 1,4-disubstituted piperidine scaffold on VMAT2 binding. 4-(2,4-Difluorophenethyl)piperidine was reacted with potassium carbonate and 1-(2-bromoethyl)-3-methoxybenzene to yield the final product, 4-(2,4-difluorophenethyl)-1-(3-methoxyphenethyl)piperidine (JPC-100) after purification via silica gel column chromatography.

1H NMR (300 MHz, $CDCl_3$): δ 1.31-2.01 (m, 9H), 2.57-3.05 (m, 8H), 3.79 (s, 3H), 6.72-6.81(m, 5H), 7.11-7.26 (m, 2H) ppm.

^{13}C NMR (75 MHz, $CDCl_3$): δ 25.9, 32.3, 34.0, 35.5, 37.2, 54.1, 55.4, 61.0, 103.7, 111.1, 111.2, 111.4, 114.6, 121.2, 129.5, 130.8, 130.88, 130.91, 142.1, 159.7 ppm.

MS (EI) m/z 359 (M^+).

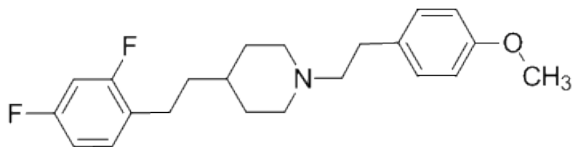


Figure 3.28 Structure of 4-(2,4-difluorophenethyl)-1-(4-methoxyphenethyl)piperidine (JPC-101) Chemical Formula: $C_{22}H_{27}F_2NO$ Molecular Weight: 359.45

This molecule was designed to evaluate the effect of introducing the combination of a 4-methoxy substituent into the phenyl ring of the phenethyl linker attached to N1, and 2,4-difluoro substituents into the phenyl ring of the phenethyl linker attached to C4 of the piperidine ring in the 1,4-disubstituted piperidine scaffold on VMAT2 binding. 4-(2,4-Difluorophenethyl)piperidine was reacted with potassium carbonate and 1-(2-bromoethyl)-4-methoxybenzene to yield the final product 4-(2,4-difluorophenethyl)-1-(4-methoxyphenethyl)piperidine (JPC-101) after purification via silica gel column chromatography.

1H NMR (300 MHz, $CDCl_3$): δ 1.32-1.98 (m, 9H), 2.57-3.04 (m, 8H), 3.83 (s, 3H), 6.69-6.84(m, 5H), 7.09-7.21 (m, 2H) ppm.

^{13}C NMR (100 MHz, $DMSO-d_6$): δ 24.7, 28.4, 28.6, 32.7, 35.9, 43.3, 51.5, 55.0, 56.9, 103.5, 111.1, 111.3, 114.0, 124.4, 124.7, 124.8, 129.1, 129.6, 129.1, 131.6, 158.0 ppm.

MS (EI) m/z 359 (M^+).

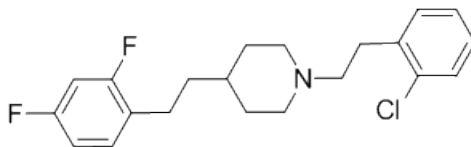


Figure 3.29 Structure of 1-(2-chlorophenethyl)-4-(2,4-difluorophenethyl)piperidine (JPC-102) Chemical Formula: $C_{21}H_{24}ClF_2N$ Molecular Weight: 363.87

This molecule was designed to evaluate the effect of introducing the combination of a 2-chloro substituent into the phenyl ring of the phenethyl linker attached to N1 and 2,4-difluoro substituents into the phenyl ring of the phenethyl linker attached to C4 of the piperidine ring in the 1,4-disubstituted piperidine scaffold on VMAT2 binding. 4-(2,4-Difluorophenethyl)piperidine was reacted with potassium carbonate and 1-(2-bromoethyl)-2-chlorobenzene to yield the final product, 1-(2-chlorophenethyl)-4-(2,4-difluorophenethyl)piperidine (JPC-102) after purification via silica gel column chromatography.

1H NMR (300 MHz, $CDCl_3$): δ 1.31-1.97 (m, 9H), 2.46-2.94 (m, 8H), 6.65-7.26 (m, 7H) ppm.

^{13}C NMR (100 MHz, $DMSO-d_6$): δ 24.7, 27.2, 28.6, 32.6, 35.8, 42.4, 43.3, 51.5, 54.9, 103.6, 109.5, 111.2, 124.6, 127.6, 128.9, 129.4, 131.1, 131.7, 133.0, 134.8, 159.5 ppm.

MS (EI) m/z 363 (M^+).

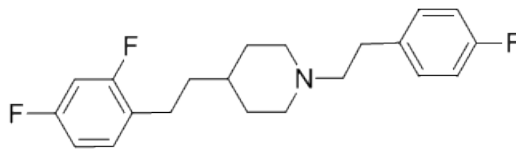


Figure 3.30 Structure of 4-(2,4-difluorophenethyl)-1-(4-fluorophenethyl)piperidine (JPC-103) Chemical Formula: $C_{21}H_{24}F_3N$ Molecular Weight: 347.42

This molecule was designed to evaluate the effect of introducing the combination of a 4-fluoro substituent into the phenyl ring of the phenethyl linker attached to N1, and 2,4-difluoro substituents into the phenyl ring of the phenethyl linker attached to C4 of the piperidine ring in the 1,4-disubstituted piperidine scaffold on VMAT2 binding. 4-(2,4-Difluorophenethyl)piperidine was reacted with potassium carbonate and 1-(2-bromoethyl)-4-fluorobenzene to yield the final product 4-(2,4-difluorophenethyl)-1-(4-fluorophenethyl)piperidine (JPC-103) after purification via silica gel column chromatography.

1H NMR (300 MHz, $CDCl_3$): δ 1.34-2.02 (m, 9H), 2.41-3.06 (m, 8H), 6.61-7.29 (m, 7H) ppm.

^{13}C NMR (100 MHz, $DMSO-d_6$): δ 24.7, 28.5, 32.7, 35.9, 37.6, 42.1, 43.3, 51.6, 56.5, 103.6, 109.5, 111.3, 115.2, 115.4, 124.4, 124.7, 130.6, 131.6, 133.5, 159.9, 162.0 ppm.

MS (EI) m/z 347 (M^+).

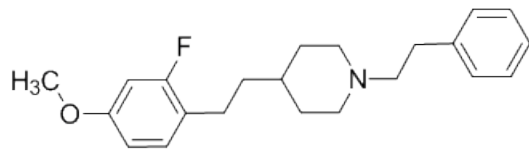


Figure 3.31 Structure of 4-(2-fluoro-4-methoxyphenethyl)-1-phenethylpiperidine (JPC-104) Chemical Formula: $C_{22}H_{28}FNO$ Molecular Weight: 341.46

This molecule was designed to evaluate the effect of introducing 2-fluoro-4-methoxy substituents into the phenyl ring of the phenethyl linker attached to C4 in the piperidine ring of the 1,4-disubstituted piperidine scaffold on VMAT2 binding. 4-Methylpyridine was subjected to Aldol condensation with 2-fluoro-4-methoxy benzaldehyde in refluxing acetic anhydride to yield (*E*)-4-(2-fluoro-4-methoxy styryl)pyridine (purified via silica gel column chromatography). Catalytic hydrogenation with Adam's catalyst (PtO_2) and hydrogen gas afforded 4-(2-fluoro-4-methoxyphenethyl)piperidine (purified via silica gel column chromatography), which was reacted with potassium carbonate and (2-bromoethyl)benzene to yield the final product 4-(2-fluoro-4-methoxyphenethyl)-1-phenethylpiperidine (JPC-104) after purification via silica gel column chromatography.

1H NMR (300 MHz, $CDCl_3$): δ 1.27-1.89 (m, 9H), 2.38-2.94 (m, 8H), 3.82 (s, 3H), 6.74-7.38 (m, 8H) ppm.

^{13}C NMR (100 MHz, $DMSO-d_6$): δ 24.6, 28.7, 29.3, 32.6, 36.1, 43.3, 51.6, 55.5, 56.6, 101.5, 109.5, 110.1, 120.1, 126.7, 128.6, 130.9, 131.0, 137.3, 157.2, 158.8, 158.9 ppm.

MS (EI) m/z 341 (M^+).

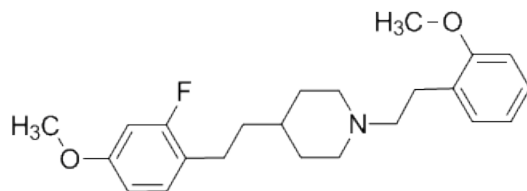


Figure 3.32 Structure of 4-(2-fluoro-4-methoxyphenethyl)-1-(2-methoxyphenethyl)piperidine (JPC-105)

Chemical Formula: $C_{23}H_{30}FNO_2$ Molecular Weight: 371.49

This molecule was designed to evaluate the effect of introducing the combination of a 2-methoxy substituent into the phenyl ring of the phenethyl linker attached to N1, and 2-fluoro-4-methoxy substituents into the phenyl ring of the phenethyl linker attached to C4 of the piperidine ring in the 1,4-disubstituted piperidine scaffold on VMAT2 binding. 4-(2-Fluoro-4-methoxyphenethyl)piperidine was reacted with potassium carbonate and 1-(2-bromoethyl)-2-methoxybenzene to yield the final product, 4-(2-fluoro-4-methoxyphenethyl)-1-(2-methoxyphenethyl)piperidine (JPC-105) after purification via silica gel column chromatography.

1H NMR (300 MHz, $CDCl_3$): δ 1.21-1.97 (m, 9H), 2.41-2.99 (m, 8H), 3.81 (s, 6H), 6.71-7.35 (m, 7H) ppm.

^{13}C NMR (100 MHz, $DMSO-d_6$): δ 24.1, 25.7, 26.2, 27.0, 36.2, 43.1, 55.2, 56.6, 58.1, 101.5, 111.2, 120.5, 126.7, 130.2, 130.5, 132.6, 158.1, 159.4, 161.2 ppm.

MS (EI) m/z 371 (M^+).

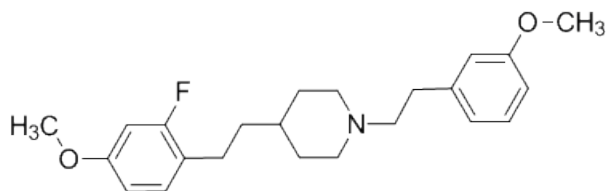


Figure 3.33 Structure of 4-(2-fluoro-4-methoxyphenethyl)-1-(3-methoxyphenethyl)piperidine (JPC-106)

Chemical Formula: $C_{23}H_{30}FNO_2$ Molecular Weight: 371.49

This molecule was designed to evaluate the effect of introducing the combination of a 3-methoxy substituent into the phenyl ring of the phenethyl linker attached to N1, and 2-fluoro-4-methoxy substituents into the phenyl ring of the phenethyl linker attached to C4 of the piperidine ring in the 1,4-disubstituted piperidine scaffold on VMAT2 binding. 4-(2-Fluoro-4-methoxyphenethyl)piperidine was reacted with potassium carbonate and 1-(2-bromoethyl)-3-methoxybenzene to yield the final product, 4-(2-fluoro-4-methoxyphenethyl)-1-(3-methoxyphenethyl)piperidine (JPC-106) was after purification via silica gel column chromatography.

^1H NMR (300 MHz, CDCl_3): δ 1.21-1.98 (m, 9H), 2.40-2.92 (m, 8H), 3.80 (s, 6H), 6.78-7.31 (m, 7H) ppm.

^{13}C NMR (100 MHz, DMSO-d_6): δ 24.2, 25.2, 26.3, 36.1, 38.0, 55.1, 57.6, 60.3, 101.5, 109.5, 112.0, 114.2, 128.1, 130.5, 142.7, 157.7, 159.9, 160.7 ppm.

MS (EI) m/z 371 (M^+).

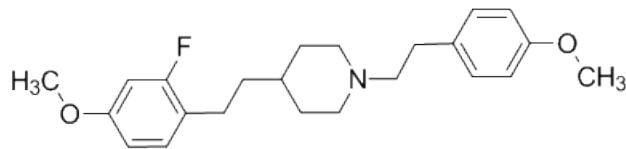


Figure 3.34 Structure of 4-(2-fluoro-4-methoxyphenethyl)-1-(4-methoxyphenethyl)piperidine (JPC-107)

Chemical Formula: $C_{23}H_{30}FNO_2$ Molecular Weight: 371.49

This molecule was designed to evaluate the effect of introducing the combination of a 4-methoxy substituent into the phenyl ring of the phenethyl linker attached to N1 and e2-fluoro-4-methoxy substituents into the phenyl ring of the phenethyl linker attached to C4 of the piperidine ring in the 1,4-disubstituted piperidine scaffold on VMAT2 binding. 4-(2-Fluoro-4-methoxy phenethyl)piperidine was reacted with potassium carbonate and 1-(2-bromoethyl)-4-methoxybenzene to yield the final product, 4-(2-fluoro-4-methoxyphenethyl)-1-(4-methoxyphenethyl)piperidine (JPC-107) after purification via silica gel column chromatography.

^1H NMR (300 MHz, CDCl_3): δ 1.27-1.97 (m, 9H), 2.32-3.04 (m, 8H), 3.82 (s, 6H), 6.71-7.21 (m, 7H) ppm.

^{13}C NMR (100 MHz, DMSO-d_6): δ 23.7, 24.9, 26.0, 34.1, 36.0, 55.1, 55.2, 60.7, 101.3, 109.2, 113.9, 130.0, 130.1, 130.3, 132.7, 157.5, 158.3, 159.2 ppm.

MS (EI) m/z 371 (M^+).

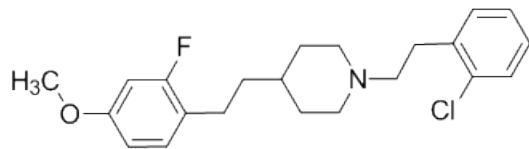


Figure 3.35 Structure of 1-(2-chlorophenethyl)-4-(2-fluoro-4-methoxyphenethyl)piperidine (JPC-108)

Chemical Formula: $C_{22}H_{27}ClFNO$ Molecular Weight: 375.91

This molecule was designed to evaluate the effect of introducing the combination of a 2-chloro substituent into the phenyl ring of the phenethyl linker attached to N1, and 2-fluoro-4-methoxy substituents into the phenyl ring of the phenethyl linker attached to C4 of the piperidine ring in the 1,4-disubstituted piperidine scaffold on VMAT2 binding. 4-(2-Fluoro-4-methoxyphenethyl)piperidine was reacted with potassium carbonate and 1-(2-bromoethyl)-2-chlorobenzene to yield the final product, 1-(2-chlorophenethyl)-4-(2-fluoro-4-methoxyphenethyl)piperidine (JPC-108) was after purification via silica gel column chromatography.

1H NMR (300 MHz, $CDCl_3$): δ 1.29-2.07 (m, 9H), 2.48-2.98 (m, 8H), 3.82 (s, 3H), 6.65-7.39 (m, 7H) ppm.

^{13}C NMR (100 MHz, $DMSO-d_6$): δ 27.0, 28.1, 30.9, 31.2, 36.1, 53.1, 55.6, 56.0, 102.1, 109.9, 127.7, 129.9, 130.1, 131.0, 131.7, 134.2, 158.2, 159.1 ppm.

MS (EI) m/z 375 (M^+).

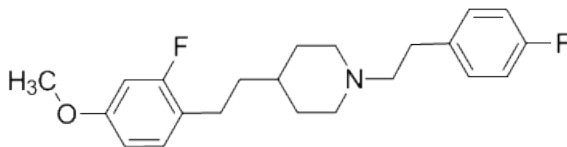


Figure 3.36 Structure of 4-(2-fluoro-4-methoxyphenethyl)-1-(4-fluorophenethyl)piperidine (JPC-109)

Chemical Formula: $C_{22}H_{27}F_2NO$ Molecular Weight: 359.45

This molecule was designed to evaluate the effect of introducing the combination of a 4-fluoro substituent into the phenyl ring of the phenethyl linker attached to N1, and 2-fluoro-4-methoxy substituents into the phenyl ring of the phenethyl linker attached to C4 of the piperidine ring in the 1,4-disubstituted piperidine scaffold on VMAT2 binding. 4-(2-Fluoro-4-methoxyphenethyl)piperidine was reacted with potassium carbonate and 1-(2-bromoethyl)-4-fluorobenzene to yield the final product, 4-(2-fluoro-4-methoxyphenethyl)-1-(4-fluorophenethyl)piperidine (JPC-109) after purification via silica gel column chromatography.

1H NMR (300 MHz, $CDCl_3$): δ 1.28-2.09 (m, 9H), 2.45-3.01 (m, 8H), 3.79 (s, 3H), 6.69-7.37 (m, 7H) ppm.

^{13}C NMR (100 MHz, $DMSO-d_6$): δ 27.1, 28.0, 30.5, 32.7, 36.0, 52.7, 55.7, 57.1, 101.9, 110.3, 114.2, 114.3, 129.8, 129.9, 130.3, 158.5, 159.9, 160.2 ppm.

MS (EI) m/z 359 (M^+).

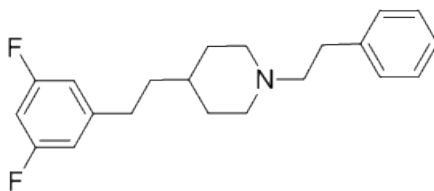


Figure 3.37 Structure of 4-(3,5-difluorophenethyl)-1-phenethylpiperidine (JPC-110) Chemical Formula: $C_{21}H_{25}F_2N$ Molecular Weight: 329.43

This molecule was designed to evaluate the effect of introducing 3,5-difluoro substituents into the phenyl ring of the phenethyl linker attached to C4 in the piperidine ring of the 1,4-disubstituted piperidine scaffold on VMAT2 binding. 4-Methylpyridine was subjected to Aldol condensation with 3,5-difluorobenzaldehyde in refluxing acetic anhydride to yield (*E*)-4-(3,5-difluorostyryl)pyridine (purified via silica gel column chromatography). Catalytic hydrogenation with Adam's catalyst (PtO_2) and hydrogen gas afforded 4-(3,5-difluorophenethyl)piperidine (purified via silica gel column chromatography), which was reacted with potassium carbonate and (2-bromoethyl)benzene to yield the final product 4-(3,5-difluorophenethyl)-1-phenethylpiperidine (JPC-110) after purification via silica gel column chromatography.

1H NMR (300 MHz, $CDCl_3$): δ 1.31-1.95 (m, 9H), 2.44-3.02 (m, 8H). 6.71-7.34 (m, 8H) ppm.

^{13}C NMR (100 MHz, $DMSO-d_6$): δ 27.7, 30.7, 32.3, 33.0, 34.9, 52.9, 59.3, 107.7, 112.9, 126.5, 127.9, 128.7, 162.1 ppm.

MS (EI) m/z 329 (M^+).

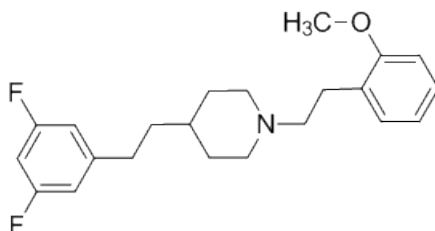


Figure 3.38 Structure of 4-(3,5-difluorophenethyl)-1-(2-methoxyphenethyl)piperidine (JPC-111)

Chemical Formula: $C_{22}H_{27}F_2NO$ Molecular Weight: 359.45

This molecule was designed to evaluate the effect of introducing the combination of a 2-methoxy substituent into the phenyl ring of the phenethyl linker attached to N1, and 3,5-difluoro substituents into the phenyl ring of the phenethyl linker attached to C4 of the piperidine ring in the 1,4-disubstituted piperidine scaffold on VMAT2 binding. 4-(3,5-Difluorophenethyl)piperidine was reacted with potassium carbonate and 1-(2-bromoethyl)-2-methoxybenzene to yield the final product, 4-(3,5-difluorophenethyl)-1-(2-methoxyphenethyl)piperidine (JPC-111) after purification via silica gel column chromatography.

1H NMR (300 MHz, $CDCl_3$): δ 1.28-1.97 (m, 9H), 2.47-3.08 (m, 8H), 3.80 (s, 3H), 6.63-7.31 (m, 7H) ppm.

^{13}C NMR (100 MHz, $DMSO-d_6$): δ 27.1, 29.2, 29.9, 30.6, 34.3, 51.7, 54.2, 57.0, 107.9, 110.5, 113.7, 120.1, 129.9, 130.3, 130.6, 158.0, 162.4 ppm.

MS (EI) m/z 359 (M^+).

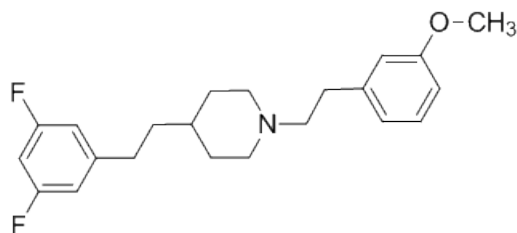


Figure 3.39 Structure of 4-(3,5-difluorophenethyl)-1-(3-methoxyphenethyl)piperidine (JPC-112)

Chemical Formula: $C_{22}H_{27}F_2NO$ Molecular Weight: 359.45

This molecule was designed to evaluate the effect of introducing the combination of a 3-methoxy substituent into the phenyl ring of the phenethyl linker attached to N1, and 3,5-difluoro substituents into the phenyl ring of the phenethyl linker attached to C4 of the piperidine ring in the 1,4-disubstituted piperidine scaffold on VMAT2 binding. 4-(3,5-Difluorophenethyl)piperidine was reacted with potassium carbonate and 1-(2-bromoethyl)-3-methoxybenzene to yield the final product, 4-(3,5-difluorophenethyl)-1-(3-methoxyphenethyl)piperidine (JPC-112) after purified via silica gel column chromatography.

1H NMR (300 MHz, $CDCl_3$): δ 1.29-2.03 (m, 9H), 2.56-3.03 (m, 8H), 3.79 (s, 3H), 6.68-6.76(m, 5H), 7.13-7.29 (m, 2H) ppm.

^{13}C NMR (75 MHz, $CDCl_3$): δ 32.6, 33.16, 34.13, 35.5, 38.0, 54.1, 55.4, 61.1, 100.9, 101.3, 101.6, 111.0, 111.32, 114.6, 121.2, 129.4, 142.3, 146.7, 154.6, 157.9, 161.3, 164.6 ppm.

MS (EI) m/z 359 (M^+).

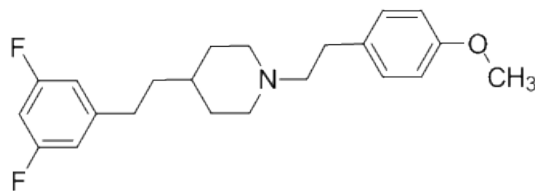


Figure 3.40 Structure of 4-(3,5-difluorophenethyl)-1-(4-methoxyphenethyl)piperidine (JPC-113)

Chemical Formula: $C_{22}H_{27}F_2NO$ Molecular Weight: 359.45

This molecule was designed to evaluate the effect of introducing the combination of a 4-methoxy substituent into the phenyl ring of the phenethyl linker attached to N1, and 3,5-difluoro substituents into the phenyl ring of the phenethyl linker attached to C4 of the piperidine ring in the 1,4-disubstituted piperidine scaffold on VMAT2 binding. 4-(3,5-Difluorophenethyl)piperidine was reacted with potassium carbonate and 1-(2-bromoethyl)-4-methoxybenzene to yield the final product 4-(3,5-difluorophenethyl)-1-(4-methoxyphenethyl)piperidine (JPC-113) after purification via silica gel column chromatography.

1H NMR (300 MHz, $CDCl_3$): δ 1.22-2.03 (m, 9H), 2.41-3.02 (m, 8H), 3.82 (s, 3H), 6.59-7.32 (m, 7H) ppm.

^{13}C NMR (100 MHz, $DMSO-d_6$): δ 28.9, 30.5, 31.8, 33.9, 36.1, 53.0, 55.1, 59.4, 108.4, 114.9, 116.0, 124.1, 159.9, 161.8 ppm.

MS (EI) m/z 359 (M^+).

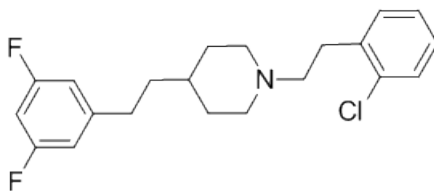


Figure 3.41 Structure of 1-(2-chlorophenethyl)-4-(3,5-difluorophenethyl)piperidine (JPC-114)

Chemical Formula: $C_{21}H_{24}ClF_2N$ Molecular Weight: 363.87

This molecule was designed to evaluate the effect of introducing the combination of a 2-chloro substituent into the phenyl ring of the phenethyl linker attached to N1, and 3,5-difluoro substituents into the phenyl ring of the phenethyl linker attached to C4 of the piperidine ring in the 1,4-disubstituted piperidine scaffold on VMAT2 binding. 4-(3,5-Difluorophenethyl)piperidine was reacted with potassium carbonate and 1-(2-bromoethyl)-2-chlorobenzene to yield the final product 1-(2-chlorophenethyl)-4-(3,5-difluorophenethyl)piperidine (JPC-114) after purification via silica gel column chromatography.

1H NMR (300 MHz, $CDCl_3$): δ 1.30-1.99 (m, 9H), 2.51-3.07 (m, 8H), 6.68-7.29 (m, 7H) ppm.

^{13}C NMR (100 MHz, $DMSO-d_6$): δ 27.9, 30.1, 31.0, 31.9, 34.7, 51.1, 54.8, 107.6, 114.2, 127.2, 127.4, 128.9, 129.7, 131.5, 161.7 ppm.

MS (EI) m/z 363 (M^+).

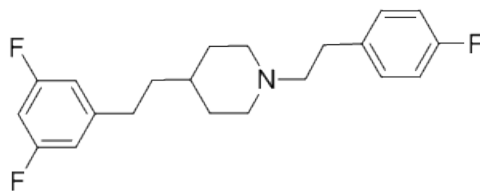


Figure 3.42 Structure of 4-(3,5-difluorophenethyl)-1-(4-fluorophenethyl)piperidine (JPC-115)

Chemical Formula: C₂₁H₂₄F₃N Molecular Weight: 347.42

This molecule was designed to evaluate the effect of introducing the combination of a 4-fluoro substituent into the phenyl ring of the phenethyl linker attached to N1, and 3,5-difluoro substituents into the phenyl ring of the phenethyl linker attached to C4 of the piperidine ring in the 1,4-disubstituted piperidine scaffold on VMAT2 binding. 4-(3,5-Difluorophenethyl)piperidine was reacted with potassium carbonate and 1-(2-bromoethyl)-4-fluorobenzene to yield the final product, 4-(3,5-difluorophenethyl)-1-(4-fluorophenethyl)piperidine (JPC-115) after purification via silica gel column chromatography.

¹H NMR (300 MHz, CDCl₃): δ 1.27-1.99 (m, 9H), 2.43-3.01 (m, 8H), 6.63-7.31 (m, 7H) ppm.

¹³C NMR (100 MHz, DMSO-d₆): δ 28.1, 30.95, 31.7, 32.9, 34.9, 51.9, 59.7, 106.8, 111.90, 112.0, 113.8, 113.93, 129.7, 161.2, 161.5 ppm.

MS (EI) m/z 347 (M⁺).

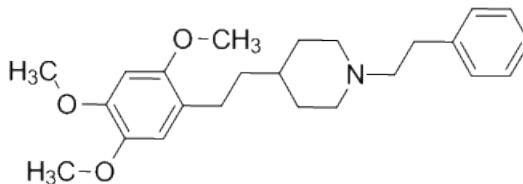


Figure 3.43 Structure of 1-phenethyl-4-(2,4,5-trimethoxyphenethyl)piperidine
(JPC-068)

Chemical Formula: $C_{24}H_{33}NO_3$ Molecular Weight: 383.52

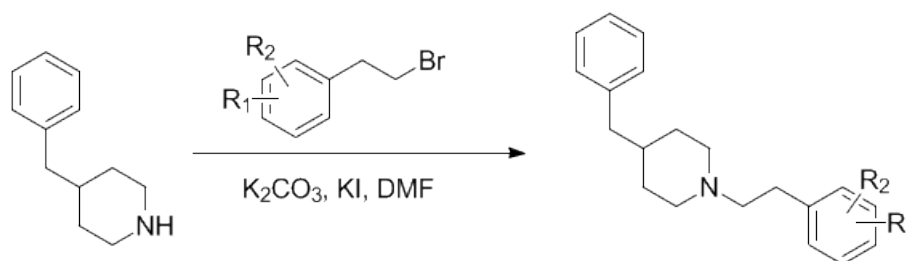
This molecule was designed to evaluate the effect of introducing 2,4,5-trimethoxy substituents into the phenyl ring of the phenethyl linker attached to C4 in the piperidine ring of the 1,4-disubstituted piperidine scaffold on VMAT2 binding. 4-Methylpyridine was subjected to Aldol condensation with 2,4,5-trimethoxybenzaldehyde in refluxing acetic anhydride to yield (*E*)-4-(2,4,5-trimethoxystyryl)pyridine (purified via silica gel column chromatography). Catalytic hydrogenation with Adam's catalyst (PtO_2) and hydrogen gas afforded 4-(2,4,5-trimethoxyphenethyl)piperidine (purified via silica gel column chromatography), which was reacted with potassium carbonate and (2-bromoethyl)benzene to yield the final product, 1-phenethyl-4-(2,4,5-trimethoxyphenethyl)piperidine (JPC-068) after purification via silica gel column chromatography.

1H NMR (300 MHz, $CDCl_3$): δ 1.24-1.97 (m, 7H), 2.47-2.98 (m, 10H), 3.72 (s, 3H), 3.77 (s, 3H), 3.80 (s, 3H), 6.44 (s, 1H), 6.62 (s, 1H), 7.12-7.24 (m, 5H) ppm.

^{13}C NMR (75 MHz, $CDCl_3$) δ 27.1, 32.6, 34.0, 35.8, 37.5, 54.3, 56.5, 56.7, 61.3, 114.1, 126.1, 128.5, 128.8, 140.6, 142.9, 147.6, 151.5 ppm.

MS (EI) m/z 383 (M^+).

A series of 1,4-disubstituted piperidine analogs were prepared with shorter alkane linker units between the C4 position of the piperidine ring and the phenyl moiety, while maintaining a substituted phenethyl linker at the N1 position of the piperidine ring, to determine the ability of the TBZ binding site on VMAT2 to recognize compounds with shorter linkers and less degrees of freedom of rotation. The synthetic route for generating these compounds is shown in Scheme 3.2, and a total of four compounds were synthesized via a one-step synthesis.



Scheme 3.2 Synthetic route to the phenethyl substituted 4-benzyl-1-phenethylpiperidine analogs of lobelane

Starting with 4-benzylpiperidine, which was readily available from Sigma Aldrich, a simple S_N2 reaction with potassium carbonate and the appropriately substituted (2-bromoethyl)benzene afforded the desired 4-benzyl-1-phenethylpiperidine product, which was purified by silica gel column chromatography. The four compounds designed and synthesized in this series, their structures, and analytical data follow in Figures 3.44 through 3.47. NMR spectra were recorded in either CDCl₃ or DMSO-d₆ (as designated) on one of three Varian instruments (300 MHz, 400 MHz, or 500 MHz) as indicated are reported in ppm relative to either TMS as internal standard or as relative to the solvent

peak present in ^{13}C spectra. GC-mass spectra were recorded on an Agilent 6890 GC incorporating an Agilent 7683 autosampler and an Agilent 5973 MSD.

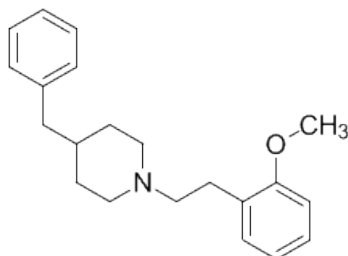


Figure 3.44 Structure of 4-benzyl-1-(2-methoxyphenethyl)piperidine (JPC-061)

Chemical Formula: $C_{21}H_{27}NO$ Molecular Weight: 309.45

This molecule was designed to evaluate the effect of incorporating a shorter methylene linker between the C4 position of the piperidine ring and the phenyl moiety, while maintaining a 2-methoxyphenethyl unit on the N1 position in the piperidine ring of the 1,4-disubstituted piperidine scaffold on VMAT2 binding. 4-Benzylpiperidine was subjected to S_N2 reaction with potassium carbonate and 1-(2-bromoethyl)-2-methoxybenzene to yield the final product 4-benzyl-1-(2-methoxyphenethyl)piperidine (JPC-061).

1H NMR (300 MHz, $CDCl_3$): δ 1.30-1.91 (m, 5H), 2.47-2.61 (m, 6H), 2.75-2.78 (m, 4H), 3.82 (s, 3H) 6.74-7.35 (m, 9H) ppm.

MS (EI) m/z 309 (M^+).

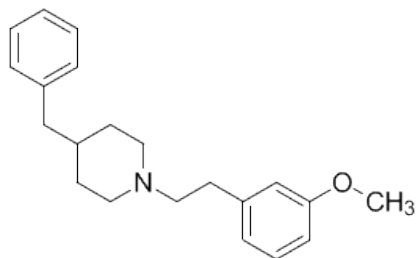


Figure 3.45 Structure of 4-benzyl-1-(3-methoxyphenethyl)piperidine (JPC-062)

Chemical Formula: $C_{21}H_{27}NO$ Molecular Weight: 309.45

This molecule was designed to evaluate the effect of incorporating a shorter methylene linker between the C4 position of the piperidine ring and the phenyl moiety while, maintaining a 3-methoxyphenethyl unit on the N1 position in the piperidine ring of the 1,4-disubstituted piperidine scaffold on VMAT2 binding. 4-Benzylpiperidine was subjected to S_N2 reaction with potassium carbonate and 1-(2-bromoethyl)-3-methoxybenzene to yield the final product, 4-benzyl-1-(3-methoxyphenethyl)piperidine (JPC-062).

1H NMR (300 MHz, $CDCl_3$): δ 1.32-1.95 (m, 5H), 2.43-2.60 (m, 6H), 2.77-2.82 (m, 4H), 3.81 (s, 3H) 6.71-7.32 (m, 9H) ppm.

MS (EI) m/z 309 (M^+).

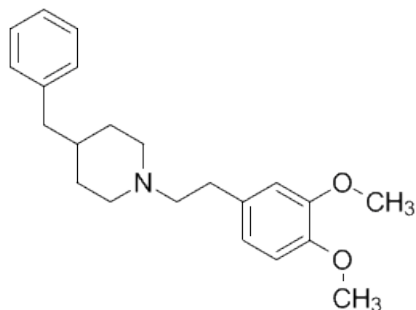


Figure 3.46 Structure of 4-benzyl-1-(3,4-dimethoxyphenethyl)piperidine (JPC-063) Chemical Formula: $C_{22}H_{29}NO_2$ Molecular Weight: 339.47

This molecule was designed to evaluate the effect of incorporating a shorter methylene linker between the C4 position of the piperidine ring and the phenyl moiety, while maintaining a 3,4-dimethoxyphenethyl unit on the N1 position in the piperidine ring of the 1,4-disubstituted piperidine scaffold on VMAT2 binding. 4-Benzylpiperidine was subjected to S_N2 reaction with potassium carbonate and 1-(2-bromoethyl)-3,4-dimethoxybenzene to yield the final product, 4-benzyl-1-(3,4-dimethoxyphenethyl)piperidine (JPC-063).

1H NMR (300 MHz, $CDCl_3$): δ 1.34-1.87 (m, 5H), 2.41-2.57 (m, 6H), 2.71-2.80 (m, 4H), 3.80 (s, 6H) 6.71-7.30 (m, 8H) ppm.

MS (EI) m/z 339 (M^+).

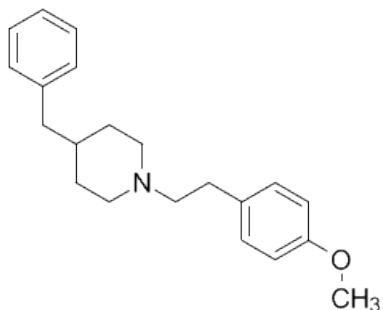


Figure 3.47 Structure of 4-benzyl-1-(4-methoxyphenethyl)piperidine (JPC-064)

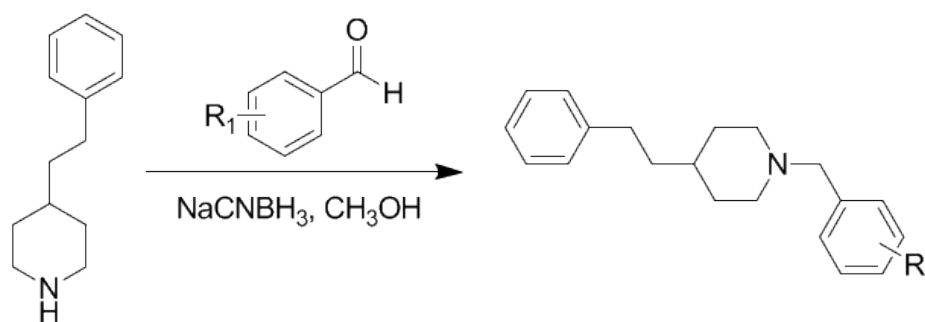
Chemical Formula: $C_{21}H_{27}NO$ Molecular Weight: 309.45

This molecule was designed to evaluate the effect of incorporating a shorter methylene linker between the C4 position of the piperidine ring and the phenyl moiety, while maintaining a 4-methoxyphenethyl unit on the N1 position in the piperidine ring of the 1,4-disubstituted piperidine scaffold on VMAT2 binding. 4-Benzylpiperidine was subjected to S_N2 reaction with potassium carbonate and 1-(2-bromoethyl)-4-methoxybenzene to yield the final product, 4-benzyl-1-(4-methoxyphenethyl)piperidine (JPC-064).

1H NMR (300 MHz, $CDCl_3$): δ 1.28-1.98 (m, 5H), 2.46-2.62 (m, 6H), 2.75-2.84 (m, 4H), 3.82 (s, 3H) 6.75-7.37 (m, 9H) ppm.

MS (EI) m/z 309 (M^+).

A series of 1,4-substituted piperidine analogs with shorter methylene linkers between the N1 position of the piperidine ring and the substituted phenyl moiety, while maintaining a substituted phenethyl linker on the C4 position, were prepared to further analyze the ability of the TBZ binding site on VMAT2 to recognize compounds with shorter linkers and less degrees of freedom of rotation (one carbon shorter) at the N1 position. The synthetic route for generating these compounds is shown in Scheme 3.3, and a total of six compounds were synthesized via a one-step synthesis.



Scheme 3.3 Synthetic route to the substituted 1-benzyl-4-phenethylpiperidine analogs of lobelane.

4-Phenethylpiperidine, which had been previously prepared in earlier syntheses, was subjected to a reductive amination reaction with an appropriately substituted benzaldehyde and sodium cyanoborohydride in methanol to yield the appropriate 1-benzyl-4-phenethylpiperidine product, which was purified by silica gel column chromatography. The six compounds designed and synthesized in this series, their structures, and analytical data follow in Figures 3.48 through 3.53. NMR spectra were recorded in either $CDCl_3$ or $DMSO-d_6$ (as designated) on one of three Varian instruments (300 MHz, 400 MHz, or 500 MHz) as indicated are reported in ppm relative to either

TMS as internal standard or as relative to the solvent peak present in ^{13}C spectra. GC-mass spectra were recorded on an Agilent 6890 GC incorporating an Agilent 7683 autosampler and an Agilent 5973 MSD.

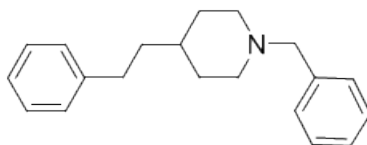


Figure 3.48 Structure of 1-benzyl-4-phenethylpiperidine (JPC-152)

Chemical Formula: $C_{20}H_{25}N$ Molecular Weight: 279.42

This molecule was designed to evaluate the effect that a shorter methylene linker (one carbon) between the N1 position on the piperidine ring and the phenyl ring, while maintaining a phenethyl linker at the C4 position in the piperidine ring of the 1,4-disubstituted piperidine scaffold would have on VMAT2 binding. 4-Phenethylpiperidine, which had been previously prepared in earlier syntheses, was subjected to reductive amination conditions with benzaldehyde and sodium cyanoborohydride in methanol to afford the final product 1-benzyl-4-phenethylpiperidine (JPC-152).

^1H NMR (300 MHz, CDCl_3): δ 1.05-1.92 (m, 9H), 2.58-2.86 (m, 4H), 3.48 (s, 2H), 7.15-7.32 (m, 10H) ppm.

^{13}C NMR (75 MHz, CDCl_3): δ 26.8, 32.6, 33.4, 35.65, 38.7, 54.1, 63.8, 125.7, 127.0, 128.25, 128.4, 128.5, 129.4, 138.8, 142.95 ppm.

MS (EI) m/z 279 (M^+).

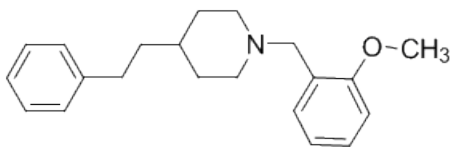


Figure 3.49 Structure of 1-(2-methoxybenzyl)-4-phenethylpiperidine (JPC-153)

Chemical Formula: $C_{21}H_{27}NO$ Molecular Weight: 309.45

This molecule was designed to evaluate the effect that a shorter methylene linker (one carbon) between the N1 position of the piperidine ring and a 2-methoxyphenyl ring, while maintaining a phenethyl linker at the C4 position in the piperidine ring of the 1,4-disubstituted piperidine scaffold would have on VMAT2 binding 4-Phenethylpiperidine was subjected to reductive amination conditions with 2-methoxybenzaldehyde and sodium cyanoborohydride in methanol to afford the final product 1-(2-methoxybenzyl)-4-phenethylpiperidine (JPC-153).

1H NMR (300 MHz, $CDCl_3$): δ 1.28-2.05 (m, 9H), 2.58-2.94 (m, 4H), 3.55 (s, 2H), 3.81 (s, 3H) 6.84-7.37 (m, 9H) ppm.

^{13}C NMR (75 MHz, $CDCl_3$): δ 26.8, 32.7, 33.5, 35.6, 38.8, 54.1, 55.7, 56.6, 110.55, 120.4, 125.7, 127.9, 128.4, 128.5, 130.7, 157.9 ppm.

MS (EI) m/z 309 (M^+).

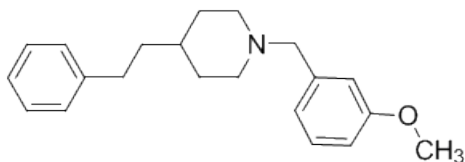


Figure 3.50 Structure of 1-(3-methoxybenzyl)-4-phenethylpiperidine (JPC-154)

Chemical Formula: $C_{21}H_{27}NO$ Molecular Weight: 309.45

This molecule was designed to evaluate the effect that a shorter methylene linker (one carbon) between the N1 position of the piperidine ring and a 3-methoxyphenyl ring, while maintaining a phenethyl linker at the C4 position in the piperidine ring of the 1,4-disubstituted piperidine scaffold would have on VMAT2 binding. 4-Phenethylpiperidine was subjected to reductive amination conditions with 3-methoxybenzaldehyde and sodium cyanoborohydride in methanol to afford the final product, 1-(3-methoxybenzyl)-4-phenethylpiperidine (JPC-154).

1H NMR (300 MHz, $CDCl_3$): δ 1.28-2.00 (m, 9H), 2.59-2.90 (m, 4H), 3.46 (s, 2H), 3.81 (s, 3H), 6.77-7.29 (m, 9H) ppm.

^{13}C NMR (75 MHz, $CDCl_3$): δ 32.6, 33.4, 35.6, 38.7, 54.1, 55.5, 63.7, 112.5, 114.8, 121.7, 125.7, 128.4, 128.5, 129.2, 141.7, 159.9 ppm.

MS (EI) m/z 309 (M^+).

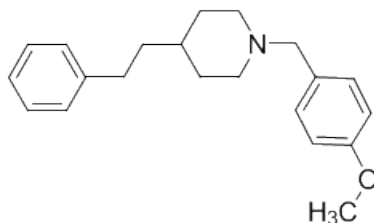


Figure 3.51 Structure of 1-(4-methoxybenzyl)-4-phenethylpiperidine (JPC-155)

Chemical Formula: $C_{21}H_{27}NO$ Molecular Weight: 309.45

This molecule was designed to evaluate the effect that a shorter methylene linker (one carbon) between the N1 position of the piperidine ring and a 4-methoxyphenyl ring, while maintaining a phenethyl linker at the C4 position of the piperidine ring of the 1,4-disubstituted piperidine scaffold would have on VMAT2 binding 4-Phenethylpiperidine was subjected to reductive amination conditions with 4-methoxybenzaldehyde and sodium cyanoborohydride in methanol to afford the final product 1-(4-methoxybenzyl)-4-phenethylpiperidine (JPC-155).

1H NMR (300 MHz, $CDCl_3$): δ 1.29-1.97 (m, 9H), 2.58-2.90 (m, 4H), 3.44 (s, 2H), 3.80 (s, 3H) 6.83-7.32 (m, 9H) ppm.

^{13}C NMR (75 MHz, $CDCl_3$): δ 26.8, 32.5, 33.4, 35.6, 38.7, 53.94, 55.51, 63.1, 113.7, 125.7, 128.41, 128.44, 130.6, 142.92, 159.5 ppm.

MS (EI) m/z 309 (M^+).

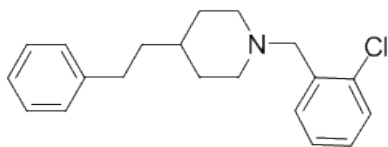


Figure 3.52 Structure of 1-(2-chlorobenzyl)-4-phenethylpiperidine (JPC-156)

Chemical Formula: $C_{20}H_{24}ClN$ Molecular Weight: 313.86

This molecule was designed to evaluate the effect that a shorter methylene linker (one carbon) between the N1 position of the piperidine ring and a 2-chlorophenyl ring, while maintaining a phenethyl linker at the C4 position of the piperidine ring of the 1,4-disubstituted piperidine scaffold would have on VMAT2 binding. 4-Phenethylpiperidine was subjected to reductive amination conditions with 2-chlorobenzaldehyde and sodium cyanoborohydride in methanol to afford the final product, 1-(2-chlorobenzyl)-4-phenethylpiperidine (JPC-156).

1H NMR (300 MHz, $CDCl_3$): δ 1.25-2.01 (m, 9H), 2.58-2.89 (m, 4H), 3.57 (s, 2H), 7.18-7.57 (m, 9H) ppm.

^{13}C NMR (75 MHz, $CDCl_3$): δ 32.73, 33.5, 35.6, 38.8, 54.3, 59.8, 125.7, 126.7, 128.0, 128.41, 128.44, 129.4, 130.4, 134.2, 136.3, 143.6 ppm.

MS (EI) m/z 313 (M^+).

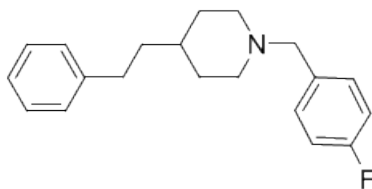


Figure 3.53 Structure of 1-(4-fluorobenzyl)-4-phenethylpiperidine (JPC-157)

Chemical Formula: $C_{20}H_{24}FN$ Molecular Weight: 297.41

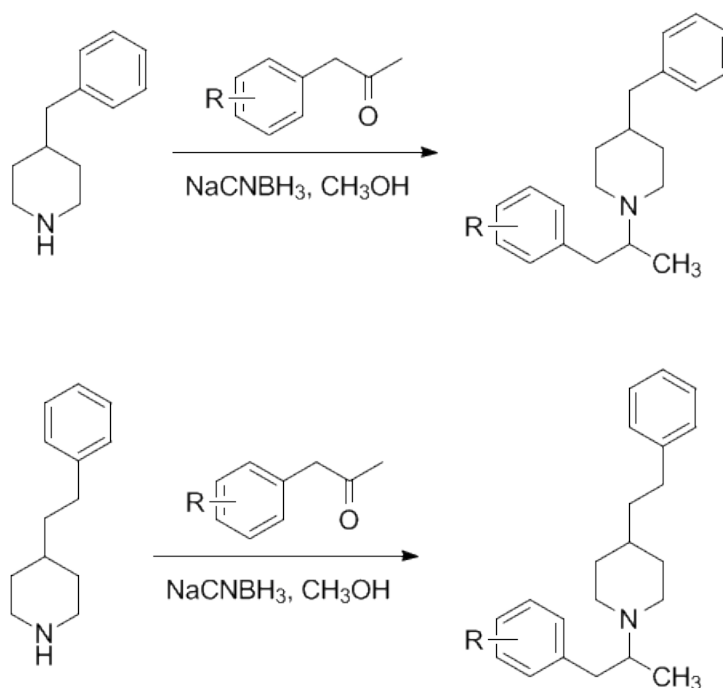
This molecule was designed to evaluate the effect that of a shorter methylene linker (one carbon) between the N1 position of the piperidine ring and a 4-fluorophenyl ring, while maintaining a phenethyl linker at the C4 position of the piperidine ring of the 1,4-disubstituted piperidine scaffold of analog would have on VMAT2 binding. 4-Phenethylpiperidine was subjected to reductive amination conditions with 4-fluorobenzaldehyde and sodium cyanoborohydride in methanol to afford the final product 1-(4-fluorobenzyl)-4-phenethylpiperidine (JPC-157).

1H NMR (300 MHz, $CDCl_3$): δ 1.05-1.65 (m, 7H), 2.31-2.73 (t, 6H), 3.60 (s, 2H), 7.18-7.47 (m, 9H) ppm.

^{13}C NMR (75 MHz, $CDCl_3$): δ 32.4, 32.8, 35.9, 38.3, 52.9, 53.14, 61.3, 114.63, 124.7, 127.7, 127.9, 130.45, 132.2, 142.6, 159.9 ppm.

MS (EI) m/z 309 (M^+).

Similarly, another series of 1,4-disubstituted piperidine analogs combined these factors with shorter linkers between the N1 position of the piperidine ring and the phenyl moiety, while maintaining a substituted phenethyl linker on the C4 position; or with shorter linkers between the C4 position of the piperidine ring and the phenyl moiety, while maintaining a substituted phenethyl linker at the N1 position, were prepared to further analyze the ability of the TBZ binding site on VMAT2 to recognize compounds with shorter linkers and less degrees of freedom of rotation (one carbon shorter) at the N1 position. This series of compounds incorporated an alkylbranch in the N1 alkyl linker to afford a racemic 1-phenylpropan-2-yl moiety attached to N1 of the piperidine ring. The combined synthetic routes for generating these compounds is shown in Scheme 3.4, and a total of four compounds were prepared via a one-step synthesis.



Scheme 3.4 Synthesis of the 4-phenethyl-1-(1-phenylpropan-2-yl)piperidine and 4-benzyl-1-(1-phenylpropan-2-yl)piperidine series of lobelane analogs

4-Benzylpiperidine or 4-phenethylpiperidine were each subjected to reductive amination conditions with the appropriately substituted 1-phenylpropan-2-one and sodium cyanoborohydride in methanol. This afforded the desired 4-phenethyl-1-(1-phenylpropan-2-yl)piperidine and 4-benzyl-1-(1-phenylpropan-2-yl)piperidine scaffolds, respectively. This synthetic route to these series of molecules also allowed for the introduction of a bromo substituted phenyl moiety into the scaffold. The final products were purified via silica gel column chromatography. The structures of four compounds from this series together with their analytical data are shown in Figures 3.54 through 3.57. NMR spectra were recorded in either CDCl₃ or DMSO-d₆ (as designated) on one of three Varian instruments (300 MHz, 400 MHz, or 500 MHz) as indicated are reported in ppm relative to either TMS as internal standard or as relative to the solvent peak present in ¹³C spectra. GC-mass spectra were recorded on an Agilent 6890 GC incorporating an Agilent 7683 autosampler and an Agilent 5973 MSD.

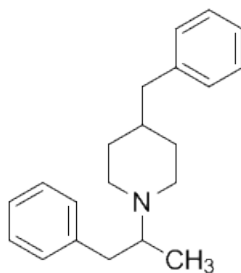


Figure 3.54 Structure of racemic 4-benzyl-1-(1-phenylpropan-2-yl)piperidine (JPC-174) Chemical Formula: $C_{21}H_{27}N$ Molecular Weight: 293.45

4-Benzylpiperidine was subjected to reductive amination conditions with 1-phenylpropan-2-one and sodium cyanoborohydride in methanol to afford the final product, (\pm)-4-benzyl-1-(1-phenylpropan-2-yl)piperidine (JPC-174).

1H NMR (300 MHz, $CDCl_3$): δ 0.97 (d, 3H), 1.02-1.88 (m, 5H), 2.21-2.96 (m, 8H), 3.10 (m, 1H), 7.15-7.36 (m, 10H) ppm.

^{13}C NMR (75 MHz, $CDCl_3$): δ 14.5, 26.7, 32.8, 33.9, 38.6, 39.4, 43.5, 48.8, 49.5, 53.7, 62.0, 125.87, 125.93, 128.2, 128.3, 129.2, 129.4, 139.7, 140.8 ppm.

MS (EI) m/z 293 (M^+).

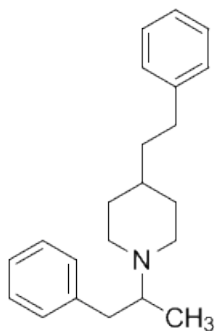


Figure 3.55 Structure of racemic 4-phenethyl-1-(1-phenylpropan-2-yl)piperidine (JPC-175) Chemical Formula: $C_{22}H_{29}N$ Molecular Weight: 307.47

4-Phenethylpiperidine was subjected to reductive amination conditions with 1-phenylpropan-2-one and sodium cyanoborohydride in methanol to afford the final product (\pm)-4-phenethyl-1-(1-phenylpropan-2-yl)piperidine (JPC-175).

1H NMR (300 MHz, $CDCl_3$): δ 0.96 (d, 3H), 1.22-1.92 (m, 7H), 2.21-2.96 (m, 8H), 3.07 (m, 1H), 7.18-7.34 (m, 10H) ppm.

^{13}C NMR (75 MHz, $CDCl_3$): δ 14.6, 33.0, 33.1, 33.4, 36.0, 38.8, 39.5, 48.9, 49.5, 62.0, 125.7, 125.9, 128.3, 128.4, 128.43, 128.51, 128.57, 129.4, 141.0, 142.9, 149.8 ppm.

MS (EI) m/z 307 (M^+).

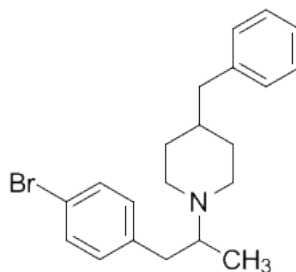


Figure 3.56 Structure of racemic 4-benzyl-1-(1-(4-bromophenyl)propan-2-yl)piperidine (JPC-171)

Chemical Formula: $C_{21}H_{26}BrN$ Molecular Weight: 372.34

4-Benzylpiperidine was subjected to reductive amination conditions with 1-(4-bromophenyl)propan-2-one and sodium cyanoborohydride in methanol to afford the final product (\pm)-4-benzyl-1-(1-(4-bromophenyl)propan-2-yl)piperidine (JPC-171).

1H NMR (300 MHz, $CDCl_3$): δ 0.97 (d, 3H), 1.07-1.84 (m, 5H), 2.25-2.99 (m, 8H), 3.15 (m, 1H), 7.15-7.46 (m, 7H), 7.86-7.90 (m, 2H) ppm.

^{13}C NMR (75 MHz, $CDCl_3$): δ 14.6, 33.0, 33.1, 33.4, 36.0, 38.8, 39.5, 48.9, 49.5, 62.0, 125.7, 125.9, 128.3, 128.4, 128.43, 128.51, 128.57, 129.4, 141.0, 142.9, 149.8 ppm.

MS (EI) m/z 372 (M^+).

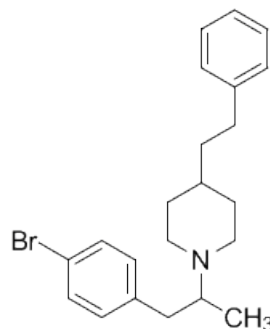


Figure 3.57 Structure of racemic 1-(1-(4-bromophenyl)propan-2-yl)-4-phenethylpiperidine (JPC-172)

Chemical Formula: $C_{22}H_{28}BrN$ Molecular Weight: 386.37

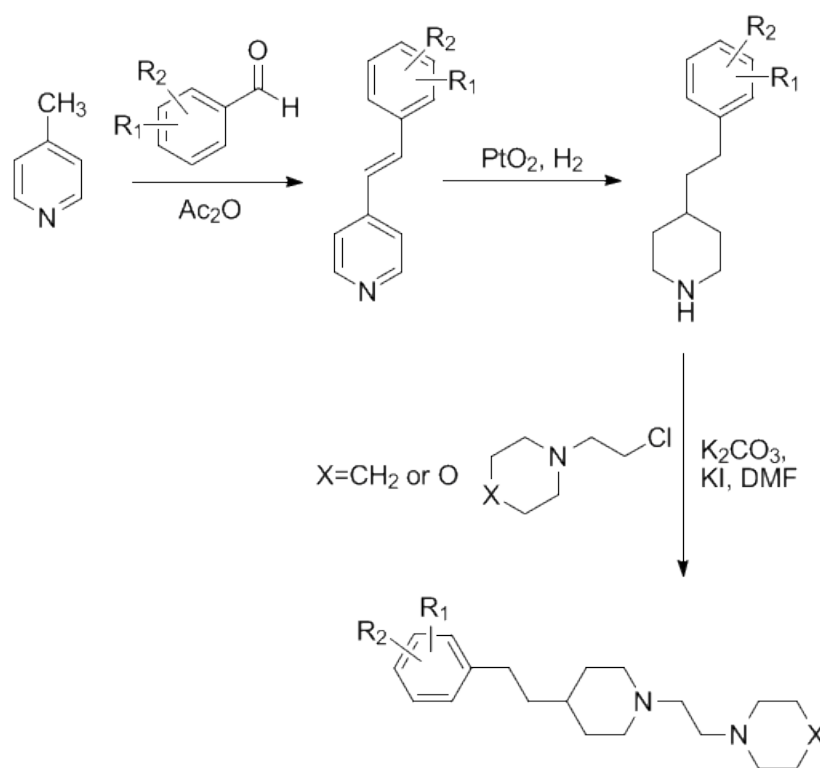
4-Phenethylpiperidine was subjected to reductive amination conditions with 1-(4-bromophenyl)propan-2-one and sodium cyanoborohydride in methanol to afford the final product, (\pm)-1-(1-(4-bromophenyl)propan-2-yl)-4-phenethylpiperidine (JPC-172).

1H NMR (300 MHz, $CDCl_3$): δ 0.98 (d, 3H), 1.22-1.80 (m, 7H), 2.28-2.94 (m, 8H), 3.13 (m, 1H), 7.24-7.65 (m, 9H) ppm.

^{13}C NMR (75 MHz, $CDCl_3$): δ 13.5, 31.2, 33.1, 35.1, 36.8, 37.3, 37.9, 38.5, 47.9, 50.3, 53.7, 62.4, 120.3, 124.0, 125.9, 126.3, 128.4, 129.5, 131.1, 131.6, 142.3, 149.7 ppm.

MS (EI) m/z 386 (M^+).

The final series of 1,4-disubstituted piperidine analogs was designed to increase the water-solubility of the scaffold by replacing the phenyl ring at the N1 phenethyl linker with saturated heterocyclic moieties, i.e. either piperidine or morpholine, and to study what effect the introduction of a more polar moiety would have on binding affinity at the TBZ site of VMAT2. Utilizing synthetic methods similar to those used in Scheme 3.1, 11 analogs were designed and synthesized in this series. The chemistry by which this series of compounds were generated is shown in Scheme 3.5.



Scheme 3.5 Synthesis of the 4-phenethyl-1-(2-(piperidin-1-yl)ethyl)piperidine and 4-(2-(4-phenethylpiperidin-1-yl)ethyl)morpholine series of lobelane analogs

The general synthetic scheme to the 4-phenethyl-1-(2-(piperidin-1-yl)ethyl)piperidine and 4-(2-(4-phenethylpiperidin-1-yl)ethyl)morpholine analogs of lobelane utilizes 4-

methylpyridine as the starting material. Similar to chemistry used to construct the 2,6-substituted scaffold, 4-methylpyridine was subjected to Aldol condensation with an appropriately substituted benzaldehyde in refluxing acetic anhydride to afford the corresponding (*E*)-4-styrylpyridine intermediate. After purification via silica gel column chromatography, the conjugated intermediate was then subjected to catalytic hydrogenation with Adam's catalyst and hydrogen gas in acetic acid, to afford the appropriate substituted 4-phenethylpiperidine intermediate. The 4-phenethylpiperidine intermediate was then subjected to a S_N2 reaction with potassium carbonate and either 1-(2-chloroethyl)piperidine or 4-(2-chloroethyl)morpholine, to yield respectively the final products of the 4-phenethyl-1-(2-(piperidin-1-yl)ethyl)piperidine and 4-(2-(4-phenethylpiperidin-1-yl)ethyl)morpholine series of lobelane analogs. The exact structures of the above compounds and the analytical data for each compound are shown in Figures 3.58 through 3.68. NMR spectra were recorded in either CDCl₃ or DMSO-d₆ (as designated) on one of three Varian instruments (300 MHz, 400 MHz, or 500 MHz) as indicated are reported in ppm relative to either TMS as internal standard or as relative to the solvent peak present in ¹³C spectra. GC-mass spectra were recorded on an Agilent 6890 GC incorporating an Agilent 7683 autosampler and an Agilent 5973 MSD.

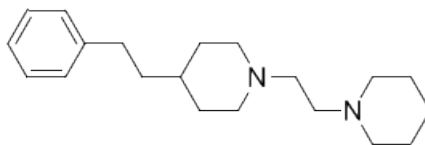


Figure 3.58 Structure of 4-phenethyl-1-(2-(piperidin-1-yl)ethyl)piperidine (JPC-116) Chemical Formula: $C_{20}H_{32}N_2$ Molecular Weight: 300.48

4-Methylpyridine was subjected to Aldol condensation with benzaldehyde in refluxing acetic anhydride to yield (*E*)-4-styrylpyridine (purified via silica gel column chromatography). Subsequent catalytic hydrogenation with Adam's catalyst (PtO_2) and hydrogen gas afforded 4-phenethylpiperidine (purified via silica gel column chromatography), which was then reacted with potassium carbonate and 1-(2-chloroethyl)piperidine in DMF to yield the final product, 4-phenethyl-1-(2-(piperidin-1-yl)ethyl)piperidine (JPC-116) after purification via silica gel column chromatography. 1H NMR (300 MHz, $CDCl_3$): δ 1.43-1.78 (m, 13H), 2.31-2.65 (m, 14H), 7.23-7.43 (m, 5H) ppm. MS (EI) m/z 300 (M^+).

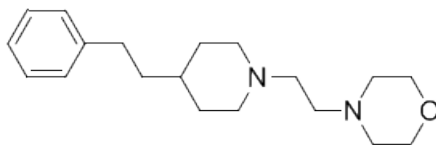


Figure 3.59 Structure of 4-(2-(4-phenethylpiperidin-1-yl)ethyl)morpholine
(JPC-117) Chemical Formula: $C_{19}H_{30}N_2O$ Molecular Weight: 302.45

4-Methylpyridine was subjected to Aldol condensation with benzaldehyde in refluxing acetic anhydride to yield (*E*)-4-styrylpyridine (purified via silica gel column chromatography). Subsequent catalytic hydrogenation with Adam's catalyst (PtO_2) and hydrogen gas afforded 4-phenethylpiperidine (purified via silica gel column chromatography), which was reacted with potassium carbonate and 4-(2-chloroethyl)morpholine in DMF to yield the final product 4-(2-(4-phenethylpiperidin-1-yl)ethyl)morpholine (JPC-117) after purification via silica gel column chromatography.

1H NMR (300 MHz, $CDCl_3$): δ 1.35-1.68 (m, 7H), 2.37-2.70 (m, 14H), 3.43-3.51 (m, 4H) 7.23-7.41 (m, 5H) ppm.

MS (EI) m/z 300 (M^+).

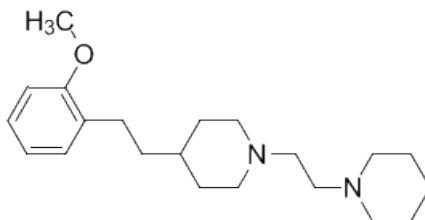


Figure 3.60 Structure of 4-(2-methoxyphenethyl)-1-(2-(piperidin-1-yl)ethyl)piperidine (JPC-118)

Chemical Formula: $C_{21}H_{34}N_2O$ Molecular Weight: 330.51

4-Methylpyridine was subjected to Aldol condensation with 2-methoxybenzaldehyde in refluxing acetic anhydride to yield (*E*)-4-(2-methoxystyryl)pyridine (purified via silica gel column chromatography). Subsequent catalytic hydrogenation with Adam's catalyst (PtO_2) and hydrogen gas afforded 4-(2-methoxyphenethyl)piperidine (purified via silica gel column chromatography), which was reacted with potassium carbonate and 1-(2-chloroethyl)piperidine in DMF to yield the final product 4-(2-methoxyphenethyl)-1-(2-(piperidin-1-yl)ethyl)piperidine (JPC-118) after purification via silica gel column chromatography.

1H NMR (300 MHz, $CDCl_3$): δ 1.47-1.68 (m, 13H), 2.30-2.67 (m, 14H), 3.82 (s, 3H), 6.81-7.23 (m, 4H) ppm.

MS (EI) m/z 330 (M^+).

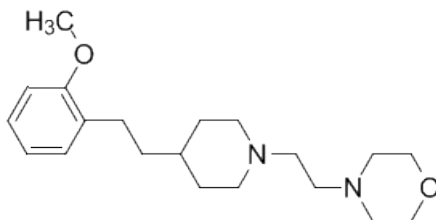


Figure 3.61 Structure of 4-(2-(4-(2-methoxyphenethyl)piperidin-1-yl)ethyl)morpholine (JPC-119)

Chemical Formula: $C_{20}H_{32}N_2O_2$ Molecular Weight: 332.48

4-Methylpyridine was subjected to Aldol condensation with 2-methoxybenzaldehyde in refluxing acetic anhydride to yield (*E*)-4-(2-methoxystyryl)pyridine (purified via silica gel column chromatography). Subsequent catalytic hydrogenation with Adam's catalyst (PtO_2) and hydrogen gas afforded 4-(2-methoxyphenethyl)piperidine (purified via silica gel column chromatography), which was reacted with potassium carbonate and 4-(2-chloroethyl)morpholine in DMF to yield the final product 4-(2-(4-(2-methoxyphenethyl)piperidin-1-yl)ethyl)morpholine (JPC-119) after purification via silica gel column chromatography.

1H NMR (300 MHz, $CDCl_3$): δ 1.32-1.64 (m, 7H), 2.44-2.68 (m, 14H), 3.48-3.58 (m, 4H), 3.81 (s, 3H), 6.81-7.23 (m, 4H) ppm.

MS (EI) m/z 332 (M^+).

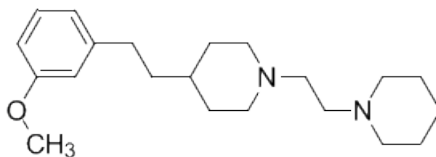


Figure 3.62 Structure of 4-(3-methoxyphenethyl)-1-(2-(piperidin-1-yl)ethyl)piperidine (JPC-120)

Chemical Formula: $C_{21}H_{34}N_2O$ Molecular Weight: 330.51

4-Methylpyridine was subjected to Aldol condensation with 3-methoxybenzaldehyde in refluxing acetic anhydride to yield (*E*)-4-(3-methoxystyryl)pyridine (purified via silica gel column chromatography). Subsequent catalytic hydrogenation with Adam's catalyst (PtO_2) and hydrogen gas afforded 4-(3-methoxyphenethyl)piperidine (purified via silica gel column chromatography), which was reacted with potassium carbonate and 1-(2-chloroethyl)piperidine in DMF to yield the final product, 4-(3-methoxyphenethyl)-1-(2-(piperidin-1-yl)ethyl)piperidine (JPC-120) after purification via silica gel column chromatography.

1H NMR (300 MHz, $CDCl_3$): δ 1.42-1.66 (m, 13H), 2.32-2.64 (m, 14H), 3.81 (s, 3H), 6.83-7.27 (m, 4H) ppm.

MS (EI) m/z 330 (M^+).

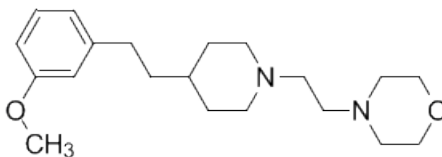


Figure 3.63 Structure of 4-(2-(4-(3-methoxyphenethyl)piperidin-1-yl)ethyl)morpholine (JPC-121)

Chemical Formula: $C_{20}H_{32}N_2O_2$ Molecular Weight: 332.48

4-Methylpyridine was subjected to Aldol condensation with 3-methoxybenzaldehyde in refluxing acetic anhydride to yield (*E*)-4-(3-methoxystyryl)pyridine (purified via silica gel column chromatography). Subsequent catalytic hydrogenation with Adam's catalyst (PtO_2) and hydrogen gas afforded 4-(3-methoxyphenethyl)piperidine (purified via silica gel column chromatography), which was reacted with potassium carbonate and 4-(2-chloroethyl)morpholine in DMF to yield the final product 4-(2-(4-(3-methoxyphenethyl)piperidin-1-yl)ethyl)morpholine (JPC-121) after purification via silica gel column chromatography.

1H NMR (300 MHz, $CDCl_3$): δ 1.38-1.67 (m, 7H), 2.44-2.67 (m, 14H), 3.47-3.60 (m, 4H), 3.82 (s, 3H), 6.78-7.19 (m, 4H) ppm.

MS (EI) m/z 332 (M^+).

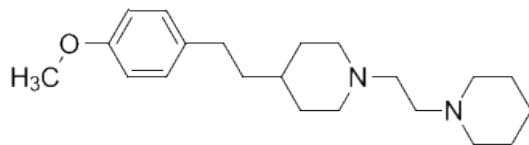


Figure 3.64 Structure of 4-(4-methoxyphenethyl)-1-(2-(piperidin-1-yl)ethyl)piperidine (JPC-122)

Chemical Formula: $C_{21}H_{34}N_2O$ Molecular Weight: 330.51

4-Methylpyridine was subjected to Aldol condensation with 4-methoxybenzaldehyde in refluxing acetic anhydride to yield (*E*)-4-(4-methoxystyryl)pyridine (purified via silica gel column chromatography). Subsequent catalytic hydrogenation with Adam's catalyst (PtO_2) and hydrogen gas afforded 4-(4-methoxyphenethyl)piperidine (purified via silica gel column chromatography), which was reacted with potassium carbonate and 1-(2-chloroethyl)piperidine in DMF to yield the final product, 4-(4-methoxyphenethyl)-1-(2-(piperidin-1-yl)ethyl)piperidine (JPC-122) after purification via silica gel column chromatography.

1H NMR (300 MHz, $CDCl_3$): δ 1.35-1.68 (m, 13H), 2.36-2.62 (m, 14H), 3.80 (s, 3H), 6.80-7.22 (m, 4H) ppm.

MS (EI) m/z 330 (M^+).

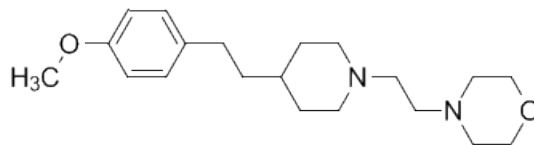


Figure 3.65 Structure of 4-(2-(4-(4-methoxyphenethyl)piperidin-1-yl)ethyl)morpholine (JPC-123)

Chemical Formula: $C_{20}H_{32}N_2O_2$ Molecular Weight: 332.48

4-Methylpyridine was subjected to Aldol condensation with 4-methoxybenzaldehyde in refluxing acetic anhydride to yield (*E*)-4-(4-methoxystyryl)pyridine (purified via silica gel column chromatography). Subsequent catalytic hydrogenation with Adam's catalyst (PtO_2) and hydrogen gas afforded 4-(4-methoxyphenethyl)piperidine (purified via silica gel column chromatography), which was reacted with potassium carbonate and 4-(2-chloroethyl)morpholine in DMF to yield the final product 4-(2-(4-(4-methoxyphenethyl)piperidin-1-yl)ethyl)morpholine (JPC-123) after purification via silica gel column chromatography.

1H NMR (300 MHz, $CDCl_3$): δ 1.31-1.62 (m, 7H), 2.48-2.70 (m, 14H), 3.45-3.62 (m, 4H), 3.84 (s, 3H), 6.73-7.26 (m, 4H) ppm.

MS (EI) m/z 332 (M^+).

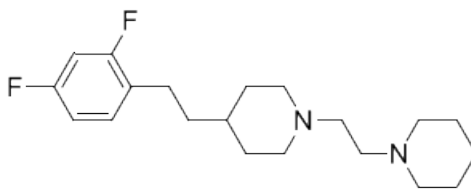


Figure 3.66 Structure of 4-(2,4-difluorophenethyl)-1-(2-(piperidin-1-yl)ethyl)piperidine (JPC-124)

Chemical Formula: $C_{20}H_{30}F_2N_2$ Molecular Weight: 336.46

4-Methylpyridine was subjected to Aldol condensation with 2,4-difluorobenzaldehyde in refluxing acetic anhydride to yield (*E*)-4-(2,4-difluorostyryl)pyridine (purified via silica gel column chromatography). Subsequent catalytic hydrogenation with Adam's catalyst (PtO_2) and hydrogen gas afforded 4-(2,4-difluorophenethyl)piperidine (purified via silica gel column chromatography), which was reacted with potassium carbonate and 1-(2-chloroethyl)piperidine in DMF to yield the final product, 4-(2,4-difluorophenethyl)-1-(2-(piperidin-1-yl)ethyl)piperidine (JPC-124) after purification via silica gel column chromatography.

1H NMR (300 MHz, $CDCl_3$): δ 1.38-1.69 (m, 13H), 2.40-2.65 (m, 14H), 6.61-7.27 (m, 3H) ppm.

MS (EI) m/z 336 (M^+).

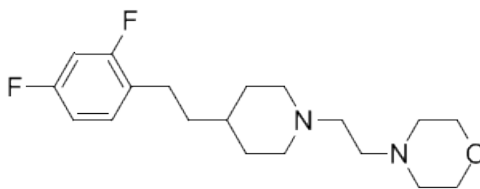


Figure 3.67 Structure of 4-(2-(4-(2,4-methoxyphenethyl)piperidin-1-yl)ethyl)morpholine (JPC-125)

Chemical Formula: $C_{19}H_{28}F_2N_2O$ Molecular Weight: 338.44

4-methylpyridine was subjected to Aldol condensation with 2,4-difluorobenzaldehyde in refluxing acetic anhydride to yield (*E*)-4-(2,4-difluorostyryl)pyridine (purified via silica gel column chromatography). Subsequent catalytic hydrogenation with Adam's catalyst (PtO_2) and hydrogen gas afforded 4-(2,4-difluorophenethyl)piperidine (purified via silica gel column chromatography), which was reacted with potassium carbonate and 4-(2-chloroethyl)morpholine in DMF to yield the final product 4-(2-(4-(2,4-difluorophenethyl)piperidin-1-yl)ethyl)morpholine (JPC-125) after purification via silica gel column chromatography.

1H NMR (300 MHz, $CDCl_3$): δ 1.35-1.63 (m, 7H), 2.38-2.63 (m, 14H), 3.48-3.55 (m, 4H) 6.64-7.23 (m, 3H) ppm.

MS (EI) m/z 338 (M^+).

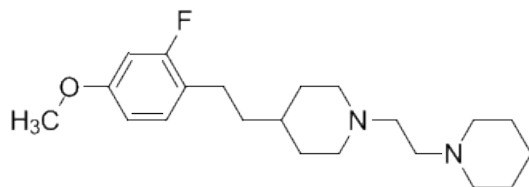


Figure 3.68 Structure of 4-(2-fluoro-4-methoxyphenethyl)-1-(2-(piperidin-1-yl)ethyl)piperidine (JPC-126)

Chemical Formula: $C_{21}H_{33}FN_2O$ Molecular Weight: 348.50

4-Methylpyridine was subjected to Aldol condensation with 2-fluoro-4-methoxy benzaldehyde in refluxing acetic anhydride to yield (*E*)-4-(2-fluoro-4-methoxy styryl)pyridine (purified via silica gel column chromatography). Subsequent catalytic hydrogenation with Adam's catalyst (PtO_2) and hydrogen gas afforded 4-(2-fluoro-4-methoxy phenethyl)piperidine (purified via silica gel column chromatography), which was reacted with potassium carbonate and 1-(2-chloroethyl)piperidine in DMF to yield the desired 4-(2-fluoro-4-methoxyphenethyl)-1-(2-(piperidin-1-yl)ethyl)piperidine (JPC-126) after purification via silica gel column chromatography.

1H NMR (300 MHz, $CDCl_3$): δ 1.35-1.62 (m, 13H), 2.37-2.70 (m, 14H), 3.80 (s, 3H) 6.73-7.27 (m, 3H) ppm.

MS (EI) m/z 348 (M^+).

3.3 Summary of the 1,4-disubstituted piperidine analog series

In summary, 68 compounds were designed and synthesized in the 1,4-disubstituted piperidine scaffold series as analogs of lobelane utilizing five distinct chemical schemes. Of the total number of compounds prepared, 43 were of the 1,4-disubstituted scaffold of lobelane, with a large variety of substituent combinations in the two phenyl rings, that included methoxy, fluoro, and chloro moieties. Another series of 11 compounds belonging to the 1,4-disubstituted piperidine scaffold were designed and synthesized for the purpose of increasing the water solubility of the scaffold by replacing the phenyl ring on the N1 phenethyl moiety with saturated heterocyclic moieties, such as piperidine or morpholine, and to study what effect the introduction of these more polar moieties would have on binding affinity at the TBZ binding site on VMAT2. The remaining 14 compounds were of three smaller series of analogs in which a change in the intramolecular distance between the substituted phenyl rings and the central piperidine ring was made. The pharmacological assay data for the above 68 compounds from these different scaffolds are discussed in Chapter 5.

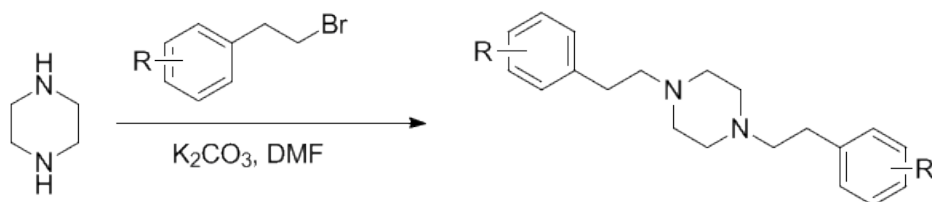
Chapter 4.

Design and Synthesis of 1,4-disubstituted piperazine and 1,4-diazapane analogs of lobelane

4.1 Experiments in the 1,4-disubstituted piperazine scaffold

As discussed in Chapter 1, (section 1.8), a series of isomerized lobelane analogs have been designed and synthesized in which compounds with different attachment positions of the phenethyl linkers on the central piperidine ring were constructed. Of these structural modifications, the analogs with the phenethyl linkers in the N1, C4 positions of the piperidine ring showed more promise for optimization and further study (data shown in Table 1.7), since their binding affinities for VMAT2 were quite similar to lobelane, while maintaining little to no affinity for $\alpha 4\beta 2^*$ & $\alpha 7^*$ nAChRs (data shown in Table 1.7). The symmetry present in the 1,4-disubstituted scaffold allowed for a relatively fast and efficient synthesis of a library of compounds with substituents in the phenyl rings. Several series of compounds were explored in Chapter 3 that possessed a central piperidine ring, and further studies into a similar scaffold were explored that inserted an additional nitrogen atom into the central piperidine ring, affording 1,4-piperazine and 1,4-diazapane scaffolds. The addition of another nitrogen atom into the central piperidine ring is predicted to improve the water solubility characteristics of the scaffold, which is a desirable property in the development of drugs with higher bioavailability than lobelane, and several series of compounds were designed and synthesized to explore these possibilities, resulting in the generation of 21 compounds.

The scheme by which the 1,4-piperazine compounds were synthesized is shown in Scheme 4.1. The structures of the compounds and the supporting analytical data are provided in Figures 4.1 through 4.21. The compounds were converted to their hydrochloride or tartrate salts (di-salts in the case of the piperazine and diazapane scaffold) prior to being submitted for pharmacological assay, and the assay data is presented in Chapter 5.



Scheme 4.1 Synthesis of the symmetrical 1,4-substituted piperazine analog scaffold.

A simple one-step reaction was used to generate six initial compounds in the symmetrical 1,4-substituted piperazine analog series. The starting material for this reaction was 1,4-piperazine (for ease of handling, the dihydrochloride salt of 1,4-piperazine was also used), which was then subjected to S_N2 reaction conditions with the appropriately substituted phenethylbromide and excess potassium carbonate as base in dimethylformamide as solvent. 2.2 equivalents of the appropriately substituted (2-bromoethyl)benzene was added drop-wise into the reaction mixture. The reaction was then heated to 70-80° Celsius for 12-18 hours until the 1,4-piperazine starting material was no longer visible by TLC chromatography (visualized with Dragendorff's reagent). The reaction was cooled, excess solvent removed under reduced pressure, adsorbed onto silica gel, and purified via silica gel chromatography to yield the desired 1,4-substituted piperazine product.

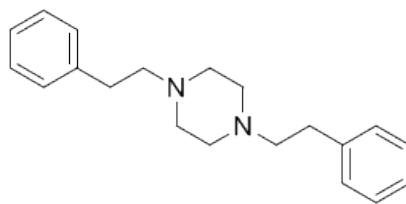


Figure 4.1 Structure of 1,4-diphenethylpiperazine (JPC-134)

Chemical Formula: $C_{20}H_{26}N_2$ Molecular Weight: 294.43

This compound incorporates a second nitrogen atom into the central ring of the 1,4-piperidine scaffold, while retaining the two phenethyl linkers that were present in lobelane. 1,4-Piperazine (readily available from Sigma Aldrich Chemical Company) was reacted via a S_N2 reaction with potassium carbonate and 2.2 equivalents of (2-bromoethyl)benzene in DMF to yield the desired product, 1,4-diphenethylpiperazine (JPC-134). The final product was purified via silica gel column chromatography.

1H NMR (300 MHz, $CDCl_3$): δ 2.59-2.65 (m, 12H), 2.80-2.85 (m, 4H), 7.20-7.32 (m, 10H) ppm.

MS (EI) m/z 294 (M^+).

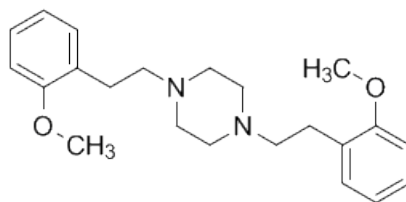


Figure 4.2 Structure of 1,4-*bis*(2-methoxyphenethyl)piperazine (JPC-135)

Chemical Formula: $C_{22}H_{30}N_2O_2$ Molecular Weight: 354.49

This compound incorporates 2-methoxy substituents into the two phenethyl linkers that are present in lobelane. 1,4-Piperazine was reacted with potassium carbonate and 2.2 equivalents of 1-(2-bromoethyl)-2-methoxybenzene in DMF to yield the desired product, 1,4-*bis*(2-methoxyphenethyl)piperazine (JPC-135). The final product was purified via silica gel column chromatography.

^1H NMR (300 MHz, CDCl_3): δ 2.56-2.72 (m, 12H), 2.81-2.87 (m, 4H), 3.82 (s, 6H), 6.83-7.26 (m, 8H) ppm.

^{13}C NMR (75 MHz, CDCl_3): δ 28.2, 53.4, 55.5, 59.0, 110.4, 120.5, 127.4, 128.8, 130.4, 157.5 ppm.

MS (EI) m/z 354 (M^+).

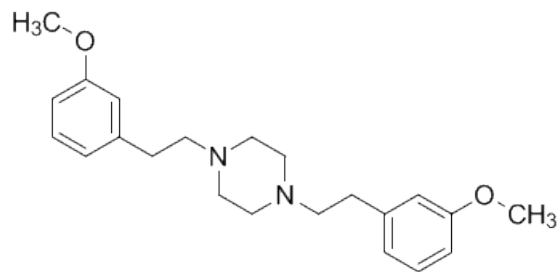


Figure 4.3 Structure of 1,4-*bis*(3-methoxyphenethyl)piperazine (JPC-137)

Chemical Formula: $C_{22}H_{30}N_2O_2$ Molecular Weight: 354.49

This compound incorporates 3-methoxy substituents into the two phenethyl linkers that are present in lobelane. 1,4-Piperazine was reacted with potassium carbonate and 2.2 equivalents of 1-(2-bromoethyl)-3-methoxybenzene in DMF to yield the desired product, 1,4-*bis*(3-methoxyphenethyl)piperazine (JPC-137). The final product was purified via silica gel column chromatography.

1H NMR (300 MHz, $CDCl_3$): δ 2.59-2.67 (m, 12H), 2.77-2.80 (m, 4H), 3.80 (s, 6H), 6.74-6.82 (m, 6H), 7.18-7.26 (m, 2H) ppm.

MS (EI) m/z 354 (M^+).

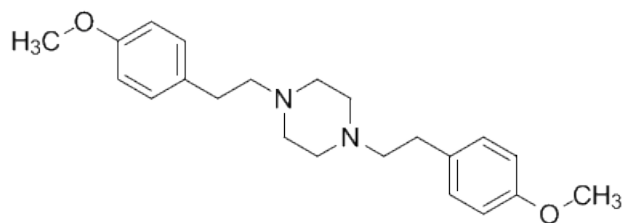


Figure 4.4 Structure of 1,4-*bis*(4-methoxyphenethyl)piperazine (JPC-138)

Chemical Formula: $C_{22}H_{30}N_2O_2$ Molecular Weight: 354.49

This compound incorporated 4-methoxy substituents into the two phenethyl linkers that are present in lobelane. 1,4-Piperazine was reacted with potassium carbonate and 2.2 equivalents of 1-(2-bromoethyl)-4-methoxybenzene in DMF to yield the desired product 1,4-*bis*(4-methoxyphenethyl)piperazine (JPC-138). The final product was purified via silica gel column chromatography.

^1H NMR (300 MHz, CDCl_3): δ 2.56-2.62 (m, 12H), 2.74-2.81 (m, 4H), 3.79 (s, 6H), 6.82-6.85 (m, 2H), 7.11-7.26 (m, 4H) ppm.

MS (EI) m/z 354 (M^+).

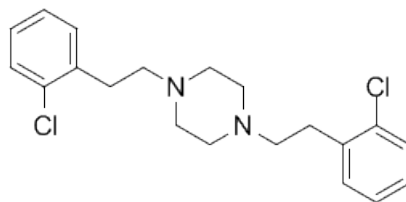


Figure 4.5 Structure of 1,4-*bis*(2-chlorophenethyl)piperazine (JPC-139)

Chemical Formula: C₂₀H₂₄Cl₂N₂ Molecular Weight: 363.32

This compound incorporated 2-chloro substituents into the two phenethyl linkers that are present in lobelane. 1,4-Piperazine was reacted with potassium carbonate and 2.2 equivalents of 1-(2-bromoethyl)-2-chlorobenzene in DMF to yield the desired product, 1,4-*bis*(2-chlorophenethyl)piperazine (JPC-139). The final product was purified via silica gel column chromatography.

¹H NMR (300 MHz, CDCl₃): δ 2.61-2.66 (m, 12H), 2.89-2.99 (m, 4H), 7.17-7.33 (m, 8H) ppm.

MS (EI) m/z 362 (M⁺).

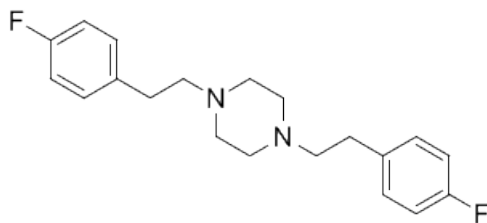


Figure 4.6 Structure of 1,4-*bis*(4-fluorophenethyl)piperazine (JPC-140)

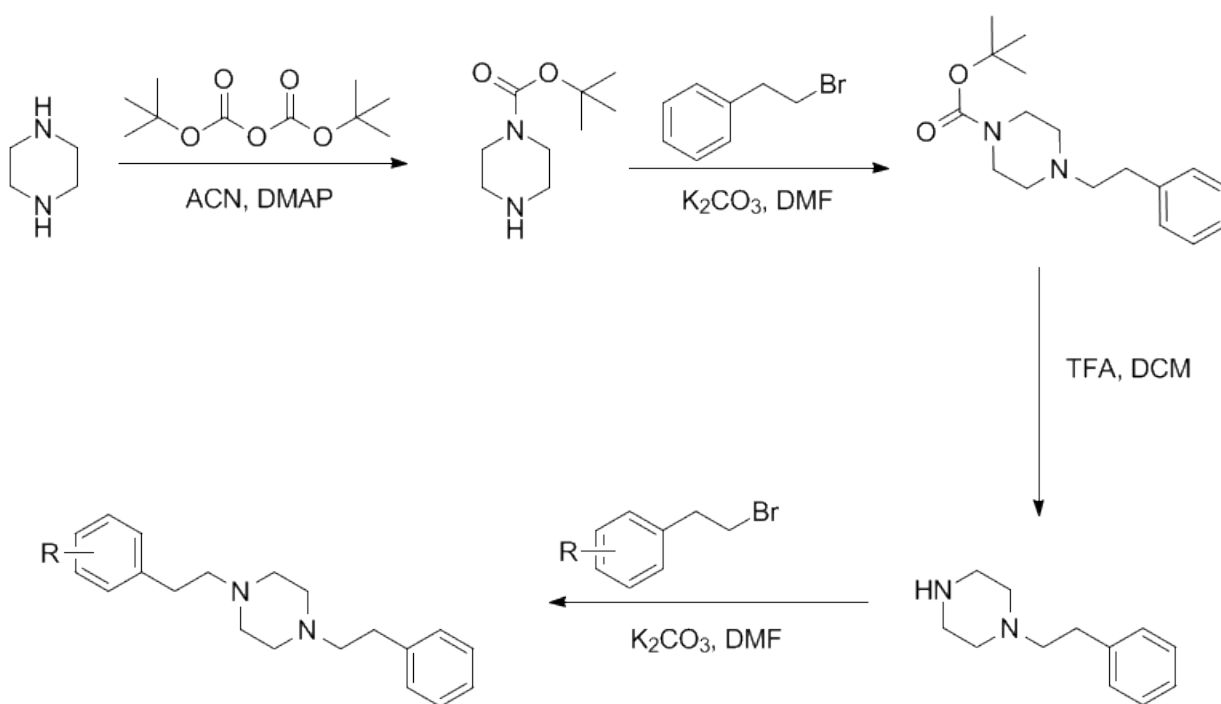
Chemical Formula: $C_{20}H_{24}F_2N_2$ Molecular Weight: 330.41

This compound incorporated 4-fluoro substituents into the two phenethyl linkers that are present in lobelane. 1,4-Piperazine was reacted with potassium carbonate and 2.2 equivalents of 1-(2-bromoethyl)-4-fluorobenzene in DMF to yield the desired product, 1,4-*bis*(4-fluorophenethyl)piperazine (JPC-140). The final product was purified via silica gel column chromatography.

1H NMR (300 MHz, $CDCl_3$): δ 2.57-2.62 (m, 12H), 2.77-2.82 (m, 4H), 6.94-7.00 (m, 4H), 7.17-7.26 (m, 4H) ppm.

MS (EI) m/z 330 (M^+).

After the symmetrical 1,4-piperazine analogs were prepared, the design and synthesis of asymmetrical 1,4-piperazine analogs was conducted. The synthetic was slightly more involved than the one step process that generated the symmetrical compounds in Figures 4.1 through 4.6, since it required a protection step (BOC protection of one amine functionality) on the 1,4-piperazine ring. The synthetic methodology is shown in Scheme 4.2.



Scheme 4.2 Synthesis of the asymmetrical 1,4-piperazine scaffold.

The starting material for this series of analogs was again 1,4-piperazine, which was subjected to BOC (butyloxycarbonyl) protection with di-*tert*-butyloxy dicarbonate in acetonitrile and a catalytic amount of DMAP (4-dimethylaminopyridine). This yielded a mixture of products, with the major product being the desired *tert*-butyl piperazine-1-

carboxylate; the other two side products were starting material and the di-protected di-*tert*-butyl piperazine-1,4-dicarboxylate. The desired product was separated via silica gel column chromatography, and was then subjected to a S_N2 reaction with (2-bromoethyl)benzene to yield the *tert*-butyl-4-phenethylpiperazine-1-carboxylate product, which was purified via silica gel column chromatography. At this point, the BOC protecting group was removed by subjecting it to a 1:3 trifluoroacetic acid:dichloromethane reaction mixture. Purification via silica gel column chromatography afforded the desired 1-phenethylpiperazine, which was utilized as the common intermediate for the synthesis of five asymmetrical compounds in this series. The 1-phenethylpiperazine was then subjected to a S_N2 reaction with the appropriately substituted (2-bromoethyl)benzene to yield the desired final products, which were purified via silica gel column chromatography. The structures and analytical data of the five compounds generated in this series are shown in Figures 4.7 through 4.11. NMR spectra were recorded in either CDCl₃ or DMSO-d₆ (as designated) on one of three Varian instruments (300 MHz, 400 MHz, or 500 MHz) as indicated are reported in ppm relative to either TMS as internal standard or as relative to the solvent peak present in ¹³C spectra. GC-mass spectra were recorded on an Agilent 6890 GC incorporating an Agilent 7683 autosampler and an Agilent 5973 MSD.

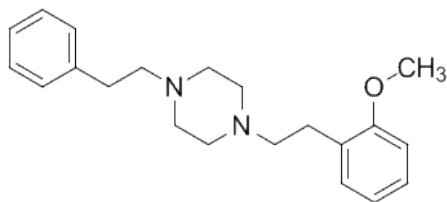


Figure 4.7 Structure of 1-(2-methoxyphenethyl)-4-phenethylpiperazine (JPC-141)

Chemical Formula: $C_{21}H_{28}N_2O$ Molecular Weight: 324.46

This compound incorporates a 2-methoxy substituent into one of the phenethyl moieties, while retaining the second phenethyl moiety that is present in lobelane. Synthesis began with 1,4-piperazine, which was subjected to BOC (butoxycarbonyl) protection via di-*tert*-butyloxy dicarbonate in acetonitrile and a catalytic amount of DMAP (4-dimethylaminopyridine). The major product, *tert*-butyl piperazine-1-carboxylate, was separated via silica column chromatography, and reacted with (2-bromoethyl)benzene to yield the *tert*-butyl 4-phenethylpiperazine-1-carboxylate, which was purified via silica gel column chromatography. Deprotection of the BOC protecting group was achieved utilizing a trifluoroacetic acid:dichloromethane 1:3 mixture. Purification of the deprotected product via silica gel column chromatography afforded the desired 1-phenethylpiperazine, which was then reacted with 1-(2-bromoethyl)-2-methoxybenzene to yield the desired final product, 1-(2-methoxyphenethyl)-4-phenethylpiperazine (JPC-141) after purification via silica column chromatography.

^1H NMR (300 MHz, CDCl_3): δ 2.60-2.66 (m, 12H), 2.78-2.86 (m, 4H), 3.82 (s, 3H), 6.81-6.92 (m, 2H), 7.15-7.38 (m, 7H) ppm.

MS (EI) m/z 324 (M^+).

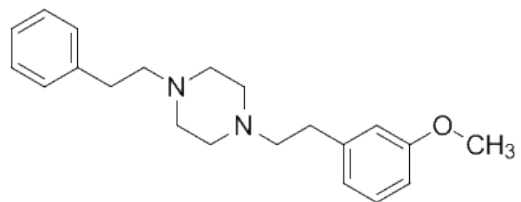


Figure 4.8 Structure of 1-(3-methoxyphenethyl)-4-phenethylpiperazine (JPC-142)

Chemical Formula: $C_{21}H_{28}N_2O$ Molecular Weight: 324.46

This compound incorporates a 3-methoxy substituent into one of the phenethyl moieties, while retaining the second phenethyl moiety that is present in lobelane. 1-phenethylpiperazine was reacted with 1-(2-bromoethyl)-3-methoxybenzene to yield the desired final product 1-(3-methoxyphenethyl)-4-phenethylpiperazine (JPC-142), which was purified via silica gel column chromatography.

1H NMR (300 MHz, $CDCl_3$): δ 2.55-2.66 (m, 12H), 2.73-2.83 (m, 4H), 3.81 (s, 3H), 6.84-6.96 (m, 2H), 7.18-7.36 (m, 7H) ppm.

MS (EI) m/z 324 (M^+).

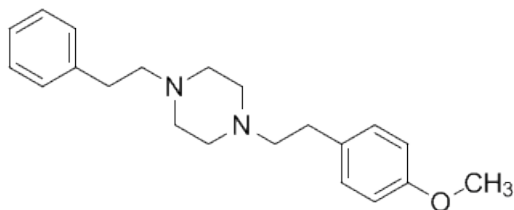


Figure 4.9 Structure of 1-(4-methoxyphenethyl)-4-phenethylpiperazine (JPC-143)

Chemical Formula: $C_{21}H_{28}N_2O$ Molecular Weight: 324.46

This compound incorporates a 4-methoxy substituent into one of the phenethyl moieties, while retaining the second phenethyl moiety that is present in lobelane. 1-Phenethylpiperazine was reacted with 1-(2-bromoethyl)-4-methoxybenzene to yield the desired final product 1-(4-methoxyphenethyl)-4-phenethylpiperazine (JPC-143), which was purified via silica gel column chromatography.

1H NMR (300 MHz, $CDCl_3$): δ 2.51-2.70 (m, 12H), 2.75-2.89 (m, 4H), 3.83 (s, 3H), 6.87-6.99 (m, 2H), 7.14-7.38 (m, 7H) ppm.

MS (EI) m/z 324 (M^+).

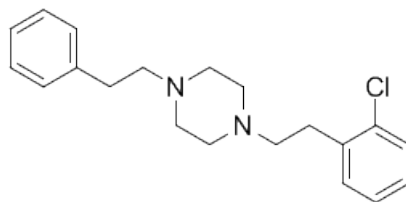


Figure 4.10 Structure of 1-(2-chlorophenethyl)-4-phenethylpiperazine (JPC-144)

Chemical Formula: $C_{20}H_{25}ClN_2$ Molecular Weight: 328.88

This compound incorporates a 2-chloro substituent into one of the phenethyl moieties, while retaining the second phenethyl moiety that is present in lobelane. 1-Phenethylpiperazine, was reacted with 1-(2-bromoethyl)-2-chlorobenzene to yield the desired final product 1-(2-chlorophenethyl)-4-phenethylpiperazine (JPC-144), which was purified via silica gel column chromatography.

1H NMR (300 MHz, $CDCl_3$): δ 2.54-2.66 (m, 12H), 2.78-2.87 (m, 4H), 7.19-7.42 (m, 9H) ppm.

MS (EI) m/z 328 (M^+).

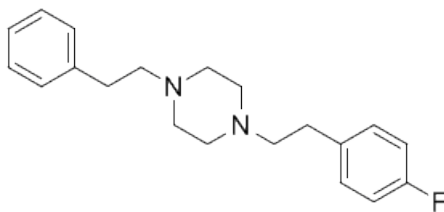


Figure 4.11 Structure of 1-(4-fluorophenethyl)-4-phenethylpiperazine (JPC-145)

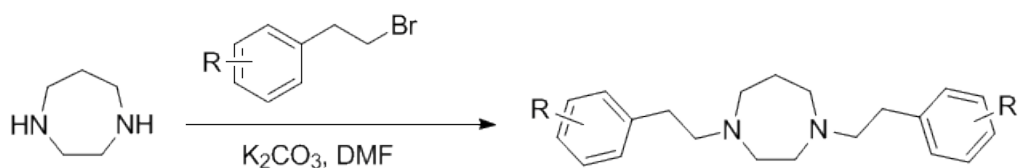
Chemical Formula: $C_{20}H_{25}FN_2$ Molecular Weight: 312.42

This compound incorporated a 4-fluoro substituent into one of the phenethyl moieties, while retaining the second phenethyl moiety that is present in lobelane. 1-Phenethylpiperazine was reacted with 1-(2-bromoethyl)-4-fluorobenzene to yield the desired final product 1-(4-fluorophenethyl)-4-phenethylpiperazine (JPC-145), which was purified via silica gel column chromatography.

$^1\text{H NMR}$ (300 MHz, CDCl_3): δ 2.53-2.64 (m, 12H), 2.73-2.84 (m, 4H), 6.96-7.31 (m, 9H) ppm.

MS (EI) m/z 312 (M^+).

After the series of asymmetrical 1,4-piperazine analogs were synthesized, further modification of the central ring of the 1,4-scaffold was explored. Thus, the central six-membered 1,4-piperazine ring was expanded to a seven-membered 1,4-diazepane ring. Six compounds were designed and synthesized in this series. The chemistry utilized to generate the symmetrical 1,4-diazepane series was very similar to that which afforded the symmetrical 1,4-piperazine series. The one-step process utilized is outlined in Scheme 4.3.



Scheme 4.3 Synthesis of the symmetrical 1,4-diazepane series of analogs

A simple one-step reaction process was used to generate six compounds in the symmetrical 1,4-substituted diazepane analog series. The starting material for this reaction was 1,4-diazepane (readily available from Sigma Aldrich Chemical Company), which was then subjected to S_N2 reaction conditions with appropriately substituted (2-bromoethyl)benzene and excess potassium carbonate as base in dimethylformamide as solvent. Once all materials were dissolved, 2.2 equivalents of the appropriately substituted (2-bromoethyl)benzene was added drop-wise into the reaction mixture. The reaction was heated to 70-80° Celsius for 12-18 hours until the 1,4-diazepane starting material was no longer visible by TLC chromatography (visualized with Dragendorff's reagent). The reaction was cooled, excess solvent removed under reduced pressure, and

the product adsorbed onto silica gel and purified via silica gel chromatography to yield the desired product in the 1,4-substituted diazepane analog series.

The structures and analytical data of the five compounds generated in this series are shown in Figures 4.12 through 4.17. NMR spectra were recorded in either CDCl₃ or DMSO-d₆ (as designated) on one of three Varian instruments (300 MHz, 400 MHz, or 500 MHz) as indicated are reported in ppm relative to either TMS as internal standard or as relative to the solvent peak present in ¹³C spectra. GC-mass spectra were recorded on an Agilent 6890 GC incorporating an Agilent 7683 autosampler and an Agilent 5973 MSD.

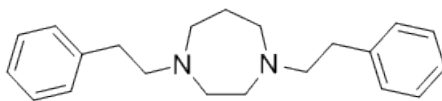


Figure 4.12 Structure of 1,4-diphenethyl-1,4-diazepane (JPC-146)

Chemical Formula: $C_{21}H_{28}N_2$ Molecular Weight: 308.46

This compound incorporates a second nitrogen atom into the central ring of the 1,4-piperidine scaffold while increasing the ring size from six-membered heterocycle to a seven-membered heterocycle and retaining the two phenethyl moieties that are present in lobelane. 1,4-Diazepane (readily available from Sigma Aldrich Chemical Company) was reacted via a S_N2 reaction with potassium carbonate and 2.2 equivalents of (2-bromoethyl)benzene in DMF to yield the desired product 1,4-diphenethyl-1,4-diazepane (JPC-146). The final product was purified via silica gel column chromatography.

1H NMR (300 MHz, $CDCl_3$): δ 1.76-1.78 (m, 2H) 2.64-3.01 (m, 16H), 7.23-7.39 (m, 10H) ppm.

MS (EI) m/z 308 (M^+).

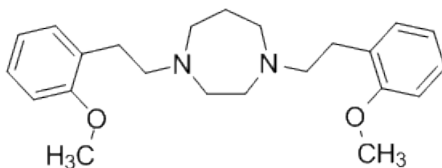


Figure 4.13 Structure of 1,4-*bis*(2-methoxyphenethyl)-1,4-diazepane (JPC-147)

Chemical Formula: $C_{23}H_{32}N_2O_2$ Molecular Weight: 368.51

This compound incorporates a 2-methoxy substituent into each of the two phenethyl moieties that are present in lobelane. 1,4-Diazepane was reacted with potassium carbonate and 2.2 equivalents of 1-(2-bromoethyl)-2-methoxybenzene in DMF to yield the desired product, 1,4-*bis*(2-methoxyphenethyl)-1,4-diazepane (JPC-147). The final product was purified via silica gel column chromatography.

^1H NMR (300 MHz, CDCl_3): δ 1.74-1.77 (m, 2H) 2.63-2.99 (m, 16H), 3.81 (s, 6H), 6.83-7.27 (m, 8H) ppm.

MS (EI) m/z 368 (M^+).

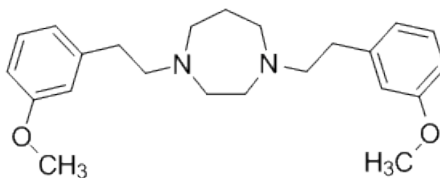


Figure 4.14 Structure of 1,4-*bis*(3-methoxyphenethyl)-1,4-diazepane (JPC-148)

Chemical Formula: $C_{23}H_{32}N_2O_2$ Molecular Weight: 368.51

This compound incorporated a 3-methoxy substituent into each of the two phenethyl moieties that are present in lobelane. 1,4-Diazepane was reacted with potassium carbonate and 2.2 equivalents of 1-(2-bromoethyl)-3-methoxybenzene in DMF to yield the desired product, 1,4-*bis*(3-methoxyphenethyl)-1,4-diazepane (JPC-148). The final product was purified via silica gel column chromatography.

^1H NMR (300 MHz, CDCl_3): δ 1.74-1.78 (m, 2H) 2.66-3.02 (m, 16H), 3.80 (s, 6H), 6.71-6.83 (m, 6H), 7.15-7.24 (m, 2H) ppm.

MS (EI) m/z 368 (M^+).

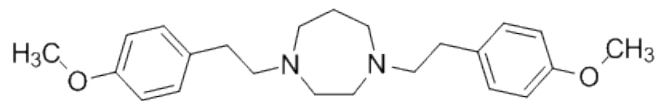


Figure 4.15 Structure of 1,4-*bis*(4-methoxyphenethyl)-1,4-diazepane (JPC-149)

Chemical Formula: $C_{23}H_{32}N_2O_2$ Molecular Weight: 368.51

This compound incorporated a 4-methoxy substituent into each of the two phenethyl moieties that are present in lobelane. 1,4-Diazepane was reacted with potassium carbonate and 2.2 equivalents of 1-(2-bromoethyl)-4-methoxybenzene in DMF to yield the desired product, 1,4-*bis*(4-methoxyphenethyl)-1,4-diazepane (JPC-149). The final product was purified via silica gel column chromatography.

^1H NMR (300 MHz, CDCl_3): δ 1.72-1.78 (m, 2H) 2.66-3.00 (m, 16H), , 3.79 (s, 6H), 6.82-6.85 (m, 2H), 7.11-7.26 (m, 4H) ppm.

MS (EI) m/z 368 (M^+).

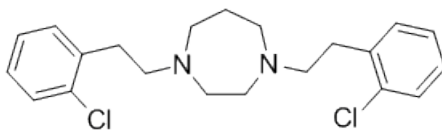


Figure 4.16 Structure of 1,4-*bis*(2-chlorophenethyl)-1,4-diazepane (JPC-150)

Chemical Formula: $C_{21}H_{26}Cl_2N_2$ Molecular Weight: 377.35

This compound incorporated a 2-chloro substituent into each of the two phenethyl moieties that are present in lobelane. 1,4-Diazepane was reacted with potassium carbonate and 2.2 equivalents of 1-(2-bromoethyl)-2-chlorobenzene in DMF to yield the desired product, 1,4-*bis*(2-chlorophenethyl)-1,4-diazepane (JPC-150). The final product was purified via silica gel column chromatography.

1H NMR (300 MHz, $CDCl_3$): δ 1.71-1.77 (m, 2H) 2.64-2.97 (m, 16H), 7.14-7.31 (m, 8H) ppm.

MS (EI) m/z 376 (M^+).

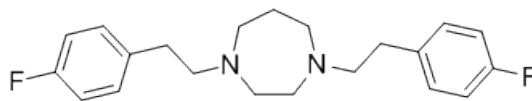


Figure 4.17 Structure of 1,4-*bis*(4-fluorophenethyl)-1,4-diazepane (JPC-151)

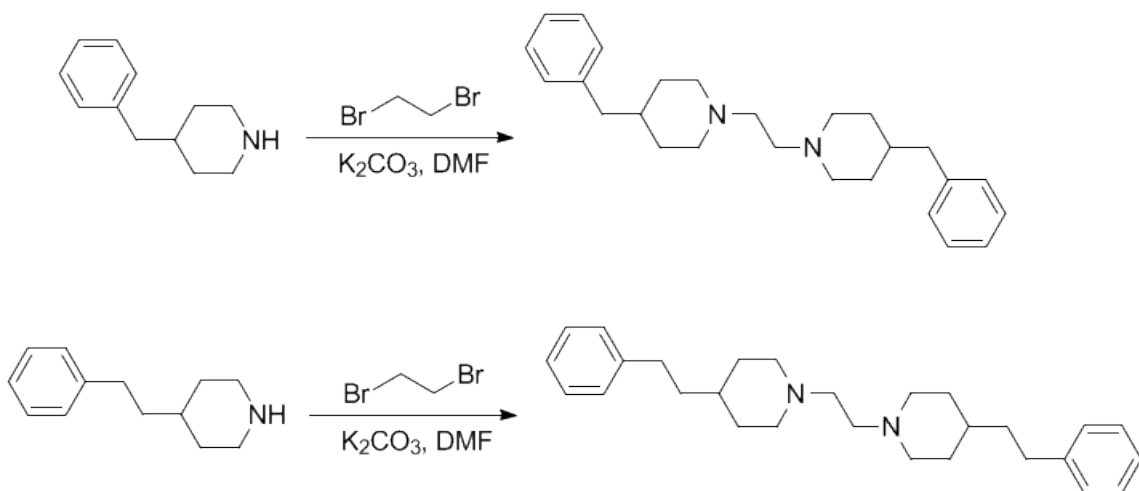
Chemical Formula: $C_{21}H_{26}F_2N_2$ Molecular Weight: 344.44

This compound incorporates a 2-chloro substituent into each of the two phenethyl moieties that are present in lobelane. 1,4-Diazepane was reacted with potassium carbonate and 2.2 equivalents of 1-(2-bromoethyl)-2-chlorobenzene in DMF to yield the desired product, 1,4-*bis*(2-chlorophenethyl)-1,4-diazepane (JPC-150). The final product was purified via silica gel column chromatography.

1H NMR (300 MHz, $CDCl_3$): δ 1.73-1.78 (m, 2H) 2.64-2.98 (m, 16H), 6.93-7.00 (m, 4H), 7.14-7.23 (m, 4H) ppm.

MS (EI) m/z 344 (M^+).

Another small series of compounds incorporating two 4-benzylpiperidine moieties linked together by an *N,N'*-ethylene bridge was also designed and synthesized, to explore the possibility that two benzyl piperidine moieties linked by an ethylene chain may be tolerated by the TBZ site on VMAT2. The synthetic methodology for the generation of the two compounds in this series is shown in Scheme 4.4.



Scheme 4.4 Synthesis of 1,2-*bis*(4-benzylpiperidin-1-yl)ethane and 1,2-*bis*(4-phenethylpiperidin-1-yl)ethane

The chemistry for generating the above two molecules is simple and quick. Two equivalents of the appropriate 4-substituted piperidine starting material was subjected to a S_N2 reaction with one equivalent 1,2-dibromoethane using potassium carbonate as a base in DMF at 70-80° C. After disappearance of the starting material (TLC monitoring of the reaction visualized with Dragendorff's reagent), the reaction material was cooled and excess solvent removed under reduced pressure. The resulting residue was purified by silica gel column chromatography to yield the desired final products. The structures of

the two compounds in this series and the supporting analytical data are shown in Figures 4.18 and 4.19. NMR spectra were recorded in either CDCl₃ or DMSO-d₆ (as designated) on one of three Varian instruments (300 MHz, 400 MHz, or 500 MHz) as indicated are reported in ppm relative to either TMS as internal standard or as relative to the solvent peak present in ¹³C spectra. GC-mass spectra were recorded on an Agilent 6890 GC incorporating an Agilent 7683 autosampler and an Agilent 5973 MSD.

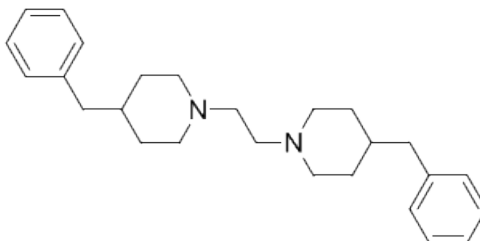


Figure 4.18 Structure of 1,2-*bis*(4-benzylpiperidin-1-yl)ethane (JPC-132)

Chemical Formula: $C_{26}H_{36}N_2$ Molecular Weight: 376.58

The synthesis began with 4-benzylpiperidine as the starting material. Two equivalents of 4-benzylpiperidine were reacted with one equivalent 1,2-dibromoethane using potassium carbonate as a base in DMF at 70-80° C. After disappearance of the starting material (TLC monitoring and visualization with Dragendorff's reagent) the reaction material was cooled and excess solvent removed under reduced pressure. The residue was purified via silica gel column chromatography to yield the desired compound, 1,2-*bis*(4-benzylpiperidin-1-yl)ethane (JPC-132).

^1H NMR (300 MHz, CDCl_3): δ 1.17-1.82 (m, 10H) 2.06-2.78 (m, 16H), 7.06-7.23 (m, 10H) ppm.

^{13}C NMR (75 MHz, CDCl_3): δ 32.6, 37.7, 43.5, 46.7, 56.2, 125.9, 128.3, 129.3, 140.9 ppm.

MS (EI) m/z 376 (M^+).

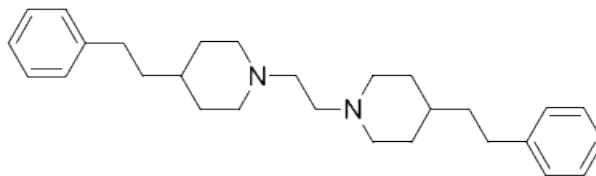


Figure 4.19 Structure of 1,2-*bis*(4-phenethylpiperidin-1-yl)ethane (JPC-133)

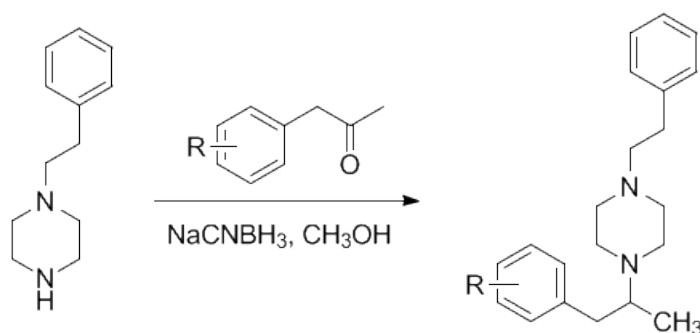
Chemical Formula: C₂₈H₄₀N₂ Molecular Weight: 404.32

Two equivalents of 4-benzylpiperidine were reacted with one equivalent of 1,2-dibromoethane using potassium carbonate as a base in DMF at 70-80° C. After disappearance of the starting material (monitored by TLC and visualized with Dragendorff's reagent) the reaction material was cooled, and excess solvent removed under reduced pressure. The residue was purified via silica gel column chromatography to yield the desired 1,2-*bis*(4-benzylpiperidin-1-yl)ethane (JPC-132).

¹H NMR (300 MHz, CDCl₃): δ 1.23-1.76 (m, 14H) 2.26-2.73 (m, 16H), 7.10-7.28 (m, 10H) ppm.

MS (EI) m/z 404 (M⁺).

One final set of two compounds were designed and synthesized to evaluate analogs that possessed a branched alkyl linker unit between one of the piperazine N-atoms and the phenyl moiety, to afford a racemic 1-phenylpropan-2-yl moiety attached to N1 of the piperazine ring, while maintaining the phenethyl linker on N4 of the piperazine ring. One of the compounds in this set also incorporated a 4-bromo substituent in the phenyl ring attached to the N1 position of the piperazine ring. The synthetic pathway for these two compounds is shown in Scheme 4.5.



Scheme 4.5 Synthesis of the 1-phenethyl-4-(1-phenylpropan-2-yl)piperazine set of compounds

Starting from 1-phenethylpiperazine, a reductive amination was carried out utilizing the appropriately substituted 1-phenylpropan-2-one to yield the two racemic 1-phenethyl-4-(1-phenylpropan-2-yl)piperazines. The structures of the two compounds in this series and the analytical data supporting their structures are shown in Figures 4.20 and 4.21. NMR spectra were recorded in either CDCl₃ or DMSO-d₆ (as designated) on one of three Varian instruments (300 MHz, 400 MHz, or 500 MHz) as indicated are reported in ppm relative to either TMS as internal standard or as relative to the solvent

peak present in ^{13}C spectra. GC-mass spectra were recorded on an Agilent 6890 GC incorporating an Agilent 7683 autosampler and an Agilent 5973 MSD.

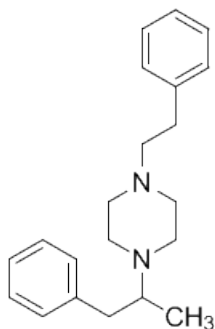


Figure 4.20 Structure of racemic 1-phenethyl-4-(1-phenylpropan-2-yl)piperazine (JPC-176) Chemical Formula: $C_{21}H_{28}N_2$ Molecular Weight: 308.46

1-Phenethylpiperazine was reacted with 1-phenylpropan-2-one under reductive amination conditions with sodium cyanoborohydride in methanol to afford the final product, (\pm)-1-phenethyl-4-(1-phenylpropan-2-yl)piperazine (JPC-176), which was purified by silica gel column chromatography.

1H NMR (300 MHz, $CDCl_3$): δ 1.01-1.03 (d, 3H), 2.43-3.18 (m, 15H), 7.22-7.34 (m, 10H) ppm.

^{13}C NMR (75 MHz, $CDCl_3$): δ 14.64, 33.9, 39.5, 48.5, 53.8, 60.8, 61.5, 125.9, 126.1, 128.3, 128.4, 128.7, 129.3, 140.60, 140.64 ppm.

MS (EI) m/z 308 (M^+).

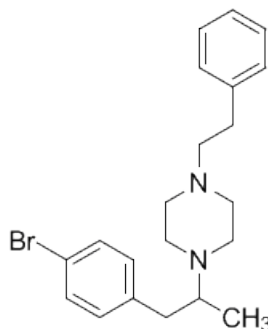


Figure 4.21 Structure of racemic 1-(1-(4-bromophenyl)propan-2-yl)-4-phenethylpiperazine (JPC-173)

Chemical Formula: $C_{21}H_{27}BrN_2$ Molecular Weight: 387.36

1-Phenethylpiperazine was reacted with 1-(4-bromophenyl)propan-2-one in methanol via reductive amination with sodium cyanoborohydride to afford the final product, (\pm)- 1-(1-(4-bromophenyl)propan-2-yl)-4-phenethylpiperazine (JPC-173), which was purified by silica gel column chromatography.

1H NMR (300 MHz, $CDCl_3$): δ 0.96-0.98 (d, 3H), 2.35-3.05 (m, 15H), 7.06-7.43 (m, 9H) ppm.

^{13}C NMR (75 MHz, $CDCl_3$): δ 14.64, 33.9, 39.0, 48.55, 53.7, 53.8, 60.9, 61.3, 119.7, 126.9, 128.5, 128.8, 131.1, 131.4, 139.7, 140.4 ppm.

MS (EI) m/z 387 (M^+).

4.2 Summary of the 1,4-disubstituted piperazine analog series

In summary, 21 compounds were designed and synthesized in the 1,4-disubstituted piperidine scaffold series by utilizing four distinct chemical approaches. Of the total number of compounds prepared, 11 were 1,4-disubstituted piperazine analogs containing a variety of aromatic substituents in each of the two phenyl rings, including methoxy, fluoro, and chloro substituents. Another series of six 1,4-disubstituted diazepane analogs were designed and synthesized to determine if an increase in the size of the central heterocyclic (1,4-piperazine) ring from six membered ring to a seven membered would improve affinity for VMAT2. Another small series of compounds were designed and synthesized to determine if two benzyl piperidine rings linked together by an ethylene chain would be tolerated by the TBZ binding site on VMAT2. The remaining two compounds were analogs that possessed a branched N1 alkyl linker in the form of a racemic 1-phenylpropan-2-yl moiety attached to N1 of the piperazine ring, as well as a phenethyl moiety at N4 of the piperazine ring. This set of compounds also included an analog containing a 4-bromophenyl moiety at the N1 position of the piperazine ring. The pharmacological assay data for these 21 compounds are discussed in Chapter 5.

Chapter 5

Pharmacology Assays and Data

5.1 [³H] Dihydropyridazine Binding Assay and [³H] Dopamine Uptake Assay

Background

Pharmacology (from Greek *pharmakon*, "poison" in classic Greek; "drug" in modern Greek; and *-λογία*, *-logia* "study of", "knowledge of") is the extension and cohesion of medicine and biology concerned with the study of drug action (De Jong et al., 2005). Just as organic and medicinal chemistry is vital to the invention and discovery of new drug molecules, pharmacology is a cornerstone of the drug discovery process. While it is the medicinal chemist that designs and synthesizes the candidate drug compound, the pharmacologist is the one who tests it for physiologic activity. A promising compound will be investigated by many other scientists to include toxicologists, microbiologists, and medical clinicians, but the initial discovery of the potential therapeutic effect by the pharmacologist must always come first. Well prior to being studied in humans, candidate drug molecules must first be studied either "*in vitro*" or "*in vivo*" in animal models. *In vivo* (Latin for "within the living") (Merriam-Webster, 2013) is experimentation using a whole, living organism as opposed to a partial or dead organism which is an *in vitro* (Latin for "within the glass", for example in a test tube or petri dish) (Merriam-Webster, 2013) within a more controlled environment.

The assays used to analyze the effectiveness of the 107 compounds described in Chapters 2 through 4 are of the "*in vitro*" variety and are described as the [³H] Dihydropyridazine Binding Assay and [³H] Dopamine Vesicular Uptake Assay.

The [³H] Dihydratetrabenazine Binding Assay was used to determine the affinity of the analogs in the synthesized compound library for the TBZ binding site on VMAT2. Potency of a compound in binding to the TBZ site of VMAT2 does not directly correlate into inhibition of VMAT2 function. It was therefore necessary to evaluate the ability of the compounds to inhibit [³H]DA uptake into synaptic vesicles as well (Nickell et al., 2010).

In the [³H] Dihydratetrabenazine Binding Assay and the [³H] Dopamine Vesicular Uptake Assay, the following materials and methods were used (Nickell et al., 2010). Assays were conducted by J. Nickell and G. Deaciuc in the laboratories of Dr. Linda Dwoskin. Methodology was developed and used in those laboratories and is shown here in original format.

Animals. Male Sprague-Dawley rats (200–250 g upon arrival) were purchased from Harlan (Indianapolis, IN). Rats were housed in the Division of Laboratory Animal Resources at the College of Pharmacy at the University of Kentucky (Lexington, KY) and had ad libitum access to food and water. Experimental protocols involving the animals were in accordance with the *National Institutes of Health Guide for the Care and Use of Laboratory Animals* and were approved by the Institutional Animal Care and Use Committee at the University of Kentucky.

Materials. [^3H]DA (specific activity, 28.0 Ci/mmol) was purchased from PerkinElmer Life and Analytical Sciences (Boston, MA). [^3H]DTBZ (specific activity, 79.0 Ci/mmol) was a gift from Dr. Michael R. Kilbourn (Department of Internal Medicine and Neurology, University of Michigan, Ann Arbor, MI). Bovine serum albumin, EDTA, EGTA, L-(-)-tartaric acid, sucrose, magnesium sulfate, polyethyleneimine, adenosine 5-triphosphate magnesium salt, HEPES, S(-)-nicotine ditartrate (nicotine), 3-hydroxytyramine (dopamine, DA), DOPAC, *d*-methamphetamine hydrochloride (methamphetamine), sodium chloride, magnesium sulfate and ascorbate oxidase were purchased from Sigma-Aldrich (St. Louis, MO). (-)-D-Glucose, L-ascorbic acid, and monobasic potassium phosphate were purchased from Aldrich Chemical Co. (Milwaukee, WI), AnalaR-BHD Ltd. (Poole, UK), and Mallinckrodt (St. Louis, MO), respectively. Perchloric acid (70%) was purchased from Mallinckrodt Baker (Phillipsburg, NJ). Ro4-1284 was obtained from Hoffman-La Roche Ltd. (Basel, Switzerland). All other commercial chemicals were purchased from Fisher Scientific Co. (Pittsburgh, PA) (Nickell et al., 2010).

[^3H]DTBZ Binding Assay. Analog-induced inhibition of [^3H]DTBZ binding was determined by use of modifications of a method described previously (Teng et al., 1998). Rat whole brain (excluding cerebellum) or striatum was homogenized in 20 ml of ice-cold 0.32 M sucrose solution with seven up-and-down strokes of a Teflon pestle homogenizer (clearance ~ 0.003 inch). Homogenates were centrifuged at 1000g for 12 min at 4°C, and the resulting supernatants were again centrifuged at 22,000g for 10 min at 4°C. Resulting pellets were incubated in 18 ml of ice-cold water for 5 min, and 2 ml of

HEPES (25 mM) and potassium tartrate (100 mM) solution were subsequently added. Samples were centrifuged (20,000g for 20 min at 4°C), and 20 µl of MgSO₄ (1 mM) solution was then added to the supernatants. Solutions were centrifuged (100,000g for 45 min at 4°C) and pellets resuspended in ice-cold assay buffer (25 mM HEPES, 100 mM potassium tartrate, 5 mM MgSO₄, 0.1 mM EDTA, and 0.05 mM EGTA, pH 7.5). Assays were performed in duplicate by use of 96-well plates. Aliquots of vesicular suspension (15 µg of protein in 100 µl) were added to wells containing 5 nM [³H]DTBZ, 50 µl of analog (1 nM to 1 mM), and 50 µl of buffer. Nonspecific binding was determined in the presence of Ro4-1284 (20 µM). Reactions were terminated by filtration (Packard Filtermate harvester; PerkinElmer Life and Analytical Sciences) onto Unifilter-96 GF/B filter plates (presoaked in 0.5% polyethyleneimine). Filters were subsequently washed five times with 350 µl of ice-cold buffer (25 mM HEPES, 100 mM potassium tartrate, 5 mM MgSO₄, and 10 mM NaCl, pH 7.5). Filter plates were dried and bottom-sealed, and each well was filled with 40 µl of scintillation cocktail (MicroScint 20; PerkinElmer Life and Analytical Sciences). Radioactivity on the filters was determined by liquid β-scintillation spectrometry (TopCount NXT; PerkinElmer Life and Analytical Sciences). Inhibition curves will be analyzed by non-linear regression and IC₅₀ values used to yield *K_i* values (Teng, et al., 1997; Teng et al., 1998; Cheng-Prusoff, 1973; Nickell et al., 2010).

Vesicular [³H]DA Uptake Assay. Inhibition of [³H]DA uptake was conducted by use of a preparation of isolated synaptic vesicles as described previously (Teng et al., 1997). In brief, rat striata were homogenized with 10 up-and-down strokes of a Teflon pestle homogenizer (clearance ~ 0.003 inch) in 14 ml of 0.32 M sucrose solution. Homogenates were centrifuged (2000g for 10 min at 4°C), and the resulting supernatants were centrifuged again (10,000g for 30 min at 4°C). Pellets were resuspended in 2 ml of 0.32 M sucrose solution and subjected to osmotic shock by adding 7 ml of ice-cold water to the preparation, followed by the immediate restoration of osmolarity by adding 900 µl of 0.25 M HEPES buffer and 900 µl of 1.0 M potassium tartrate solution. Samples were centrifuged (20,000g for 20 min at 4°C), and the resulting supernatants were centrifuged again (55,000g for 1 h at 4°C), followed by the addition of 100 µl of 10 mM MgSO₄, 100 µl of 0.25 M HEPES, and 100 µl of 1.0 M potassium tartrate solution before the final centrifugation (100,000g for 45 min at 4°C). Final pellets were resuspended in 2.4 ml of assay buffer (25 mM HEPES, 100 mM potassium tartrate, 50 µM EGTA, 100 µM EDTA, 1.7 mM ascorbic acid, 2 mM ATP-Mg²⁺, pH 7.4). Aliquots of the vesicular suspension (100 µl) were added to tubes containing assay buffer, various concentrations of analog (0.1 nM to 10 mM) and 0.1 µM [³H]DA to produce a final volume of 500 µl. Nonspecific uptake was determined in the presence of Ro4-1284 (10 µM). Reactions were terminated by filtration, and radioactivity retained by the filters was determined as described previously (Nickell et al., 2010).

5.2 [³H] Dihydratetabenazine Binding Assay and [³H] Dopamine Uptake Assay

Results

The structures of 107 JPC compounds designed and synthesized as relayed in Chapters 2-4 are presented in Tables 5.1 (18 compounds), 5.2 (68 compounds), and 5.3 (21 compounds) along with their corresponding K_i values in the [³H] Dihydratetabenazine Binding Assay and [³H] Dopamine Uptake Assay. The structures and corresponding K_i values in the [³H] Dihydratetabenazine Binding Assay and [³H] Dopamine Uptake Assay for lobeline and lobelane are included in each table for comparison convenience.

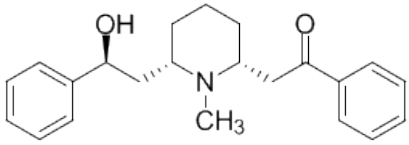
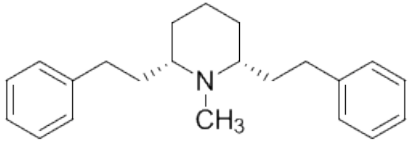
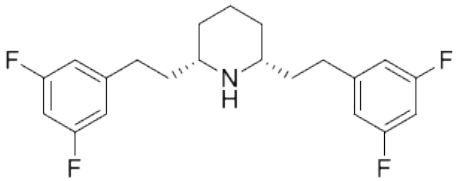
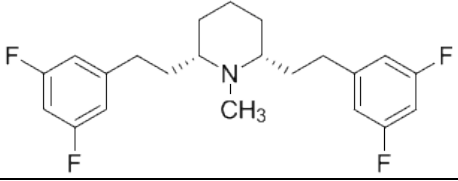
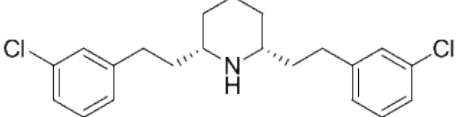
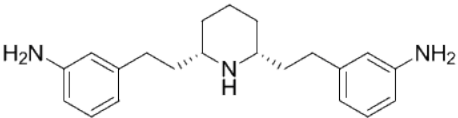
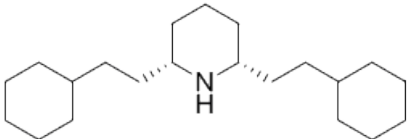
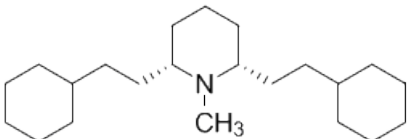
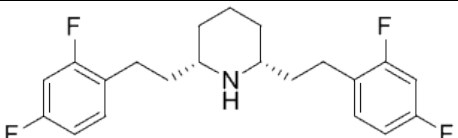
Compound Code	Structure	VMAT2 [³ H]DTBZ Binding Assay; K _i ± SEM (μM)	VMAT2 [³ H]DA Uptake; K _i ± SEM (μM)
Lobeline		2.04 ± 0.64	0.47 ± 0.045
lobelane		0.97 ± 0.19	0.045 ± 0.002
JPC-001		5.24 ± 1.81	0.043 ± 0.0034
JPC-011		0.29 ± 0.03	0.156 ± 0.0323
JPC-002		3.88 ± 0.43	*
JPC-008		30.6	*
JPC-003		5.09 ± 1.37	0.084 ± 0.0071
JPC-007		3.09 ± 0.60	0.19 ± 0.025
JPC-130A		2.24 ± 0.15	0.056 ± 0.026

Table 5.1 (continued)

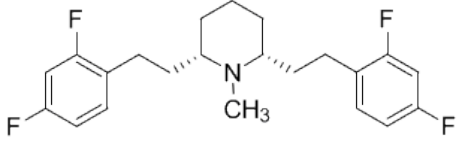
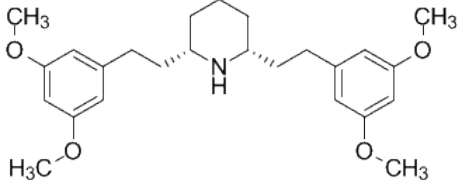
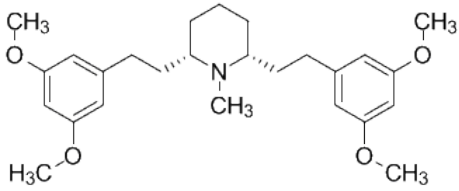
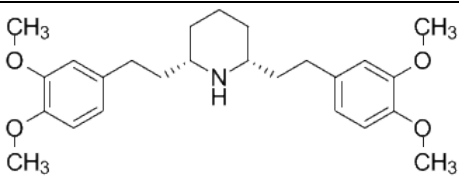
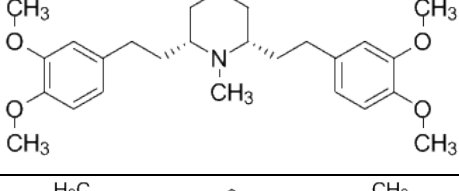
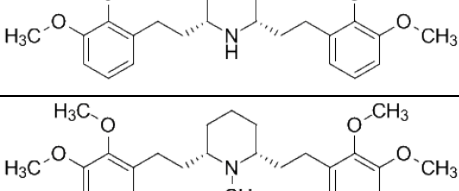
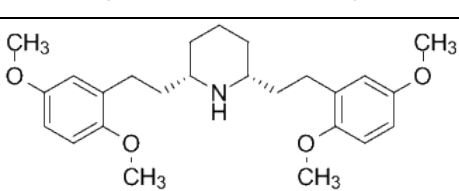
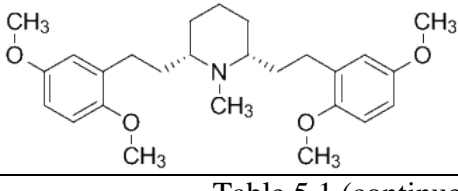

JPC-130B		0.43 ± 0.050	0.030 ± 0.0017
JPC-004		2.57 ± 0.48	0.30 ± 0.080
JPC-010		2.87 ± 0.83	0.23 ± 0.023
JPC-033		29.0 ± 5.0	0.58 ± 0.096
JPC-034		5.93 ± 1.40	0.99 ± 0.079
JPC-035		2.08 ± 0.098	0.23 ± 0.065
JPC-036		0.62 ± 0.020	0.30 ± 0.077
JPC-041		2.70 ± 0.70	0.14 ± 0.033
JPC-042		0.56 ± 0.082	0.13 ± 0.0087

Table 5.1 (continued)

JPC-161B		2.25 ± 0.28	0.032 ± 0.0022
JPC-161C		0.35 ± 0.042	0.036 ± 0.010

Table 5.1 [^3H] Dihydrotrabenzazine Binding Assay Data and [^3H] Dopamine Uptake Assay Data for JPC compounds in the 2,6-substituted piperidine analog scaffold of lobelane

Compound Code	Structure	VMAT2 [^3H]DTBZ Binding Assay; $K_i \pm \text{SEM}$ (μM)	VMAT2 [^3H]DA Uptake; $K_i \pm \text{SEM}$ (μM)
Lobeline		2.04 ± 0.64	0.47 ± 0.045
lobelane		0.97 ± 0.19	0.045 ± 0.002
JPC-057		0.255 ± 0.026	0.030 ± 0.0020
JPC-058		2.80 ± 0.11	0.056 ± 0.009

Table 5.2 (continued)

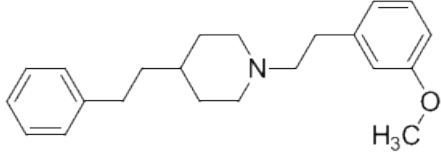
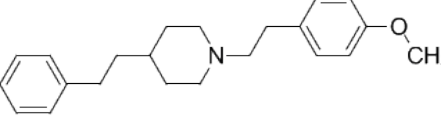
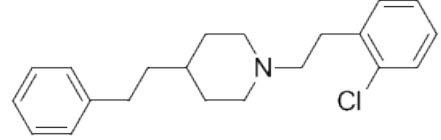
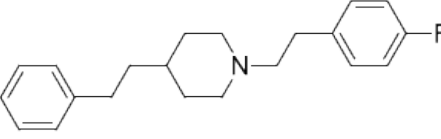
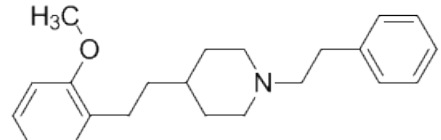
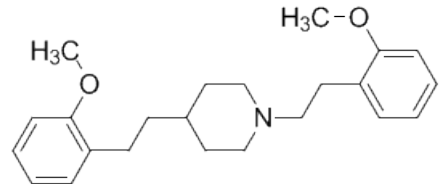
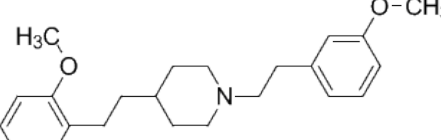
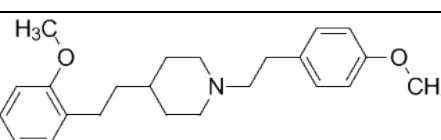
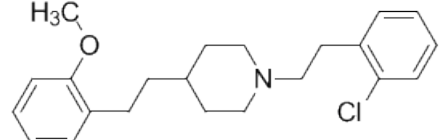
JPC-059		0.265 ± 0.038	0.022 ± 0.00087
JPC-060		1.62 ± 0.19	0.046 ± 0.0037
JPC-072		0.38 ± 0.0058	0.047 ± 0.0063
JPC-073		1.82 ± 0.0058	0.032 ± 0.0038
JPC-078		0.69 ± 0.050	0.022 ± 0.0028
JPC-077		0.19 ± 0.0088	0.0093 ± 0.0006
JPC-094		0.15 ± 0.0058	0.013 ± 0.0015
JPC-095		0.50 ± 0.10	0.043 ± 0.0028
JPC-096		0.19 ± 0.020	0.020 ± 0.0030

Table 5.2 (continued)

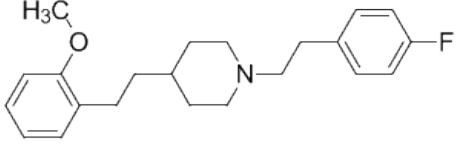
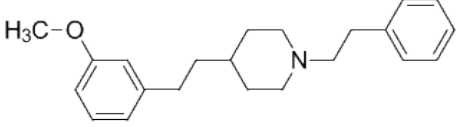
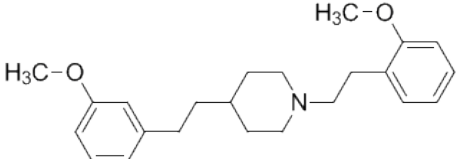
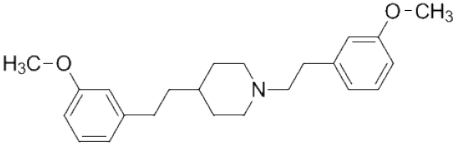
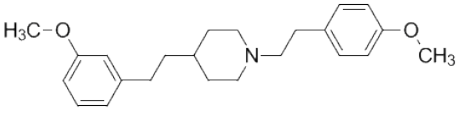
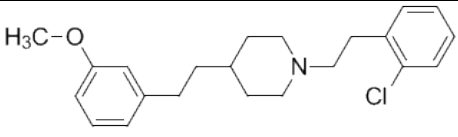
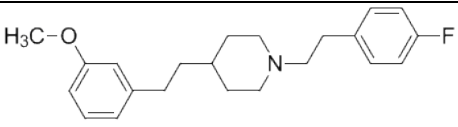
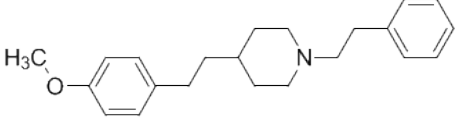
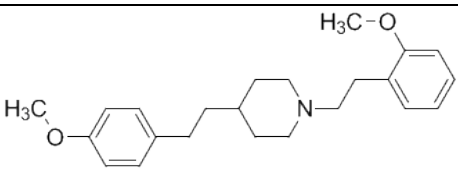
JPC-097		0.40 ± 0.097	0.013 ± 0.0021
JPC-079		0.32 ± 0.015	0.056 ± 0.0086
JPC-080		0.32 ± 0.055	0.040 ± 0.0075
JPC-081		0.23 ± 0.019	0.085 ± 0.010
JPC-082		0.45 ± 0.13	0.13 ± 0.023
JPC-083		0.46 ± 0.098	0.42 ± 0.049
JPC-084		0.96 ± 0.047	0.069 ± 0.004
JPC-085		0.51 ± 0.087	0.11 ± 0.007
JPC-086		0.42 ± 0.019	0.083 ± 0.009

Table 5.2 (continued)

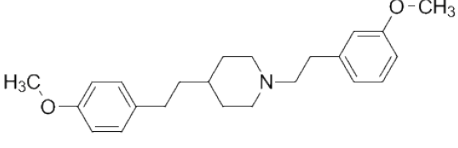
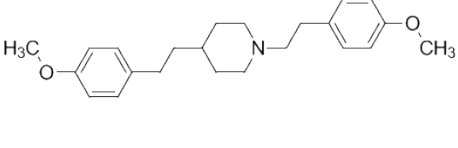
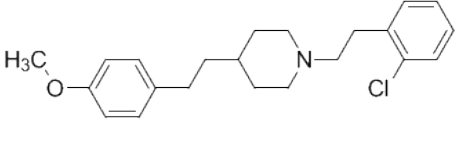
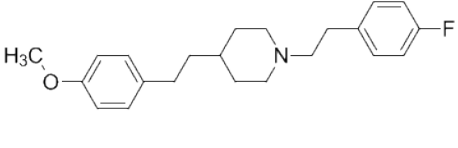
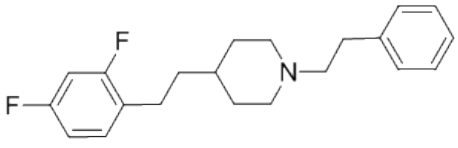
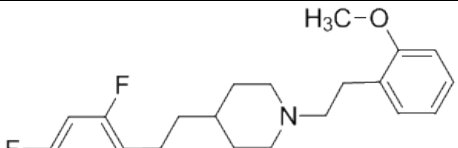
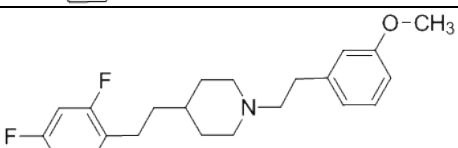
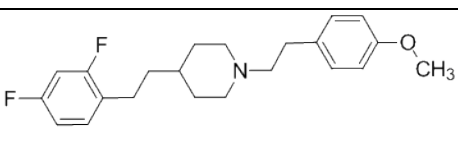
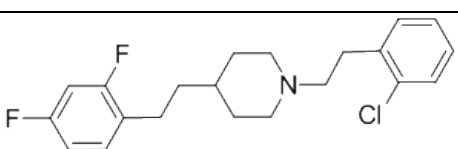
JPC-087		0.23 ± 0.047	0.075 ± 0.004
JPC-088		2.47 ± 0.27	0.16 ± 0.012
JPC-089		0.23 ± 0.020	0.040 ± 0.007
JPC-090		0.47 ± 0.067	0.060 ± 0.005
JPC-098		0.53 ± 0.11	0.053 ± 0.0055
JPC-099		0.35 ± 0.048	0.041 ± 0.012
JPC-100		0.27 ± 0.015	0.029 ± 0.0055
JPC-101		1.30 ± 0.17	0.070 ± 0.0051
JPC-102		0.24 ± 0.038	0.11 ± 0.019

Table 5.2 (continued)

JPC-103		1.45 ± 0.24	0.043 ± 0.014
JPC-104		0.29 ± 0.064	0.12 ± 0.0085
JPC-105		0.33 ± 0.018	0.076 ± 0.010
JPC-106		0.19 ± 0.009	0.083 ± 0.0038
JPC-107		1.61 ± 0.078	0.044 ± 0.0033
JPC-108		0.23 ± 0.015	0.067 ± 0.021
JPC-109		0.60 ± 0.075	0.060 ± 0.0082
JPC-110		1.10 ± 0.087	0.051 ± 0.0035

Table 5.2 (continued)

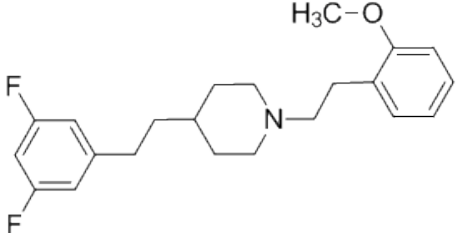
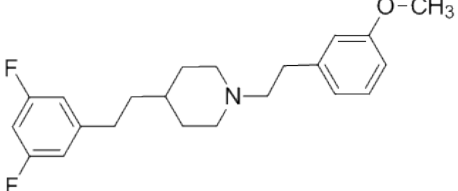
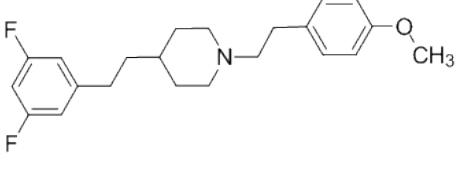
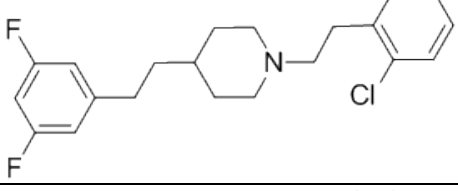
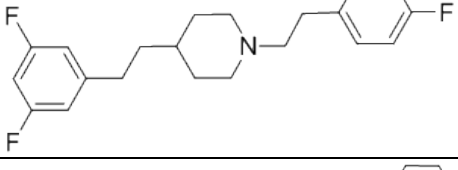
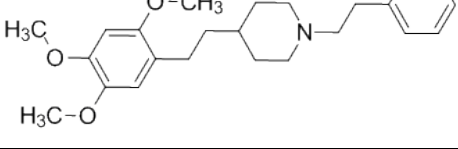
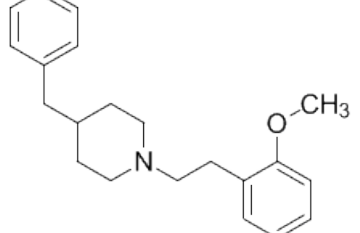
JPC-111		0.41 ± 0.038	0.034 ± 0.0039
JPC-112		0.25 ± 0.003	0.028 ± 0.0027
JPC-113		2.03 ± 0.13	0.12 ± 0.028
JPC-114		0.66 ± 0.058	0.18 ± 0.068
JPC-115		1.43 ± 0.28	0.068 ± 0.016
JPC-068		0.38 ± 0.049	0.094 ± 0.0096
JPC-061		2.76 ± 0.31	0.13 ± 0.015

Table 5.2 (continued)

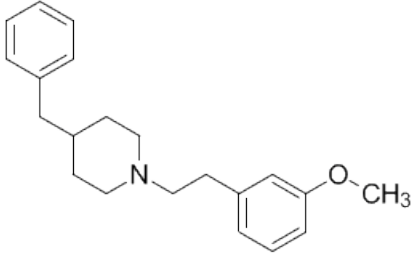
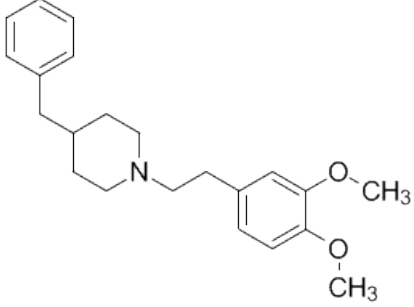
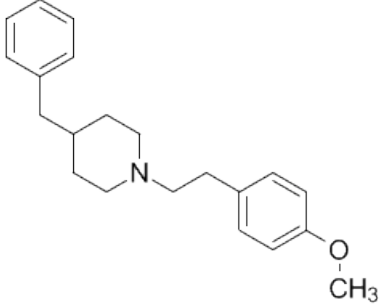
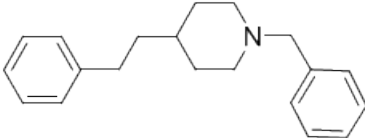
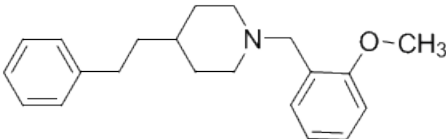
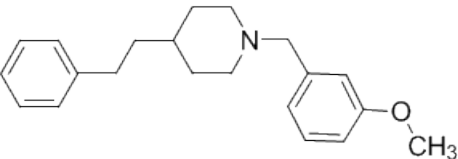
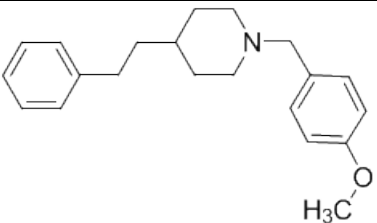
JPC-062		1.53 ± 0.10	0.077 ± 0.0098
JPC-063		2.99 ± 0.17	0.24 ± 0.034
JPC-064		1.94 ± 0.43	0.18 ± 0.011
JPC-152		21.7 ± 2.08	0.19 ± 0.63
JPC-153		9.36 ± 1.32	0.070 ± 0.0075
JPC-154		12.7 ± 4.28	0.19 ± 0.020
JPC-155		6.23 ± 0.56	0.25 ± 0.027

Table 5.2 (continued)

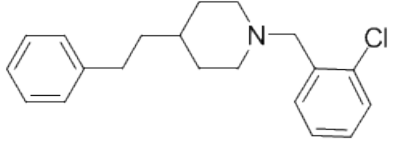
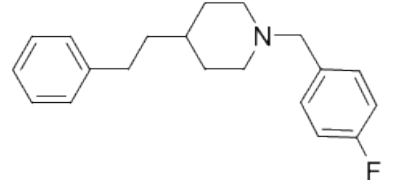
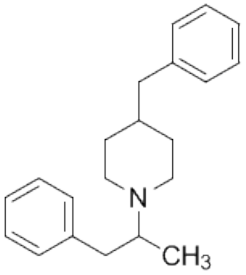
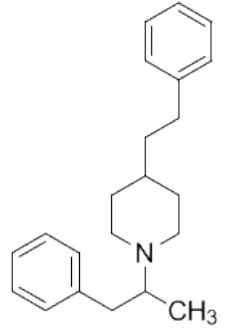
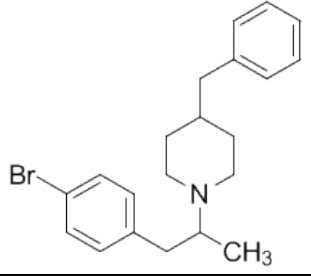
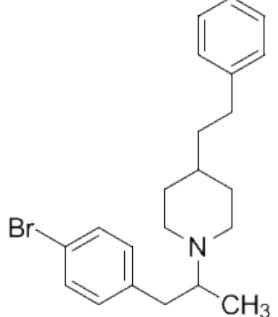
JPC-156		44.5 ± 17.8	0.27 ± 0.042
JPC-157		10.1 ± 0.58	0.21 ± 0.012
JPC-174		*	0.020 ± 0.0082
JPC-175		2.32 ± 0.26	0.073 ± 0.0008
JPC-171		2.56 ± 0.34	0.21 ± 0.052
JPC-172		0.257 ± 0.37	0.30 ± 0.032

Table 5.2 (continued)

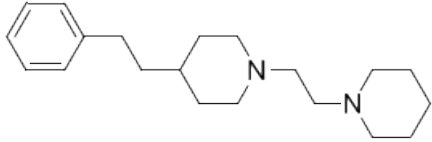
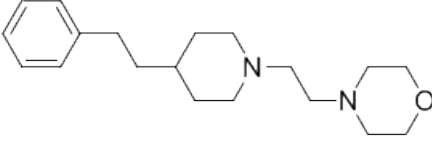
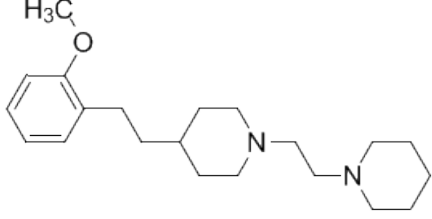
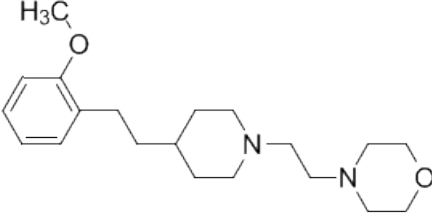
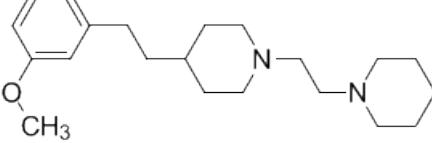
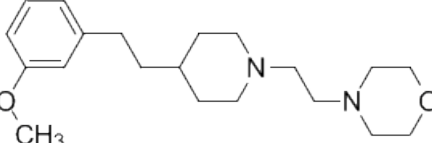
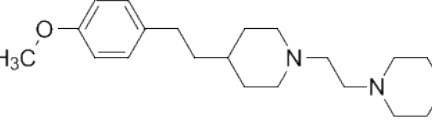
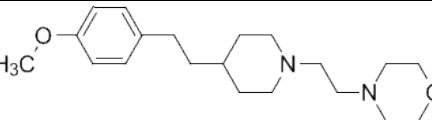
JPC-116		30.3 ± 5.97	2.32 ± 0.50
JPC-117		>100	6.28 ± 0.39
JPC-118		11.5 ± 0.80	2.19 ± 0.37
JPC-119		>100	3.74 ± 1.03
JPC-120		9.26 ± 1.27	1.18 ± 0.12
JPC-121		>100	2.90 ± 0.36
JPC-122		14.1 ± 2.36	0.36 ± 0.050
JPC-123		22.0 ± 4.48	1.12 ± 0.19

Table 5.2 (continued)

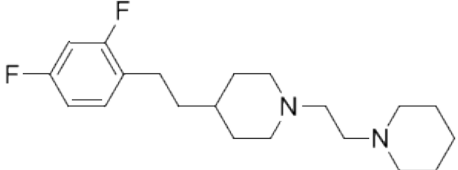
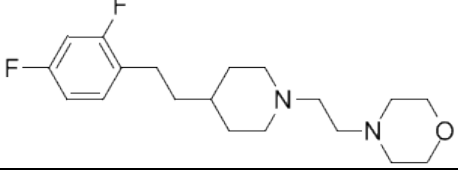
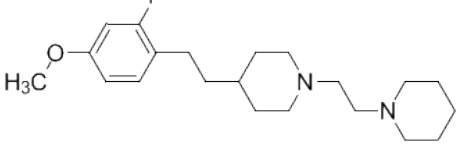
JPC-124		19.7 ± 4.40	0.60 ± 0.11
JPC-125		22.9 ± 1.9	2.00 ± 0.32
JPC-126		6.27 ± 0.22	0.42 ± 0.04

Table 5.2 [^3H] Dihydrotrabenzazine Binding Assay Data and [^3H] Dopamine Uptake

Assay Data for JPC compounds in the 1,4-substituted piperidine analog scaffold of
lobelane

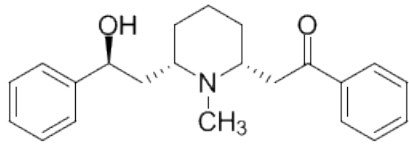
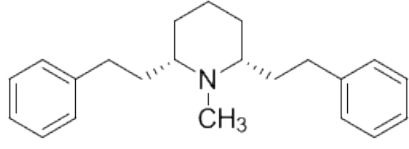
Compound Code	Structure	VMAT2 [^3H]DTBZ Binding Assay; $K_i \pm \text{SEM}$ (μM)	VMAT2 [^3H]DA Uptake; $K_i \pm \text{SEM}$ (μM)
Lobeline		2.04 ± 0.64	0.47 ± 0.045
lobelane		0.97 ± 0.19	0.045 ± 0.002

Table 5.3 (continued)

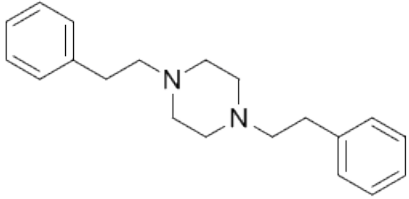
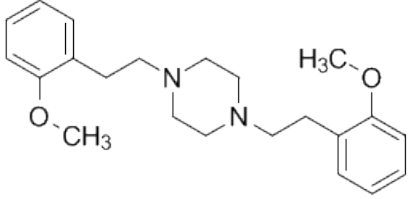
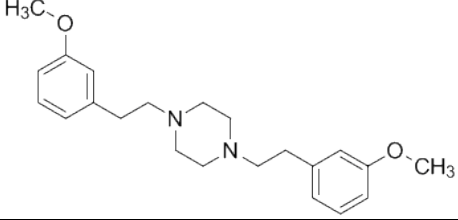
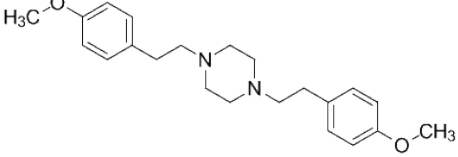
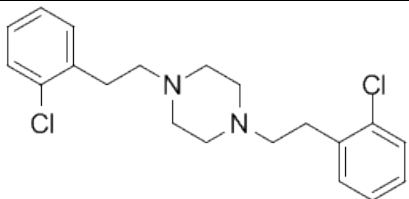
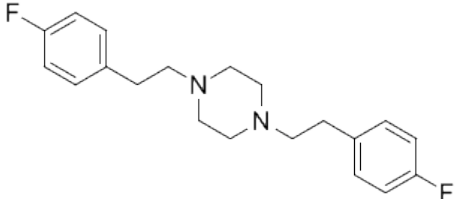
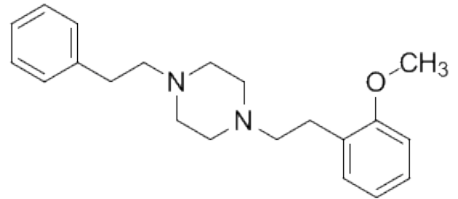
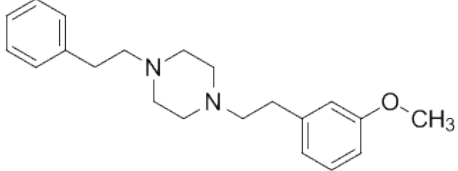
JPC-134		3.05 ± 0.64	0.11 ± 0.012
JPC-135		1.17 ± 0.13	0.035 ± 0.0012
JPC-137		1.05 ± 0.087	0.060 ± 0.004
JPC-138		6.63 ± 0.84	0.41 ± 0.005
JPC-139		0.37 ± 0.038	0.048 ± 0.003
JPC-140		3.71 ± 0.48	0.058 ± 0.012
JPC-141		1.07 ± 0.25	0.037 ± 0.0005
JPC-142		1.30 ± 0.33	0.098 ± 0.016

Table 5.3 (continued)

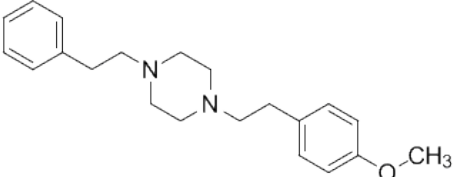
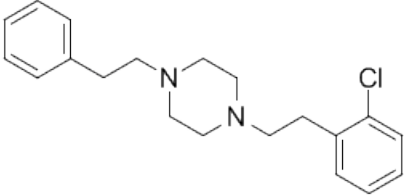
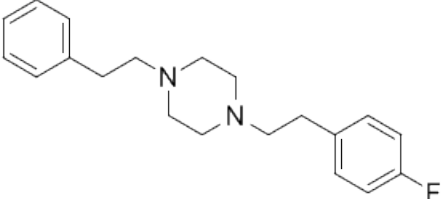
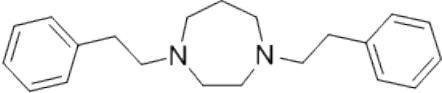
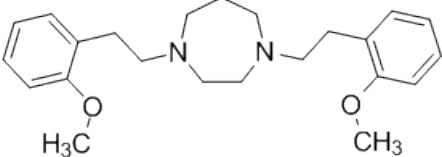
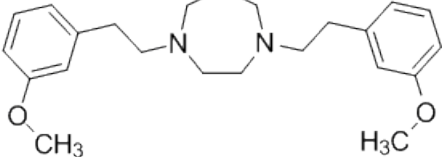
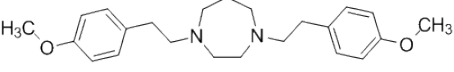
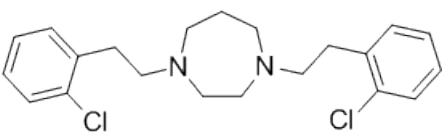
JPC-143		4.63 ± 1.31	0.10 ± 0.011
JPC-144		1.59 ± 0.26	0.063 ± 0.0069
JPC-145		3.86 ± 1.01	0.088 ± 0.0069
JPC-146		3.17 ± 0.55	0.17 ± 0.017
JPC-147		2.02 ± 0.11	0.18 ± 0.011
JPC-148		2.24 ± 0.53	0.10 ± 0.010
JPC-149		2.88 ± 0.25	0.25 ± 0.015
JPC-150		0.93 ± 0.021	0.17 ± 0.025

Table 5.3 (continued)

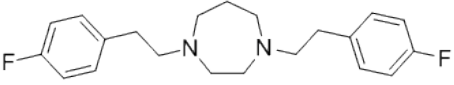
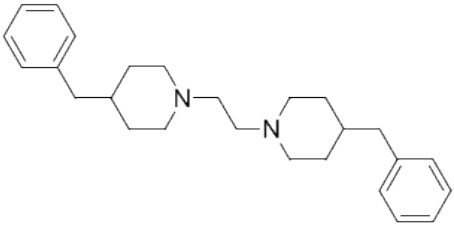
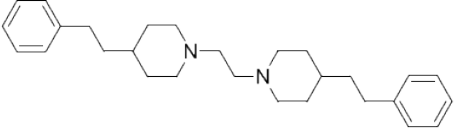
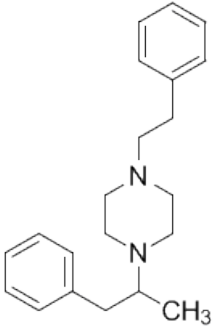
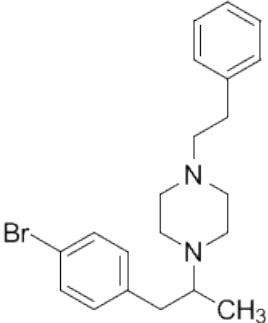
JPC-151		5.05 ± 0.77	0.085 ± 0.0052
JPC-132		0.82 ± 0.19	0.26 ± 0.019
JPC-133		3.42 ± 0.34	0.11 ± 0.0087
JPC-176		13.3 ± 1.10	0.15 ± 0.015
JPC-173		4.55 ± 0.94	0.31 ± 0.005

Table 5.3 [^3H] Dihydrotrabenazine Binding Assay Data and [^3H] Dopamine Uptake Assay Data for JPC compounds in the 1,4-substituted piperazine and diazepane analog scaffolds of lobelane and similar compounds

5.3 [³H] Dihydrotetrabenazine Binding Assay and [³H] Dopamine Uptake Assay Results Discussion

The 107 JPC compounds designed, synthesized, and assayed for activity and function at VMAT2 can and have been assigned to one of three groups based on structure. These groups are 1) the 2,6-substituted piperidine analog scaffold of lobelane, 2) the 1,4-substituted piperidine analog scaffold of lobelane, and 3) the 1,4-substituted piperazine and diazepane analog scaffolds of lobelane. Groups 2 and 3 can be divided further into subgroups based on structure to allow later SAR discussions to better describe trends. In order for a compound to be selected for further testing in the whole animal model, it must meet two requirements: 1) be among the most potent compounds if not the most potent compound among a designated series or scaffold of compounds and 2) have a potency in the functional [³H] Dopamine Uptake Assay of better than 100 nM. Compounds that have been selected from the 107 JPC compounds that were designed and synthesized have been marked in bold face font within the tables present in Chapter 5.

The 2,6-substituted piperidine analog scaffold of lobelane contained 18 compounds that are similar in scaffold structure to remain in one group without further division. The compounds differed in their [³H]DTBZ affinities by as much as two orders of magnitude, with the best compound (JPC-011) having an affinity for the TBZ binding site on VMAT2 of 0.29 μM and the least effective compound (JPC-008) having a binding affinity for the TBZ binding site on VMAT2 of 30.6 μM. The compounds that did not possess a *N*-methyl substituent (*nor*-compounds) were generally 10-fold less potent than their *N*-methyl containing counterparts, a trend that is in line with previous data collected in our laboratories with other compounds in the 2,6-substituted piperidine analog scaffold. The two compounds that possessed completely saturated cyclohexyl moieties in

place of the phenyl rings found in lobelane (JPC-003 and JPC-007) had 3-5 fold less affinity for the TBZ site on VMAT2, so again the presence of two hydrophobic phenyl rings is shown to be necessary for the TBZ site of VMAT2 to recognize a ligand molecule.

The analogs that possessed two substituents in each of the phenyl rings showed interesting binding characteristics. Compounds JPC-011 and JPC-130B that contained two very electronegative (and therefore electron withdrawing) fluoro moieties (3,5-difluoro and 2,4-difluoro respectively), had the best affinities for the TBZ binding site on VMAT2 with K_i values of 0.29 μM (JPC-011) and 0.43 μM (JPC-130B). Analogs that possess less localized electron density present in the phenyl rings appears to bind slightly better to VMAT2. The analogs that possess dimethoxy functionalities in the phenyl rings showed large differences in affinity depending on the attachment point of the methoxy groups. The analog that has methoxy functionalities in the 3,5-positions of the phenyl rings (JPC-010) had approximately 2.5 fold less affinity for VMAT2 ($K_i = 2.57 \mu\text{M}$) than lobelane (0.97 μM), and when the methoxy moieties were moved to the 3,4-positions of the phenyl rings (JPC-034), the affinity decreased 6-fold ($K_i = 5.93 \mu\text{M}$) compared to lobelane. Analogs that contain methoxy functionalities in the 2,3-positions of the phenyl rings (JPC-036) and in the 2,5-positions of the phenyl rings (JPC-042) had affinities ($K_i = 0.62 \mu\text{M}$ and $K_i = 0.56 \mu\text{M}$), for the TBZ binding site on VMAT2 similar to lobelane, if not slightly stronger. It is postulated that when the methoxy groups are in the 3,5 and 3,4 positions of the phenyl rings, a steric effect must be occurring in the binding site that does not allow those analogs to bind as tightly, while when methoxy substituents are located in the 2,3 and 2,5 positions of the phenyl rings, the steric issues can be avoided.

The analog containing both a methoxy functionality and a fluoro functionality (JPC-161C) supports this idea, as the methoxy group is in the meta (3) position of the phenyl rings and the fluoro is in the para (4) position of the phenyl rings (same 3,4-substitution pattern as JPC-034), and the binding affinity was almost 17-fold greater for JPC-161C ($K_i = 0.35$) than for JPC-034 ($K_i = 5.93$).

In comparison to compounds previously generated that contained mono-substituted phenyl rings, the compounds that contain two functionalities in each phenyl ring met with mixed results in reference to affinity at VMAT2. Compounds that possessed two methoxy moieties were comparable to their mono-methoxy substituted counterparts, as two methoxy substitution patterns (2,3 and 2,5) on the phenyl rings yielded analogs with comparable to equal affinities, while two substitution patterns on the phenyl rings (3,4 and 3,5) yielded analogs with moderately less affinity for the TBZ site on VMAT2. Compounds that possessed two fluoro substituents or one fluoro and one methoxy substituents in the phenyl rings displayed affinities for VMAT2 that were equal to slightly (2-4 fold) better than their mono-substituted counterparts synthesized previously.

The best compound in the 2,6-substituted piperidine analog scaffold with respect to the DTBZ binding assay was JPC-011. None of the compounds within the 2,6-substituted piperidine analog series showed tremendous potency with respect to the functional vesicular [^3H]DA uptake assay and therefore none have yet been selected for further study in the whole animal model. While half of the dimethoxy substituted analogs fared reasonably well in the [^3H]DTBZ binding assay, all of the dimethoxy substituted compounds were equal in functional potency when compared to lobelane, as

most of them were an order of magnitude less potent in the functional vesicular [^3H]DA uptake assay. Compounds JPC-001, JPC-130A, JPC-130B, JPC-161B, and JPC-161C were similar in potency to lobelane.

The second group of compounds to be discussed are those within 1,4-substituted piperidine analog scaffold of lobelane. This series, which consists of 68 compounds, will be divided into subgroups for discussion: 1) the 1,4-substituted isomeric analogs of lobelane, 2) the 4-benzyl-1-phenethylpiperidine and 1-benzyl-4-phenethylpiperidine analogs, 3) the 4-phenethyl-1-(1-phenylpropan-2-yl)piperidine and 4-benzyl-1-(1-phenylpropan-2-yl)piperidine analogs, and 4) the 4-phenethyl-1-(2-(piperidin-1-yl)ethyl)piperidine and 4-(2-(4-phenethylpiperidin-1-yl)ethyl)morpholine analogs.

The 43 designed and synthesized 1,4-substituted isomeric analogs of lobelane ranged from 5-fold greater affinity to 2.5-fold less affinity for the TBZ site on VMAT2 when compared to lobelane. The six compounds that began the series possessed a phenethyl linker attached to the C4 position of the piperidine ring and a substituted phenethyl linker attached to the N1 position of the piperidine ring. Compounds JPC-057 and JPC-059 contain methoxy functionalities in the ortho (2) and meta (3) positions of the phenethyl linker attached to the N1 position of the piperidine ring, respectively. These two compounds displayed affinities 4-fold stronger than lobelane, with JPC-057 displaying a $K_i = 0.255 \mu\text{M}$ and JPC-059 displaying a $K_i = 0.265 \mu\text{M}$. Both JPC-057 and JPC-059 displayed potencies in the functional vesicular [^3H]DA uptake assay slightly better than lobelane. Again, as was seen in the 2,6-substituted piperazine series, compounds containing a methoxy moiety in the ortho or meta position of the phenyl ring appear to be recognized by the TBZ site on VMAT2 better than compounds without

substituents or with methoxy substituents in the para position. Addition of a 2-chloro substituent (JPC-072) did improve affinity in the [³H]DTBZ binding assay ($K_i = 0.38 \mu\text{M}$) by 3-fold compared to lobelane, and had nearly identical potency in the functional vesicular [³H]DA uptake assay ($K_i = 0.047 \mu\text{M}$). Three of the six compounds had slightly less affinity at the TBZ site on VMAT2 when compared to lobelane (JPC-058, JPC-060, and JPC-073) with affinities of $K_i = 2.80 \mu\text{M}$, $K_i = 1.62 \mu\text{M}$, $K_i = 1.82 \mu\text{M}$ respectively. These compounds did, however, have comparable affinities in the functional vesicular [³H]DA uptake assay with $K_i = 0.056 \mu\text{M}$, $K_i = 0.046 \mu\text{M}$, $K_i = 0.032 \mu\text{M}$, correspondingly.

The next subseries of compounds possessed a 2-methoxy moiety in the phenyl ring of the phenethyl linker attached to the C4 position of the piperidine ring. This entire group of six compounds had stronger affinity for the TBZ site on VMAT2, so placing a methoxy group in the ortho position of the phenyl ring attached to the linker at C4 is beneficial to the recognition of the molecule at the binding site. These six analogs have K_i 's in the [³H]DTBZ binding assay ranging from $0.15 \mu\text{M}$ to $0.69 \mu\text{M}$. The most potent three compounds in this subseries are JPC-077, JPC-094, and JPC-096 with nearly identical affinity values in [³H]DTBZ binding assay (K_i 's = $0.19 \mu\text{M}$, $K_i = 0.15 \mu\text{M}$, $K_i = 0.19 \mu\text{M}$, respectively). It should be noted that the three moieties in the phenethyl substituents attached at the N1 position that continue to give the highest affinities in each subseries are 2-methoxy, 3-methoxy, and 2-chloro. The same three compounds that were most potent in binding to the TBZ site on VMAT2 were among the best in their ability to inhibit DA uptake into the vesicle, with functional vesicular [³H]DA uptake assay values of $K_i = 0.0093 \mu\text{M}$, $K_i = 0.013 \mu\text{M}$, $K_i = 0.020 \mu\text{M}$, correspondingly. JPC-077 was the

most potent compound in the entire 43 designed and synthesized 1,4-substituted isomeric analogs in inhibiting DA uptake into the vesicle, with potency nearly 5-fold stronger than lobelane.

The next subseries of compounds possessed a 3-methoxy moiety in the phenyl ring of the phenethyl linker attached to the C4 position of the piperidine ring. Again, this entire group of six compounds had stronger affinity for the TBZ site on VMAT2, so placing a methoxy group in the meta position of the phenyl ring attached to the linker at C4 is also beneficial to the recognition of the molecule at the binding site. These six analogs have K_i 's in the [³H]DTBZ binding assay ranging from 0.15 μ M to 0.69 μ M. The most potent three compounds in this subseries are JPC-079, JPC-080, and JPC-081 with nearly identical affinity values in [³H]DTBZ binding assay (K_i 's = 0.32 μ M, K_i = 0.32 μ M, K_i = 0.23 μ M, respectively). Again, the best two compounds possessed a 2-methoxy or 3-methoxy moiety in the phenyl ring of the phenethyl linker attached to the N1 position of the piperidine ring. A significant trend is seen developing, as molecules containing 2-methoxy and 3-methoxy moieties in either one or both phenyl rings are continuing to be recognized better by the TBZ binding site on VMAT2. This series of six compounds did not fare as well in the functional assay, with potencies comparable to lobelane if not slightly inferior.

The next subseries of compounds possessed a 4-methoxy moiety in the phenyl ring of the phenethyl linker attached to the C4 position of the piperidine ring, and displayed similar trends. Five analogs in this group of six compounds had stronger affinity than lobelane for the TBZ site on VMAT2, so placing a methoxy group in the para position of the phenyl ring attached to the linker at C4 is also beneficial to the

recognition of the molecule at the binding site, but it can be said that compounds containing 4-methoxy substituents in both phenyl rings is not as well tolerated, as JPC-088 has this feature, and has a $K_i = 2.47 \mu\text{M}$, which is 2.5-fold less potent than the parent compound with just two unsubstituted phenyl rings as well as 2.5-fold less potent than lobelane, and JPC-088 is 5-10 fold less potent than the other compounds in this subseries. It should be again be noted that the three moieties in the phenethyl substituents attached at the N1 position that continue to give the highest affinities in each subseries are 2-methoxy, 3-methoxy, and 2-chloro (K_i 's = $0.42 \mu\text{M}$, $K_i = 0.23 \mu\text{M}$, $K_i = 0.23 \mu\text{M}$, respectively). The same three compounds that were most potent in binding to the TBZ site on VMAT2 were also the best in their ability to inhibit DA uptake into the vesicle, with functional vesicular [^3H]DA uptake assay values of $K_i = 0.083 \mu\text{M}$, $K_i = 0.075 \mu\text{M}$, $K_i = 0.040 \mu\text{M}$, correspondingly, which is comparable to lobelane.

The next subseries of compounds possessed 2,4-fluoro substituents in the phenyl ring of the phenethyl linker attached to the C4 position of the piperidine ring, and displayed similar trends. Four analogs in this group of six compounds had stronger affinity than lobelane for the TBZ site on VMAT2, with the other two comparable to lobelane, so placing 2,4-fluoro substituents the phenyl ring attached to the linker at C4 is also beneficial to the recognition of the molecule at the binding site. Again, it should be noted that the three moieties in the phenethyl substituents attached at the N1 position that continue to give the highest affinities in each subseries are 2-methoxy (JPC-099), 3-methoxy (JPC-100), and 2-chloro (JPC-102), with affinities in the [^3H]DTBZ binding assay ranging from $0.24 \mu\text{M}$ to $0.35 \mu\text{M}$ (K_i 's = $0.35 \mu\text{M}$, $K_i = 0.27 \mu\text{M}$, $K_i = 0.24 \mu\text{M}$, respectively). Analogs JPC-100 and JPC-101 were again the most potent in the

functional vesicular [³H]DA uptake assay values of $K_i = 0.041 \mu\text{M}$, $K_i = 0.029 \mu\text{M}$, correspondingly, which is comparable to lobelane (slightly more potent) and continues the trend.

The next subseries of compounds possessed 2-fluoro, 4-methoxy substituents in the phenyl ring of the phenylethyl linker attached to the C4 position of the piperidine ring, and displayed similar trends. Five analogs in this group of six compounds had stronger affinity than lobelane for the TBZ site on VMAT2, with the other comparable to lobelane, so placing 2-fluoro, 4-methoxy substituents the phenyl ring attached to the linker at C4 is also beneficial to the recognition of the molecule at the binding site. Once again, the three moieties in the phenethyl substituents attached at the N1 position that continue to give the highest affinities in each subseries are 2-methoxy (JPC-105), 3-methoxy (JPC-106), and 2-chloro (JPC-108), with affinities in the [³H]DTBZ binding assay ranging from $0.19 \mu\text{M}$ to $0.33 \mu\text{M}$ (K_i 's = $0.33 \mu\text{M}$, $K_i = 0.19 \mu\text{M}$, $K_i = 0.23 \mu\text{M}$, respectively). Compound JPC-108 is the first analog that possessed the combination of three different moieties in the two phenyl rings. All compounds in this subseries displayed similar potencies in the functional vesicular [³H]DA uptake assay comparable to lobelane.

The next subseries of compounds possessed 3,5-difluoro substituents in the phenyl ring of the phenylethyl linker attached to the C4 position of the piperidine ring, and displayed similar trends. Four analogs in this group of six compounds had stronger affinity than lobelane for the TBZ site on VMAT2, with the other comparable to lobelane, so placing 3,5-difluoro substituents the phenyl ring attached to the linker at C4 is also beneficial to the recognition of the molecule at the binding site. Once again, the

three moieties in the phenethyl substituents attached at the N1 position that continue to give the highest affinities in each subseries are 2-methoxy (JPC-111), 3-methoxy (JPC-112), and 2-chloro (JPC-114), with affinities in the [³H]DTBZ binding assay ranging from 0.25 μM to 0.66 μM (K_i 's = 0.41 μM, K_i = 0.25 μM, K_i = 0.66 μM, respectively). Analogs JPC-111 and JPC-112 were again the most potent in the functional vesicular [³H]DA uptake assay values of K_i = 0.034 μM, K_i = 0.028 μM, correspondingly, which is comparable to lobelane (slightly more potent) and continues the trend.

The final compound in this group of 43 among the 1,4-substituted piperidine analog scaffold of lobelane is JPC-068. This analog contains a 2,4,5-trimethoxy substituent in the phenyl ring of the phenethyl linker attached to the C4 position of the piperidine ring, and an unsubstituted phenethyl linker attached to the N1 position. Previously, in the 2,6-substituted piperidine series, compounds with multiple methoxy groups present in the meta and para positions in both phenyl rings were 5-6 fold less potent in the [³H]DTBZ binding assay, and this was postulated to be due to steric issues. This compound had only one phenyl ring substituted with multiple methoxy substituents, and has an affinity for the TBZ site on VMAT2 3-fold more potent than lobelane. It appears that if steric hindrance is the issue for earlier compounds not being able to bind as strongly, it is only on one portion of the binding site, as this compound was tolerated quite well. Despite having a 3-fold better binding affinity at the TBZ binding site, JPC-068 did not improve upon lobelane in the functional vesicular [³H]DA uptake assay, with values comparable but not enhanced.

The next series of series of 1,4-substituted piperidine analogs was designed and synthesized with shorter linkers between the C4 position of the piperidine ring while

maintaining a substituted phenethyl linker on the N1 position were prepared to further analyze the ability of the TBZ binding site on VMAT2 to recognize compounds with shorter linkers and less degrees of freedom of rotation (one carbon shorter on the C4 attached linker). Four compounds were generated in this series and all had weaker affinity than lobelane for the TBZ site on VMAT2, with the other comparable to lobelane, so placing shorter linkers between the C4 position of the piperidine ring is not beneficial to the recognition of the molecule at the binding site. The most appealing compound among the four in the series is JPC-062, which has a 3-methoxy substituent in the phenyl ring attached to the N1 position of the piperidine ring. Affinity at the TBZ site of VMAT2 was comparable ($K_i = 1.53 \mu\text{M}$) to lobelane, and effectiveness in the functional vesicular [^3H]DA uptake assay was comparable ($K_i = 0.077 \mu\text{M}$), but was not enhanced.

A series of 1,4-substituted piperidine analogs with shorter linkers between the N1 position of the piperidine ring while maintaining a substituted phenethyl linker on the C4 position were prepared to further analyze the ability of the TBZ binding site on VMAT2 to recognize compounds with shorter linkers and less degrees of freedom of rotation (one carbon shorter) on the N1 attached linker. The entire series of six compounds had less affinity for the TBZ site on VMAT2 with K_i values ranging from $6.23 \mu\text{M}$ to $44.5 \mu\text{M}$. One analog, JPC-153, containing a 2-methoxy substituent in the phenyl ring attached by a one carbon linker to the N1 position of the piperidine ring did have effectiveness in the functional vesicular [^3H]DA uptake assay was comparable ($K_i = 0.070 \mu\text{M}$), but all others were 4-6 fold less potent than lobelane. It is clear that reducing the length of the linker between the N1 position of the piperidine ring and the phenyl ring is not beneficial, and

has a detrimental effect on how the TBZ binding site on VMAT2 recognizes the molecule.

Similarly, another series of 1,4-substituted piperidine analogs combined these factors with shorter linkers between the N1 position of the piperidine ring while maintaining a substituted phenethyl linker on the C4 position or with shorter linkers between the C4 position of the piperidine ring while maintaining a substituted phenethyl linker on the N1 position were prepared to further analyze the ability of the TBZ binding site on VMAT2 to recognize compounds with shorter linkers and less degrees of freedom of rotation (one carbon shorter) on the N1 attached linker. This series of compounds was designed to possess a branch in the N1 alkyl linker in the form of a racemic 1-phenylpropan-2-yl functionality attached to N1 of the piperidine ring. Four compounds were generated in this series, and had similar affinities as lobelane for the TBZ site on VMAT2 with one exception. JPC-172, containing a 4-bromo substituent on the phenyl ring of the 1-phenylpropan-2-yl linker attached to the N1 position of the piperidine ring displayed a $K_i = 0.257 \mu\text{M}$ in the [^3H]DTBZ binding assay, approximately 4-fold more potent than lobelane. JPC-174 and JPC-175 exhibited effectiveness in the functional vesicular [^3H]DA uptake assay was comparable ($K_i = 0.073 \mu\text{M}$ and $K_i = 0.073 \mu\text{M}$, respectively) to lobelane.

The final series of compounds of 1,4-substituted piperidine analogs was designed to increase the water solubility of the scaffold by replacing the phenyl ring on the N1 phenethyl linker with saturated heterocyclic moieties, either piperidine or morpholine and to study what effect the introduction of a more polar moiety would have on binding affinity at the TBZ site of VMAT2. Of the 11 compounds generated in this series, all had

much lower affinity in the [³H]DTBZ binding assay than compounds possessing two phenyl rings. Values in the [³H]DTBZ binding assay ranged from $K_i = 6.27 \mu\text{M}$ to $>100 \mu\text{M}$. Effectiveness in the functional vesicular [³H]DA uptake assay was also greatly diminished with K_i 's ranging from 0.36 to 6.28 μM . Clearly, attempting to increase water solubility by replacing one of the phenyl rings with a piperidine or morpholine moiety is not effective. The next series of compounds attempted to maintain the two phenyl rings while increasing the water solubility characteristics of the analogs by placing a second amino moiety inside the central saturated ring.

The series of 1,4-piperazine and 1,4-diazepane analogs were designed and synthesized to add the second amino functionality into the central ring of the lobelane scaffold. The addition of another polar functionality into the central ring will increase the water solubilizing characteristics of the scaffold, which is desirable in development of drugs with higher bioavailability than lobelane, and several series of compounds were designed and synthesized to explore these possibilities, resulting in the generation of 21 compounds.

The first series of six compounds consisted of symmetrical 1,4-piperazine analogs. Of these six compounds, all had affinities for the TBZ site on VMAT2 similar to that possessed by lobelane, ranging from slightly better ($K_i = 0.37 \mu\text{M}$) to slightly worse (6.63 μM). Considering that this series of compounds should be at least 2-3 times as soluble in water as their piperidine counterparts, these affinities are remarkably effective, especially when one considers the large loss of affinity found when replacing one of the phenyl rings of the piperidine scaffold with a water solubilizing piperidine or morpholine moiety. It was not surprising, however, that the three most potent analogs in

both the [³H]DTBZ binding assay and the functional vesicular [³H]DA uptake assay maintained the same trend as seen before. Analogs that possessed a 2-methoxy (JPC-135), a 3-methoxy (JPC-137), or a 2-chloro (JPC-139) functionality in both of the two phenyl rings had the strongest affinity for the TBZ site on VMAT2 with K_i 's of 1.17 μ M, 1.05 μ M, and 0.37 μ M, respectively. In the functional vesicular [³H]DA uptake assay the same three analogs displayed K_i 's of 0.035 μ M, 0.060 μ M, and 0.048 μ M, respectively, which were all quite similar to lobelane.

The second series of five compounds were asymmetrical 1,4-piperazine analogs containing an unsubstituted phenethyl linker attached to N4 position of the piperazine ring, and a substituted phenethyl linker attached to the N1 position of the piperazine ring. Of these five compounds, all had affinities for the TBZ site on VMAT2 similar to that possessed by lobelane, ranging from the same ($K_i = 1.07 \mu$ M) to slightly worse (4.63 μ M). As is nearly standard by this point, the three compounds that have the best affinity for the TBZ site on VMAT2 were those that possessed a 2-methoxy (JPC-141), a 3-methoxy (JPC-142), or a 2-chloro (JPC-144) functionality in the phenyl ring attached to the N1 position of the piperazine ring, K_i 's of 1.07 μ M, 1.30 μ M, and 1.59 μ M, respectively. In the functional vesicular [³H]DA uptake assay the same three analogs displayed K_i 's of 0.037 μ M, 0.098 μ M, and 0.063 μ M, respectively, which were all quite similar to lobelane.

After the series of asymmetrical 1,4-piperazine analogs were synthesized, further modification of the central ring of the 1,4-scaffold was desired. Enlarging the central six-membered piperazine ring to a seven-membered 1,4-diazepane ring was explored, with six compounds designed and synthesized to explore this series. All analogs in this series

displayed affinities for the TBZ site on VMAT2 similar to that possessed by lobelane, ranging from the same ($K_i = 0.93 \mu\text{M}$) to slightly worse ($5.05 \mu\text{M}$). These compounds did not fare as well as the 1,4-piperazine analogs in the functional vesicular [^3H]DA uptake assay, ranging from 2-5 fold less potent than lobelane.

The next small series of compounds, JPC-132 and JPC-133, contain two amine moieties central to the molecule and were designed and synthesized to explore the idea that two piperidine rings linked by ethylene chain may be tolerated by the TBZ site on VMAT2. While JPC-132 displayed an affinity in the [^3H]DTBZ binding assay slightly better ($K_i = 0.82 \mu\text{M}$) than lobelane, it had less potency in the functional vesicular [^3H]DA uptake assay ($K_i = 0.26 \mu\text{M}$), or 5-fold less potent than lobelane.

The final series of compounds in the library consisted of two compounds were designed and synthesized to evaluate analogs that possess a branch in the N1 alkyl linker in the form of a racemic 1-phenylpropan-2-yl functionality attached to N1 of the piperazine ring, while maintaining the phenethyl linker on N4 of the piperazine ring. This series also explored the addition of a 4-bromo moiety in the phenyl ring attached to the N1 position of the piperazine ring. This mirrored a similar series generated in the piperidine scaffold, and the results in the assays were of a similar nature. JPC-176 had 10-fold less affinity for the TBZ site on VMAT2 than lobelane, and JPC-173, which contained the 4-bromo substituent, was 5-fold less potent than lobelane.

Of the 107 compounds generated in the library, many showed improved affinity in the [^3H]DTBZ binding and the functional vesicular [^3H]DA uptake assay when compared to the first and second generation analogs that were prepared previously. The

compounds selected for further evaluation are: JPC-077, JPC-078, JPC-089, JPC-141, JPC-142, and JPC-143, and these improved compounds were chosen to undergo further *in vivo* evaluation in rat models of behavior. These experiments are still ongoing, but preliminary results look quite promising. JPC-077 has displayed the ability to inhibit METH self-administration in the rat model as well as the ability to prevent METH induced locomotor response in rats. JPC-078 also shows potential, as it has shown the ability to prevent METH induced locomotor response in rats. JPC-141, a 1,4-piperazine analog, has also displayed the capability to prevent METH induced locomotor response in the rat model. The other three compounds are still in the process of evaluation.

Chapter 6

Ligand based pharmacophore modeling of the VMAT2 binding site

6.1 Background of computational modeling

Modern SAR efforts require the use of computational resources and programs that use mathematical models of the drug molecule and target. This part of the drug discovery pathway has become more and more complex as it evolves. Entire research groups are dedicated to the “virtual synthesis” and “virtual screening” of molecules and drug targets. These virtual efforts go hand in hand with traditional drug discovery procedures, and are mainly used to support the continuing synthetic efforts to make more and more efficient drug candidates. By taking advantage of the information gleaned from prior synthetic efforts and biological experimentation, computational SAR can uncover the required molecular features of the lead compounds from past generations of synthesis and provide direction and novel ideas for structural chemical modification.

The computational methods for SAR differ depending on the circumstances and information at hand. The different methods are described as: 1.) development of ligand-receptor models (also known as docking models), and these are used specifically for situations where the receptor or biomolecular target structure has been previously identified through methods such as x-ray crystallography, or 2.) development of a pharmacophore-based model, also known as a ligand based model, which consists of SAR modeling based on certain molecular features of the ligand molecules from the constructed compound library; these methods used in situations where little information

is known about the drug target, or when the critical molecular structural features of the target are not well defined, as in this case with VMAT2.

6.2 Model Methods of automatic pharmacophore modeling of VMAT2 inhibitors.

Computational pharmacophore modeling has emerged as one of the major computational techniques in pharmaceutical drug design, especially in the absence of a protein 3D structure. For instance, when active compounds are available, chemists use the geometric and electronic structures of the chemical compounds to naturally define a chemical model of how a particular ligand or a series of structurally related ligands interact with the receptor, and/or to deduce structure-activity relationships.

In the current study, pharmacophore modeling has been performed using the small molecule ligands that have been discovered to bind to the TBZ site on VMAT2 by conventional screening procedures. The discovered compounds demonstrated what can be considered strong inhibitory activity in the [³H]DTBZ binding assay and the functional vesicular [³H]DA uptake assay. In order to understand the specific chemical features that are responsible for the activity of the compounds, the elucidation of the pharmacophore has been performed.

MOE software was utilized extensively for the pharmacophore modeling. Two kinds of pharmacophore modeling can be performed, 1.) manual pharmacophore generation, and 2.) automatic pharmacophore generation. Briefly, manual pharmacophore modeling can be performed by using each of the most active compounds from the current series of compounds. Automatic pharmacophore generation can be performed when one or more active compounds with a similar binding mode at the targeted binding site are

available in the library of compounds. Since the compounds reported in this study are all analogs of similar structural scaffolds, and since the binding modes of the compounds cannot be generated due to the absence of a defined binding site structure, for now, we must assume that all the inhibitors bind in a similar binding mode.

The three major steps involved in automatic pharmacophore modeling are:

1. Conformation generation
2. Alignment
3. Pharmacophore query elucidation.

Prior to running the pharmacophore application in MOE, all the compounds have to be imported into the MOE database along with the [³H]DTBZ binding and the functional vesicular [³H]DA uptake assay data. Briefly, the input database must contain in one field molecules either in 2D or 3D format. The pharmacophore elucidator in MOE only works with 3D conformations, and if the 2D structures are provided, MOE can automatically convert the 2D structures to 3D conformations, or the conformations of the compounds can be generated with any other method or software and imported into the MOE database. For the current work, the internal MOE conformation generator was used on the library of compounds (which were all protonated and charged at biological pH) utilizing a Stochastic search. In general, it is best to use the same method for generating conformations as is used for preparing the 3D search databases. The generated conformations per compound were stored in the molecule field of the database. In the second field, the activity data (biological assay data) is provided. If no limit of activity is

specified, the MOE elucidator will assume all the compounds to be active, therefore, in the current study, all the compounds with affinities in the [³H]DTBZ binding assay that were less than 1.0 μM were treated as active and all compounds with affinities > 1.0 μM were treated as inactive compounds. After the input database is prepared, the next step is to specify a scheme. In MOE the modeling of H-donor and H-acceptor features depends on the selected pharmacophore scheme. There are six schemes supplied with MOE: PCH, PCHD, PCH_All, PPCH, PPCH_All, and CHD. The default CHD scheme was selected for use in the current work. Finally, before generation of the pharmacophore queries, molecular geometric alignments from the collection of input conformations was done by considering all possible discrete geometries and all possible combinations of feature query expressions. The default CHD contains a feature limit of 5, which means the pharmacophore with a maximum of 5 features are generated, and this is due to the preliminary nature of this study. Pharmacophore queries with higher numbers of features to be matched predictably tend to match fewer molecules outside the input database, which would be less useful in this early process.

6.3 Results of automatic pharmacophore modeling of VMAT2 inhibitors.

A total of 177 different pharmacophore models (queries) were generated by using the CHD scheme and the above mentioned method. The best pharmacophore is displayed and discussed further. The pharmacophore query resulting from the MOE pharmacophore elucidator is shown in Figure 6.1 and Figure 6.2. The statistics of the pharmacophore model are shown in Table 6.1, with descriptions below to describe the different categorical results. The model was developed based on the input that all compounds with

affinities for the TBZ site on VMAT2 $>1 \mu\text{M}$ are treated as inactive and all others as active compounds.

Query	Cover	Overlap	Accuracy	acc1	No. of features
HHH+	10	7.3009	1.0	1.0	4

Table 6.1 Statistics of best pharmacophore model query obtained by using the MOE pharmacophore elucidator (automatic pharmacophore modeling).

Cover: The number of active molecules that match the query.

Overlap: The score of the alignment. This number varies between [0,n] where n is the number of active molecules, therefore the larger this number, the better the alignments.

Accuracy: The accuracy of the query in separating actives and inactives. A value of 1.0 (the value actually obtained) signifies that the query matched all active compounds, and did not match any inactive compounds. The accuracy is measured on clustered conformations.

acc1: The accuracy of the query in matching the active compounds. The value of 1.0 (the value actually obtained) signifies that all actives were matched, while a value 0.0 would mean that none were matched. The accuracy is measured on clustered conformations.

The best pharmacophore generated by this method is shown in Figure 6.1. The quality of the pharmacophore query or model depends on the hit rate, which in other words can be defined as number of active compounds (true positives) that were captured

leaving behind the inactive compounds. The pharmacophore model shown in Figure 6.1 retrieves the known active compounds with an accuracy of 100.0% (see Table 6.1).

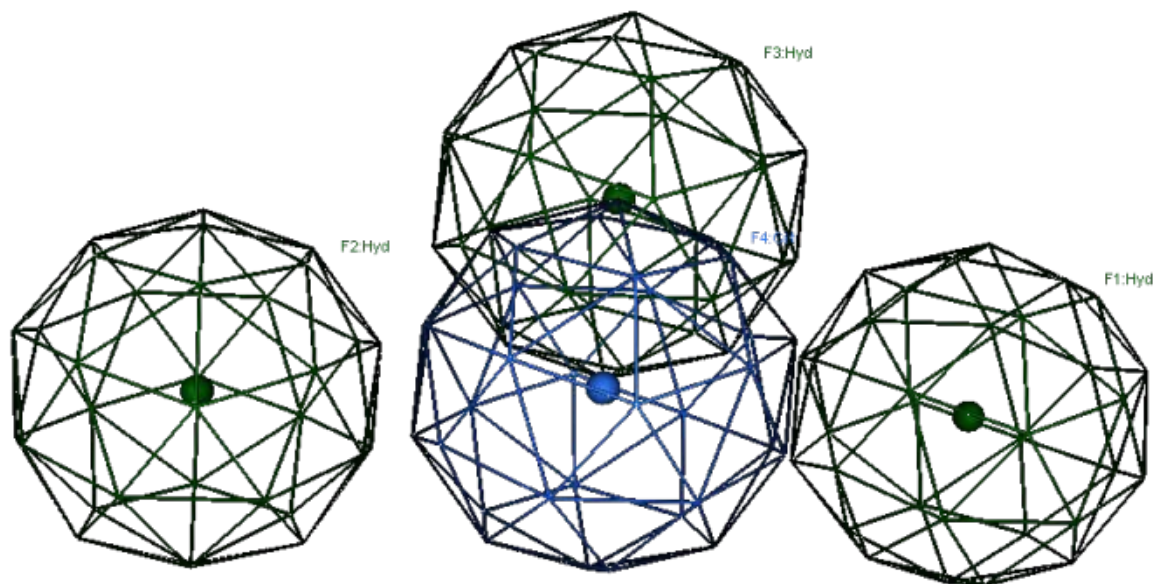


Figure 6.1 The most reliable pharmacophore model generated by automatic pharmacophore model generation in the MOE pharmacophore elucidator. The spheres in green represent the hydrophobic features and the blue sphere represents the central cation feature.

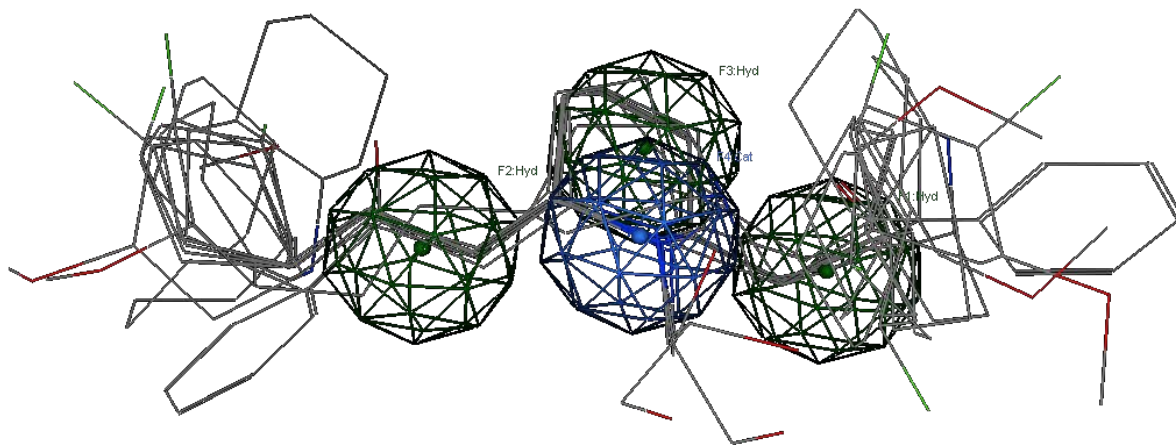


Figure 6.2 The most reliable pharmacophore model generated by automatic pharmacophore model generation in the MOE pharmacophore elucidator with all active compounds aligned in their best fit to the pharmacophore model.

The pharmacophore query produced by the MOE pharmacophore elucidator contains three hydrophobic features and a cation feature. The query has an overlap of 7.3 and accuracy of 100% which means the query could match all the 10 active compounds which were used as input. When we run the query against the 66 compound input database with active compounds, this query was able to retrieve 61 out of 66 compounds of input database, which suggests that the query describes the chemical features with huge significance.

In addition to running the pharmacophore model against the known active compounds, the query was used to run on an external database of 1000 random compounds from NCI, which resulted in 74 hits being retrieved from the NCI database. In summary, the pharmacophore query resulting from the MOE pharmacophore

elucidator suggests that hydrophobic features in the middle of the compounds and two hydrophobic features one each on either side of the central hydrophobic feature and one cation feature to the bottom of the central hydrophobic feature are necessary for the biological activity of the compounds. These observations can be used in further designing and synthesizing the similar analogs to the current series of compounds.

6.4 Model Methods of manual pharmacophore modeling of VMAT2 inhibitors.

In the manual pharmacophore modeling, two compounds with best inhibitory activity were selected. The conformations of all the compounds were generated in the same way as conformations generated by automatic pharmacophore modeling (stochastic method). The conformations with lowest energy were finally utilized as input for the pharmacophore modeling. Manual pharmacophore modeling was performed with each compound separately, therefore, two pharmacophore queries were generated.

In the first step, JPC-077 has been manually imported into the MOE environment and used to create the pharmacophore. MOE's pharmacophore query editor detected the pharmacophore features automatically and quickly generated four features which best describe the compound for biological activity. One hydrophobic and one cation and donor feature were created in the center of the compound (JPC-077) and two hydrophobic but slightly anionic features, one at either end of the compound (due to the aromatic methoxy functionalities). The compound JPC-077 with its manually created pharmacophoric query is shown in Figure 6.3. Likewise, the pharmacophore query of an active compound from the library, namely lobelane was created and shown in Figures

6.4. Finally, a manual pharmacophore model of lobeline was completed and is shown in Figure 6.5. Briefly, the pharmacophore models for lobeline and *cis*- contain three hydrophobic features and a cation and donor feature at different locations in the structure of the compounds and with different spherical volume.

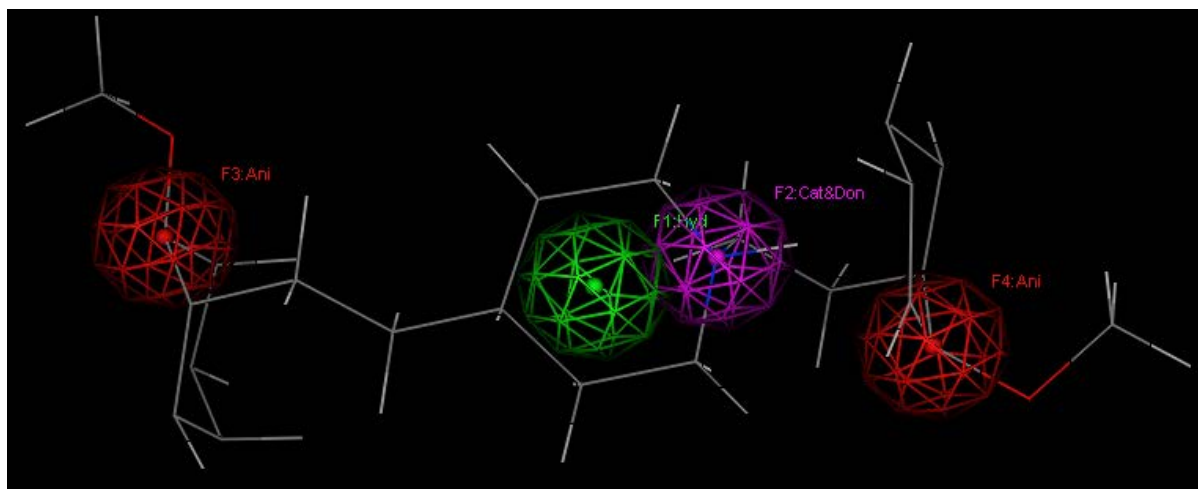


Figure 6.3 Pharmacophoric features derived manually using compound JPC-077. The four pharmacophore features are displayed in red (anionic/acceptor), green (hydrophobic), and purple (cationic/donor) colored spheres.

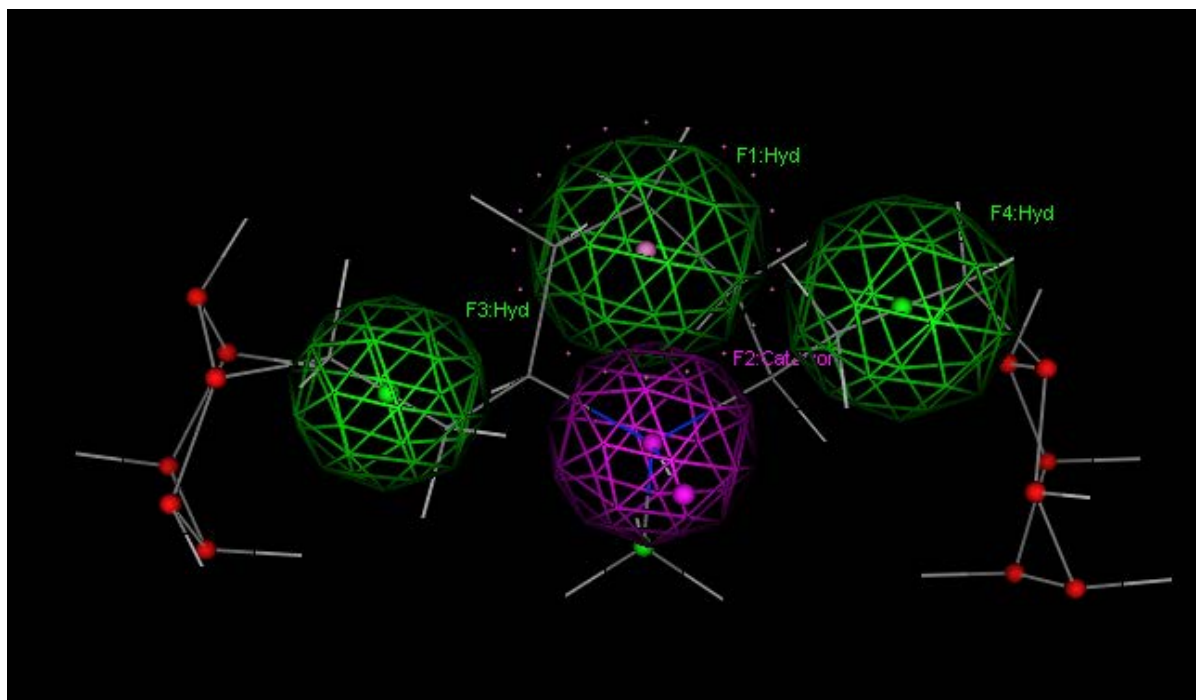


Figure 6.4 Pharmacophoric features derived manually using lobelane. The four pharmacophore features are displayed in green (hydrophobic) and purple (cationic/donor) colored spheres.

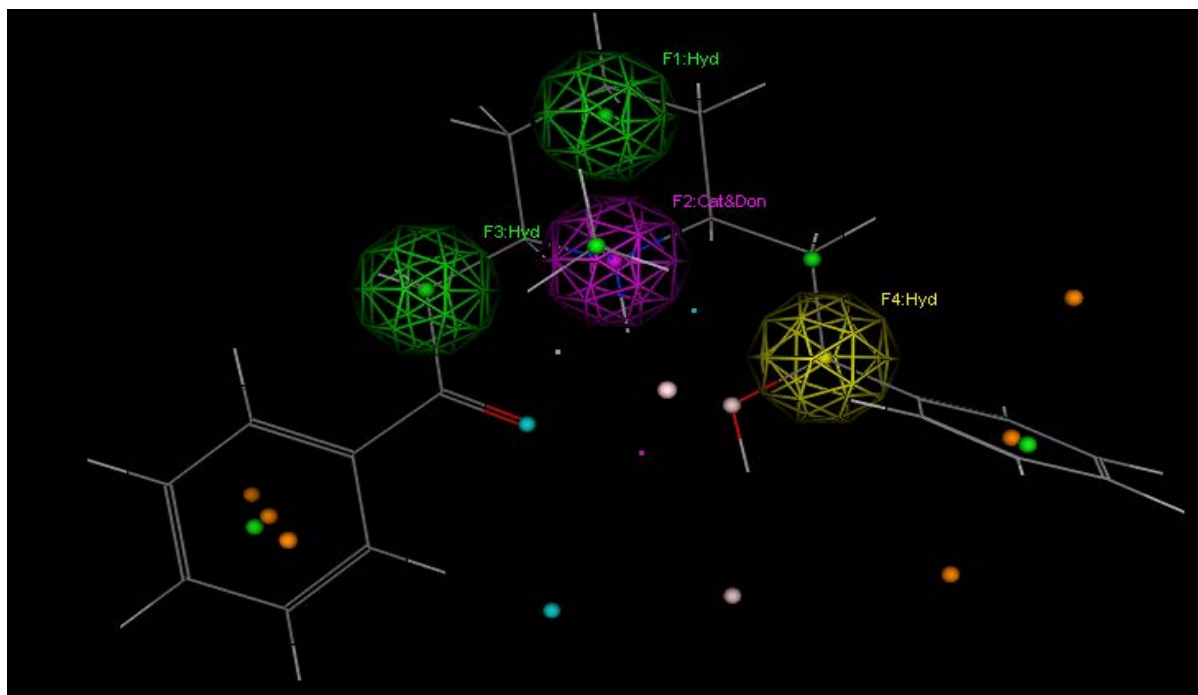


Figure 6.5 Pharmacophoric features derived manually using the compound lobeline. The four pharmacophore features are displayed in yellow (hydrophobic), green (hydrophobic) and purple (cationic/donor) colored spheres.

6.5 Results of manual pharmacophore modeling of VMAT2 inhibitors.

All the three above mentioned queries differs from each other in several significant ways. Only the hydrophobic feature at the center of molecule and the cationic and donor features are features that are considered common among all the queries, and even then, each one differs by the spherical volume. Also, the anionic features of JPC-077 were not included in the other two queries; instead, hydrophobic features on either side of the central hydrophobic feature are used. All four of the pharmacophore queries were able to retrieve approximately 50 compounds (varying by only one or two hits) of

the 66 active compounds of the current library. The pharmacophore queries suggest that the presence of a hydrophobic feature in the center of the molecule, a cationic and donor feature, and another two hydrophobic features on either side of the central hydrophobic feature, and possibly an anionic feature at the terminal aromatic methoxy group containing phenyl rings, are responsible for the biological activity of the compounds.

In perspective, following the initial pharmacophore modeling, much more could be done in the future. Possible next steps in molecular modeling to include building a homology model of VMAT2, which is as close to an actual crystal structure as possible with this trans-membrane transporter (Vardy et al., 2004). This step would be followed by docking and molecular dynamics simulation to provide insights into the interaction between the inhibitors and the protein structure, and finally, this would be followed by virtual screening, using the pharmacophore query and docking for discovering possible new inhibitors.

Chapter 7

Review and Discussion

Psychostimulant abuse has become a severe worldwide problem that has shown no sign of lessening the hold that it has on much of mainstream society. There exists an ongoing need for new therapies and medications that can provide efficacy in the treatment of psychostimulant abuse. METH especially is identified as an addictive and increasingly popular psychostimulant drug, and there are no effective, Food and Drug Administration (FDA) approved pharmacological treatments available for the addicts who wish to quit. This project has been designed to address the needs of those people who currently abuse psychostimulants such as METH, and who need an effective therapy that will help them break away from their addiction. The design and synthesis of a library of analogs similar to lobelane has been completed, with structural alterations designed into the molecules to make them more potent at the target protein: VMAT2. The overriding goal of this study was to provide one or multiple potential drug candidates that could ultimately become a treatment for psychostimulant abuse for that part of the population that currently abuses psychostimulants but wishes to quit.

Three distinct scaffolds were designed and synthesized. The first scaffold was based directly on lobelane. Further optimization and study was needed to ascertain if addition of different aromatic substituents into the phenyl rings would enhance binding affinity at VMAT2. Addition of two aromatic substituents into each of the two phenyl rings was also explored in order to determine if multiple substituents could also improve affinity. Eighteen compounds in this series were designed and synthesized. JPC-011 was

found to be the most potent compound within this series in the [³H]DTBZ binding assay (was 4-fold more potent than lobelane), but was disappointing in potency in the functional vesicular [³H]DA uptake assay, which better predicts how it will effect METH self-administration in the rat model and correspondingly the human model. In the second scaffold, further optimization and study was needed to ascertain if the addition of different aromatic substituents into the phenyl rings of the 1,4-substituted lobelane scaffold would enhance binding affinity at VMAT2. Addition of multiple aromatic substituents into the phenyl rings was also explored. 43 compounds in this series were designed and synthesized, and of those 43 analogs, 32 had improved affinity for the TBZ site on VMAT2 when compared to lobelane, with some compounds exhibiting as much as 5-fold improvement compared to lobelane and 13 compounds exhibited significant improvement in the functional vesicular [³H]DA uptake assay compared to lobelane, with JPC-077 displaying a 5-fold enhancement over lobelane.

The third scaffold was designed to increase the water-solubility of the analogs while maintaining, if not improving the compound's affinity and function at VMAT2. The addition of another N-atom into the central heterocyclic piperidine ring was predicted to improve the water solubilizing characteristics of the scaffold, which is desirable property in the development of drugs that have a higher bioavailability than lobelane, and several series of compounds were designed and synthesized to explore these possibilities, resulting in the generation of 21 novel compounds. Of these 21 analogs, seven displayed affinities for the TBZ site on VMAT2 that either maintained the affinity exhibited by lobelane, or improved it by as much as 3-fold (JPC-139). Six compounds had comparable potency in the functional vesicular [³H]DA uptake assay

when compared to lobelane. Considering that these analogs have at least 2-3 fold improved water solubility compared to lobelane and other related analogs in the piperidine series of compounds, these results are encouraging, and may lead to clinical candidates with greater oral bioavailability.

In summary, of the 107 compounds generated in the current library, many showed improved affinity in both the [³H]DTBZ binding assay, and the functional vesicular [³H]DA uptake assay, when compared to the first and second generation analogs that were prepared earlier. The compounds selected for further evaluation are: JPC-077, JPC-078, JPC-089, JPC-141, JPC-142, and JPC-143, and these improved compounds were chosen to undergo further *in vivo* evaluation in rat models of behavior. These experiments are still ongoing, but preliminary results look quite promising. JPC-077 has displayed the ability to inhibit METH self-administration in a rat model of METH addiction, as well as the ability to prevent METH-induced locomotor responses in rats. JPC-078 also shows potential as a clinical candidate, since it has been shown to prevent METH-induced locomotor responses in rats. JPC-141, a 1,4-piperazine analog, is also able to prevent METH-induced locomotor responses in the rat model. The other three JPC compounds are still in the process of evaluation.

A preliminary ligand-based pharmacophore model has been generated utilizing the SAR data accumulated from the library of compounds and their evaluation in the binding and functional assays. It proved to be very accurate in retrieval of the active compounds from the library.

This study involved three central hypotheses. One hypothesis of this work was that structural analogs of lobelane that maintain the 2,6-disubstituted piperidine scaffold, but incorporated preferred aromatic substituents into the two phenyl rings present in the lobelane structure, can improve binding affinity at the Vesicular Monoamine Transporter-2 (VMAT2), and can also improve functional inhibition of VMAT2. A second hypothesis of this work was that structural analogs of lobelane in which the phenethyl moieties present in the C2 and C6 positions of the piperidine ring can be structurally modified to afford analogs in which these moieties are located on the N1 and C4 positions of the piperidine ring, and these 1,4-disubstituted analogs have increased affinity for VMAT2 and increased potency as functional inhibitors of VMAT2. A third hypothesis of this work was that introduction of an additional N-atom into the piperidine ring of the lobelane scaffold will increase water-solubility while maintaining similar binding affinity and functional inhibition potency for VMAT2 when compared to lobelane.

As a summary of the results pertaining to the three initial hypotheses, the first hypothesis was valid in part: examples are present where structural analogs of lobelane that maintain the 2,6-disubstituted piperidine scaffold, but incorporated preferred aromatic substituents into the two phenyl rings present in the lobelane structure improved binding affinity at the Vesicular Monoamine Transporter-2 (VMAT2), but were not shown to also improve functional inhibition of VMAT2. The second and third hypotheses were shown to be valid, in that several examples from each series of compounds in the study displayed both greater affinity for the TBZ site on VMAT2 and greater potency as functional inhibitors at VMAT2 when compared to lobelane.

The data presented in this work have further demonstrated that VMAT2 is a valid target for the treatment of methamphetamine abuse, and should continue to strengthen that argument as the data from the whole animal model studies are revealed. With *in-vivo* studies currently underway and initial results for several compounds generated within this library looking promising, the primary three hypotheses of the study were addressed through well designed and executed experiments and initiative. The experiments detailed here have successfully expanded our knowledge and understanding of the properties of these novel compounds, as they relate to their binding and functional inhibition of VMAT2, and several JPC compounds are currently being evaluated as potential candidates for the treatment of METH abuse. It is highly possible that several of the compounds were presented in this manuscript and were designed and synthesized by this author will go into human clinical trials for the treatment of methamphetamine abuse, and if one proves effective in the human, this work will have not only verified that VMAT2 is an excellent target for the treatment of methamphetamine abuse, but will also have made available a pharmacological treatment for the addicts who wish to quit.

REFERENCES

- Alachkar, A.; Brotchie, J. M.; Jones, O. T. Locomotor response to L-DOPA in reserpine-treated rats following central inhibition of aromatic L-amino acid decarboxylase: Further evidence for non-dopaminergic actions of L-DOPA and its metabolites. *Neuroscience Research*, **2012**, 68, 44-50.
- Amara, S. G.; Sonders, M. S. Neurotransmitter Transporters as Molecular Targets for Addictive Drugs. *Drug Alcohol Dependence*, **1998**, 51, 87–96.
- Barlow, R. B.; Johnson, O. Relations between Structure and Nicotine-like Activity—X-ray Crystal-Structure Analysis of (-)-Cytisine and (-)-Lobeline Hydrochloride and a Comparison with (-)-Nicotine and other Nicotine-like Compounds. *Br. J. Pharmacol.*, **1989**, 98, 799–808.
- Barr, A.; Panenka, W.; MacEwan, G.; Thornton, A.; Lang, D.; Honer, W. The need for speed: an update on methamphetamine addiction. *Journal of Psychiatry and Neuroscience*, **2006**, 31, 301-313.
- Bates, A. T.; Chamberlain, S.; Champion, M.; Foley, L.; Hughes, E.; Jani, B.; Mehta, H.; Smith, S. E. (1995). Pholedrine: A substitute for hydroxyamphetamine as a diagnostic eyedrop test in Horner's syndrome". *Journal of neurology, neurosurgery, and psychiatry*. **1995**, 58, 215–217.
- Bevan, J. A.; Hughes, T. Inhibition of gastric contraction following stimulation of intrathoracic sensory endings. *Arch. Int. Pharmacodyn. Ther.*, **1966**, 161, 334-342.
- Birman, V. B.; Jiang, H.; Li, X. Enantioselective Synthesis of Lobeline via Nonenzymatic Desymmetrization. *Org. Lett.*, **2007**, 9, 3237–3240.
- Blickle, F. F.; Zienty, F. B. Antispasmodics (IV). *J. Am. Chem. Soc.* **1939**, 61, 774-776.
- Briggs, C. A.; McKenna, D. G.; Activation and inhibition of the human alpha 7 nicotinic acetylcholine receptor by agonists. *Neuropharmacology*, **1998**, 37, 1095-1102.
- Brioni, J. D.; Oneill, A. B.; Kim, D. J.; Decker, M. W. Nicotinic receptor agonists exhibit anxiolytic-like effects on the elevated plus-maze test. *Eur. J. Pharmacol.*, **1993**, 238, 1-8.
- Brown, J. M.; Hanson, G. R.; Fleckenstein, A. E. Regulation of the Vesicular Monoamine Transporter-2: A Novel Mechanism for Cocaine and Other Psychostimulants. *J. Pharmacol. Exp. Ther.*, **2001**, 296, 762–767.

- Brown, J. M.; Hanson, G. R.; Fleckenstein, A. E. Cocaine-Induced Increases in Vesicular Dopamine Uptake: Role of Dopamine Receptors. *J. Pharmacol. Exp. Ther.* **2001**, *298*, 1150–1153.
- Callaghan, R.; Cunningham, J.; Sykes, J.; Kish, J. Increased risk of Parkinson's disease in individuals hospitalized with conditions related to the use of methamphetamine or other amphetamine-type drugs. *Drug and Alcohol Dependence*, **2011**.
- Cashman, J.; Xiong, Y.; Xu, L.; Janowsky, A. N-oxygenation of amphetamine and methamphetamine by the human flavin-containing monooxygenase (form 3): role in bioactivation and detoxication. *J Pharmacol Exp Ther.* **1999**, *288*, 1251–1260.
- Chang, L., Cloak, C., Patterson, K., et al. Enlarged striatum in abstinent methamphetamine abusers: a possible compensatory response. *Biol Psychiatry*, **2005**, *57*, 967-974.
- Chang, L.; Alicata, D.; Earnst, T.; Bolkow, N. Structural and metabolic brain changes in the striatum associated with methamphetamine abuse. *Addiction*, **2007**, *102*, 16-32.
- Cheng, Y. and Prusoff, W. H. Relationship between the inhibition constant (K_i) and the concentration of inhibitor which causes 50 percent inhibition (I_{50}) of an enzymatic reaction. *Biochemical Pharmacology*, **1973**, *22*, 3099-3108.
- Compere, D.; Marazano, C.; Das, B. C. Enantioselective Access to Lobelia Alkaloids. *J. Org. Chem.*, **1999**, *64*, 4528–4532.
- Court, J.; Perry, E.; Spurden, D.; Lloyd, S.; Gillespie, J.; Whiting, P.; Barlow, R. Comparison of the binding of nicotinic agonists to receptors from human and rat cerebral cortex and from chick brain ($\alpha(4)\beta(2)$) transfected into mouse fibroblasts with ion-channel activity. *Brain Res.*, **1994**, *667*, 118-122.
- Crooks, P.; Zheng, G.; Vartak, A.; Culver, J.; Zheng, F.; Horton, D.; Dwoskin, L. Design, Synthesis and Interaction at the Vesicular Monoamine Transporter-2 of Lobeline Analogs: Potential Pharmacotherapies for the Treatment of Psychostimulant Abuse. *Current Topics in Medicinal Chemistry*, (Sharjah, United Arab Emirates), **2011**, *11(9)*, 1103-1127.
- Damaj, M. I.; Patrick, G. S.; Creasy, K. R.; Martin, B. R. Pharmacology of Lobeline, a Nicotinic Receptor Ligand. *J. Pharmacol. Exp. Ther.*, **1997**, *282*, 410–419.
- Daniels, A. J.; Reinhard, J. F., Jr. Energy-Driven Uptake of the Neurotoxin 1–Methyl-4-phenylpyridinium into Chromaffin Granules via the Catecholamine Transporter. *J. Biol. Chem.*, **1988**, *263*, 5034–5036.
- Darchen, F.; Scherman, D; Henry, J. P. Reserpine Binding to Bovine Chromaffin Granule Membranes. *Mol. Pharmacol.*, **1984**, *25*, 113–122.

- Darchen, F.; Scherman, D.; Henry, J. P. Characteristics of the Transport of Quaternary Ammonium 1 Methyl-4-phenylpyridinium by Chromaffin Granules. *Biochem. Pharmacol.* **1988**, *37*, 4381–4387.
- Darchen, F.; Scherman, D.; Laduron, P. M.; Henry J. P. Ketanserin Binds to the Monoamine Transporter of Chromaffin Granules and of Synaptic Vesicles. *Mol. Pharmacol.* **1988**, *33*, 672–677.
- Darchen, F.; Scherman, D.; Henry, J. P. Reserpine Binding to Chromaffin Granules Suggests the Existence of Two Conformations of the Monoamine Transporter. *Biochemistry*, **1989**, *28*, 1692–1697.
- Dasgupta, A., Langman, L. *Pharmacogenomics of Alcohol and Drugs of Abuse*. CRC Press, **2012**, 132.
- Davis, F. A.; Zhang, J.; Li, Y.; Xu, H.; DeBrosse, C. Asymmetric Synthesis of 2,4,5-Trisubstituted Piperidines from Sulfinimine-Derived D-Amino B-Ketoesters. Formal Synthesis of Pseudodistomin B Triacetate. *J. Org. Chem.*, **2005**, *70*, 5413–5419.
- Decker, M. W.; Majchrzak, M. J.; Arneric, S. P. Effects of Lobeline, a Nicotinic Receptor Agonist, on Learning and Memory. *Pharmacol., Biochem. Behav.*, **1993**, *45*, 571–576.
- Defalque R. J., Wright A. J. (April 2011). Methamphetamine for Hitler's Germany: 1937 to 1945". *Bull. Anesth. Hist.* **29** (2): 21–24, 32.
- De Jong, L. A. A.; Uges, D. R. A.; Franke, J. P.; Bischoff, R. Receptor–ligand binding assays: Technologies and Applications. *Journal of Chromatography B*, **2005**, *829* (1–2), 1–25.
- Dimatelis, J. J.; Russell, V. A.; Stein, D. J.; Daniels, W. M. The effects of lobeline and naltrexone on methamphetamine-induced place preference and striatal dopamine and serotonin levels in adolescent rats with a history of maternal separation. *Metabolic Brain Disease*, **2012**, *27*(3), 351–361.
- Disbrow, J. K.; Ruth, J. A. Greatly Extended Viability of Rat Brain Storage Vesicles in an Intracellular Medium Based Upon a Non-Permeant Polyanion. *Life Sci.* **1981**, *29*, 1989–1996.
- Drews, G. Drug Discovery: A Historical Perspective. *Science*, **2000**, *287*, 1960–1964.
- Dwoskin, L. P.; Crooks, P. A. A Novel Mechanism of Action and Potential Use for Lobeline as a Treatment for Psychostimulant Abuse. *Biochem. Pharmacol.*, **2002**, *63*, 89–98.
- Ebnöther, A. Alkaloids. IX. Mutarotation of Lobeline. Cis-Trans Isomers in the Lobelia Alkaloid Series. *Helv. Chim. Acta* **1958**, *41*, 386–396.

- Eiden, L. E.; Schäfer, M. K.; Weihe, E.; Schütz, B. The Vesicular Amine Transporter Family (SLC18): Amine/Proton Antiporters Required for Vesicular Accumulation and Regulated Exocytotic Secretion of Monoamines and Acetylcholine. *Plfuegers Arch.* **2004**, *447*, 636–640.
- Erickson, J. D.; Eiden, L. E.; Hoffman, B. J. Expression Cloning of a Reserpine-Sensitive Vesicular Monoamine Transporter. *Proc. Natl. Acad. Sci.*, **1992**, *89*, 10993–10997.
- Erickson, J. D.; Eiden, L. Functional Identification and Molecular Cloning of a Human Brain Vesicle Monoamine Transporter. *J. Neurochem.*, **1993**, *61*, 2314–2317.
- Erickson, J. D.; Schafer, M. K.; Bonner, T. I.; Eiden, L. E.; Weihe E. Distinct Pharmacological Properties and Distribution in Neurons and Endocrine Cells of Isoforms of the Human Vesicular Monoamine Transporter. *Proc. Natl. Acad. Sci.*, **1996**, *93*, 5166–5171.
- Eyerman, D. J.; Yamamoto, B. K. Lobeline Attenuates Methamphetamine-Induced Changes in Vesicular Monoamine Transporter 2 Immunoreactivity and Monoamine Depletions in the Striatum. *J. Pharmacol. Exp. Ther.*, **2005**, *312*, 160–169.
- Fel'pin, F. X.; Lebreton, J. A Highly Stereoselective Asymmetric Synthesis of (-)-Lobeline and (-)-Sedamine. *J. Org. Chem.*, **2002**, *67*, 9192–9199.
- Fel'pin, F. X.; Lebreton, J. History, Chemistry and Biology of Alkaloids from *Lobelia inflata*. *Tetrahedron*, **2004**, *60*, 10127–10153.
- Flammia, D.; Dukat, M.; Damaj, M. I.; Martin, B.; Glennon, R. A. Lobeline: Structure-Affinity Investigation of Nicotinic Acetylcholinergic Receptor Binding. *J. Med. Chem.*, **1999**, *42*, 3726–3731.
- Fleckenstein, A. E.; Brown, J. M.; Sandoval, V.; Riddle, E. L.; Hansen, J. P.; Ugarte, Y. V.; Gibb, J. W.; Hanson, G. R. D2 Receptor-Mediated Regulation of Vesicular Dopamine Uptake. *Advances in Behavioral Biology*, **2002**, *53*, 39–42.
- Fleckenstein, A. E.; Hanson, G. R. Impact of Psychostimulants on Vesicular Monoamine Transporter Function. *Eur. J. Pharmacol.*, **2003**, *479*, 283–289.
- Fleckenstein, A. E.; Volz, T. J.; Riddle E. L.; Gibb, J. W.; Hanson, G. R. New Insights into the Mechanism of Action of Amphetamines. *Annual Review of Pharmacology and Toxicology*, **2007**, *47*, 681–698.
- Fudala, P. J.; Iwamoto, E. T. Further studies on nicotine-induced conditioned place preference in the rat. *Pharmacol. Biochem Behav.*, **1986**, *25*, 1041–1049.
- Gasnier, B.; Krejci, E.; Botton, D.; Massoulié, J.; Henry, J. P. Expression of a Bovine Vesicular Monoamine Transporter in COS Cells. *FEBS Lett.* **1994**, *342*, 225–229.

- Gasnier, B. The Loading of Neurotransmitters into Synaptic Vesicles. *Biochimie*, **2000**, 82, 327–337.
- German, D. C.; Sonsalla, P. K. A Role for the Vesicular Monoamine Transporter (VMAT2) in Parkinson's Disease. *Advances in Behavioral Biology*, **2003**, 54, 131–137.
- Gopalakrishnan, A.; Sievert, M.; Ruoho, A. E. Identification of the Substrate Binding Region of Vesicular Monoamine Transporter-2 (VMAT-2) Using Iodoaminoflisopolol as a Novel Photoprobe. *Mol. Pharmacol.* **2007**, 72, 1567–1575.
- Gros, Y.; Schuldiner, S. Directed Evolution Reveals Hidden Properties of VMAT, a Neurotransmitter Transporter. *J. Biol. Chem.*, **2010**, 285, 5076–5084.
- Grobler, Sias R.; Chikte, Usuf; Westraat, Jaco (2011). "The pH Levels of Different Methamphetamine Drug Samples on the Street Market in Cape Town". *ISRN Dentistry* **2011**
- Hamann, S. R.; Martin, W. R. Hyperalgesic and Analgesic Actions of Morphine, U50-488, Naltrexone, and (-)-Lobeline in the Rat Brainstem. *Pharmacol. Biochem. Behav.*, **1994**, 47, 197–201.
- Hansen, J. P.; Riddle, E. L.; Sandoval, V.; Brown, J. M.; Gibb, J. W.; Hanson, G. R.; Fleckenstein, A. E. Methylenedioxymethamphetamine Decreases Plasmalemmal and Vesicular Dopamine Transport: Mechanisms and Implications for Neurotoxicity. *J. Pharmacol. Exp. Ther.* **2002**, 300, 1093–1100.
- Hansson, S. R.; Mezey, E; Hoffman, B. J. Ontogeny of Vesicular Monoamine Transporter mRNAs VMAT1 and VMAT2, II. Expression in Neural Crest Derivatives and Their Target Sites in the Rat. *Dev. Brain Res.*, **1998**, 110, 159–174.
- Harrod, S. B.; Phillips, S. B.; Green, T. A.; Crooks, P. A.; Dwoskin, L. P.; Bardo M. T. α -Lobeline attenuates methamphetamine self-administration, but does not serve as a reinforcer in rats. *Soc. Neurosci. Abstr.*, **2000**, 26, 789.
- Harrod, S. B.; Dwoskin, L. P.; Crooks, P. A.; Klebaur, J. E.; Bardo, M. T. Lobeline Attenuates D-Methamphetamine Self-Administration in Rats. *J. Pharmacol. Exp. Ther.*, **2001**, 298, 172–179.
- Harrod, S. B.; Dwoskin, L. P.; Green, T. A.; Gehrke, B. J.; Bardo, M. T. Lobeline Does Not Serve as a Reinforcer in Rats. *Psychopharmacol.*, Berlin, Germany, **2003**, 165, 397–404.
- Hart, N.; Rocha, A.; Miller D. K.; Nation, J. R. Dose-dependent attenuation of heroin self-administration with lobeline. *Psychopharmacol.*, London, United Kingdom, **2010**, 24(1), 51-55.

Henry, J. P.; Botton, D.; Sagne, C.; Isambert, M. F.; Desnos, C.; Blanchard, V.; Raisman-Vozari, R.; Krejci, E.; Massoulie, J.; Gassnier, B. Biochemistry and Molecular Biology of the Vesicular Monoamine Transporter from Chromaffin Granules. *J. Exp. Biol.* **1994**, *196*, 251–262.

Henry, J. P.; Sagne, C.; Bedet, C.; Gasnier, B. The Vesicular Monoamine Transporter: From Chromaffin Granule to Brain. *Neurochem. Int.* **1998**, *32*, 227-246.

Henry, J. P.; Sagné, C.; Botton, D.; Isambert, M. F.; Gasnier, B. Molecular Pharmacology of the Vesicular Monoamine Transporter. *Advances in Pharmacology*, **1998**, *42*, 236–239.

Hillmer, A. T.; Wooten, D. W.; Farhoud, M.; Barhart, T. E.; Mukherjee, J.; Christian B. T. The effects of lobeline on $\alpha 4\beta 2^*$ nicotinic acetylcholine receptor binding and uptake of [¹⁸F]nifene in rats. *Journal of Neuroscience Methods*, **2013**, *214*, 163-169.

Hoffman, K.; Stoffel, W. A. Database of Membrane Spanning Protein Segments. *Biological Chemistry Hoppe-Seyler*, **1993**, *374*, 166.

Hojahmat, M.; Horton, D. B.; Norrholm, S. D.; Miller, D. K.; Grinevich, V. P.; Deaciuc, A. G.; Dwoskin, L. P.; Crooks, P. A. Lobeline Esters as Novel Ligands for Neuronal Nicotinic Acetylcholine Receptors and Neurotransmitter Transporters. *Bioorg. Med. Chem. Lett.*, **2010**, *18*, 640–649.

Horton, D. B.; Siripurapu, K. B.; Norrholm, S. D.; Culver, J. P.; Hojamat, M.; Beckman, J. S.; Harrod S. B.; Deaciuc, A. G.; Bardo, M. T.; Crooks, P. A.; Dwoskin, L. P. *meso*-Transdiene analogs inhibit vesicular monoamine transporter-2 function and methamphetamine-evoked dopamine release. *JPET*, **2011**, *336*(3), 940-951.

Horton, D. B.; Siripurapu, K. B.; Zheng, G.; Crooks P. A.; Dwoskin, L. P. Novel N-1, 2-dihydroxypropyl analogs of lobelane inhibit vesicular monoamine transporter-2 function and methamphetamine-evoked dopamine release. *JPET*, **2011**, *339*(1), 286-297.

Howell, M.; Shirvan, A.; Stern-Bach, Y.; Steiner-Mordoch, S.; Strasser, J.E.; Dean, G.E.; Schuldiner, S. Cloning and Functional Expression of a Tetrabenazine-Sensitive Vesicular Monoamine Transporter from Bovine Chromaffin Granules. *FEBS Lett.*, **1994**, *338*, 16–22.

“*in vitro*” Merriam-Webster.com. Merriam-Webster, **2013**, Web. 12 February 2014.

“*in vivo*” Merriam-Webster.com. Merriam-Webster, **2013**, Web. 12 February 2014.

Iyo M, Namba H, Yanagisawa M, et al. Abnormal cerebral perfusion in chronic methamphetamine abusers: a study using ^{99m}Tc-HMPAO and SPECT. *Prog Neuropsychopharmacol Biol Psychiatry.*, **1997**, *21*, 789-96.

- Iyo, M.; Sekine, Y.; Mori, N. Neuromechanism of developing methamphetamine psychosis: a neuroimaging study. *Ann. N. Y. Acad. Sci.*, **2004**, *1025*, 288-295.
- Kaniakova, M.; Lindovsky, J.; Krusek, J.; Adamek, S.; Vuskocil, F. Dual effect of lobeline on $\alpha 4\beta 2$ rat neuronal nicotinic receptors. *European Journal of Pharmacology*, **2011**, *658*, 108-113.
- Johnson, R. G. Accumulation of Biological Amines into Chromaffin Granules: A Model for Hormone and Neurotransmitter Transport. *Physiol. Rev.*, **1988**, *68*, 232–307.
- Katritzky, A. R.; Cui, X. L.; Yang, B.; Steel, P. J. Asymmetric Syntheses of 2-Substituted and 2,5-Disubstituted Pyrrolidines from (3s,5r,7ar)-5-(Benzotriazol-1-Yl)-3-phenyl[2,1-B]oxazolopyrrolidine. *J. Org. Chem.*, **1999**, *64*, 1979–1985.
- Kirschner, N. Uptake of Catecholamines by a Particulate Fraction of the Adrenal Medulla. *J. Biol. Chem.* **1962**, *237*, 2311–2317.
- Klingler, F.-D.; Sobotta, R. (Boehringer Ingelheim Pharma GmbH & Co. KG, Germany, US Patent, **2006**, p. 4.
- Knoth, J.; Isaacs, J. M.; Njus, D. Amine Transport in Chromaffin Granule Ghosts. pH Dependence Implies Cationic Form is Translocated. *J. Biol. Chem.* **1981**, *256*, 6541–6543.
- Knoth, J.; Zallakian, M.; Njus, D. Stoichiometry of H⁺-Linked Dopamine Transport in Chromaffin Granule Ghosts. *Biochemistry*, **1981**, *20*, 6625–6629.
- Koob, G. F. Ann. Neural Mechanisms of Drug Reinforcement. *N Y Acad. Sci.*, **1992**, *654*, 171–191.
- Korczyn, A. D.; Bruderma. I.; Braun, K. Cardiovascular Effects of Lobeline. *Archives Internationales de Pharmacodynamie et de Thérapie* **1969**, *182*, 370–375.
- Krejci, E.; Gasnier, B., Botton, D.; Isambert, M. F.; Sagné, C.; Gagnon, J.; Massoulié, J.; Henry, J. P. Expression and Regulation of the Bovine Vesicular Monoamine Transporter Gene. *FEBS Lett.* **1993**, *335*, 27–32.
- Krueger, S.; Williams, D. Mammalian flavin-containing monooxygenases: structure/function, genetic polymorphisms and role in drug metabolism. *Pharmacol Ther.* **2005**, *106*: 357–387.
- Li, C.; Ji, X.; Hui, G.; Zhang, J.; Zhou, W.; Wei, B.; Xingyao, G. L. Effects of lobeline on dopamine uptake by plasma membrane dopamine transporter. *Zhonghua Shenjing Waike Jibing Yanjiu Zazhi*, **2007**, *6(3)*, 247-249.

- Liu, Y.; Edwards, R. H. The Role of Vesicular Transport Proteins in Synaptic Transmission and Neural Degeneration. *Annual Review of Neuroscience*, **1997**, *20*, 125–156.
- Lohoff, F. W.; Dahl, J. P.; Ferraro, T. N.; Arnold, S. E.; Gallinat, J.; Sander, T.; Berrettini, W. H. Variations in the Vesicular Monoamine Transporter 1 Gene (VMAT1/SLC18A1) are Associated with Bipolar 1 Disorder. *Neuropsychopharmacology*, **2006**, *31*, 2739–2747.
- Lotharius, J.; O'Malley, K. L. The Parkinsonism-Inducing Drug 1 Methyl-4-phenylpyridinium Triggers Intracellular Dopamine Oxidation. A Novel Mechanism of Toxicity. *J. Biol. Chem.* **2000**, *275*, 38581–38588.
- McCann U. D.; Wong D. F.; Yokoi, F. et al. Reduced striatal dopaminetransporter density in abstinent methamphetamine and methcathinone users: evidence from positron emission tomography studies with [11C]WIN-35,428. *J. Neurosci.*, **1998**, *18*, 8417-8422.
- McCurdy, C. R.; Miller, R. L.; Beach, J. W. Lobeline: A Natural Product with High Affinity for Neuronal Nicotinic Receptors and a Vast Potential for Use in Neurological Disorders. *Biolog. Active Nat. Prod.*, **2000**, 151–162.
- McIntosh A. Carotid artery dissection and middle cerebral artery stroke following methamphetamine use. *Neurology*, **2006**, *67*; 2259-60.
- Merickel, A.; Rosandich, P.; Peter, D.; Edwards, R. H. Identification of Residues Involved in Substrate Recognition by a Vesicular Monoamine Transporter. *J. Biol. Chem.*, **1995**, *270*, 25798–25804.
- Meyer, A. C.; Neugebauer, N. M.; Zheng, G.; Crooks, P. A.; Dwoskin, L. P.; Bardo, M. T. Effects of VMAT2 inhibitors lobeline and GZ-793A on methamphetamine-induced dopamine release, metabolism and synthesis in vivo. *Journal of Neurochemistry*, **2013**, *127* (1&2), 187-198.
- Merickel, A.; Kaback, H. R.; Edwards, R. H. Charged Residues in Transmembrane Domains II and XI of a Vesicular Monoamine Transporter Form a Charge Pair That Promotes High Affinity Substrate Recognition. *J. Biol. Chem.*, **1997**, *272*, 5403–5408.
- Miller, D. K.; Crooks, P. A.; Dwoskin, L. P. Lobeline Inhibits Nicotine-Evoked [³H]Dopamine Overflow from Rat Striatal Slices and Nicotine-Evoked 86Rb (+) Efflux from Thalamic Synaptosomes. *Neuropharmacology*, **2000**, *39*, 2654–2662.
- Miller, D. K.; Crooks, P. A.; Teng, L. H.; Witkin, J. M.; Munzar, P.; Goldberg, S. R.; Aciri, J. B.; Dwoskin, L. P. Lobeline Inhibits the Neurochemical and Behavioral Effects of Amphetamine. *J. Pharmacol. Exper. Ther.*, **2001**, *296*, 1023–1034.

- Miller, D. K.; Harrod, S. B.; Green, T. A.; Wong, M. Y.; Bardo, M. T.; Dwoskin, L. P. Lobeline Attenuates Locomotor Stimulation Induced by Repeated Nicotine Administration in Rats. *Pharmacol., Biochem. Behav.*, **2003**, *74*, 279–286.
- Miller, D. K.; Crooks, P. A.; Zheng, G.; Grinevich, V. P.; Norrholm, S. D.; Dwoskin, L. P. Lobeline Analogs with Enhanced Affinity and Selectivity for Plasmalemma and Vesicular Monoamine Transporters. *J. Pharmacol. Exp. Ther.* **2004**, *310*, 1035–1045.
- Miller, D. K.; Lever, J. R.; Rodvelt, K. R.; Baskett, J. A.; Will, M. J.; Kracke, G. R. Lobeline, a Potential Pharmacotherapy for Drug Addiction, Binds to Mu Opioid Receptors and Diminishes the Effects of Opioid Receptor Agonists. *Drug and Alcohol Dependence* **2007**, *89*, 282–291.
- Miller, D. K.; Polston, J. E.; Rodvelt, K. R.; Will, M. J. Lobeline attenuates the locomotor-activating properties of repeated morphine treatment in rats. *Tropical Journal of Pharmaceutical Research*, **2011**, *10(4)*, 421-429.
- Millsbaugh, C. F. *Lobelia Inflata in: American Medicinal Plants: An Illustrated and Descriptive Guide to Plants Indigenous to and Naturalized in the United States Which Are Used in Medicine*; Dover: New York, **1974**; pp. 385–388.
- National Institute on Drug Abuse. Drugs of Abuse and Related Topics: *Methamphetamine*. NIH Publication Number 13-4210. Available at: <http://www.drugabuse.gov/DrugPages/Methamphetamine.html>.
- Neugebauer, N. M.; Harrod, S. B.; Stairs, D. J.; Crooks, P. A.; Dwoskin, L. P.; Bardo, M. T. Lobelane Decreases Methamphetamine Self-Administration in Rats. *Eur. J. Pharmacol.*, **2007**, *571*, 33–38.
- Nickell, J. R.; Krisnamurthy, S.; Norrholm, S.; Deaciuc, G.; Siripurapu, K. B.; Zheng, G.; Crooks, P. A.; Dwoskin, L. P. Lobelane inhibits methamphetamine-evoked dopamine release via inhibition of the vesicular monoamine transporter-2. *JPET*, **2010**, *332(2)*, 612-621.
- Nickell, J. R.; Zheng, G.; Deaciuc, A. G.; Crooks, P. A.; Dwoskin, L. P. Phenyl ring substituted lobelane analogs: inhibition of [³H]dopamine uptake at the vesicular monoamine transporter-2. *JPET*, **2011**, *336(3)*, 724-733.
- Njus, D.; Kelley, P. M.; Harnadek, G. J. Bioenergetics of Secretory Vesicles. *Biochim. Biophys. Acta* **1986**, *853*, 237–265.
- Parsons, S. M. Transport Mechanisms in Acetylcholine and Monoamine Storage. *FASEB J.* **2000**, *14*, 2423–2434.
- Partilla, J. S.; Dempsey, A. G.; Nagpal, A. S.; Blough, B. E.; Baumann, M. H.; Rothman, R. B. Interaction of Amphetamines and Related Compounds at the Vesicular Monoamine Transporter. *J. Pharmacol. Exp. Ther.* **2006**, *319*, 237–246.

- Peter, D.; Jimenez, J.; Liu, Y.; Kim, J.; Edwards, R. H. The Chromaffin Granule and Synaptic Vesicle Amine Transporters Differ in Substrate Recognition and Sensitivity to Inhibitors. *J. Biol. Chem.*, **1994**, *269*, 7231–7237.
- Peter, D.; Liu Y.; Sternini, C.; de Giorgio, R.; Brecha, N.; Edwards, R. H. Differential Expression of Two Vesicular Monoamine Transporters. *J. Neurosci.*, **1995**, *15*, 6179–6188.
- Peter, D.; Vu, T.; Edwards, R. H. Chimeric Vesicular Monoamine Transporters Identify Structural Domains That Influence Substrate Affinity and Sensitivity to Tetrabenazine. *J. Biol. Chem.*, **1996**, *271*, 2979–2986.
- Pletscher, A. Effect of Neuroleptics and Other Drugs on Monoamine Uptake by Membranes of Adrenal Chromaffin Granules. *Br. J. Pharmacol.*, **1977**, *59*, 419–424.
- Polston, J. E.; Cunningham, C. S.; Rodvelt, K. R.; Miller, D. K. Lobeline Augments and Inhibits Cocaine-Induced Hyperactivity in Rats. *Life Sci.*, **2006**, *79*, 981–990.
- Pothos, E. N.; Larsen, K. E.; Krantz, D. E.; Liu, Y.; Haycock, J. W.; Setlik, W.; Gershon, M. D.; Edwards, R. H.; Sulzer, D. Synaptic Vesicle Transporter Expression Regulates Vesicle Phenotype and Quantal Size. *J. Neurosci.* **2000**, *20*, 7297–7306.
- Quinn, G. P.; Shore, P. A.; Brodie, B. B. Biochemical and Pharmacological Studies of RO 1-9569 (Tetrabenazine), a Nonindole Tranquilizing Agent with Reserpine-Like Effects. *J. Pharmacol. Exp. Ther.* **1959**, *127*, 103–109.
- Rasmussen, T.; Swedberg, M. D. B. Reinforcing Effects of Nicotinic Compounds: Intravenous Self-Administration in Drug-Naïve Mice. *Pharmacol., Biochem. Behav.*, **1998**, *60*, 567–573.
- Riddle, E. L.; Topham, M. K.; Haycock, J. W.; Hanson, G. R.; Fleckenstein, A. E. Differential Trafficking of the Vesicular Monoamine Transporter-2 by Methamphetamine and Cocaine. *Eur. J. Pharmacol.* **2002**, *449*, 71–74.
- Riddle, E. L.; Fleckenstein, A. E.; Hanson, G. R. Role of Monoamine Transporters in Mediating Psychostimulant Effects. *American Association of Pharmaceutical Scientists Journal*, **2005**, *7*, E847-E851.
- Rudnick, G. Bioenergetics of Neurotransmitter Transport. *Journal of Bioenergetics and Biomembranes*, **1998**, *30*, 173–185.
- Sandoval, V.; Riddle, E. L.; Hanson, G. R.; Fleckenstein, A. E. Methylphenidate Alters Vesicular Monoamine Transport and Prevents Methamphetamine-Induced Dopaminergic Deficits. *J. Pharmacol. Exp. Ther.* **2003**, *304*, 1181-1187.
- Scherman, D.; Jaudon, P.; Henry, J. P. Characterization of the Monoamine Carrier of Chromaffin Granule Membrane by Binding of [2-3H]Dihydrotetrabenazine. *Proc. Natl. Acad. Sci. USA*, **1983**, *80*, 584–588.

Scherman, D.; Raisman, R.; Ploska, A.; Agid, Y. [³H]Dihydrotrabenzazine, a New In Vitro Monoaminergic Probe for Human Brain. *J. Neurochem.* **1988**, *50*, 1131–1136.

Scherman, D.; Henry, J. P. Radioligands of the Vesicular Monoamine Transporter and Their Use as Markers of Monoamine Storage Vesicles. *Biochem. Pharmacol.*, **1989**, *38*, 2395–2404.

Scheuing, G.; Winterhalder, L. Synthesis of Lobelia Alkaloids. *Justus Liebigs Annalen der Chemie* **1929**, *473*, 126–136.

Schoepf, C.; Mueller, E. Absolute Configuration of (-)-Lobeline and of Its Reduction Products. *Liebigs Ann. Chem.*, **1965**, *687*, 241–250.

Schopf, C.; Lehmann, G. Syntheses and Transformations of Natural Products Under Physiological Conditions (Model Experiments on the Question of the Biogenesis of Natural Products). Iv. Syntheses of Tropinone, Pseudopelletierine, Lobelanine, and Related Alkaloids Under Physiological Conditions. *Liebigs Annalen der Chemie* **1935**, *518*, 1–37.

Schuldiner, S.; Steiner-Mordoch, S.; Yelin, R.; Wall, S. C.; Rudnick, C. Amphetamine Derivatives Interact with Both Plasma Membrane and Secretory Vesicle Biogenic Amine Transporters. *Mol. Pharmacol.* **1993**, *44*, 1227–1231.

Schuldiner, S. A. A Molecular Glimpse of Vesicular Monoamine Transporters. *J. Neurochem.* **1994**, *62*, 2067–2078

Schuldiner, S.; Shirvan, A.; Linial, M. Vesicular Neurotransmitter Transporters: From Bacteria to Humans. *Physiology Review*, **1996**, *75*, 369–392.

Sekine, Y.; Iyo, M.; Ouchi, Y. et al. Methamphetamine-related psychiatric symptoms and reduced brain dopamine transporters studied with PET. *Am. J. Psychiatry*, **2001**, *158*, 1206–1214.

Shoptaw SJ, Kao U, Heinzerling K, Ling W. "Treatment for amphetamine withdrawal". In Shoptaw SJ. *Cochrane Database Syst. Rev.* (2), **2009**.

Sievert, M. K.; Ruoho, A. E. Peptide Mapping of the [125I]Iodoazidoketanserin and [125I]2-N-[(3'-iodo-4'-azidophenyl)Propionyl]trabenzazine Binding Sites for the Synaptic Vesicle Monoamine Transporter. *J. Biol. Chem.*, **1997**, *272*, 26049–26055.

Slotkin, T. A.; Seidler, F. J.; Whitmore, W. L.; Lau, C.; Salvaggio, M.; Kirksey, D. F. Rat Brain Synaptic Vesicles: Uptake Specificities of [³H]Norepinephrine and [³H]Serotonin in Preparations from Whole Brain and Brain Regions. *J. Neurochem.* **1978**, *31*, 961–968.

- Smith, A. M.; Wellmann, K. A.; Lundblad, T. M.; Carter, M. L.; Barron, S.; Dwoskin, L. P. Lobeline attenuates neonatal ethanol-mediated changes in hyperactivity and dopamine transporter function in the prefrontal cortex in rats. *Neuroscience (Amsterdam, Netherlands)*, **2012**, *206*, 245-254.
- Sneader, W. *Drug Discovery* (Wiley, New York, 1985).
- Stern-Bach, Y.; Keen, J. N.; Bejerano, M.; Steiner-Mordoch, S.; Wallach, M.; Findlay, J. B.; Schuldiner, S. Homology of a Vesicular Amine Transporter to a Gene Conferring Resistance to 1-Methyl-4-phenylpyridium. *Proc. Natl. Acad. Sci. USA*, **1992**, *89*, 9730–9733.
- Stolerman, I. P.; Garcha, H. S., Mirza N. R. Dissociations between the locomotor stimulant and depressant effects of nicotinic agonists in rats. *Psychopharmacology*, **1995**, *117*, 430-437.
- Stuhmer, W.; Elbrachter, E. N-Substituierte bis(3,3'-phenylpropyl)amine. *Arch. Pharmacol.* **1954**, *287*, 139-142.
- Sulzer, D.; Rayport, S. Amphetamine and other Psychostimulants Reduce pH Gradients in Midbrain Dopaminergic Neurons and Chromaffin Granules: A Mechanism of Action. *Neuron*, **1990**, *5*, 797–808.
- Sulzer, D.; Maidment, N. T.; Rayport, S. Amphetamine and Other Weak Bases Act to Promote Reverse Transport of Dopamine in Ventral Midbrain Neurons. *J. Neurochem.*, **1993**, *60*, 527–535.
- Sulzer, D.; Chem, T. K.; Lau, Y. Y.; Kristensen, H.; Rayport, S.; Ewing, A. Amphetamine Redistributes Dopamine from Synaptic Vesicles to the Cytosol and Promotes Reverse Transport. *J. Neurosci.*, **1995**, *15*, 4102–4108.
- Sulzer, D.; Pothos, E. N. Regulation of Quantal Size by Presynaptic Mechanisms. *Reviews in the Neurosciences*, **2000**, *11*, 159–212.
- Sulzer, D.; Sonders M.; Poulsen N.; Galli A. Mechanisms of neurotransmitter release by amphetamines: a review. *Prog Neurobiol.* **2005**, *75*: 406-433.
- Takahashi, N.; Miner, L. L.; Sora, I.; Ujike, H.; Revay, R.S.; Kostic, V.; Jackson-Lewis, V.; Przedborski, S.; Uhl, G.R. VMAT2 Knockout Mice: Heterozygotes Display Reduced Amphetamine-Conditioned Reward, Enhanced Amphetamine Locomotion and Enhanced MPTP Toxicity. *Proc. Natl. Acad. Sci. USA*, **1997**, *94*, 9938–9943.
- Tatsuta, T.; Kitanaka, N.; Kitanaka, J.; Morita, Y.; Takemura, M. Lobeline Attenuates Methamphetamine-Induced Stereotypy in Adolescent Mice. *Neurochem. Res.*, **2006**, *31*, 1359–1369.

- Teng, L. H.; Crooks, P. A.; Sonsalla, P. K.; Dwoskin, L. P. Lobeline and Nicotine Evoke [³H]Overflow from Rat Striatal Slices Preloaded with [³H]Dopamine: Differential Inhibition of Synaptosomal and Vesicular [³H]Dopamine Uptake. *J. Pharmacol. Exp. Ther.*, **1997**, *280*, 1432–1444.
- Teng, L.; Crooks, P. A.; Dwoskin, L. P. Lobeline Displaces [³H]Dihydrotetrabenazine Binding and Releases [³H]Dopamine from Rat Striatal Synaptic Vesicles: Comparison with D-Amphetamine. *J. Neurochem.*, **1998**, *71*, 258–265.
- Thiriot, D. S.; Ruoho, A. E. Mutagenesis and Derivatization of Human Vesicle Monoamine Transport 2 (VMAT2) Cysteines Identifies Transporter Domains Involved in Tetrabenazine Binding and Substrate Transport. *J. Biol. Chem.*, **2001**, *276*, 27304–27315.
- Thiriot, D. S.; Sievert, M. K.; Ruoho, A. E. Identification of Human Vesicle Monoamine Transporter (VMAT2) Lumenal Cysteines That Form an Intramolecular Disulfide Bond. *Biochemistry*, **2002**, *41*, 6346–6353.
- Tong, J.; Wilson, A. A.; Boileau, I.; Houle, S.; Kish, S. J. Dopamine Modulating Drugs Influence Striatal (+)-[¹C]DTBZ Binding in Rats: VMAT2 Binding is Sensitive to Changes in Vesicular Dopamine Concentration. *Synapse*, **2008**, *62*, 873–876.
- Torres, G.; Gainetdinov, R.; Caron, M. Plasma membrane monoamine transporters: structure, regulation and function. *Nat. Rev. Neurosci.*, **2003**, *4* (1): 13–25.
- Ugarte, Y. V.; Rau, K. S.; Riddle, E. L.; Hanson, G. R.; Fleckenstein, A. E. Methamphetamine Rapidly Decreases Mouse Vesicular Dopamine Uptake: Role of Hyperthermia and Dopamine D2 Receptors. *Eur. J. Pharmacol.* **2003**, *472*, 165–171.
- Vardy, E.; Arkin, I. T.; Gottschalk, K. E.; Kaback, H. R.; Schuldiner, S. Structural Conservation in the Major Facilitator Superfamily as Revealed by Comparative Modeling. *Protein Sci.*, **2004**, *13*, 1982–1840.
- Varkat, A. P.; Nickell, J. R.; Chagkutip, J.; Dwoskin, L. P.; Crooks, P. A. Pyrrolidine Analogs of Lobeline: Relationship of Affinity for the Dihydrotetrabenazine-Binding Site with Function of the Vesicular Monoamine Transporter (VMAT2). *J. Med. Chem.*, **2009**, *52*, 7878–7882.
- Varkat, A.P.; Deaciuc, A.G.; Dwoskin, L.P.; Crooks, P.A. Quintobelane: A Water-Soluble lobelane Analogue and Inhibitor of VMAT2. *Bioorg. Med. Chem. Lett.*, **2010**, *20*, 3584–3587.
- Vazquez, E.; Galindo, A.; Gnecco, D.; Bernes, S.; Teran, J. L.; Enriquez, R. G. Unexpected Retro-Michael Reaction of (-)-(1's,4as,8ar)- and (+)-(1's,4ar,8as)-4a-ethyl-1-(1-phenylethyl)octahydroquinolin-7-ones. *Tetrahedron: Asymmetry* **2001**, *12*, 3209-3211.

Vermont Department of Health. "Historical overview of methamphetamine". Retrieved January 2013.

Volkow, N. D.; Chang, L.; Wang G. J. et al. Loss of dopamine transporters in methamphetamine abusers recovers with protracted abstinence. *J. Neurosci.* **2001**, *21*, 9414-9418.

Volkow N. D.; Chang, L.; Wang G. J. et al. Association of dopamine transporter reduction with psychomotor impairment in methamphetamine abusers. *Am. J. Psychiatry*, **2001**, *158*, 377-382.

Volkow N. D.; Chang, L.; Wang G. J. et al. Low level of brain dopamine D2 receptors in methamphetamine abusers: association with metabolism in the orbitofrontal cortex. *Am. J. Psychiatry*, **2001**, *158*, 2015-2021.

Volz, T. J.; Hanson, G. R.; Fleckenstein, A. E. The Role of the Plasmalemmal Dopamine and Vesicular Monoamine Transporters in Methamphetamine-Induced Dopaminergic Deficits. *J. Neurochem.* **2007**, *101*, 883–888.

Wang, Y. M.; Gainetdinov, R. R.; Fumagalli, F.; Xu, F.; Jones, S. R.; Bock, C. B.; Miller, G. W.; Wightman, R. M.; Caron, M. G. Knockout of the Vesicular Monoamine Transporter 2 Gene Results in Neonatal Death and Supersensitivity to Cocaine and Amphetamine. *Neuron*, **1997**, *19*, 1285–1296.

Weihe, E.; Schafer M. K.; Erickson J. D.; Eiden L. E. et al. Localization of Vesicular Monoamine Transporter Isoforms (VMAT1 and VMAT2) to Endocrine Cells and Neurons in Rat. *J. Mol. Neurosci.*, **1994**, *5*, 149–164.

Wieland, H. Alkaloids of the Lobelia Plant. I. (Preliminary Communication.). *Berichte der Deutschen Chemischen Gesellschaft*, **1921**, *54B*, 1784–1788.

Wieland, H.; Dragendorff, O. Lobelia alkaloids. Iii. Constitution of the Lobelia Alkaloids. *Liebigs Annalen der Chemie* **1929**, *473*, 83–101.

Wieland, H.; Schopf, C.; Hermsen, W. Lobelia Alkaloids. Ii. *Liebigs Annalen der Chemie* **1925**, *444*, 40–68.

Wieland, H.; Drishaus, I. Lobelia Alkaloids. Iv. Synthesis of Lobelia Alkaloids. *Liebigs Annalen der Chemie* **1929**, *473*, 102–118.

Wieland, H.; Koschara, W.; Dane, E. Lobelia alkaloids. V. Several Bases Accompanying Lobeline and the Reciprocal Relations of the Lobelia Alkaloids. *Liebigs Annalen der Chemie* **1929**, *473*, 118–126.

Wilhelm, C. J.; Johnson, R. A.; Lysko, P. G.; Eshleman, A. J.; Janowsky, A. Effects of Methamphetamine and Lobeline on Vesicular Monoamine and Dopamine Transporter-Mediated Dopamine Release in a Cotransfected Model System. *J. Pharmacol. Exp. Ther.*, **2004**, *310*, 1142–1151.

- Wilhelm, C. J.; Johnson, R. A.; Eshleman, A. J.; Janowsky, A. Hydrogen Ion Concentration Differentiates Effects of Methamphetamine and Dopamine on Transporter-Mediated Efflux. *J. Neurochem.*, **2006**, *96*, 1149–1159.
- Wilhelm, C. J.; Johnson, R. A.; Eshleman, A. J.; Janowsky, A. Lobeline Effects on Tonic and Methamphetamine-Induced Dopamine Release. *Biochem. Pharmacol.*, **2008**, *75*, 1411–1415.
- Wilson, J. M.; Kalasinsky, K. S.; Levey, A. I. et al. Striatal dopamine nerve terminal markers in human, chronic methamphetamine users. *Nat. Med.* **1996**, *2*, 699–703.
- Wimalasena, D. S.; Wimalasena, K. Kinetic Evidence for Channeling of Dopamine Between Monoamine Transporter and Membranous Dopamine-Beta-Monooxygenase in Chromaffin Granule Ghosts. *J. Biol. Chem.* **2004**, *279*, 15298–15304.
- Wimalasena, D. S.; Perera, R. P.; Heyen, B. J.; Balasooriya, I. S.; Wimalasena, K. Vesicular Monoamine Transporter Substrate/Inhibitor Activity of MPTP/MPP+ Derivatives: A Structure-Activity Study. *J. Med. Chem.* **2008**, *51*, 760–768.
- Wimalasena, K. Vesicular Monoamine Transporters: Structure-Function, Pharmacology, and Medicinal Chemistry. *Medical Research Review*, **2011**, *31*, 483–519.
- Wise, R. A.; Bozarth, M. A. A Psychostimulant Theory of Addiction. *Psychol. Rev.*, **1987**, *94*, 469–492.
- Yamada, H.; Baba, T.; Hirata, Y.; Oguri, K.; Yoshimura, H. Studies on the N-demethylation of methamphetamine by liver microsomes of guinea pigs and rats: the role of flavin-containing monooxygenase and cytochrome P-450 systems. *Xenobiotica*. **1984**; *14*:861–866.
- Yelin, R.; Schuldiner, S. Vesicular Neurotransmitter Transporters: Pharmacology, Biochemistry, and Molecular Analysis. In *Neurotransmitter Transporters: Structure, Function, and Regulation*. 2nd Ed.; Reith, M., Ed.; Humana Press: Totowa, NJ, 2002; pp 313–354.
- Zheng, G.; Dwoskin, L. P.; Crooks, P. A. Indirect Trapping of the Retroconjugate Addition Reaction Intermediate Involved in the Epimerization of Lobeline: Application to the Synthesis of (-)-Sedamine. *J. Org. Chem.*, **2004**, *69*, 8514–8517.
- Zheng, G.; Dwoskin, L. P.; Deaciuc, A. G.; Crooks, P. A. Synthesis and Evaluation of a Series of Tropane Analogues as Novel Vesicular Monoamine Transporter-2 Ligands. *Bioorg. Med. Chem. Lett.*, **2005**, *15*, 4463–4466.
- Zheng, G.; Dwoskin, L. P.; Deaciuc, A. G.; Norrholm, S. D.; Crooks, P. A. Defunctionalized Lobeline Analogues: Structure-Activity of Novel Ligands for the Vesicular Monoamine Transporter. *J. Med. Chem.*, **2005**, *48*, 5551–5560.

Zheng, G.; Dwoskin, L. P.; Deaciuc, A. G.; Zhu, J.; Jones, M. D.; Crooks, P. A. Lobelane Analogues as Novel Ligands for the Vesicular Monoamine Transporter-2. *Bioorg. Med. Chem.*, **2005**, *13*, 3899–3909.

Zheng, G.; Dwoskin, L. P.; Crooks, P. A. Vesicular Monoamine Transporter 2: Role as a Novel Target for Drug Development. *American Association of Pharmaceutical Scientists*, **2006**, *8*, E682–E692.

Zheng, G.; Horton, D. B.; Deaciuc, A. G.; Dwoskin, L. P.; Crooks, P. A. Des-Keto Lobeline Analogs with Increased Potency and Selectivity at Dopamine and Serotonin Transporters. *Bioorg. Med. Chem. Lett.*, **2006**, *16*, 5018–5021.

Zheng, G.; Dwoskin, L. P.; Deaciuc, A. G.; Crooks, P. A. Synthesis and Evaluation of a Series of Homologues of lobelane at the Vesicular Monoamine Transporter-2. *Bioorg. Med. Chem.*, **2008**, *18*, 6509–6512.

Vita

John Paul Culver

I. Education

Western Kentucky University

B.Sc. Chemistry/Biology/minor in Biophysics 2005

II. Professional Research Experience

Research Scientist: ChemSolutions. 10/2010-present

Doctoral Research: University of Kentucky, College of Pharmacy. 2005-2010
Compound synthesis, molecular model development
Dr. Peter Crooks

Undergraduate Research: Western Kentucky University. 2002-2005
Compound Synthesis, Mechanistic Studies, Carbene catalysis synthesis.
Dr. Donald Slocum and Dr. Colin Abernethy

III. Teaching Activity

General Chemistry Lab (1 credit, major responsibility), Western Kentucky University, Department of Chemistry.

Organic Chemistry Lab (2 credits, teaching assistant), Western Kentucky University, Department of Chemistry.

Introduction to Chemistry Lab (1 credit, teaching assistant), Western Kentucky University, Department of Chemistry.

MCAT Preparation Course (major responsibility), Western Kentucky University, South Central Area Health Education Center (AHEC).

IV. Awards & Honors

Honors Department Scholarship, Western Kentucky University (2002 - 2005)

College Heights Foundation Golf Classic Scholarship, Western Kentucky University (2003-2005)

Outstanding Senior in Chemistry, Western Kentucky University (2005)

Funded by NIDA Training Grant T32 DA016176 (2006-2010)

V. Memberships in Professional Organizations

Member of the American Chemical Society

Member of the American Association of Pharmaceutical Scientists

VI. Publications

Original Research Articles Published

1. "N-heterocyclic carbene adducts of high-oxidation-state metal halides". M. Spicer, C. Dodds, **John P. Culver**, Colin D. Abernethy. Chapter 18 in Modern Aspects of Main Group Chemistry, Lattman, M.; Kemp, R. (Eds) American Chemical Society Symposium Series, November 2005.

2. “Metalations in hydrocarbon solvents; media effects on n-BuLi reactivity”. Donald W. Slocum, Angela Carroll, Paul Dietzel, Sally Eilerman, **John P. Culver**, Ben McClure, Scott Brown, Robert Holman. Tetrahedron Letters (2006), 47(6), 865-868.
3. “cis-2,6-Dibenzylcyclohexanone”. **John P. Culver**, Sean Parkin, Peter A. Crooks. Acta Crystallographica, Section E: Structure Reports Online (2009), E65(3), o551, o551/1-o551/7.
4. “Design, Synthesis and VMAT2 Binding of Lobeline Analogs as Potential Therapeutic Agents for Treating Psychostimulant Abuse”. Peter A. Crooks, Guangrong Zheng, Ashish Vartak, **John Culver**, Fang Zheng, A. Gabi Deaciuc, and Linda P. Dwoskin, Current Topics in Medicinal Chemistry, (Sharjah, United Arab Emirates) (2011), 11(9), 1103-11275.
5. “meso-Transdiene analogs inhibit vesicular monoamine transporter-2 function and methamphetamine-evoked dopamine release”. Horton, David B.; Siripurapu, Kiran B.; Norrholm, Seth D.; **Culver, John P.**; Hojahmat, Marhaba; Beckmann, Joshua S.; Harrod, Steven B.; Deaciuc, Agripina G.; Bardo, Michael T.; Crooks, Peter A.; et al. Journal of Pharmacology and Experimental Therapeutics (2011), 336(3), 940-951.
- 6.) “Exploring the effect of N-substitution in nor-lobelane on the interaction with VMAT2: discovery of a potential clinical candidate for treatment of methamphetamine abuse”. Zheng, Guangrong; Horton, David B.; Penthala, Narsimha Reddy; Nickell, Justin R.; **Culver, John P.**; Deaciuc, Agripina G.; Dwoskin, Linda P.; Crooks, Peter A. MedChemComm (2013), 4(3), 564-568.

Original Research Articles currently submitted or in preparation

1. “Synthesis and evaluation of a series of aromatic substituted lobelane analogues as ligands for the vesicular monoamine transporter-2”. John P. Culver, Guangrong Zheng, Linda P. Dwoskin, Justin R. Nickell, Agripina G. Deaciuc, Peter A. Crooks * Currently in preparation and formatted for Bioorg Med Chem Lett.
2. “Synthesis and evaluation of 1,4-substituted Piperidines as Novel Ligands for the Vesicular Monoamine Transporter-2 (VMAT2) Authors: John P. Culver, Guangrong Zheng, Linda P. Dwoskin, Justin R. Nickell, Agripina G. Deaciuc, Peter A. Crooks *. Currently in preparation and formatted for Bioorg Med Chem.

Symposium Abstracts

1. “High-oxidation state early transition metal complexes containing N-heterocyclic carbene ligands”. Colin D. Abernethy, John P. Culver, Mary C. Garrison, Dustin M. Jenkins, Alanna K. Storey. Department of Chemistry, Western Kentucky University. 87th Canadian Chemistry Conference in London, Ontario, 2004.
2. “Early transition state metal complexes featuring N-heterocyclic carbene ligands”. Colin D. Abernethy, John P. Culver, Courtney R. Phillips, Kirsty N. Thompson, Mark D. Spicer. Department of Chemistry, Western Kentucky University. 229th ACS National Meeting, San Diego, CA, United States, March 13-17, 2005.
3. “Western Kentucky University Student Affiliate Chapter”. Kayla Milner, Abigail M. Hobbs, John P. Culver, Kevin M. Williams. Department of Chemistry, Western Kentucky University. 229th ACS National Meeting, San Diego, CA, March 13-17, 2005.
4. “Phenylation of o-lithio intermediates: Coupling of DoM and benzyne-formation methodologies”. Donald W. Slocum, Troy Reece, Julia Raymer, John P. Culver,

Karen Lalonde, Kelley Moran. Department of Chemistry, Western Kentucky University. 230th ACS National Meeting, Washington, DC, August 28-September 1, 2005.

5. “Metalations in hydrocarbon solvents: Detection of the ‘complex’ in the complex-induced proximity effect paradigm”. Donald W. Slocum, Ben McClure, John P. Culver, Scott Brown, Robert Holman. Department of Chemistry, Western Kentucky University. 230th ACS National Meeting, Washington, DC, August 28-September 1, 2005.

6. "Design and synthesis of lobelane analogs targeting the Vesicular Monoamine Transporter (VMAT2) as a potential treatment for methamphetamine abuse". John P. Culver, Agripina G. Deaciuc, Linda P. Dwoskin, Peter A. Crooks. College of Pharmacy, University of Kentucky. 233rd ACS National Meeting, Chicago, IL, March 25-29, 2007.

8. “Synthesis of lobelane Analogs Targeting the Vesicular Monoamine Transporter-2 (VMAT2).” Culver JP, Dwoskin LP, Deaciuc AG, Crooks PA. AAPS National Conference, San Diego, CA, Fall 2007.

9. “Development of lobelane Isomers Targeting the Vesicular Monoamine Transporter-2 (VMAT2)”. Culver JP, Dwoskin LP, Deaciuc AG, J. Chagkutip, Crooks PA. AAPS National Conference, Atlanta, GA, Fall 2008.

10. “Synthesis and Evaluation of Analogs of lobelane Targeting the Vesicular Monoamine Transporter-2 (VMAT2)” Culver JP, Dwoskin LP, Nickell, JR, Deaciuc AG, Crooks PA. AAPS National Conference, Los Angeles, CA, Fall 2009.

11. “Synthesis and Evaluation of Structurally Diverse Analogs of lobelane Targeting the Vesicular Monoamine Transporter-2 (VMAT2)” Culver JP, Dwoskin LP, Nickell, JR, Deaciuc AG, Crooks PA. AAPS National Conference, New Orleans, LA, Fall 2010.